



UNIVERSITA' DEGLI STUDI DI MESSINA

Department of Chemical, Biological, Pharmaceutical and Environmental Sciences

PhD in: APPLIED BIOLOGY AND EXPERIMENTAL MEDICINE

XXXI Cycle

Coordinator: Prof.ssa Maria Assunta Lo Gullo

NEW OMICS APPROACHES IMPROVING CLASSIFICATION AND PERSONALIZED RETINITIS PIGMENTOSA DIAGNOSIS

PhD Student:

Dott. LUIGI DONATO

Tutor:

Illustrious Professor

ANTONINA SIDOTI

ACADEMIC YEAR 2015/16

SUMMARY		Page
1. INTRODUCTION AND OBJECTIVES OF THE WORK		1
2. CLINICAL, BIOCHEMICAL, MOLECULAR AND GENETIC ASPECTS OF RP		4
2.1. Clinical signs in RP		4
2.2. Family history		5
2.3. Ophthalmic trial		6
2.3.1. The classic RP instrumental examination		6
2.3.2. Ocular findings linked to RP		7
2.4. Retinal functionality		8
2.5. Retinal imaging		10
2.6. Differential diagnosis for non – syndromic retinitis pigmentosa		14
2.7. Clinical aspects of RP genetic subtypes		32
2.8. Associated genes and proteins		39
2.8.1. The phototransduction pathway		40
2.8.2. Visual cycle cascade		43
2.8.3. Connecting cilium trafficking		45
2.8.4. Photoreceptor outer segment assembly		47
2.8.5. The interphotoreceptor matrix		49
2.9. Handling of RP		51
2.9.1. Ophthalmic and genetic counseling		51
2.9.2. Visual rehabilitation		53
2.9.3. RP treatment possibilities		53
3. MATERIALS AND METHODS		57
3.1. Genomics		57
3.1.1. Patients' clinical features		57
3.1.2. Genotyping (Sanger sequencing)		63
3.1.3. Whole Genome Sequencing (WGS)		64
3.1.4. In silico functional prediction analyses of variant effects		69
3.2. Transcriptomics		71
3.2.1. Cell cultures		71
3.2.2. Total RNA sequencing		72
3.2.3. Quality validation and read mapping		72
3.2.4. Differential gene and non – coding RNA expression and statistical analysis		73
3.2.5. Functional gene annotations		74
3.2.6. Filtering and annotation of non – coding RNAs		75
3.2.7. Coding and non – coding genes pathway analyses		79
3.3. Functional and validation assays		82
3.3.1. Sanger validation and family member genotyping		82
3.3.2. Population screening		82
3.3.3. Data validation by qRT – PCR		82
3.3.4. Dual luciferase assay		83

	SUMMARY	Page
4. RESULTS		86
4.1. Genomics		86
4.1.1. Combined effects of known variants in genes still not associated to RP		86
4.1.2. Combined effects of known variants and haplotypes in Stargardt disease causative genes		94
4.1.3. Novel mutations in already known RP causative genes		98
4.2. Transcriptomics		100
4.2.1. Expression changes in RP candidate genes caused by oxidative stress		100
4.2.2. Discovery of new regulative “hot – spot” withing new found biochemical pathways		111
5. DISCUSSION		128
5.1. Classification of new RP forms by new genotype – phenotype associations		128
5.2. Impaired bidirectional neurotransmission in the inner retina layers as RP pathogenic mechanism (and not as effect)		139
5.3. Evaluation of new consequences determined by already known variants in RP causative genes		145
5.4. Classification of new non – syndromic RP forms by discovery of new biochemical pathways		153
5.4.1. Candidate “macro – pathways” analysis		154
5.4.2. Pathway analysis of altered genes yet associated to retinal diseases		160
5.4.3. New candidate genes and their possible impact on RP etiopathogenesis		164
5.5. Classification of new non – syndromic RP forms caused by alterations in regulation of new specific pathways		176
6. CONCLUSIONS		184
7. BIBLIOGRAPHY		186

1. INTRODUCTION AND OBJECTIVES OF THE WORK

Retinitis Pigmentosa (RP) is a heterogeneous inherited ocular disease characterized by progressive retinal degeneration. It is considered an uncommon condition, but worldwide prevalence refutes this data, varying approximately from 1:9000 to 1:750 (Na et al., 2017), depending on the geographic location. RP affects 1-5 in 10,000 in Italy, while no data is available on RP frequency in Sicily. The term “pigmentosa” refers to the characteristic appearance of abnormal areas of pigment in the retina in the advanced stages of the disease. Such adjective was first coined by the eminent Dutch ophthalmologist F.C. Donders in 1857, although his colleague A.C. van Trigt described RP four years earlier, by the use of an ophthalmoscope (Naz et al., 2010). Interestingly, already during 19th century several forms of retinal degenerations had already been reported. Among them, we report that in 1744 R.F. Ovelgün described a form of familial night blindness closely resembling RP (Heckenlively, 1987), and the description by F.A. von Ammon of patients with poor vision and pigmented retinal lesions (Marre & Walther, 1990).

RP comprises a group of progressive inherited retinal dystrophies (IRDs), generally characterized by the early degeneration of rod photoreceptors, followed by the loss of cone photoreceptors (O'Neal & Luther, 2018). The first symptom is usually reduced night vision, followed by a progressive loss of the peripheral visual field (tunnel vision). Macula function is usually relatively well conserved until later stages of the disease. As already mentioned, fundus abnormalities include particular bone spicule pigmentation predominantly in the periphery and/or mid-periphery, along with attenuation of retinal vessels and a waxy pallor of the optic nerve head. Electroretinography can help to reveal the characteristic loss of photoreceptor function, primarily among rods rather than cones in early stages of the disease.

RP is clinically different from other IRDs, including IRDs occurring at birth or within the first few months of life (e.g. Leber congenital amaurosis, or LCA), dystrophies in which cone degeneration precedes rod degeneration (e.g. cone-rod dystrophy), macular dystrophies, and not – progressive disorders like achromatopsia and congenital stationary night blindness (CSNB) (Broadgate, Yu, Downes, & Halford, 2017). Additionally, about 25% of RP patients shows a syndromic form associated

with extra-ocular abnormalities. Collectively, these disorders constitute a big group of retinal dystrophies with significantly overlapping clinical and/or genetic findings (Fig. 1). This overlap represents the biggest challenge in IRDs specific classification. Moreover, only few therapeutic options are currently available in daily clinical practice. For that reason, it is fundamental to provide the patient with the best possible information about the expected clinical course and inheritance pattern. In order to realize such purpose, developing a classification system which merges the clinical diagnosis with the underlying genetic factors can provide precious prognostic information about the rate of progression and long-term outcome.

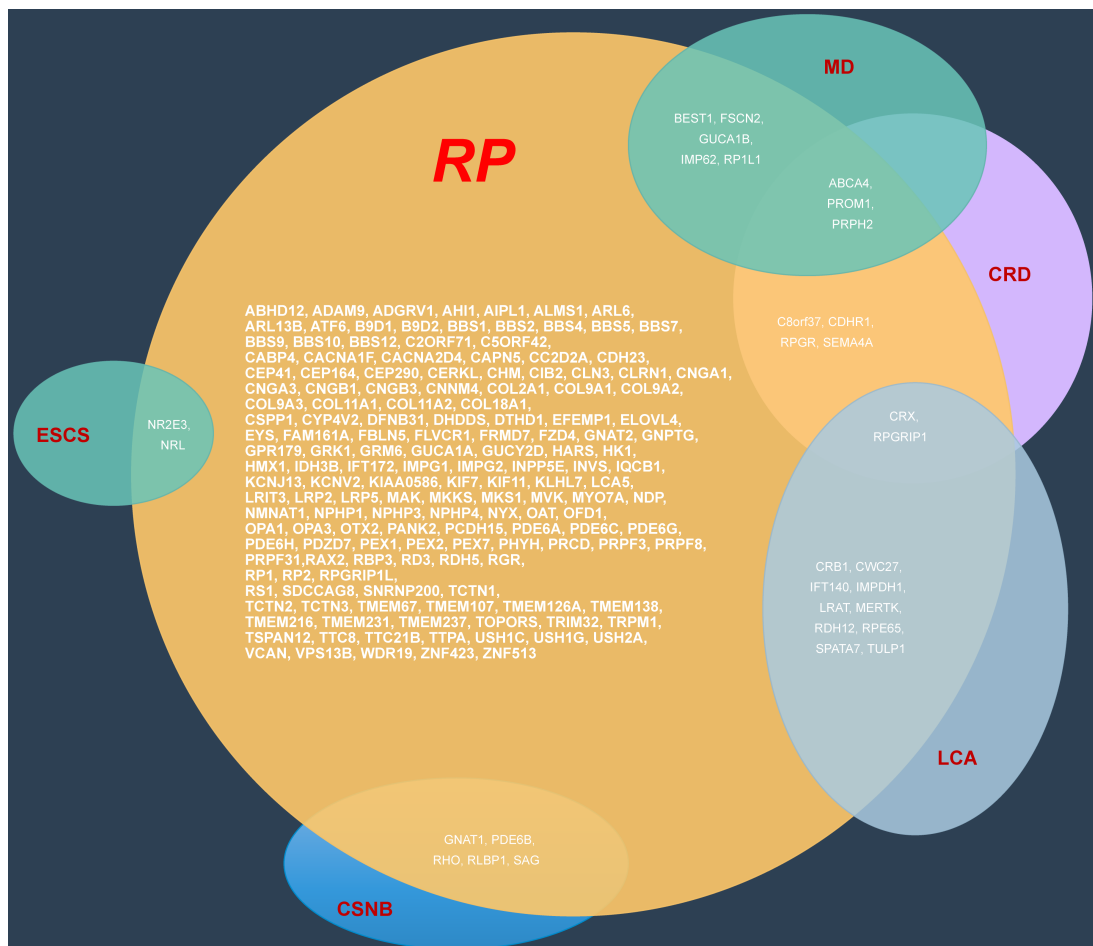


Fig. 1. Venn diagram summarizing the genetic overlap between RP and other inherited retinal dystrophies. Each circle represents a specific clinical diagnosis. The gene names listed in the overlapping areas indicate that mutations in these genes can lead to different phenotypes. Genes marked with an asterisk are candidate genes for non-syndromic RP.; Abbreviations: CRD: cone-rod dystrophy, CSNB: congenital stationary night blindness, ESCS: enhanced S-cone syndrome, LCA: Leber congenital amaurosis, MD: macular dystrophy, RP: retinitis pigmentosa.

The high heterogeneity showed by RP patients is excellently illustrated by the wide number of genetic defects associated with RP. During the early 90s, the rhodopsin (*RHO*) gene was identified as the first gene involved in autosomal dominant RP (Shokravi & Dryja, 1993). Since then, mutations in more than 80 genes have been involved in non-syndromic RP (Ali, Rahman, Cao, & Yuan, 2017), and each year new genes are added to this list. Each of these genes belongs to a gene-specific subtype of RP with a specific spectrum of phenotypes. Furthermore, lots of factors can change widely within each of these particular subtypes, even between affected family members, suggesting the presence of unknown genetic and/or environmental factors that could influence the RP phenotype.

The main purpose of our work is to improve the classification of RP orphan forms, along with the clarification of etiopathogenesis mechanisms of already known ones. Such goals were realized by an omics approach, which exploits the modern technique of Next Generations Sequencing and derived “Big Data” to bring out the innermost and heterogeneous genetic sides of retinitis pigmentosa. We start providing a comprehensive overview of the clinical features associated with the different genetic subtypes of non-syndromic and syndromic RP. Additionally, in order to define the state of art about genotype – phenotype associations, we also discuss the role of proteins encoded by causative RP genes in the structure and function of the retina. Finally, we discuss the current therapeutic options and future perspectives for all analyzed RP forms.

2. CLINICAL, BIOCHEMICAL, MOLECULAR AND GENETIC ASPECTS OF RP

2.1. CLINICAL SIGNS IN RP

RP leads to a progressive photoreceptor and retinal pigment epithelium (RPE) degeneration, determining tunnel vision, night blindness and a gradual reduction of central vision. Nevertheless, the clinical findings in RP vary widely due to the huge number of genes involved, each of which can have several alleles. Now we examine the common clinical features considered representative of RP.

- *Age of onset and progression rate*: age of onset varies widely among RP patients. Several patients develop symptomatic visual loss during early childhood, while others can remain relatively asymptomatic up to mid-adulthood. Generally, difficulties with dark adaptation begin in adolescence, whereas typical visual loss during the mid-peripheral field becomes evident during young adulthood. Nevertheless, children's ability to compensate for peripheral visual loss, along with dark adaptation difficulties detecting caused by our artificially illuminated nighttime environment, complicate the exact age of onset knowledge. Almost always, RP subtypes showing symptoms early in life tend to progress more rapidly. Additionally, pathology severity is correlated with the specific Mendelian pattern of inheritance. Generally, patients affected by X-linked forms (about 10% of RP patients) evidence a more severe disease course compared to patients with autosomal recessive ones (about 55% of RP patients), while autosomal dominant affected individuals (about 35% of RP patients) have the best long-term prognosis with great chances to maintain central vision (Farrar et al., 2017).
- *Symptomatology*: the beginning symptoms of RP include nyctalopia (night blindness) and dark adaptation difficulties. Interestingly, RP can also show loss

of the mid-peripheral visual field, although this is rarely reported as an initial symptom. Generally, the central retina maintains its integrity until the final stages of the pathology, even if anatomical abnormalities can appear early during the development of the disease. Such possibility is characteristic of middle age patients, in which central cone degeneration leads to visual acuity decrease. A large number of RP patients preserve the light detection ability, due to residual macular function or thanks to the retained integrity of peripheral temporal retinal island (Aleman et al., 2011). Photopsia is a widespread but often underestimated symptom (Ohguro et al., 2002) which can be very troubling to patients. This pathological manifestation may be caused by an impairment of afferent nerve synapses following photoreceptor degeneration or spontaneous self-signaling activity as consequence of inner retina remodeling (Jones, Marc, & Pfeiffer, 1995). Although photopsia can occur during early stages of RP, the most striking and disturbing effects are typical of the later stages of the disease (Bittner, Haythornthwaite, Diener-West, & Dagnelie, 2012). In advanced RP, as in Charles Bonnet syndrome (Franke, Rauschenberger, & Fluri, 2018), visual hallucinations can take animate forms. Finally, RP affected patients can also exhibit dyschromatopsia and photophobia (Riveiro-Alvarez et al., 2015).

2.2. FAMILY HISTORY

A detailed analysis of family history is very important in any patient suspected for RP. A pedigree for each proband is useful to assess the pattern of inheritance and may also help during diagnoses. For example, if an X-linked inheritance is suspected, *RP2* and *RPGR* genes should be sequenced before using next generation sequencing (NGS) approaches. A pedigree may also exemplify which family members could develop RP and indicate subjects where non-penetrance should be suspected, as for mutations in *HK1* gene.

2.3. OPHTHALMIC TRIAL

2.3.1. *The classic RP instrumental examination*

Three clinical hallmarks represent the typical signs of RP: attenuation of retinal vessels, a waxy pallor of the optic nerve and, above all, bone spicule pigmentation. In the initial stages of RP, ocular fundus may appear normal, as bone spicule-shaped pigment accumulation is either absent or sparse, vascular attenuation is not yet pronounced, and the optic disc appears typical. Before such representative RP alterations, some patients may manifest aspecific abnormalities such as discontinuous whitish lesions localized around RPE, broadening of the foveal reflex and irregular reflexes from the internal limiting membrane.

Retinal vessel shrinkage in RP is not yet defined. Firstly, this clinical aspect was attributed to decreased metabolic demand following ganglion cell death after photoreceptor loss. Another possibility links the loss of oxygen-consuming photoreceptors to a hyperoxic state of the residual inner retina, leading to vasoconstriction and slowing down blood flow in retinal vessels (Sorrentino, Bonifazzi, & Perri, 2015). Moreover, Li et al. found that thinning of the extracellular matrix between the retinal vessels and the migrated RPE cells implies narrowing of the vessels (Z. Y. Li, Possin, & Milam, 1995). At last, Stone et al. hypothesized that an impairment of synaptic input determined by photoreceptor cell death, along with the subsequent depleting of trophic factors, decreases the metabolism of the inner retinal cells, promoting vascular remodeling followed by vessel thickness (Grunwald, Maguire, & Dupont, 1996). Alternatively, Cellini et al. suggested that ocular blood flow was decreased more than expected by retinal atrophy, turning the debate on whether vascular changes in RP patients play a central role in the onset of RP or are simply secondary to neuroretinal remodeling (D'Orazi, Suzuki, & Wong, 2014). Regarding this, a crucial role for the vasoconstrictor endothelin-1 has been proposed, even if both boosted and reduced plasma levels of this protein have been described among RP patients, thus suggesting the need for further study (Olivares-Gonzalez, Martinez-Fernandez de la Camara, Hervas, Millan, & Rodrigo, 2018). Finally, because most of RP associated genes are involved in either the photoreceptor-RPE complex or

the inter-photoreceptor matrix, the most probable hypothesis give a secondary role to these vascular alterations.

About the waxy pallor of the optic disc, typical of disease progression, it is probably determined by glial cell accumulation both on the surface and inside the optic disc, increasing light reflectance (Al Rashaed, Khan, Nowilaty, Edward, & Kozak, 2016).

Curiously, not all RP patients develop characteristic bone spicules, substituted by dust-like pigmentation or nummular hyperpigmentation. The hyperpigmentation level can change among patients and it is not consequently related to the severity of the disease. Bone spicule pigmentation is the histological representation of RPE cell detaching from Bruch membrane after photoreceptor degeneration, cell that migrate to intraretinal perivascular sites, where they constitute melanin pigment deposits (Jaissle et al., 2010). These bone spicules frequently arise in the mid-periphery, where the density of rods is the highest (Berson, 1993). Due to the high level of interdependence with the choriocapillaris and photoreceptors, the RPE migration might be triggered by the attenuation between the inner retinal vessels and the RPE itself, following photoreceptor degeneration in RHO knock-out mice (G. L. Wang et al., 2005).

2.3.2. Ocular findings linked to RP

Many other different eye – affecting conditions, such as disease-associated refractive error, nystagmus and macular complications, are frequently associated with RP, and several are responsive to treatment. Cystoid macular edema (CME), together with macular hole and epiretinal membrane formation, represent the most displeasing conditions. CME, the most frequent of them, could be determined by several mechanisms: 1) Müller cell edema and dysfunction, 2) blood-retina barrier disruption, 3) vitreomacular traction, 4) RPE pumping activity alterations, and 5) anti-retinal antibodies (Strong, Liew, & Michaelides, 2017). About 40% of RP patients evidences epiretinal membrane constitution (Fujiwara et al., 2016), probably as consequence of idiopathic preretinal glial cell proliferation or of inflammatory processes (G. Liu, Du, Keyal, & Wang, 2017). The involvement of inflammatory pathways in RP is

abundantly proved but, if it was primarily considered as an event following rod and cone death, today inflammatory cells are believed to induce retinal degeneration by their cytotoxic effect on photoreceptors (Massengill, Ahmed, Lewin, & Ildefonso, 2018). Inflammation could be also associated to posterior subcapsular cataract, affecting about 45% of RP patients, which seriously impairs vision, but which can be resolved even during macular compromise (Bruno, Nebbioso, Rigoni, Gagliardi, & Vingolo, 2015). Furthermore, additional but uncommon abnormalities that can arise during RP are represented by vitreous cysts (N. Yoshida et al., 2015) and proteolipidic accumulation in optic nerve head and fiber layer (Garcia-Cazorla, Mochel, Lamari, & Saudubray, 2015). Finally, RP seems to be one of the most frequent hidden pathology in patients affected by secondary retinal vasoproliferative tumors (Honavar, 2018).

2.4. RETINAL FUNCTIONALITY

- *Perimetry*: one of distinguishing RP feature is progressive loss of the visual field. It is characterized by significant bilateral symmetry (Massof et al., 1979) and arises with mid-peripheral isolated scotomas which gradually merge in a partial or complete ring scotoma. During advanced stages of disease, this annular scotoma expands both inward and outward. Even in the absence of ring scotoma, other known patterns of visual field impairment could occur, as concentric or arcuate (from superior to inferior retina) visual field loss (Bellingrath et al., 2017). Kinetic perimetry is best suitable evaluation method of peripheral visual field loss; the annual rate of decline for target V4e of the Goldmann perimeter varies between 2 and 12%, in relation to gene-specific subtypes (A. Oishi et al., 2013). The degree of central visual field impairment is usually verified by static perimetry, but it was superseded by recent fundus-driven perimetry. Microperimetry, for example, exploits accurate eye tracking throughout the analysis, and provides direct structure-function correlations generating an annotated image of the posterior pole.

- *Color vision*: generally, dyschromatopsia is representative of later stages of RP, with the so-called type III (blue) acquired color vision impairments more diffused than type I (red-green) (Abdelhakim & Rasool, 2018). Blue cone defect has been attributed to the insufficient and irregular distribution of these short-wavelength cones at the fovea (leading to pericentral retinal function loss and tritanopia (blue-yellow color blindness) (Durlu, Koroglu, & Tolun, 2014). Reduction of visual acuity and associated central photoreceptor death increases the probability of developing a type I color dysfunction (Pokorny, Lutze, Cao, & Zele, 2008). Alternatively, vision impairment caused by CME should not have serious effect on color vision (Pinckers, van Aarem, & Keunen, 1993).
- *Dark adaptometry*: an altered dark-adapted threshold is a typical sign of RP. Reduction of rod sensitivity and related delayed recovery generally increase rod threshold (Birch, Wen, Locke, & Hood, 2011). Recent analyses highlighted increases in both photoreceptor thresholds, a delay in reaching the asymptotic rod threshold, or the entire loss of rod function (Bennett, Klein, Locke, Kiser, & Birch, 2017).
- *Electroretinography*: the quantitative evaluation of RP severity and progression is primarily realized by full-field electrophysiological testing, according to the ISCEV guidelines (Robson et al., 2018). Electroretinogram (ERG) alterations occur early and precede nyctalopia symptoms and fundus abnormalities (Fig. 2.). On the dark-adapted (scotopic), bright flash (mixed rod-cone) ERG, the a-wave is below the physiological standard. Moreover, isolated rod responses to a scotopic dim flash are delayed, decreased or absent in a full-field ERG recording. Cone responses may also be impaired in the early stages of RP, but this generally occurs after the onset of rod dysfunction. When present, cone compromise appears in the light-adapted (photopic) ERG as a delayed and reduced response to a bright flash and 30-Hz flicker stimuli. Oscillatory potentials may also be weakened in RP patients (Goo, Ahn, Song, Ryu, & Kim, 2011). The decay in central cone function is slower (Galli-Resta et al., 2013), as evidenced by a heterogeneous patient cohort including all three

inheritance patterns (autosomal recessive, autosomal dominant, and X-linked) and syndromic subtypes (Falsini et al., 2012). As the disease progresses, the full-field ERG may become unrecordable, even if a residual visual field is present. Such conditions require the use of full-field stimulus threshold (FST) or a multifocal ERG (mfERG) to obtain responses to follow RP progression, and delayed responses in the mfERG might predict visual field loss in a healthy-appearing retina (Lopez Torres, Turksever, Schotzau, Orgul, & Todorova, 2015).

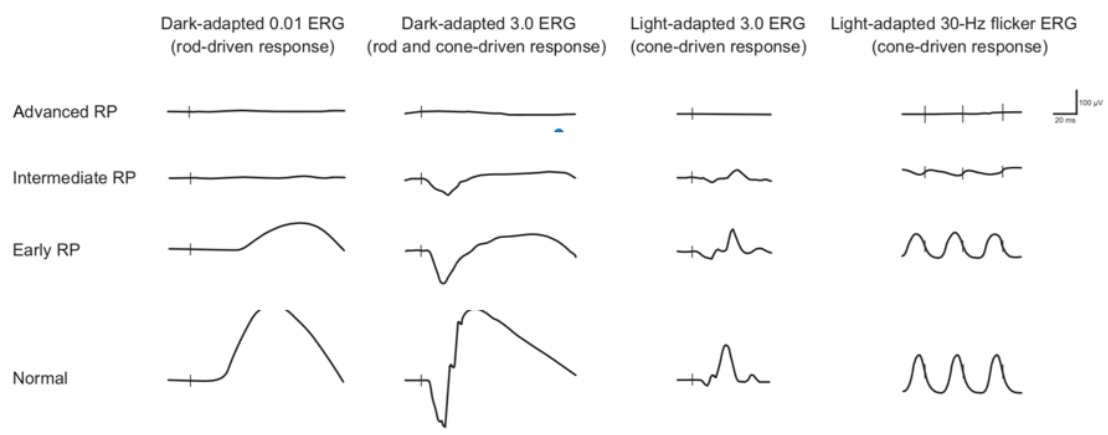


Fig. 2. Schematic representation of ERG recordings in different stages of RP (i.e. early, intermediate and advanced RP). Vertical lines indicate the moment of stimulus flash. As the RP progresses, the amplitude of responses decreases, and the implicit time may increase. Cone dysfunction typically lags behind the onset of rod dysfunction. Eventually, the ERG—under both scotopic and photopic conditions—is extinguished.

2.5. RETINAL IMAGING

- *Fundus imaging*: standard fundus photography covers a visual field of of 30 – 50 degrees of the retina, with a decreased coverage for the peripheral area. Typical color fundus photography is qualitative superior, but limited by media opacities and insufficient pupillary dilation, thus requiring a high patient compliance. A better method could be represented by ultra-wide field imaging, which exploits confocal scanning laser ophthalmoscopy (cSLO) with red and green laser light. Although such technique captures up to 200 degrees of retina in a single acquisition (Dysli, Schurch, Pascal, Wolf, & Zinkernagel, 2018), it

presents several disadvantages: the peripheral image appears distorted due to the two dimensional reduced image of the three-dimensional globe, the colors are artificial, and many artefacts could have been created by structures placed anterior to the retina (e.g. eyelashes and vitreous opacities). A recent method is multicolor imaging, which uses the reflectance of three lasers with a specific wavelength, to analyze the different layers of the retina. The final image results from merging of reflectance images from the individual lasers, and the coloring is also artificial. In RP patients, multicolor imaging improves border definition of the intact macular area compared to standard fundus photography (Andersen, Sauer, Gensure, Hammer, & Bernstein, 2018).

- *Optical coherence tomography*: thinning of photoreceptor outer segments represent the first histopathological RP (Milam et al., 1998). Such change is highlighted in a spectral-domain optical coherence tomography (SD-OCT) image as disorganization of the outer retinal layers, starting from the interdigitation zone, following with the ellipsoid zone, and ending at the external limiting membrane (Battaglia Parodi et al., 2016) (Fig. 3a). RP progression determines dimensional reduction of the outer segments and of the outer nuclear layer, which includes photoreceptor cell nuclei, then completely loss during the advanced phases of RP (Hood, Lazow, Locke, Greenstein, & Birch, 2011). On the other hand, the inner retinal layers, as the deep nuclear layer and the ganglion cell layer, remain quite untouched, even if their thickening could occur, as consequence of edema creation in the retinal nerve fiber layer and/or neuronal-glia retinal remodeling following the thinning of the outer retina (Aleman et al., 2007). In advanced stages, several patients could show other retinal tubulations (N. R. Goldberg, Greenberg, Laud, Tsang, & Freund, 2013). Hyperreflective foci, reflex of RPE cells migration from ellipsoid area, are a frequently found in both nuclear layers and/or the in the subretinal space, and often fundoscopically visible as hyperpigmentation. Interestingly, many studies evidenced a correlation between visual acuity and the width of ellipsoid zone, also linearly correlated to an impairment of visual field and attenuation of the outer segments (G. Liu, Liu, Li, Du, & Wang, 2016). Finally, OCT exams may also help to detect other macular alterations present in more than

50% of all RP patients (Makiyama et al., 2014). Among them, CME is the most frequent, followed by vitreomacular traction syndrome, epiretinal membrane formation and macular hole. During CME development, cystoid spaces are mainly distributed in the inner nuclear layer, but they can also occur in the outer layers and/or in the ganglion cell layer (Hariri et al., 2016).

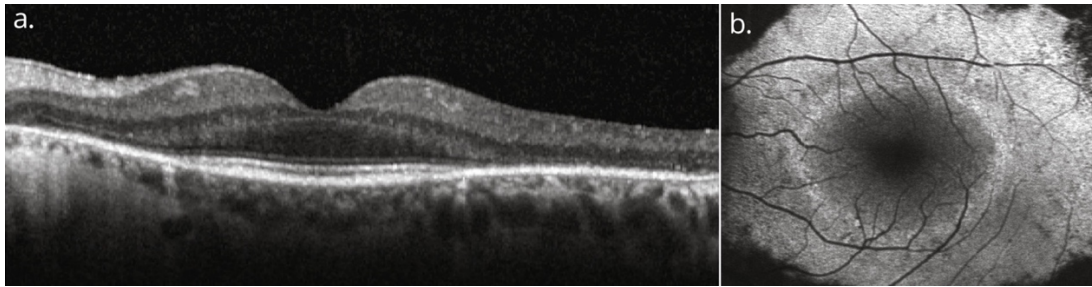


Fig. 3. Horizontal spectral-domain optical coherence tomography (SD-OCT; a) and fundus autofluorescence (FAF; b) images of the left eye of a patient with RP. The OCT image shows the perifoveal loss of the outer retinal layers. The central preservation of the ellipsoid zone corresponds to the internal edges of the hyperautofluorescent ring visible on FAF.

- Fundus autofluorescence imaging: fundus autofluorescence (FAF) can RPE metabolism abnormalities undetectable with other methods. With short-wavelength (SW) - FAF, using green or blue light, the signal derives predominantly from RPE lipofuscin aggregates (Delori et al., 1995), while near-infrared (NIR)-FAF shows also the autofluorescence signal from choroidal melanin or related fluorophores (Keilhauer & Delori, 2006). FAF represents an optimal technique to assess and monitoring the progression of RP, even if no detailed informations about the increased susceptibility to light toxicity dystrophic retinas - rich in photosensitizers as lipofuscin - can be obtained (Teussink et al., 2017). An abnormal foveal ring or curvilinear arc of amplified auto-fluorescence (Fig. 3b), detectable only by SW-FAF and NIR-FAF, occurs in more than 55% of RP patients (Mendis & Lois, 2014). Such hyperautofluorescent ring, generally characterized by a high interocular symmetry (Sujirakul et al., 2015), outlines a transition zone between altered (center of the ring) and undamaged (outside of the ring) retinal function. Autofluorescence degree immediately outside of the ring is generally conserved, even if retinal function is impaired. Additionally, photoreceptor degeneration in areas external to the ring corresponds to the loss of the ellipsoid

zone and the outer limiting membrane, along with thinning or depletion of the outer nuclear layer in an SD-OCT image (Lima et al., 2009). The autofluorescent ring itself reflects an area of outer segment dysgenesis and lipofuscin production, with progressive retinal attenuation, generally associated to dysregulation of the ellipsoid zone around the internal edge of the ring (Kominami et al., 2017). Most of patients do not show quantitative differences of the auto - fluorescence measured inside the ring compared to healthy eye (Schuerch et al., 2017). During disease progression, the ring diameter shrinks, with a high reduction rate for relatively large rings. Commonly, the increasing of cone dysfunction is reflected by the inner edge of the constricting ring, while rod sensitivity impairment is more diffused and involves the parafoveal area within the ring. Ultimately, the ring may disappear, as consequence of a widespread loss of sensitivity and visual acuity (Robson et al., 2012). Microperimetry in RP patients highlights that visual sensitivity is quite preserved within the ring, decreased in the ring zone itself, and frequently unrecordable outside the ring (Duncker et al., 2013). Besides the hyperfluorescent ring, other autofluorescence patterns can be detected. In the most of adult patients with RP, wide-field FAF reveals patchy and/or decreased autofluorescence in the mid-periphery, probably following the loss of peripheral vision (M. Oishi et al., 2014). Furthermore, central vision impairment could be reflected by an altered pattern of increased autofluorescence at the central macula (Wakabayashi, Sawa, Gomi, & Tsujikawa, 2010).

- *Fluorescein angiography*: fluorescein angiography represents a technique little used today for RP diagnosis. The angiogram shows chorioretinal atrophy, starting from periphery and expanding to the posterior pole. Generally, delay in the filling of retinal vessels is absent, but some leakage of dye could be present, due to vessels own attenuation. Moreover, CME presence and the uncommon choroidal neovascularization can be depicted by fluorescein angiography, even if the optical coherence tomography angiography (OCTA) is less invasive and more used today (Inooka et al., 2018).

- *Adaptive optics scanning laser ophthalmoscopy*: adaptive optics scanning laser ophthalmoscopy (AOSLO) is the most recent, non-invasive imaging technique that allows the visualization of photoreceptors at a microscopic level by correcting for ocular aberrations. In RP patients, the high resolution of AOSLO could early detect photoreceptor damage, as well as possible cone density reduction before the visual acuity is impaired, since a significant cone decrease is possible before the visual acuity becomes affected (Salmon et al., 2017). Summarizing, AOSLO represents a highly sensitive imaging method that may improve disease progression monitoring and evaluating treatment safety and efficacy in clinical trials.

2.6. DIFFERENTIAL DIAGNOSIS FOR NON-SYNDROMIC RETINITIS PIGMENTOSA

IRDs constitute a very heterogeneous and widespread family, made of disorders that especially affect the macula (e.g., Sorsby's fundus dystrophy and Stargardt disease) and of stationary disorders such as CSNB and achromatopsia. The inclusion criteria of RP depend on ophthalmological aspects (symptoms, fundus abnormalities and ERG results), as well as less objective evaluations, such as the patient's age at onset and/or historical factors. Finally, in order to minimize overlapping phenotypes, more evident at the late stages of disease, it has to be considered the whole pathology course when classifying an IRD. A comprehensive overview of the parameters take in account for differential diagnoses in RP is highlighted in Table 1.

- *Other inherited retinal dystrophies*: two retinal dystrophies, clinically and genetically indistinguishable, unclearly classified by the age of onset, are early-onset RP and Leber Congenital Amaurosis (LCA). Frequently, patients who manifest symptoms at birth or within the first few months of life are considered to be affected by LCA (Sharif & Sharif, 2017). In LCA, the excessively early loss of visual ability determines a group of symptoms that include photophobia,

poor pupillary response, nystagmus, and particular oculo-digital signs such as, pressing, poking and rubbing the eyes. Visual acuity is usually lower than 20/400, and the fundus can vary from a normal appearance to a wide atrophic RP-like pigmentary retinopathy. Scotopic and photopic ERG are frequently unrecordable or severely reduced. Early-onset RP can exhibit many of previously described symptoms, and the number of shared genes reflects the overlap with LCA (Fig. 1). Another IRD sharing clinical and genetic aspects with RP is cone-rod dystrophy. ERG exam is not always sufficient to assess which photoreceptors are primarily affected, especially during the later phases of the disease. Nevertheless, the early symptoms of cone-rod dystrophy, such as early loss of visual acuity, variable achromatopsia, intense photophobia, and the initial absence of night blindness, can help to distinguish between cone-rod dystrophy and RP (Inui et al., 2014). Other specific retinal dystrophies show rod-cone degeneration, but their own particular phenotypes distinguish them from RP. Among them, most diffuse examples are gyrate atrophy (well-defined circular chorioretinal atrophy accompanied by high ornithine levels), choroideremia (patchy chorioretinal atrophy with physiological appearing retinal vessels) and late-onset retinal degeneration (perimacular drusen-like lesions together with long anterior lens zonules) (Stanton et al., 2017). Retinitis punctata albescens, even if presents a highly particular phenotype has been considered an RP subtype throughout most of the literature. Congenital stationary night blindness (CSNB) is an example of a stationary disorder principally identified by rod abnormalities. Affected patients, generally present a normal fundus, except two particular subtypes of CSNB, called Oguchi disease and fundus albipunctatus. Nevertheless, CSNB evidences a significant gene overlap with RP, especially for RDH5, RLBP1, PDE6B, SAG and RHO (Koenekoop, 2018).

- *Pseudoretinitis pigmentosa*: lots of disturbs can mimic the clinical features of RP (phenocopy) and are categorized as pseudoretinitis pigmentosa. Unlike real RP forms, the family of pseudoretinitis pigmentosa could be treatable and do not present an essential genetic base. Therefore, to distinguish them from

typical RP, a deep history, including lack of interocular symmetry, current and past medications, and lack of disease progression, is fundamental. For example, several patients who were diagnosed with “unilateral RP” fall in this category, even if a germline mutation in the RP1 gene was documented in a patient affected by strictly unilateral RP (Mukhopadhyay, Holder, Moore, & Webster, 2011).

Disease	Clinical Features
Syndromic forms of retinitis pigmentosa	
Ciliopathies	
Usher syndrome	RP with partial or complete neurosensory hearing loss, sometimes vestibular dysfunction.
Bardet-Biedl syndrome	RP and obesity, postaxial polydactyly, hypogonadism, renal dysfunction, cognitive impairment.
Cohen syndrome	RP and myopia, mental retardation, hypotonia, fascial dysmorphism, short stature, neutropenia.
Joubert syndrome	RP/LCA with dysmorphic facial features, congenital hypotonia evolving in ataxia, developmental delay and unusual fast or slow breathing. Oculomotor apraxia and nystagmus may be present. The hallmark feature is the ‘molar tooth sign’ on MRI.
Senior-Løken syndrome	RP/LCA and nephronophthisis (NPHP).
Sensenbrenner syndrome (cranioectodermal dysplasia)	RP and craniosynostosis, ectodermal abnormalities.
Short-rib thoracic dysplasia with or without polydactyly (includes Jeune, Mainzer- Saldino, Ellis-van Creveld and short rib- polydactyly syndrome)	RP and thoracic hypoplasia, short stature, brachydactyly, polydactyly, chronic renal failure, (sometimes lethal) respiratory insufficiency.
Metabolic disorders	
Alfa-tocopherol transfer protein deficiency (familial isolated vitamin E deficiency)	RP with (Friedrich-like) ataxia, dysarthria, reduced proprioception and hyporeflexia.
Bassen-Kornzweig syndrome (abetalipoproteinemia)	Atypical RP with onset 1 st -2 nd decade. Wide spectrum of abnormalities including progressive cerebellar ataxia, gastrointestinal disorders, acanthocytosis and absence of apo-B containing lipoproteins.
Mucopolysaccharidoses	Group of disorders with RP, cloudy cornea and glaucoma and numerous symptoms in varying degree: cognitive impairment, developmental delay, hearing loss, hydrocephalus, facial abnormalities, dwarfism and hepato-splenomegaly.
Neuronal ceroid-lipofuscinoses, childhood onset (Batten disease)	RP with early vision loss, FAG: diffuse RPE atrophy with stippled hyperfluorescence, progressive neurodegeneration, seizures, may cause early death.
Refsum disease (phytanic acid oxidase deficiency)	RP and anosmia, miosis, attenuated effect of mydriatica, elevated phytanic acid levels, anosmia,

	hearing loss, ataxia, polyneuropathy, ichthyosis, cardiopathy.
Mevalonate kinase deficiency (mevalonic aciduria (MEVA) and hyper-immunoglobulin D and periodic fever syndrome (HIDS)	Spectrum of clinical phenotypes, sometimes with RP. HIDS: recurrent febrile attacks lymphadenopathy, arthralgia, gastrointestinal disturbances, skin rash and increased levels of serum immunoglobulin D. MEVA is the most severe form with psychomotor retardation, progressive cerebellar ataxia, dysmorphic features, recurrent febrile crises, and failure to thrive.
HARP syndrome (hypoprebetalipoproteinemia, acanthocytosis, RP and pallidal degeneration)	Part of the pantothenate kinase-associated neurodegeneration (PKAN) spectrum. RP with hypoprebetalipoproteinemia, acanthocytosis and pallidal degeneration (eye of the tiger sign on MRI).
PHARC syndrome (polyneuropathy, hearing loss, ataxia, RP, and cataract)	RP with polyneuropathy, hearing loss, cerebellar ataxia and early-onset cataract.
Mitochondrial disorders	
Kearns-Sayre Syndrome	RP with progressive external ophthalmoplegia, heart conduction defect, cerebellar ataxia or elevated protein concentration in cerebrospinal fluid. Onset <20 years.
NARP syndrome (Neuropathy, Ataxia, RP)	RP and peripheral neuropathy, neurogenic muscle weakness, ataxia.
Inherited retinal dystrophies	
Progressive retinal disease	
Cone-rod dystrophy	Patients typically present with VA loss, dyschromatopsia and photoaversion. May experience nyctalopia. Primary loss of cone function on the ERG, followed by rod impairment. Syndromal associations.
Cone dystrophy	Progressive loss of VA and dyschromatopsia often accompanied by photoaversion and photophobia. Macula: ranging from normal to a bull's eye maculopathy or RPE atrophy. Reduced or nonrecordable photopic ERG.
Leber congenital amaurosis	Early-onset retinal dystrophy at birth or in first months of life, nystagmus, hyperopia, amaurotic pupils, oculo- digital sign, extinguished photopic and scotopic ERG. Syndromal associations.
Macular dystrophies (Stargardt disease, Sorsby fundus dystrophy)	Progressive loss of VA, advanced disease sometimes associated with night blindness and loss of peripheral vision.
Bietti crystalline corneoretinal dystrophy	Yellow-white crystalline retinal deposits throughout posterior pole and sometimes in corneal limbus. Sclerosis of the choroidal vessels. Often marked asymmetry in retinal findings.
Late-onset retinal degeneration	Perimacular yellow-white drusen-like lesions, long anterior zonules, and hyperpigmentation in the midperiphery. Gradual loss of dark adaptation in fifth-sixth decade. Reduced visual acuity in advanced stages caused by scalloped areas of RPE atrophy or neovascularization, accompanied by ERG changes (rod-cone pattern). Normal caliber of retinal vessels.

Stationary retinal disease	
Congenital stationary night blindness	Largely non-progressive. Nightblindness. Nystagmus and myopia with decreased VA if onset early in life. Most common ERG is 'negative' dark-adapted ERG. Oguchi disease and fundus albipunctatus are forms of CSNB.
Chorioretinal dystrophies	
Choroideremia	X-linked, pigment clumping at RPE level, followed by patchy loss of RPE and choriocapillaris with visible underlying large choroidal vessels and sclera. Normal appearing retinal vessels.
Gyrate atrophy	Well demarcated, circular areas of chorioretinal atrophy often starting in far periphery, early onset cataract formation, myopia, CME, elevated plasma ornithine, type II muscle fiber atrophy, hair thinning.
Helicoid peripapillary chorioretinal degeneration (Sveinsson chorioretinal atrophy)	Autosomal dominant, peripapillary chorioretinal atrophy with radially extending wing-shaped atrophy, no attenuation of retinal vessels.
Progressive bifocal chorioretinal atrophy	Slowly progressive, large atrophic lesions in macula and nasal to the optic disc. Nystagmus and myopia.
Vitreoretinal dystrophies	
X-linked juvenile retinoschisis	VA loss from the 1 st /2 nd decade of life. Cystoid macular lesions, typically in an spoke-wheel pattern, peripheral schisis in 50% of patients. ERG: selective reduction in b-wave amplitude.
Enhanced S-cone syndrome/Goldmann- Favre Syndrome	ERG: enhanced S-cone sensitivity (pathognomic). Variable phenotype, hallmarks are nummular pigmentations at RPE level and cystoid or schisis-like maculopathy. Night blindness from birth and decreased VA.
Wagner syndrome/erosive vitreoretinopathy	Optically empty vitreous with avascular vitreous strands and veils, presenile cataract, moderate myopia, progressive chorioretinal atrophy sometimes with diffuse pigmentary changes, reduced VA, night blindness and visual field constriction. Retinal detachment in advanced stages of disease.
Snowflake vitreoretinopathy	Autosomal dominant, corneal guttae, cataract, fibrillar degeneration of the vitreous, retinal detachment, and peripheral retinal degeneration, including crystalline deposits referred to as snowflakes, vascular attenuation and chorioretinal pigmentation.
Female carriers of inherited retinal dystrophies	
Retinitis pigmentosa	Female carriers of XL-RP: highly variable presentation; from no abnormalities to RP phenotype. Tapetal-like reflex possible.
Choroideremia	Female carriers are generally asymptomatic, although chorioretinal atrophy and ERG changes similar to those in affected males can be observed.
Ocular albinism	Female carriers <i>GPR143</i> gene (OA1): patchy hypopigmentation of the RPE, iris transillumination.

Pseudoretinitis pigmentosa	
Drug-induced	
Thioridazine and chlorpromazine	Nummular areas with loss of RPE and choriocapillaris perfusion. Chlorpromazine often leads to posterior subcapsular cataract.
Quinolines (e.g. (Hydroxy)chloroquine)	Bull's eye maculopathy, Asian patients: pericentral retinopathy. In case of poisoning: initially fixed dilated pupils, later miosis. Late fundus appearance.
Chorioretinal infections	
Syphilis, Lyme disease, acute retinal necrosis and other viral infections (rubella, chicken pox, measles, cytomegalovirus)	Often unilateral or sectorial retinal disease. History of infectious retinal disease.
List of inflammatory disease	
Sarcoidosis	Ocular clinical criteria: mutton-fat or small granulomatous KPs and/or iris nodules; nodules in trabecular meshwork or tent-shaped PAS; vitreous snowballs; peripheral chorioretinal lesions; nodular/segmental periphlebitis; optic disc nodule(s) and/or solitary choroidal nodule; bilaterality. Extraocular granulomas in: lymph nodes, lungs, skin, liver, spleen, salivary glands, heart, bones and nervous system.
Acute posterior multifocal placoid pigment epitheliopathy	Sudden loss of VA, blurred vision and central scotomas. Often self-limiting, good prognosis with visual recovery.
Birdshot chorioretinopathy	Gradual decline in VA due to CME and retinal atrophy, nyctalopia, floaters, glare, dyschromatopsia and photopsia. Cream-colored, irregular or elongated choroidal lesions radiating from optic disc. Supportive: HLA-A29+ and retinal vasculitis.
Serpiginous choroidopathy	Symptoms: VA loss, metamorphopsia or central scotoma. Signs: recurrent gray-yellowish subretinal infiltrates, centrifugally spreading from peripapillary region in a serpiginous manner. They resolve in atrophy. Bilateral, but often asymmetric.
Diffuse unilateral subacute neuroretinitis (DUSN)	Early stage: vitritis, papillitis, clustered yellow-gray-white lesions. Later stage: optic atrophy, arteriolar narrowing, increased ILM reflex (Oréfiçe's sign), subretinal tunnels (Garcia's sign), diffuse RPE degeneration, and afferent pupillary defect. Nematode sometimes visible.
Systemic lupus erythematosus (SLE)	Extraocular SLE characteristics (fever, joint pain, rash, etc), cotton wool spots.
Miscellaneous	
Vitamin A deficiency	Xerophthalmia and nightblindness. Yellow and white retinal spots may be present in the periphery. Symptoms may be reversible with vitamin A treatment.
Paraneoplastic	Photopsias, history of primary tumor; most often breast - or lung carcinoma or melanoma.
Trauma	Patient history, unilateral.

Siderosis bulbi	Patient history, unilateral, inner retinal layers more severely affected than outer layers.
Old retinal detachment	Unilateral, history of retinal detachment.
Pigmented paravenous retinochoroidal atrophy (PPRCA)	Pigment accumulation solely along retinal veins, no or very slow progression, often asymptomatic. Etiology unclear.
Acute zonal occult outer retinopathy	Acute onset, often initially unilateral; however, majority develops bilateral disease, scotoma, photopsias, fundus examination often apparently normal, later RPE disturbances. ERG: delayed implicit time of 30-Hz cone flicker response. EOG: reduction in the light rise.

Tab. 1. Differential diagnoses for non-syndromic retinitis pigmentosa. Abbreviations: CME: cystoid macular edema, ERG: electroretinography, ILM: internal limiting membrane, FAG: fluorescein angiography, KPs: keratic precipitates, PAS: peripheral anterior synechiae, RP: retinitis pigmentosa, RPE: retinal pigment epithelium, VA: visual acuity.

- *Syndromic RP*: the highest number of RP syndromic forms is related to mutations in genes involved in ciliary activities. The most common ciliopathy is Usher syndrome, whose symptomatology is specifically characterized by variable degree of neurosensory hearing loss (Mathur & Yang, 2015). Another well-known syndromic form of RP is Bardet-Biedl syndrome which presents, in addition to retinopathy, renal dysfunction, postaxial polydactyly, obesity, hypogonadism, and/or cognitive impairment (Forsythe, Kenny, Bacchelli, & Beales, 2018). Type and degree of such extra-ocular features are mainly related to the specific gene involved and the specific mutation within that gene. Syndromic RP is also associated with mitochondrial and systemic metabolic disorders. The extra-ocular features in syndromic RP can be extremely hidden (e.g. an impaired sense of smell) or easily detected by the examining clinician (e.g. evaluating cardiovascular and/or renal disease). An important element regards the possibility to surgically correct features, such as polydactyly, at an early stage. When, initially, clinical exams could not detect any extra-ocular anomalies, the unique distinguishing criteria that may help to diagnose syndromic forms of RP is the genetic testing. However, even if extra – ocular impairments are evident, it is necessary to match such abnormalities to involved genes, in order to assess a syndromic disease. Moreover, several genes associated with non - syndromic RP (e.g. USH2A and BBS1) may also determine syndromic RP (Table 2). Concluding, correct diagnosis of

syndromic RP could improve patients' management until save his life, as for patients affected by metabolic disorders like Kearns – Sayre syndrome, a mitochondrial disease frequently associated to cardiac dysfunction (Shemesh & Margolin, 2018).

Gene/locus	RP type	Inher. Pattern	Decade of onset	Visual function	Ophthalmic features	ERG	Syndromic associations	Other IRD phenotypes
<i>ABCA4</i>	19	AR	1	VA is severely affected: FC to NLP at higher age.	Bone spicule-like pigmentation may reach into the macular region. Severe chorioretinal atrophy.	Rod-cone pattern, later both responses NR	-	STGD, CRD (may occur simultaneously in RP families)
<i>AGBL5</i>	75	AR	1-2	VA loss is highly variable. At 40-50 years, VA may range from 20/40 to NLP.	Macular involvement: macular atrophy, CME. PSC.	Rod-cone pattern	Mental retardation (correlation with <i>AGBL5</i> unknown)	-
<i>AHI1</i>	NA	AR	3-4	VA in 3 rd decade can range from 20/32 to HM or even LP.	Macular involvement. PSC.	Rod-cone pattern	JS type 3	-
<i>ARHGEF18</i>	78	AR	3-4	VA: 20/30-20/60 in 4 th decade, but may decrease to CF in the 6 th decade. Photopsias.	Nummular pigment clumping, CME. Vitreous opacities (in 1 patient)	Rod-cone pattern	-	-
<i>ARL2BP</i>	66 ^s	AR	3	Relative early loss of VA: HM (or even LP) in the 4 th decade of life. Yet, other patients may retain a VA of 20/40 up to the 6 th decade of life.	Marked macular atrophy, PSC, ERM.	NR	Situs inversus, primary ciliary dyskinesia (respiratory failure), otitis media	-
<i>ARL6</i>	55	AR	NA	No information on the visual function available.	No information on the retinal phenotype available.	No further information available	BBS type 3	-
<i>BBS1</i>	NA	AR	1-2, (earliest: 1y)	Severe visual loss, may reach LP by 5 th - 6 th decade of life. Severe constriction of VFs up to 5°-10° in the 4 th decade.	Nystagmus, possible macular atrophy, cataract (PSC and cortical).	Generally NR, severely disturbed in rod-cone pattern in 2 nd decade	BBS type 1	-
<i>BBS2</i>	74	AR	1-2	Severe, relative early visual loss: HM or LP before the age 60. VFs are severely constricted.	Macular atrophy, bull's eye maculopathy, PSC, ERM.	NR	BBS type 2	-

<i>BBS9</i>	NA	AR	NA	No further information available.	No information on the retinal phenotype available.	No further information available	BBS type 9	-
<i>BEST1</i>	50	AD AR (1 family)	1-2, (5)	Nightblindness may be absent. Loss of VA is a prominent symptom.	Yellow fundus flecks in the mid-periphery, pigmentation in far periphery, CME, ERM. Macula relatively spared unless serous macular detachments.	NR scotopic responses, residual photopic responses	-	BVMD, AVM D, ARB, ADVI RC
<i>C2orf71</i>	54	AR	1-2 (2 cases <5y)	Night blindness may be absent. Ring scotomas in 4 th -5 th decade of life. Photophobia may occur.	Foveal atrophy. Early onset associated with severe chorioretinal atrophy.	Rod-cone pattern, often NR	Hearing loss, ataxia and cerebellar atrophy (digenic with RP1L1)	-
<i>C8orf37</i>	64	AR	1-2	Severe visual loss to HM/LP in the 4 th decade. The VF is constricted to 5°. Sometimes photophobia.	High myopia, cataract. Marked geographic macular atrophy.	Generally NR	BBS type 21	CRD
<i>CA4</i>	17	AD	2-3	VA levels of 20/200 (age 11) and LP (58 years).	Pigment clumping at the level of the RPE has been described (in 1 patient).	Reduced or NR photopic and scotopic responses	-	-
<i>CDHR1</i>	65	AR	2	VA loss to HM by the 4 th or 5 th decade of life. Severe color vision defects and VF constriction to 5-10°, sometimes with mid-peripheral residue. Photophobia (3 rd decade).	In early stage: sparse bone spicule pigment migration. Later stages: dense pigment migration, macular atrophy.	Generally NR, although ERG may show recordable rod- and cone-driven responses	-	CRD
<i>CERKL</i>	26	AR	2-3 (mean: 23y)	VA generally severely affected and may decrease to LP around the 5 th decade. Photophobia.	Early macular involvement, sometimes with hyperpigmentation. Pericentral localization of bone spicules. Normal appearance of optic disc.	Responses are SR in a rod-cone pattern, may be NR in the 3 rd decade	-	-
<i>CLN3</i>	NA	AR	1-5	VA loss to HM by the 5 th decade reported. Severe constriction of VFs up to 5°-10° in the 6 th decade.	Sparse bone spicule pigmentation, macular atrophy, CME	NR or rod-cone pattern	JNCL	CRD
<i>CLRNI</i>	61	AR	NA	Classic RP phenotype.	Typical RP features.	Rod-cone pattern	USH type 3	-
<i>CNGAI</i>	49	AR	1	A gradual decrease in VA may occur from the 4 th decade onwards. Concentric constriction of the VF during the 3 rd decade of life.	Sometimes macular atrophy. Pericentral RP (described once).	NR	-	-

<i>CNGBI</i>	45	AR	1-2	Macular involvement with VA loss to LP. VF loss from a mean age of 33 years (13- 40). Sometimes photophobia.	Macular atrophy, pericentral RP (described once).	Rod-cone pattern	-	-
<i>CRBI</i>	12	AR	1-5 (median: 4y)	50% of patients have a VA <20/200 at age 35 years.	Nystagmus (±40%), hyperopia, CME (50%), PPRPE, Coats-like vasculopathy, optic disc drusen, retinal vascular sheathing, asteroid hyalosis, thickened retina with loss of the retinal laminations, bull's eye maculopathy and yellow round deposits in the posterior pole. Occasional dense pigmentation.	NR from 2 nd – 3 rd decade	Nanophthalmos	LCA, PPRCA
<i>CWC27</i>	NA	AR	1	VF is severely constricted early in the disease course.	No information on the retinal phenotype available.	No further information available	Brachydactyly, craniofacial abnormalities, short stature, neurologic defects	LCA
<i>DHDDS</i>	59	AR	2-3	VA is generally mildly affected, although in some eyes VA decreases to LP levels.	Occasional CME. Parafoveal atrophy of the RPE. Pericentral localization of pigmentation (reported once).	SR or NR rod- and cone-driven responses from the 2 nd decade.	-	-
<i>EYS</i>	25	AR	2-3 (range 8-62y)	VA loss from the 4 th decade to levels of 20/200 to NLP in the 7 th decade.	Variable levels of bone spicule pigmentation and macular atrophy. PSC.	Rod-cone pattern, but often NR	-	-
<i>FAMI61A</i>	28	AR	2-3	Legally blind in 6 th – 7 th decade. Constriction of to 10°.	Limited number of bone spicules. Macular atrophy. PSC.	NR	Hearing problems, hyposmia	-
<i>FSCN2</i>	30	AD	1	VA and VF relatively spared until the 4 th decade, then VA loss to levels of HM.	Early vessel attenuation. Incidental macular atrophy.	SR at early ages, generally NR from the 4 th decade	-	MD
<i>GNATI</i>	NA	AR	2	Variable VA: 20/20 (80 years) to 20/80 (32 years).	Round pigment clumps and typical bone spicules. ERM.	Rod-cone pattern or NR	-	CSNB
<i>GUCAIB</i>	48	AD	NA	Variable visual function: 20/20 (62 years) – 20/100 (47 years).	Highly variable retinal expression in Japanese patients: normal fundi, sector RP with macular involvement, only macular atrophy or diffuse RP.	NR in patients with diffuse RP. Sector RP with macular atrophy leads to reduced scotopic and photopic responses	-	MD
<i>HGSNAT</i>	73	AR	1-2 5-6	Severe VA loss to CF at age 60 years. VA is more preserved in case	CME, ERM, pericentral RP (described once).	Reduced or NR rod- and cone-driven responses	MPS type IIIC	-

of late disease onset.									
<i>HK1</i>	79	AD, NP ≤15%	1-4 (range 4y-mid- 30s)	Highly variable VA loss. VA loss to CF in 3 rd decade reported. Photophobia.	Bull's eye maculopathy, pericentral RP.	Rod-cone pattern	HMSN, nonspherocytic hemolytic anemia	-	-
<i>IDH3A</i>	NA	AR	1-2 (range 1- 11y)	VA loss dependent on the presence of macular pseudocoloboma.	Macular pseudocoloboma, CME.	SR or NR rod-drive responses, cone- responses SR	-	-	-
<i>IDH3B</i>	46	AR	NA	Classic RP phenotype.	Typical RP features, PSC.	SR amplitudes of both scotopic and photopic responses	-	-	-
<i>IFT140</i>	NA	AR	1-4 (range 2y-early- 30s)	Vision loss from 3 rd - 5 th decade, VA may eventually reduce to LP.	Macular atrophy, CME, ERM, early cataract or white dots. Dense pigmentation in 7 th decade reported.	SR in a rod- cone pattern	SRTD type 9	LCA	-
<i>IFT172</i>	71	AR	1-2	Night blindness is the initial symptom. Further symptoms have not been specified.	Variable macular involvement: macular atrophy, CME, ERM.	No further information available	SRTD type 10, BBS type 20	-	-
<i>IMPDH1</i>	10	AD AR: (Asp226 Asn)	1-3	<i>AD disease:</i> variable degrees of VA loss. Legal blindness before the age of 40 has been described.	<i>AD disease:</i> CME, significant vitreous disturbances, PSC.	<i>AD disease:</i> SR or NR rod and cone responses	-	LCA	-
				<i>AR disease:</i> no information on the visual function available.	<i>AR disease:</i> macular involvement.	<i>AR disease:</i> NR	-	-	
<i>IMPG2</i>	56	AR	1-2	Central vision generally affected.	Macular atrophy and bull's eye maculopathy. Sheathing of peripheral vessels.	SR in a rod- cone pattern or NR	-	VMD	-
<i>KIZ</i>	69	AR	2	Classic RP phenotype.	Macular thinning (in 1 patient).	NR at the age of 35 years	Obesity, hearing problems (correlation with <i>KIZ</i> unknown)	-	-
<i>KLHL7</i>	42	AD	3	VA remains (near) normal up to the 5 th or 6 th decade. VF loss usually is the initial symptom.	Fundus appearance can be normal up to the 4 th decade. Later: CME and parafoveal atrophy.	Rod-cone pattern, eventually NR. The mean (SD) decline in light- adapted 31- Hz flicker response is 3.0% (3.0) per year.	CISS	-	-

<i>LRAT</i>	NA	AR	1 (earliest: 2y)	Severe, early VA loss to 20/100-20/200 and VF constriction to 30°-60° before the age of 10 years. Photophobia.	High hyperopia, nystagmus, poorly reactive pupils. Sparse or absent bone spicules (age 9 years). RPA. Reduced FAF signal.	SR in a rod-cone pattern or NR	-	LCA
<i>MAK</i>	62	AR	2-5	May show initial preservation of nasal VF.	Macula generally not involved, but sometimes CME (in 1 patient) or macular atrophy.	Reduced in a rod-cone pattern, but often NR	-	-
<i>MERTK</i>	38	AR	1-2 (earliest: 3y)	VA loss to $\leq 20/200$ in the 2 nd decade. Variable VF loss: normal VF (3 rd decade) – 5° (2 nd decade). Legal blindness: ± 40 years. Impaired color discrimination.	Nystagmus, bull's eye maculopathy, macular atrophy. Pallor of the optic disc may be absent.	Photopic responses become NR during the 1 st decade. Scotopic responses are NR	-	LCA
<i>MVK</i>	NA	AR	3	VF loss may be the initial symptom.	Arterial tortuosity, PSC, ERM, thickening of the nerve fiber layer on OCT, CME (described once).	SR in a rod-cone pattern	MKD (MEVA or HIDS)	-
<i>NEK2</i>	67	AR	NA	No information on the visual function available.	No information on the retinal phenotype available.	No further information available	-	-
<i>NR2E3</i>	37	AD, AR	1-3 (earliest: 3y)	<i>AD disease:</i> VF loss from the 2 nd -3 rd decade.	<i>AD disease:</i> nummular and spicular pigmentation. Early-onset cataract. FAF: 2 or 3 hyperfluorescent rings may be visible. Pericentral RP.	<i>AD disease:</i> rod-cone pattern. Rod responses are SR, and become NR in advanced disease. Cone-driven responses are affected late.	-	ESCS
				<i>AR disease:</i> early VA loss.	<i>AR disease:</i> clumped pigment	<i>AR disease:</i> rod-cone pattern		
<i>NRL</i>	27	AD, AR	1 (earliest: 1y)	<i>AD disease:</i> VA loss from the 4 th decade: 20/20 – 20/00. VF diameters: 50-60° in the 3 rd decade and decrease up to 10° in the 8 th decade.	<i>AD disease:</i> nystagmus, minimal or absent hyperpigmentation in 2 nd decade. Round pigment clumps. Chorioretinal atrophy, macular atrophy, bull's eye maculopathy, PSC. Peripheral retinal telangiectasis (which may cause serous retinal detachment).	NR	-	-
				<i>AR disease:</i> visual function is more severely affected compared to AD disease.	<i>AR disease:</i> peripheral pigment clumps. Retinal features are similar to NR2E3- associated enhanced S-cone syndrome.			
<i>OFD1</i>	23	XL	1 (<2y)	Early loss of central vision. Only temporal and inferior VF residues.	Grayish spots at the level of the RPE. Granularity of macular RPE.	NR	JS, OFDS type 1, SGBS type 2	-

<i>PANK2</i>	NA	AR	5	VA reduction to HM in the 6 th decade.	No information on the retinal phenotype available.	No further information available	HARP syndrome, NBIA1 (also termed HSS)	-
<i>PDE6A</i>	43	AR	1	Marked peripheral VF loss.	CME, PSC and dense pigmentation.	Rod-cone pattern	-	-
<i>PDE6B</i>	40	AR	1	Loss of peripheral VF is a prominent symptom that occurs during the 2 nd -3 rd decade.	CME, PSC, dense pigmentation at high age (80 years), pericentral RP.	Rod-cone pattern <i>Carriers:</i> rod-driven responses may be reduced	-	CSNB
<i>PDE6G</i>	57	AR	1	Marked constriction of the VF up to 5-10°.	Normal vessels and optic discs in young patients. CME in all patients (1 family).	Both rod- and cone-driven responses are NR within the 1 st decade of life.	-	-
<i>POMGNT1</i>	76	AR	1-2 (3-4)	Variable VA loss, may decrease to LP. VF constriction to 5° in the 6 th -7 th decade.	Macular involvement, CME.	NR	MEB	-
<i>PRCD</i>	36	AR	1-3	Relative early visual loss.	Various macular involvement: bull's eye maculopathy, macular atrophy, CME, ERM, PSC. Fairly normal-colored optic disc.	Scototically and phototically NR in an early stage of disease (earliest described: age 6 years)	-	-
<i>PROM1</i>	41	AR	1	Visual loss during the 1 st decade.	Large inter- and intrafamilial variability: from isolated (bull's eye) maculopathy to pericentral RP and severe RCD. Nystagmus.	NR	Polydactyly	CRD, AD MD
<i>PRPF3</i>	18	AD, full penetrance	1 (4, once)	Classic RP phenotype.	Classic RP phenotype.	Rod-cone pattern Rod-driven responses are abolished from the 2 nd decade, cone-driven responses are SR by then	-	-
<i>PRPF4</i>	70	AD	2-3	Variable visual loss, may reach HM. VF constriction to 5-10° in the 6 th decade.	Variable degree of macular atrophy.	Generally NR	-	-

<i>PRPF6</i>	60	AD	2-4	VA initially spared, but may decrease to LP. Constriction of VFs to 30-40° (4 th decade) and ±10° (6 th decade).	Macular atrophy in later stages. Optic nerve heads may initially be normal. PSC.	SR responses in the earlier phases of the disease. Scotopic responses become NR over time, photopic responses tend to diminish more slowly.	-	-
<i>PRPF8</i>	13	AD	1-2	VA may remain normal up to the 3 rd – 4 th decade, with progression to 20/200 in the 7 th decade. VF constriction to ±10° in 4 th decade.	Dense intraretinal pigment migration (in 1 patient).	NR	-	-
<i>PRPF31</i>	11	AD NP ≤10%	1-2	Variable presentation. Incomplete penetrance suggested in asymptomatic patients. Mean annual VF loss: 6.9%. Legal blindness: 4 th decade.	Macular atrophy, CME, PSC. May present with para-arteriolar absence of pigmentation or pericentral RP (described once). No abnormalities observed in patients that lack penetrance.	The mean (SD) decline in light-adapted 30-Hz flicker response is 9.2% per year. Responses may be normal in patients that lack penetrance	-	-
<i>PRPH2 (formerly known as RDS)</i>	7	AD digenic with ROM1	2-6	VA usually spared, but dependent on the degree of macular involvement.	Variable macular involvement, CME, RPA, pericentral RP (described once).	Rod-cone pattern, will become NR during 6 th decade	-	MD, PD, CRD, LCA
<i>RBP3</i>	66 ^s	AR	<i>Early onset: 1</i>	<i>Early-onset disease: early visual loss. Strabismus.</i>	<i>Early-onset disease: (high) myopia, PSC.</i>	<i>Early-onset disease: SR responses, most often in a rod-cone pattern, although cone-rod patterns also occur.</i>	-	-
			<i>Late-onset: 4-6</i>	<i>Late-onset disease: blurred vision is an early symptom; night blindness may be absent.</i>	<i>Late-onset disease: PSC, (high) myopia.</i>	<i>Late-onset disease: SR rod- and cone-driven responses, often NR</i>		
<i>RDH12</i>	53	AD, AR	<i>AD disease: 2-5</i>	<i>AD disease: classic RP phenotype.</i>	<i>AD disease: typical RP features.</i>	<i>AD disease: no further information available</i>	-	LCA

				<i>AR disease:</i> VA at presentation: 20/40- 20/200, may reach HM-LP. VF constriction to <5° in the 2 nd – 3 rd decade. Central scotoma may occur. Photophobia.	<i>AR disease:</i> nystagmus, macular atrophy, dense intraretinal pigment migration with para-arteriolar sparing. Hyperpigmentation may reach into the macular region. Preservation of peripapillary RPE. CME, PSC.	<i>AR disease:</i> NR or SR in both scotopic and photopic conditions.		
<i>REEP6</i>	77	AR	1-2	Gradual VA loss, although a decline to 20/400 at the age of 32 has been described.	CME, PSC, vascular sheathing.	SR in a rod-cone pattern or NR	Anosmia	-
<i>RGR</i>	44	AR	NA	VA loss to ≤20/200. Severe VF constriction.	Macular atrophy in patients with severely affected VA.	Responses are reduced in a rod-cone pattern	-	-
<i>RHO</i>	4	AD, AR	1-2, (4)	Highly variable clinical course (also intrafamilial). Annual VA decline: 1.6%. Annual VF loss: 2.6%. Legal blindness: 6 th – 8 th decade.	Sector RP, and to a lesser extent pericentral RP. CME. Late-onset chorioretinal atrophy in patients with p.Met207Lys mutation.	Rod-cone pattern. Mean annual decline: 7.7 - 8.7%.	-	CSNB
<i>RLBP1</i>	NA	AR	2	Variable VF loss from the 3 rd decade, to <5° residues.	Minimal or absent bone spicules, RPA.	Rod-cone pattern	-	BRD, NFRC D, FA
<i>ROM1</i>	NA	Digenic (<i>ROM1</i> : Leu185Pro + <i>PRPH2</i>)	NA	No information on the visual function available.	No information on the retinal phenotype available.	SR scotopic and photopic responses	-	-
<i>RP1</i>	1	AD, AR	<i>AD disease:</i> 2-3	<i>AD disease:</i> moderate decrease in VA in 4-5 th decade.	<i>AD disease:</i> PSC. RP sine pigmento (described once).	Rod-cone pattern	-	-
			<i>AR disease:</i> 1	<i>AR disease:</i> relative early loss of VA to CF or HM in the 5 th decade. VF constriction to 10° in the 3 rd decade.	<i>AR disease:</i> macular atrophy, CME, myopia.			
<i>RP1L1</i>	NA	AR	4-5	Moderate decrease in VA to ±20/80. VF constriction to 5° in the 8 th decade.	Typical RP features.	NA	Hearing loss, ataxia, cerebellar atrophy (digenic with C2orf71)	OMD
<i>RP2</i>	2	XL	1	Early loss of central vision. Central scotoma in 50% of patients. Severe VF constriction in 2 nd decade. Large	Myopia. Bull's eye maculopathy, macular atrophy, sometimes choroideremia-like degeneration. A tapetal-like reflex (reported once).	Rod-cone pattern	-	-

				intrafamilial differences.					
				<i>Female carriers:</i> can be affected as well. Presentation highly variable.					
<i>RP9</i>	9	AD NP	1-2	Highly variable presentation. Incomplete penetrance suggested in asymptomatic patients. Relative early VF constriction: <20° in 3 rd decade.	PSC, CME, macular atrophy. Early stage: regional (or 'patchy') loss of rod and cone function.	Highly variable, varying from normal to NR responses.	-	-	
<i>RPE65</i>	20	AD (NP described), AR	<i>AD disease:</i> 2-5	<i>AD disease:</i> incomplete penetrance suggested in asymptomatic patients. Early loss of central vision.	<i>AD disease:</i> (sparse) nummular and spicular pigmentation. Extensive chorioretinal atrophy, macular atrophy. PSC.	Scotopic responses are generally NR, residual photopic responses may be present, but often NR.	-	LCA	
			<i>AR disease:</i> 1	<i>AR disease:</i> severely, relative early visual loss: CF or HM in the 1 st decade. Photophobia is generally absent.	<i>AR disease:</i> nystagmus, macular atrophy. Bone spicule pigmentation is often sparse. Lack of FAF.				
<i>RPGR</i>	3	XL	1-2	Early loss of central vision. Annual VF loss: 4.7-9%. Mean age legally blind: 45 years.	Variable macular involvement: from no abnormalities to atrophic lesions. Coats-like vasculopathy (1 patient). OCT: Ellipsoid zone width constriction ±175 µm/year; ONL thinning ±2,50 µm/year.	Rod-cone pattern, but often NR. Annual decline in cone ERG amplitude: 7.1%	Hearing loss, respiratory infections	CRD, CD, MD	
				<i>Females carriers:</i> can be affected as well. Presentation highly variable.	<i>Female carriers:</i> tapetal-like reflex possible.				
<i>RPGRIP1</i>	NA	AR	1-2	Relative early VA loss to levels of 20/200- CF in 3 rd decade.	Nystagmus, macular atrophy, pigmentary changes may be sparse or absent.	NR	-	LCA, CRD	
<i>SAG</i>	47	AD, AR	2	<i>AD disease:</i> VF constriction to 10°.	<i>AD disease:</i> typical RP features, hyperreflective foci on OCT.	Rod-cone pattern	-	Oguchi disease, (can occur simultaneously within families)	
				<i>AR disease:</i> VA loss may precede NB.	<i>AR disease:</i> macular atrophy, CME Golden-yellow fundus reflex with Mizuo- Nakamura phenomenon.				

<i>SAMD11</i>	NA	AR	3-4	Loss of VA from the 6 th decade, may eventually reach HM. VF constriction to <10°. Incidental photophobia.	Foveal atrophy, ERM, PSC. Incidental: CME, corneal guttata.	NR	-	-
<i>SEMA4A</i>	35	AD	NA	No information on the visual function available.	No information on the retinal phenotype available.	No further information available	-	CRD
<i>SLC7A14</i>	68	AR	1-2	Visual loss, may reach HM in the 4 th decade.	Extensive chorioretinal atrophy, including macular atrophy.	NR	-	-
<i>SNRNP200</i>	33	AD, NP described	1-4 (mainly 2)	Variable progression. Generally slow VA loss to HM in the 8 th decade. VF constriction to 10°.	Macular atrophy, CME. May present with heavy pigment clumping. PSC (patients >45 years).	SR or NR	-	-
<i>SPATA7</i>	NA	AR	1	Considerable VA loss in case of macular involvement. Severe VF constriction.	Nystagmus, maculopathy, PSC.	NR, although a cone-rod pattern has been described in early disease	LCA with fertility- or auditory dysfunction	LCA
<i>TOPORS</i>	31	AD	2-5	VA is maintained in most patients. Constriction of VF to 10°.	Pericentral RPE atrophy in young patients, which progresses to a diffuse pigmentary retinopathy with choroidal sclerosis.	Rod-cone pattern	-	-
<i>TTC8</i>	51	AR	1-2	NB and photophobia are early symptoms. Early VA loss to 20/200.	May include macular atrophy, sparse bone spicule pigmentation.	NR	BBS type 8	-
<i>TULP1</i>	14	AR	1 (onset <5y possible)	Rapid progression. VA: 20/200 at age 20, may decrease to HM or even LP. VF loss to 10°.	Nystagmus, hyperopia, PSC, macular atrophy; yellow perifoveal annular ring, pericentral RP (described once).	Scotopic and photopic responses are SR or NR	-	LCA
<i>USH2A</i>	39	AR	3 (mean: 25y)	VA relatively intact to 3 rd to 4 th decade, then annual VA decline: 2.6%. Annual loss V4e VF area: 7.0% Legal blindness (based on VA): 6 th - 7 th decade.	CME can be observed. FAF: distinctive pattern of diffuse and homogeneous peripheral hypoautofluorescence. RP sine pigmento (reported once), pericentral RP.	Photopic responses are SR early in disease course, and become NR as the disease progresses. Mean annual decline in amplitude to 30 Hz flashes is 13.2%.	USH type 2A	-
<i>ZNF408</i>	72	AR	2-4	VA generally remains ≥20/40 in the 5 th decade VF constriction to 10° at age 50 years.	High myopia. Vitreous condensations, PSC, ERM, CME (in 1 patient).	SR in a rod-cone pattern or NR	-	FEVR

				Photophobia is common.					
<i>ZNF513</i>	58	AR	1	Visual loss to 20/200 - LP.	Macular atrophy in all patients, sometimes with hyperpigmentation.	Loss of both rod- and cone-driven responses.	-	-	
<i>NEURODI</i>	NA	AR	2	VA loss from the 3 rd decade.	PSC has been reported.	Reduced or NR rod and cone responses	MODY/late-onset diabetes, neurological abnormalities	-	
Loci									
RP6 locus	6	XL	1-2 (generally <13)		<i>Female carriers:</i> tapetal-like reflex.	Reduced scotopic and photopic responses	CGD, McLeod phenotype, mental retardation	-	
RP17 locus	17*	AD	NA	VA in 3 rd decade can range from 20/20 to 20/200. Variable VF constriction: from pericentral scotoma to 10° residue.	Atrophic patches, pigment dispersion, granular aspect of the RPE.	MR scotopic and photopic responses.	-	-	
RP22 locus	22	AR	1	Rapidly progressive decline in VA, leading to severe visual impairment at the age of 40.	Absence of pigmentation has been described.	NR. <i>Female carriers:</i> rod-driven responses may be reduced	Obesity, mental retardation, hypogonadism, hexadactyly.	-	
RP24 locus	24	XL	1	Peripheral VF loss in 4 th decade. <i>Female carriers:</i> asymptomatic, although perimetry reveals sensitivity losses.	Typical RP features.	SR or NR rod-driven responses in 2 nd decade. Cone-driven responses: initially normal, average annual decline: 0.1 log unit during 1 st and 2 nd decade.	-	-	
RP29 locus	29	AR	2-3	Onset VA loss: 3 rd decade. VA may decrease to NLP in 5 th decade.	Anterior and posterior polar cataracts, vitreous cells, obliteration of peripheral blood vessels.	No further information available	-	-	
RP32 locus	32	AR	1	Severely, relatively early visual loss: HM in 3 rd decade to LP or worse in 4 th -5 th decade.	Generalized grayish carpet-like retinal degeneration. Bull's eye maculopathy, macular atrophy.	SR responses in 1 st -2 nd decade, later NR.	-	-	
RP34 locus	34	XL	2	Nyctalopia is the initial symptom, despite a cone-rod pattern on ERG. Early impaired color vision.	Typical RP features.	Cone-rod pattern	-	-	
RP63 locus	63	AD	2-5	Blurred vision is an early symptom. Yet,	Macular atrophy in some patients.	Both rod- and cone-driven	-	-	

VA generally is normal or near normal.	responses are generally only MR
--	---------------------------------

Tab. 2. Genetic subtypes and specific characteristics of non-syndromic RP. Abbreviations: AD: autosomal dominant, ADVIRC: autosomal dominant vitreoretinopathopathy, ARB: autosomal recessive bestrophinopathy, AVMD: adult onset vitelliform macular dystrophy, AR: autosomal recessive, BBS: Bardet-Biedl syndrome, BRD: Bothnia retinal dystrophy, BVMD: Best vitelliform macular dystrophy, CACD: central areolar choroidal dystrophy, CD: cone dystrophy, CGD: Chronic granulomatous disease, CISS: Cold-induced sweating syndrome, CF: counting fingers, CRD: cone-rod dystrophy, CSNB: congenital stationary night blindness, DG: digenic, ERM: epiretinal membrane, ESCS: enhanced S-cone syndrome, FA: fundus albipunctatus, FAF: fundus autofluorescence, HARP: hypoprebetalipoproteinemia, acanthocytosis, RP and pallidal degeneration, HIDS: hyper-immunoglobulin D and periodic fever syndrome, HM: hand movements, HMSN: hereditary motor and sensory neuropathy, HSS: Hallervorden-Spatz syndrome, IP: inheritance pattern, IRD: inherited retinal dystrophy, JNCL: juvenile neuronal ceroid-lipofuscinoses, JS: Joubert syndrome, LCA: Leber congenital amaurosis, LP: light perception, MD: macular dystrophy, MEB: muscle-eye-brain disease, MEVA: mevalonic aciduria, MODY: maturity-onset diabetes of the young, MPS: mucopolysaccharidosis, MR: moderately reduced, MRCS: microcornea, rod-cone dystrophy, cataract, posterior staphyloma, MVK: mevalonate kinase deficiency, NA: not available, NB: night blindness, NBIA1: neurodegeneration with brain iron accumulation 1, NFRCD: Newfoundland rod-cone dystrophy, NLP: no light perception, NP: non-penetrance, NR: nonrecordable, OCT: optical coherence tomography, OFDS: orofaciocigital syndrome, OMD: occult macular dystrophy, PD: pattern dystrophy, PPRPE: preserved para-arteriolar retinal pigment epithelium, PSC: posterior subcapsular cataracts, RPA: retinitis punctata albescens, RPE: retinal pigment epithelium, SGBS: Simpson-Golabi-Behmel syndrome, SIFD: sideroblastic anemia, B-cell immunodeficiency, recurrent fevers and developmental delay, SR: severely reduced, SRTD: Short-rib thoracic dysplasia, STGD: Stargardt disease, USH: Usher syndrome, VA: visual acuity, VF: visual field, VMD: vitelliform macular dystrophy. Table was been reworded from (Verbakel et al., 2018).

2.7. CLINICAL ASPECTS OF RP GENETIC SUBTYPES

Previously we described commonly features attributed to RP. Nevertheless, the heterogeneous manifestations of these symptoms imply to better analyze the clinical findings specific for each genetic subtype of RP. Initial studies were based on non-genotyped RP cohorts and seldom subdivided the patients according to their inheritance pattern. Recently the applied approach changed but, even if phenotypes for a specific causative genes are described, the limited numbers of patients and/or a lack of clinical details represent a serious challenge to face. Tables 2 and Fig. 4, show a comprehensive overview of the specific clinical features attributed to various subtypes. However, it has to remember that a specific subtype could show noticeable phenotypic variation due to the variable effects of mutations, genetic modifiers and environmental factors.

- *Nomenclature*: frequently RP subtypes nomenclature is not very clear, so it results fundamental considering its origins. Initially, subtypes were named with

numbers related to the order in which the RP-linked loci were discovered (e.g. the *RPI* locus at chromosome 1 was the first discovered). Nevertheless, the order followed by various RP-associated identified genes diverges from this locus-based numbering system. The classic example is represented by rhodopsin gene (*RHO*), the first RP-associated gene identified, whose mutation - related RP subtype is actually called RP4, as the *RHO* locus was the fourth to be identified. Over the years, new ways to categorize RP subtypes have been proposed, and several of them, such as RP8, RP15 and RP21, were deprecated. Nowadays, the most accepted RP classification follows the underlying gene (or locus if the causative gene has not yet been identified), criterion which is less subject to change, more informative, and frequently provides a direct link to the related mechanism, as well as possible therapeutic options.

- Age of onset: the RP age of onset shows a great range of variation. LCA and early forms of RP, sharing many causative genes, generally occur before the fifth year of life. Among late – onset forms, instead, *HGSNAT*-, *CRX*- and *RBP3*-linked RP represent the most diffused. It is important to remember that patients developing symptomatology at a later stage, the possibility of a pseudoretinitis must be taken into account.
- Refractive errors: hyperopia and myopia show a high prevalence in RP patients rather than general population (Hendriks et al., 2017). LCA affected patients commonly present hyperopia, especially in forms caused by mutation in *RPGRIP1*, *GUCY2D*, *CEP290* or *CRX* genes (Hanein et al., 2006). Moreover, hyperopia is very diffused among RP patients carrying mutations in *LRAT* (Y. Chen et al., 2018), *CRBI* (K. N. Khan et al., 2018) or *NR2E3* (Mahajan & Votruba, 2017) genes. Myopia, instead, is linked to two X-linked (*RPGR* and *RP2*) and three autosomal recessive (*RBP3*, *RP1* and *ZNF408*) RP genetic subtypes, as well as to Usher syndrome (Habibi, Chebil, Kort, Schorderet, & El Matri, 2017).

- Pigmentary anomalies:
 - ◇ Peripheral retinal pigmentation: in addition to the already cited bone spicule pigmentation, arising from the retinal mid-periphery and prevalently diffused through the perivascular area, other localizations and/or shapes have also been described. BEST1- associated RP present pigments generally localized in the outermost periphery of the retina (Dalvin et al., 2016). Round clump – shape pigment deposits typically characterize patients with RP caused by mutations in *GNATI* (Carrigan et al., 2016), *ARHGEF18* (Arno et al., 2017), *NRL* (M. Gao et al., 2016) or *NR2E3* (Escher et al., 2012) genes. Para-arteriolar absence of pigmentation, instead, is specific of RP patients carrying mutations in *RDH12* (Zou et al., 2018), *CRB1* (Talib et al., 2017) or *PRPF31*.
 - ◇ Retinal hyperpigmentation loss: several RP subtypes, named RP sine pigmento, could reveal an absence or deficiency of characteristic hyperpigmentation, even if such situation may also be linked to unavailability during the early stages of RP (North, Gelman, & Tsang, 2014). Pigmentation lack was reported in RP patients over 20 years of age and carrying variants in *RPGRIP1* (A. O. Khan, Abu-Safieh, Eisenberger, Bolz, & Alkuraya, 2013), *RLBP1* (Burstedt et al., 2013), *USH2A* (Xu et al., 2011) and *RPI* (Ma et al., 2013) genes. Several hypotheses were proposed to clarify the etiology of this phenomenon, and the most probable is related to myopic degeneration observed in some RP patients (Bandah-Rozenfeld et al., 2010). Slightest pigmentary variations have also been linked to mutations in the BBS genes, but this is mostly related to syndromic cases (Priya, Nampoothiri, Sen, & Sripriya, 2016). Therefore, even if an absence of pigmentation could be related to other disorders, it could not be used as a criterion to exclude a diagnosis of RP, especially in young patients.
 - ◇ Macular pigmentary abnormalities: particular RP subtypes, highlighting early atrophy and early central RPE alterations, implies a fast decrease of visual acuity (Flynn, Cukras, & Jeffrey, 2018) and result very difficult to distinguish from a cone-rod dystrophy. Patients carrying mutations in *IDH3A* (Pierrache et al., 2017) or *DHX38* (Ajmal et al., 2014) show a

macular atrophy frequently referred to as macular pseudocoloboma, in order to discriminate it from “true” coloboma, caused by a closure defect in the embryonic fissure during developmental stages. Alternatively, deposits of macular pigments, ranging from the periphery to the macular region, have been reported in early-onset RP subtypes as biological consequence of mutations in *RDH12* and *ABCA4* genes (Schuster et al., 2007). Additionally, in other subtypes, the macula generally does not show pigment clumping.

- *Cystoid macular edema*: CME is largely diffused among RP patients, regardless of age (Gorovoy et al., 2013) and of subtype, but with high prevalence in autosomal dominant form of RP (Liew, Moore, Webster, & Michaelides, 2015). Children carrying mutations in *RPI* or *CRBI* genes, as well as young adults with variants in *USH2A* and *PRPF31*, manifested a combination of CME and cells in the vitreous body (Murro et al., 2017). Such mixed clinical aspects can lead to an incorrect diagnosis of intermediate uveitis, especially in RP affected children with hidden or absent retinal abnormalities (Verhagen et al., 2016).
- *Vascular abnormalities*: coats-like exudative retinopathy, identified by lipid deposits, exudative retinal detachment and retinal telangiectasia, has been documented in about 11% of patients carrying variants in *CRBI* (Mathijssen et al., 2017) and in a single patient with a mutation in *RPGR* gene (Demirci, Rigatti, Mah, & Gorin, 2006). The Coats-like phenotype in RP patients is commonly bilateral, while the real Coats' disease is generally unilateral (Chebil & El Matri, 2016). Nevertheless, several affected siblings do not exhibit Coats-like phenotype, suggesting the involvement of non - genetic factors (den Hollander et al., 2001). Finally, a vascular covering has been documented in various patients with mutations in *IMPG2* (van Huet et al., 2014), *CRBI* (van den Born et al., 1994) or *REEP6* genes.

- Localized forms of RP:
 - ◇ Sector RP: even if RP is considered a widespread photoreceptor dystrophy, several patients show only localized retinal abnormalities, as ones limited to the inferonasal quadrant of both eyes. This atypical RP form is defined as sector RP and is characterized by symmetrical areas of regional pigmentary alterations, general limited to the inferior quadrants of the retina (Van Woerkom & Ferrucci, 2005). Frequently, visual field impairments often match the boundaries of these retinal pigmentary abnormalities, even if the variations visible on fluorescein angiography and ERG can continue over the affected areas observed with ophthalmoscopy (Abraham, Ivry, & Tsvieli, 1976). Sector RP generally evidences a slow course, but can progress to a panretinal RP phenotype (Ramon et al., 2014). Sector RP was analyzed in autosomal dominant RP forms caused by variants in *GUCA1B* and *RHO* genes (Napier et al., 2015), as well as in *RPGR*-associated X-linked forms (Charng et al., 2016). However, the real reason why the atrophic pigmentary variations are initially regionalized, even if underlying molecular abnormalities are most probable expressed ubiquitously in the retina, is not yet totally clear. One hypothesis refers to sectorialized differences in the retina's exposure to light, as described in RP patients carrying mutations in *RHO* gene (Ramon et al., 2014).
 - ◇ Pericentral pigmentary retinopathy: an interesting group of RP genes have been linked to pigmentary abnormalities and annular chorioretinal atrophy that range temporal from the optic disc along to the vascular arcade, tending to spare the far periphery (Ramon et al., 2014). The clinical aspects documented in this pericentral pigmentary retinopathy (PPR) differ widely among patients, including both stationary and slow progression forms of the disease (Matsui et al., 2015). PPR represent a relevant feature of the RP phenotype, especially in patients with a history of night blindness, progressive disease, annular scotoma and decreased rod activity. PPR looks like pigmented paravenous retinochoroidal atrophy (PPRCA) and postinflammatory variations in retinal pigmentation.

- *Retinitis punctata albescens*: different patients affected by RP can show white punctate deposits widely spread throughout the retina and frequently reduced in number before the onset of atrophy. Such clinical phenotype has been depicted as a distinct form of retinal dystrophy called retinitis punctata albescens, but today is better included in non-syndromic RP subtypes. Retinitis punctata albescens etiology is related to *PRPH2* (Shastry & Trese, 1997), *RHO* (Souied et al., 1996), *RLBP1* (Bagheri et al., 2017) and *LRAT* (Littink et al., 2012) mutations. Moreover, *RLBP1* variants have also been identified as causative of Newfoundland rod-cone and Bothnia retinal dystrophies, two particular RP subtypes presenting the same white punctate deposits characteristic of retinitis punctata albescens (Hipp et al., 2015). The previous cited white deposits are probably originated from accumulation of all-trans-retinyl esters in the RPE (K. A. Lee, Nawrot, Garwin, Saari, & Hurley, 2010), even if such chemical compounds result absent in LRAT subtype (Dessalces et al., 2013).
- *Miscellaneous*: one of the most common histological observation in RP patients is represented by optic disc drusen, particularly in CRB1 subtypes (Talib et al., 2017). Another particular finding, reported in female carriers of RPGR – associated and X – linked RP2 (Flaxel et al., 1999), is a tapetal-like fundus reflex with a yellow-golden appearance. Such reflex, on one hand similar to the Mizuo-Nakamura phenomenon of Oguchi disease, but on the other different because it does not disappear after dark adaption, is best visualized using near-infrared or red-free reflectance (Acton et al., 2013). Furthermore, several FAF features other than the well-detected hyperautofluorescent ring, have been reported in specific genetic RP subtypes. Among them, variants in visual cycle involved genes *LRAT* and *RPE65* can reduce or delete signal on FAF imaging (Arno et al., 2016), while mutations in *NR2E3* could be related to the presence of 2 or 3 hyperautofluorescent rings (Escher et al., 2012).

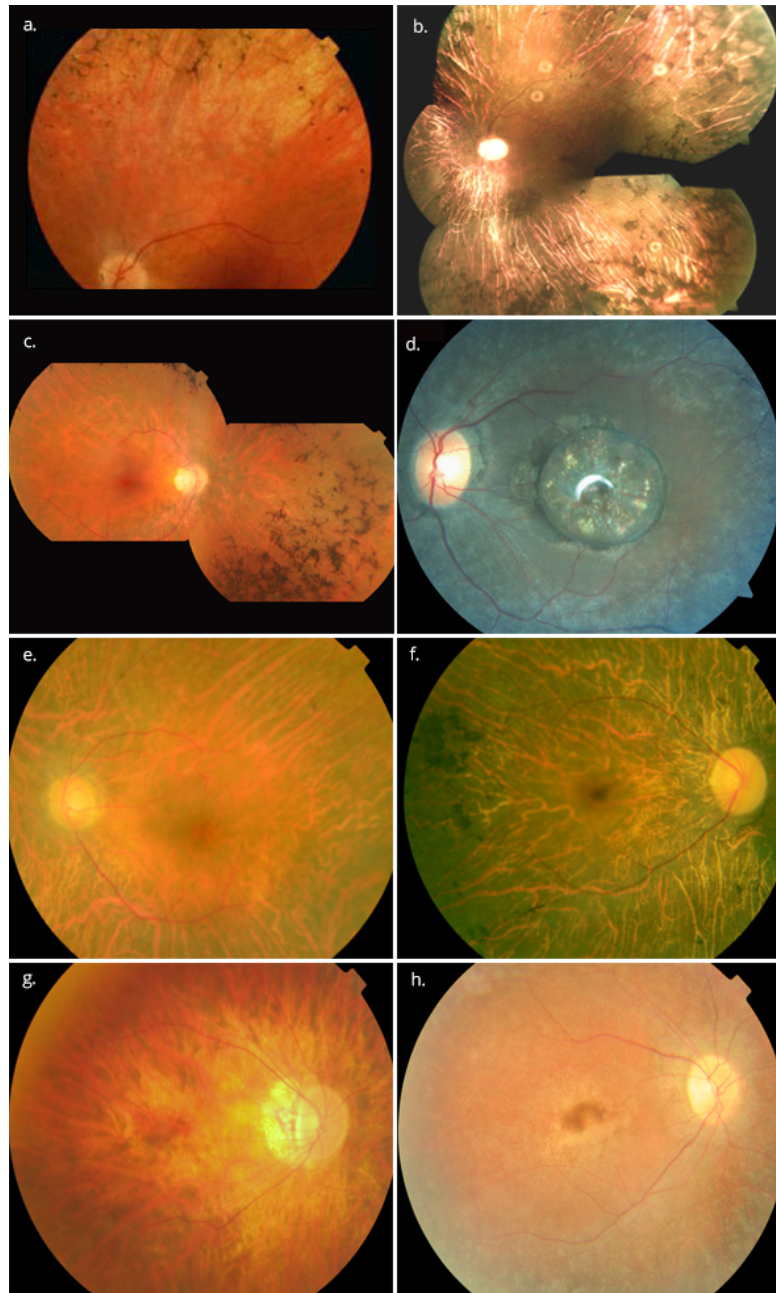
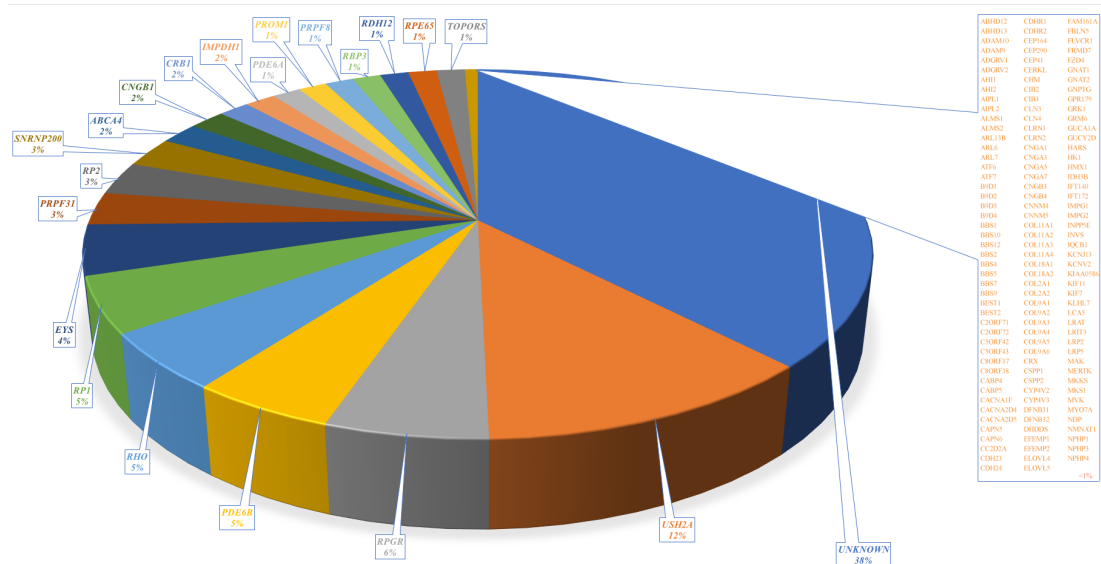


Fig. 4. Fundus photographs of patients with various non-syndromic RP subtypes. a. Fundus photograph of a 48-year old female with *ABCA4* – associated RP, showing peripheral bone spicule pigmentations, mild attenuation of vessels, and mid-peripheral atrophy. Reprinted from Klevering et al., 2004. b. Composite fundus photograph of a 50-year old male with *C2orf71* – associated RP, showing peripheral bone spicule pigmentation, attenuation of retinal vessels, severe retinal atrophy, and pallor of the optic disc. 4 round reflection artefacts. Reprinted from Collin et al., 2010. c. Composite fundus photographs of a 49-year old female with *CNGA1* – associated RP, showing mid-peripheral bone spicule pigmentation, attenuated vessels and parapapillary atrophy. Reprinted from Verbakel et al., 2018. d. Fundus photograph of a 26-year old female with *IDH3A* – associated RP, showing bone spicule pigmentary changes, and macular pigmentation with severe pseudocoloboma-like atrophy. Reprinted from Pierrache et al., 2017. e. Fundus photograph of a 59-year old female with *RHO* – associated autosomal dominant RP, showing attenuated vessels and severe RPE atrophy. Reprinted from Verbakel et al., 2018. f. Fundus photograph of a 56-year old female with *RP1* – associated RP, showing profound RPE atrophy, temporal pigment clumping, attenuated vessels, and a pale optic disc. Reprinted from Verbakel et al., 2018. g. Fundus photograph of a 29-year old male with *RP2* – associated RP, showing severely attenuated retinal vessels, and extensive RPE atrophy. Reprinted from Verbakel et al., 2018. h. Fundus photograph of a 13-year old female with *RPE65* – associated autosomal recessive RP, showing attenuated retinal vessels, optic disc pallor, and relative absence of retinal hyperpigmentation. Reprinted from Verbakel et al., 2018.

2.8. RP – ASSOCIATED GENES AND PROTEINS

Nowadays, about 163 genes (Fig. 5) have been related to syndromic and non-syndromic RP. Each protein encoded by these genes is directly involved in many essential processes within the RPE and/or neuroretina, such as the phototransduction cascade, or an underlying structure, as the connecting cilium. For that reason, mutations in a single gene within a specific sub-pathway could be sufficient to impair irreparably the whole pathway. Generally, genetic variants which alter a pathway's activity can expand phenotype or genetic heterogeneity of pathologies involving a common pathway, even if RP subtypes caused by mutations in genes associated with a shared pathway exhibit a specific degree of clinical overlap. Therefore, identifying the biochemical pathways involving in non-syndromic RP is fundamental to clarify the underlying etiopathogenesis. Now the RP most well – associated pathways (phototransduction cascade, visual cycle, ciliary transport and interphotoreceptor matrix) are going to be described, while new discovered ones will be discussed in experimental section.



2.8.1. *The phototransduction pathway*

Phototransduction consists of consecutive reactions starting from the excitation of the opsin molecule by a photon, transduced in an electrical signal then transmitted via the optic nerve to the visual cortex, permitting the perception of an image (Fig. 6). Cascade composition is almost the same in rods and cones, with little differences due to their different functions in dim light versus bright light. Rod outer segment shows a lipid bilayer membrane arranged as flattened “discs” (optical discs), which is strictly packed with the photopigment rhodopsin. Rhodopsin (encoded by *RHO*) is a member of the superfamily of seven-helix, G-protein–coupled receptor proteins (GPCRs). Differently from chemosensing GPCRs, rhodopsin presents its ligand, the light-absorbing “chromophore” retinaldehyde, prebound. The bound form, 11-*cis* retinal, acts as a strong antagonist, holding rhodopsin in its completely inactive state. Absorption of a photon of light isomerizes the chromophore to the the all-*trans* configuration, which rapidly triggers a conformational change in the protein, activating rhodopsin as an enzyme, the photoactive meta-rhodopsin II. The conformational change triggered by light causes rhodopsin’s absorption spectrum to shift into the UV, so that the pigment loses its visible color and is said to “bleach”. In addition to rhodopsin (R), which is packed into the disc membrane at high density, three other classes of protein cooperate into activation of the photoresponse: 1) an heterotrimeric G - protein (G), called transducin (encoded by *GNAT1*) in rods, with a 1:10 stochiometry to rhodopsin; 2) the cyclic nucleotide phosphodiesterase (PDE, whose subunits are encoded by the *PDE6A*, *PDE6B* and *PDE6G*), activated by transducin, which hydrolyzes cyclic GMP (cGMP), the second cytoplasmic messenger, present at about 100 units per rhodopsin one; and (3) the cyclic nucleotide – gated channels (CNGCs channels, whose subunits are encoded by *CNGA1* and *CNGB1*) of the plasma membrane, which control the flow of electrical current into the outer segment, and which close due to reduced cGMP concentration. Such molecular events strongly decrease the intracellular calcium concentration, with the final consequence of plasma membrane hyperpolarization which leads to glutamate release reduction at the photoreceptor's synapse. Long after signaling is complete, the system is reset to the unactivated state by the following

steps: i) metarhodopsin II phosphorylation by rhodopsin kinase and the consequent binding of arrestin (encoded by the *SAG* gene), which suspends transducin activity (McCarthy & Akhtar, 2002); ii) the Schiff – base bond that attaches the all – trans retinal is hydrolyzed, permitting the retinoid to dissociate from the apo – protein, opsin, by the retinoid (visual) cycle; iii) transducin deactivation by GTPase-accelerating proteins, determining the phosphodiesterase inactivation (X. J. Zhang, Gao, Yao, & Cote, 2012); iv) normalization of intracellular cGMP levels by guanylate cyclase (encoded by *GUCY2D*), triggered by guanylate cyclase-activating protein (encoded by the *GUCAI* cluster) (Haeseleer et al., 1999). After all-trans-retinal dissociation from opsin, 11-cis-retinal binds to opsin and produces rhodopsin, which then dissociates from arrestin. Finally, rhodopsin is dephosphorylated by protein phosphatase 2A. Therefore, in the dark, rhodopsin is prevalently in the unphosphorylated state.

Most of proteins involved in the rod phototransduction present a homolog that plays a similar role in cones, even if the whole process shows few differences. Cones express three different opsins, each one is characteristic, even though less sensitive, to a particular wavelength. These cone opsins exhibit faster kinetics than rod ones and are almost unsaturable, leading to a possible shorter recovery phase. The most supported hypothesis to explain such behavior involves faster phosphorylation of activated cone pigments, dissociation rate of all-trans-retinal and/or transducin inactivation kinetics (Tachibanaki & Kawamura, 2005). Finally, rod rate-limiting reaction is represented by hydrolysis of transducin-bound GTP, while cones contain 10X higher concentrations of the GTPase-accelerating protein complex.

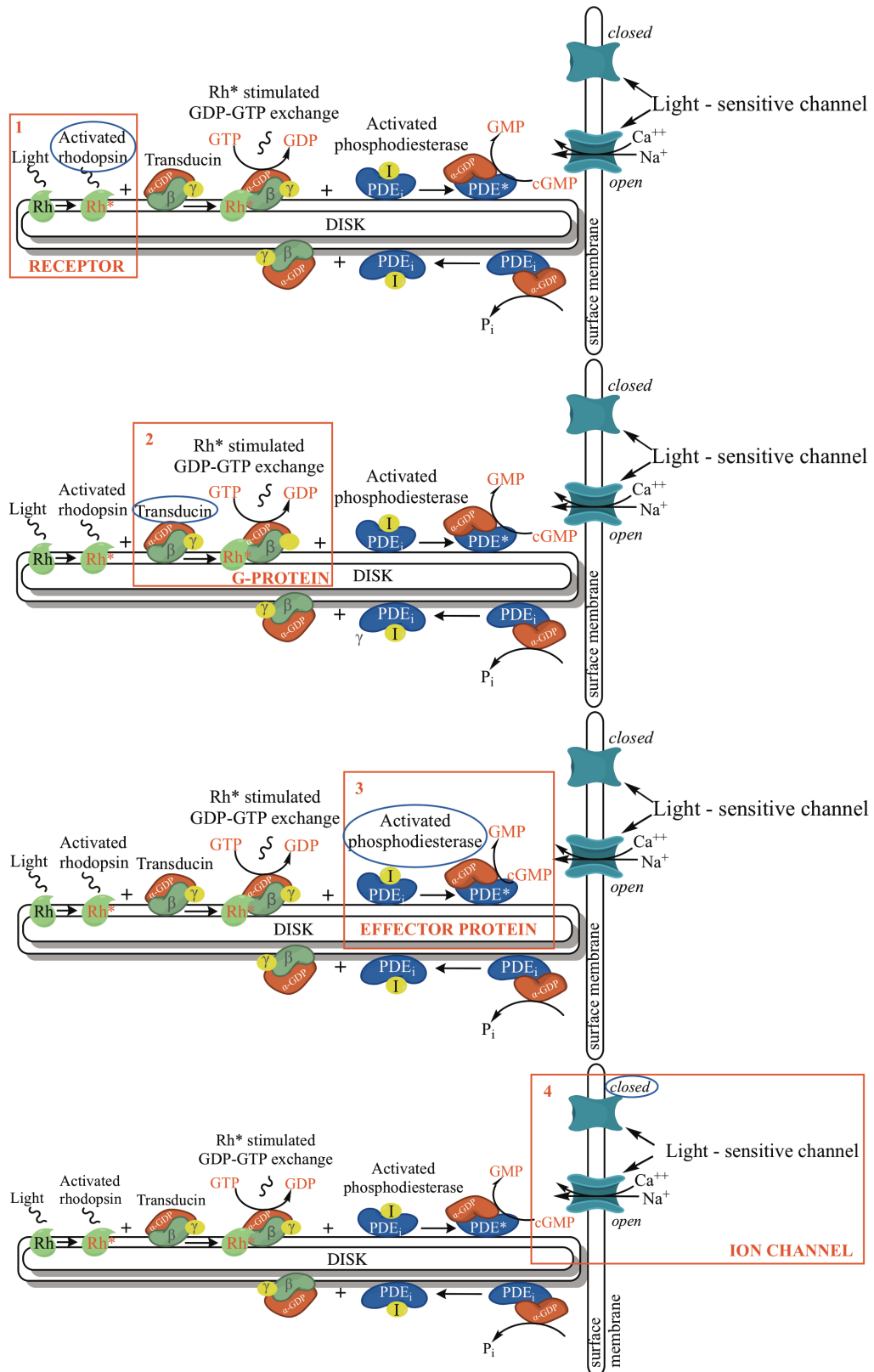


Fig. 6. Phototransduction steps. 1) activation of the receptor protein in rods, that is rhodopsin (1 photon for 1 rhodopsin); 2) the activated receptor protein stimulates the G-protein transducin, with GTP converted to GDP in the process (1 rhodopsin \rightarrow 100 transducins); 3) in turn, activated transducin activates the effector protein phosphodiesterase, converting cGMP to GMP (1 transducin \rightarrow 100 PDE/s); 4) Falling concentrations of cGMP cause the transduction channels to close, decreasing Na^{+} current (1 PDE \rightarrow 1000 GMP/s).

2.8.2. *Visual cycle cascade*

The 11-cis-retinal, derived from vitamin A (all-trans-retinol), represents a fundamental component in the phototransduction cascade. Dietary vitamin A is absorbed from the blood and converted to converted to 11-cis-retinal in RPE. The regeneration of 11-cis-retinal from all-trans-retinal obtained during phototransduction (Fig. 7) represents the core of visual cycle.

When photoactivation begins, all-trans-retinal is released from the activated visual pigment into the lumen of the outer segment discs, where it interacts with phosphatidylethanolamine to produce N-retinylidene-phosphatidylethanolamine (Liu et al., 2000). Thanks to the ABC (ATP-binding cassette) transporter ABCR (encoded by *ABCA4*), all-trans-retinal is flipped into photoreceptor cytoplasm, where it is reduced to all-trans-retinol by the all-trans-retinal dehydrogenase (encoded by *RDH8*, *RDH12* and *RDH14*) (Rattner, Smallwood, & Nathans, 2000). Soon after, all-trans-retinol is carried to the subretinal space, where it binds to interphotoreceptor retinoid-binding protein (IRBP, encoded by *RBP3*) before being translocated to the RPE. Once arrived within RPE cell, all-trans-retinol reacts with cellular retinol-binding protein (encoded by *CRBP1*) and isomerizes again through a biochemical pathway involving, consecutively, lecithin-retinol acyltransferase (LRAT), retinoid isomerohydrolase (RPE65), retinal G protein-coupled receptor (RGR) and 11-cis-retinol dehydrogenase (encoded by *RDH5* and *RDH11*) (Moiseyev et al., 2006). Subsequently, the obtained 11-cis-retinal is transferred to the inter-photoreceptor matrix by cellular retinaldehyde-binding protein (CRALBP, encoded by *RLBP1*) and soon after recovered towards photoreceptor cytoplasm by IRBP. At this point, 11-cis-retinal binds to opsin and constitutes a new rhodopsin molecule. In addition to previously described canonical visual cycle, whose purpose is the re-isomerization of retinal in rods, a second non – canonical visual cycle occurs in cones, precisely in their outer segments, and in Müller cells. This time the 11-cis-retinal regenerations exhibits a 20X faster rate (P. H. Tang, Kono, Koutalos, Ablonczy, & Crouch, 2013), even if many involved proteins are still unidentified. Non – canonical pathway starts with cone-specific opsin photobleach and all-trans-retinal release into cell cytosol, where retinol dehydrogenases (encoded by

RDH8 and *RDH14*) and the cone-specific enzyme retSDR1 (encoded by *DHRS3*) reduced it to all-trans-retinol (Sahu & Maeda, 2016). Soon after, produced all-trans-retinol binds to IRBP and moves towards Müller cells, where the direct isomerization of all-trans-retinol to 11-cis-retinol, 9-cis-retinol and 13-cis-retinol occurs by dihydroceramide desaturase-1 (*DES1*, encoded by *DEGS1*) (P. H. Tang et al., 2013). Such reaction is reversible so, in order to avoid the re-isomerization of just obtained 11-cis-retinol, the cell uses two mechanisms: 1) a multifunctional O-acyltransferase (*MFAT*, encoded by *AWAT2*) can esterify the 11-cis-retinol to 11-cis-retinyl-ester; 2) newly produced 11-cis-retinol can be caught by CRALBP, and this step is needed to activate a 11-cis-retinol-ester hydrolase to convert 11-cis-retinyl-ester to 11-cis-retinol (Stecher, Gelb, Saari, & Palczewski, 1999). After the interaction with CRALBP, 11-cis-retinol is released into the interphotoreceptor matrix, where it binds IRBP and is carried to cone outer segment (Saari, Nawrot, Stenkamp, Teller, & Garwin, 2009). At this level, an unknown RDH oxidizes 11-cis-retinol to 11-cis-retinal, which then binds to opsin and constitutes a new pigment molecule. This final oxidation step is unique for cones (P. H. Tang et al., 2013), explaining why the non-canonical visual cycle is specific to cone cells.

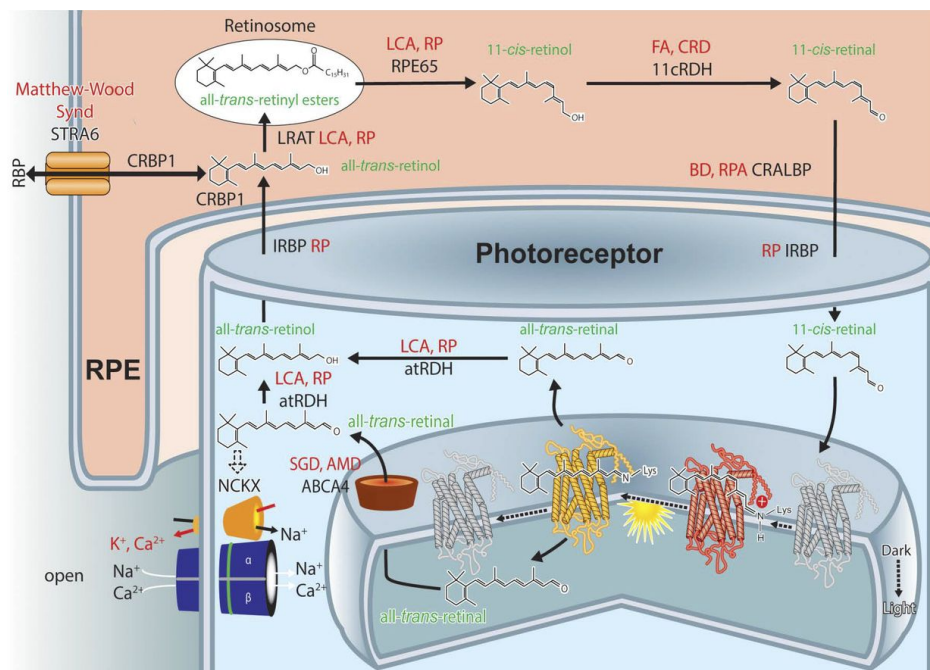


Fig. 7. Scheme of rod visual cycle. After absorption of light, the visual pigment chromophore, 11-cis retinal is isomerized to all-trans retinal. All-trans retinal is detached from opsin and reduced by RDH8 to all-trans retinol in the presence of a cofactor, NADPH. This retinol is transferred to the RPE where the all-trans form is isomerized to the 11-cis form and is oxidized to 11-cis retinal; 11-cis retinal is transferred back to the OS of a rod to regenerate visual pigment.

2.8.3. *Connecting cilium trafficking*

Surface of most mammalian cells presents microtubule – based projections called cilia, whose length and shape vary based on specific cytotype (Pedersen, Schroder, Satir, & Christensen, 2012). Cilia can be motile, supporting the movement of ciliary fluid of particular organs (e. g. clearance of mucus from the airways) or non-motile (primary), widespread on non-motile eukaryotic cells, acting as sensory elements in most sensory organs (McIntyre, Hege, & Berbari, 2016). Due to very wide distribution of cilia, mutations in genes encoding ciliary proteins can lead to specific pathologies called ciliopathies, that frequently determine syndromic phenotypes (Reiter & Leroux, 2017). Photoreceptors present a highly specialized sensory cilium constituted by the connecting cilium which links the associated basal body to the apical outer segment, an extremely specialized structure dedicated to phototransduction (Roepman & Wolfrum, 2007). The importance of such transport process, facilitated by intraflagellar transport (IFT), derives from the necessity to transfer molecules synthesized and pre-assembled in the inner segment to the outer one, because the latter lacks biosynthetic machinery. Moreover, IFT is also needed for cilia assembly and maintaining (Shamoto, Narita, Kubo, Oda, & Takeda, 2018). Nowadays, more than 30 ciliary protein–encoding genes could be causative of non-syndromic retinal diseases, most of them involved in IFT function/regulation or ciliary structure. IFT is a cargo transport system which exploits microtubule motor proteins for anterograde (from the cilia's base to the tip) and retrograde (from the tip to the base) transport of thousands of molecules (e. g. RHO and transducing) per second in each photoreceptor (Wren et al., 2013). Many genes linked to non-syndromic RP encode proteins that are involved in various phases of ciliary transport (Fig. 8). Two of them, RP2 and ARL3, regulate the localization of motor units at the ciliary tip (Schwarz et al., 2017a). Moreover, IFT is modulated by the the two complexes (A and B) of IFT family proteins (e.g., IFT172), which bind and transfer ciliary cargo (Taschner et al., 2016). Additionally, the BBSome complex (BBS is the acronym of Bardet-Biedl syndrome) acts as adaptor between cargo and the IFT proteins (Nager et al., 2017). Mutations in eight BBSome subunits (BBS1, -2, -4, -5, -7, -8 (TTC8), -9, and -18) are causative of Bardet-Biedl syndrome, even if other four BBSome subunits encoding genes (BBS1, BBS2, BBS9,

and TTC8) and ARL6 (encoding for a protein involved in the recruitment of the BBSome complex to the membrane) result associated with non-syndromic RP (Estrada-Cuzcano, Roepman, Cremers, den Hollander, & Mans, 2012). IFT – mediated cargo bidirectional transport to and from the structurally isolated outer segment is modulated by the specialized “ciliary gate”, a structure localized at the base of the primary cilium which acts as a general barrier against periciliary particle diffusion (Goncalves & Pelletier, 2017). In order to realize its function, gate needs the support of transition fibers, distal projections that anchor the cilium to the plasma membrane, and the transition zone, a modular structure consisting of Y-shaped linkers which probably serve as “molecular filter” in order to selectively control the ciliary cargo trafficking. The photoreceptor connecting cilium is structurally and functionally similar to just described transition zone, although the increased length of cilium is necessary to support the high trafficking rate for transporting biosynthetic material needed for daily renewal of outer segment. Furthermore, a homologous of nuclear pore complex, the so-called ciliary pore complex, behaves as an active molecule gate at the base of the cilium (W. Luo et al., 2017). Transition zone assembly and gating are regulated by the Meckel/Joubert syndrome (MKS/JBTS) and nephronophthisis (NPHP) associated modules (Garcia-Gonzalo et al., 2011). These complexes consist of different ciliopathy-associated proteins and interact with adjacent transition zone components (e.g., the BBSome complex) and a system which includes the *RPGR* encoded protein, whose mutations represent about 80% of X-linked RP and about 15% of all RP cases (Goncalves & Pelletier, 2017). The *RPGR* protein is docked to the connecting cilium by *RPGR* interacting protein 1 (*RPGRIP1*), whose localization is determined by another ciliary protein, spermatogenesis-associated protein 7 (*SPATA7*). Complex made of three previously cited proteins could play a fundamental role in opsins specific transport, thus alterations in such system could lead to opsins mislocalization (Dharmat et al., 2018).

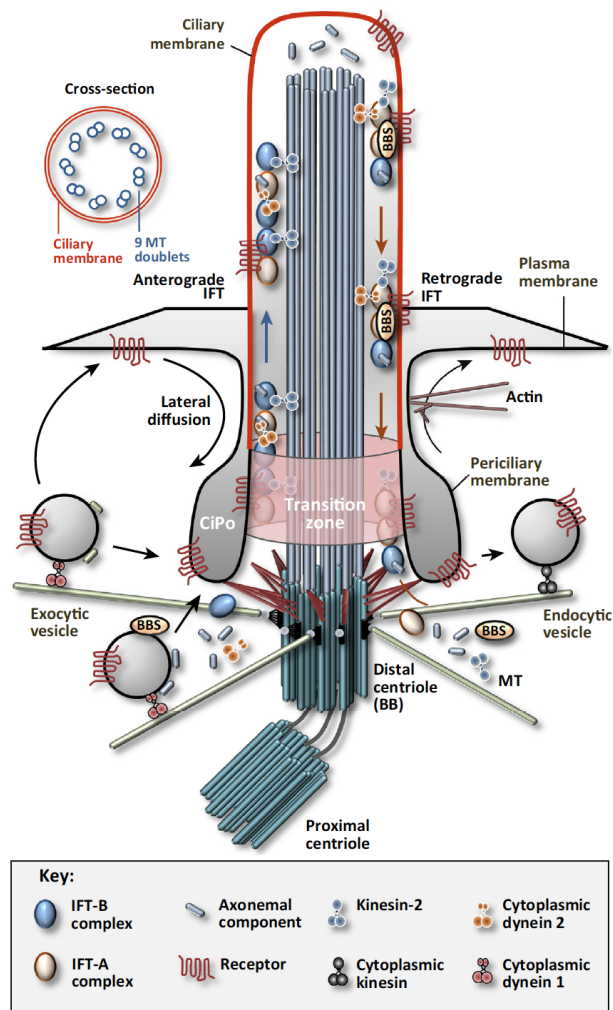


Fig. 8. Overview of Trafficking Pathways Involved in Ciliary Assembly and Homeostasis. Diagram illustrating the structures of the primary cilium, intraflagellar transport (IFT), and trafficking processes that control ciliary assembly and targeting of receptors to the ciliary membrane.

2.8.4. Photoreceptor outer segment assembly

Photoreceptor outer segment represents an extremely specialized compartment presenting stacks of intracellular lamellae (in cones) or discs (in rods). Several non-syndromic RP subtypes show association with proteins involved in development and/or orientation of outer segment discs (Fig. 9). Such discs origin from the connecting cilium as plasma membrane evaginations that are afterwards internalized to constitute a stack of intracellular discs (Ding, Salinas, & Arshavsky, 2015). The initial step of new disc evagination needs crosslinks and bundles of F-actin

microfilaments localized at basal axonemal microtubules, mediated by retinal fascin homolog 2 encoded by the RP-associated *FSCN2*. Additionally, mutations in peripherin-2 (PRPH2), involved in disc stability and shedding, as well as in the formation of the outer segment disc rim could lead to the loss of outer segment discs (A. F. Goldberg, Moritz, & Williams, 2016). Interestingly, it was reported that the photoreceptor cilium can release a huge number of ectosomes (Salinas et al., 2017), analogous to the process recently described in primary cilia, characterized by ciliary G protein-coupled receptor dispatch in extracellular signaling-competent vesicles by actin-mediated ectocytosis (Nager et al., 2017). PRPH2 maintains the adequate levels for this process, permitting retained ectosomes to morph into outer segment discs (Salinas et al., 2017). The rod outer segment membrane protein-1 (ROM1) protein modulate the genesis of PRPH2, thereby controlling the disc internalization process (Molday, Molday, & Loewen, 2004). The first step of outer segment disc production needs the membrane-bound protein prominin-1 (PROM1), localized to the arising disc edge, which links outer segment disc rims and helps to stabilize the stack (A. F. Goldberg et al., 2016). Cadherin-related family member 1 (encoded by *CDHRI*) is localized in the same area of PROM1, with whom cooperatively acts to form disc rim (Fu et al., 2018). Furthermore, the photoreceptor-specific cytosolic protein RP1 is required for outer segment disc morphogenesis, probably linking outer segment discs to the axoneme. Moreover, RP1 synergistically interact with RP1L1, a protein which exhibits a similar localization pattern and also fundamental for outer segment morphogenesis (Yamashita et al., 2009).

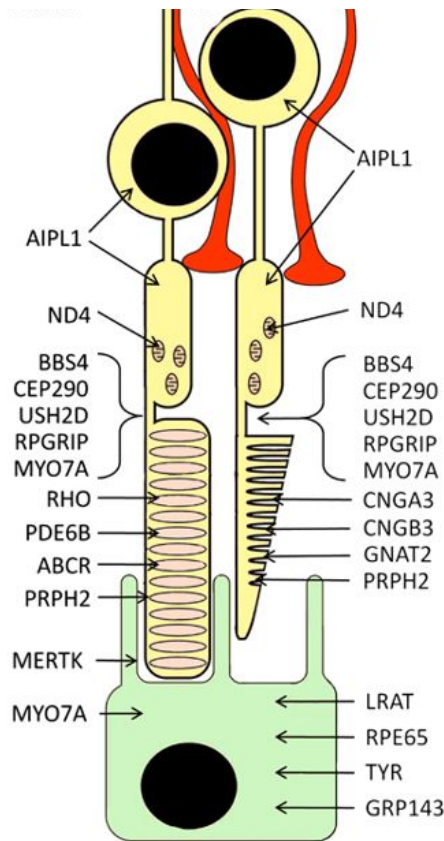


Fig. 9. Main protein expressed in outer membrane segments. Retina layers express a huge number of proteins, especially in photoreceptor outer portions. The most of gene coding for such proteins are causative, when mutated, of several RP forms.

2.8.5. The interphotoreceptor matrix

The interphotoreceptor matrix occupies the subretinal space, ranging from the external limiting membrane, represented by Müller cells basal ends, to the apical side of RPE (Fig. 10). In addition, the inner and outer portions of photoreceptors are also comprised within this space (Hollyfield, 1999). Contrary to what was believed until few years ago, the interphotoreceptor matrix takes part in many key processes, including: 1) retinal adhesion to the RPE (Hageman, Marmor, Yao, & Johnson, 1995); 2) retinoid metabolism; 3) matrix turn-over; 4) support of outer segment shedding and phagocytosis by the RPE; 5) growth factor presentation; 6) modulation of oxygen and nutrients transport to photoreceptors (Ishikawa, Sawada, & Yoshitomi, 2015); 7) photoreceptor alignment. Furthermore, this extracellular matrix could help the clinical presentation of progressive retinal degeneration (Al-Ubaidi, Naash, & Conley, 2013).

The interphotoreceptor matrix consists of carbohydrates and proteins secreted by photoreceptors and RPE cells. Among main components, hyaluronic acid, proteoglycans, elastin and collagen represent the most abundant, as well as laminins, fibronectin and fibrillin. The three-dimensional mesh network (Hollyfield, 1999), principally constituted by interconnected hyaluronic acid polymers, is linked to the RPE by RHAMM (receptor for hyaluronic acid-mediated motility)-type binding motifs containing proteins and to Müller cells via CD44. Moreover, other extracellular matrix components such as SPACRCAN, SPACR, pigment epithelium-derived factor (PEDF), and IRBP also present RHAMM-binding motifs, and are also connected to the hyaluronic acid network (Hollyfield, 1999). Three genes (*RBP3*, *IMPG2* and *EYS*) associated with non-syndromic RP encode proteins linked to the hyaluronic acid network (van Huet et al., 2014). *RBP3* encodes IRBP, the principal soluble protein in the interphotoreceptor matrix, already described in relation to the visual cycle. *IMPG2* encodes SPACRCAN, a proteoglycan able to bind hyaluronic acid and chondroitin sulfate, involved in several pathways such as modulation of the growth and maintenance of the photoreceptor outer segment and organization of the interphotoreceptor matrix (Acharya et al., 2000). *EYS*, one of the widest genes expressed in the retina, encodes the human ortholog of the *Drosophila* eyes shut protein, rich of different sites for the glycosaminoglycans side chains attachment. In *Drosophila*, this protein is an extracellular protein. Thus, due to the high degree of homology between the human and *Drosophila* orthologs, the human counterpart could also act in the extracellular matrix. Nevertheless, human protein presents four isoforms, also localized in subcellular compartments and in the axoneme of the connecting cilium. Interestingly, arresting *EYS* expression in zebrafish implies mislocalization of outer segment proteins, suggesting a possible role in ciliary transport (Lu et al., 2017). Additionally, posttranslational modifications may permit the protein to be targeted to specific locations (Alfano et al., 2016). Finally, the RP1 protein also includes hyaluronic acid-binding motifs and may interact with the hyaluronic acid scaffold when associated with photoreceptor plasma membrane (Hollyfield, 1999).

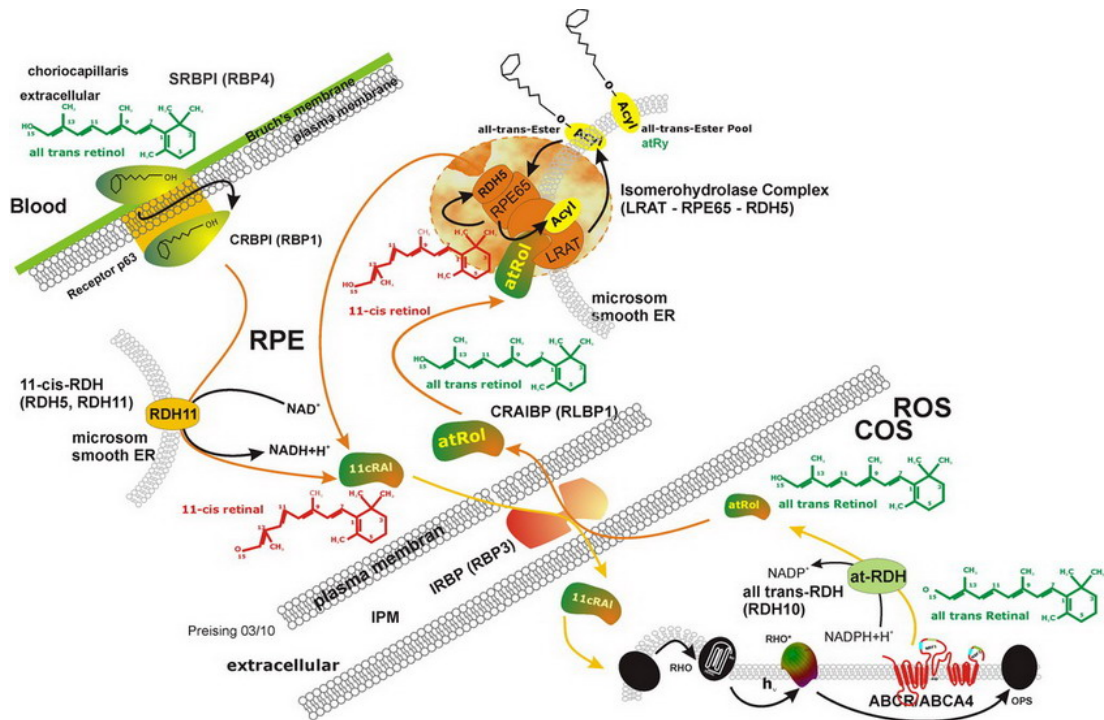


Fig. 10. Interphotoreceptor matrix role in visual physiology. *atRol* diffuses through the plasma membrane into the interphotoreceptor space where it is bound to Interphotoreceptor Retinoid-binding Protein (IRBP). IRBP, which is synthesised by the neural retina and secreted by photoreceptor cells, is the predominant protein of the IPM. It predominantly binds *atRAI* and *atRol*, although IRBP can also bind other lipid ligands. Due to its retinoid binding properties IRBP is the protein that shuttles the chromophore between the RPE and the photoreceptor outer segment, from and to regeneration.

2.9. HANDLING OF RP

Retinitis pigmentosa is a pathology which could extremely impact the physical and emotional sides of patients' lives and of their families, to whom is fundamental providing suitable support.

2.9.1. Ophthalmic and genetic counseling

The best approach to improve diagnostic process and long – term management of RP combines genetic and ophthalmic counseling services (Branham & Yashar, 2013). Today, sequencing all known genes implicated in RP simultaneously seems the best current approach for the definitive molecular diagnosis of RP, and next-generation

sequencing (NGS) is currently considered a powerful tool for mutation screening. With about 30-60% of previously unrecognized RP cases already characterized, this high-throughput method represents a promising tool for detecting novel disease-causing genes and genotype-phenotype correlation, which may lead to substantial improvement of our understanding of allele pathogenicity, protein function, and population genetics. Moreover, several centers switched from targeted sequencing to exome sequencing (WES), applying a vision-related gene filter to avoid the risk of incidental findings in genes that are not necessarily related to the pathology (Haer-Wigman et al., 2017). Main advantage of exome sequencing is the possibility to readily expand the search towards other genes if the causative one is not found among the known RP genes, thereby potentially discovering novel RP-related genes. The principal limits of WES are represented by structural rearrangements and mutations in non-coding and/or GC-rich regions, that are better suited for Sanger sequencing (Carss et al., 2017). In such cases fall RPGR mutations, accounting for about 75% of all X-Linked RP patients, due to the highly repetitive, purine-rich ORF15 region characteristic of this gene (Huang, Wu, Lv, Zhang, & Jin, 2015). However, the routine application of whole-genome sequencing in diagnostics will probably further increase the ability to obtain molecular diagnoses, although discovering the functional role of many of these candidate causative variants will remain a challenge.

Genetic testing frequently elicits a a huge number of questions, and patients are generally referred for genetic counseling to address questions about the reliability of the test results and the consequences for patient and his/her relatives. Even if many clinicians claim that performing presymptomatic and/or predictive testing at too early an age may increase the probability of a negative impact on quality of life (Godino, Turchetti, Jackson, Hennessy, & Skirton, 2016), the availability of new treatment options, which ideally are applied in the earliest possible stage of the disease, may justify testing at a younger age.

Even if genotyping usually improves the conclusions of ophthalmic counseling, the number of unique described phenotypes for a specific genetic subtype is generally limited, and phenotypes can range widely within a subtype and even between family members who share the same variants. Regardless of such heterogeneity, the features discussed in section 2.1 can support the clinician in evaluation of clinical aspects

related to the various genetic subtypes. Two examples are given by rapid central vision impairment frequently caused by variants in the *CERKL* gene, and by long – term preservation of visual acuity in RP patients carrying mutations in the *TOPORS* gene. Therefore, understanding the specific genotype – phenotype associations will help provide a more reliable clinical prognosis. Waiting for such in-depth genetic analyses, detailed follow-up checkups that include visual field examination, FAF and SD-OCT, will monitor the clinical progression of the retinal dystrophy, as well as predict the impairment of visual function.

2.9.2. Visual rehabilitation

Recently, a multidisciplinary approach focusing on patients’ functional abilities and necessities was exploited for visual rehabilitation of RP patients with low visual acuity (Herse, 2005). Strong support, including orientation and mobility training, along with low-vision aids (e. g. flashlights, reverse telescopes and night-vision goggles), are provided by vision rehabilitation centers in order to optimize residual visual function. Moreover, in advanced stages of disease, the patients’ independence and functional quality of life can be improved using text-to-speech software and guide dogs.

2.9.3. RP treatment possibilities

By improving the knowledge about the genetic causes of RP, innovative strategies towards disease treating have been developed (Yue, Weiland, Roska, & Humayun, 2016). Such strategies can be classified into 1) gene – specific and mutation-specific approaches, or 2) genetic – independent approaches.

- *Gene-specific and mutation-specific approaches*: because the most of RP causative genes encode proteins expressed either in photoreceptors or in the

RPE, efficient gene-specific and/or mutation-specific approaches have to target these cells; therefore, percentage of success is the highest during the early stages of the disease, before cell death. The most interesting approach is based on gene augmentation therapy, in which a construct driving the expression of a wild-type copy of the mutated gene cDNA is delivered into the target cells, trying to restore wild-type expression. In RP and related disease procedures, intravitreal or sub-retinal injection of virus-based vectors, such as adeno-associated viruses (AAVs), represent the first choice to deliver the genetic cargo to retinal target cells. The first reported study describing the cited approach regarded *RPE65* in patients with LCA or early-onset RP caused by bi-allelic mutations (Bainbridge, 2009). The encouraging results obtained from these studies led to phase I/II clinical trials designed to test gene therapy-based approaches for treating other different genetic subtypes of retinal disease, such as *MERTK*-associated RP (Ghazi et al., 2016), choroideremia (Patricio, Barnard, Xue, & MacLaren, 2018), *PDE6A*-associated RP, *CNGA3*-associated achromatopsia, retinoschisis, *RPGR*-associated X-linked RP and Stargardt disease. Recently, phase 3 study in *RPE65*-dependent inherited retinal dystrophy patients treated with voretigene neparvovec, validated treatment safety and efficacy, exhibited by improved visual fields, light sensitivity and navigational ability under dim light (Russell et al., 2017). Such positive results led to the first US FDA approved gene therapy for retinal disease. However, several serious challenges must be overcome before gene augmentation approach can be widely implemented: 1) one-time administration of a therapeutic vector could not provide long-lasting/long-term clinical benefits; 2) many RP causative genes are too large (e. g. *USH2A*, *EYS* or *ABCA4*) to be hosted by the most commonly used viral vectors; 3) dominant-negative mechanisms; 4) difficulties in expression level control; 5) the relative small number of patients for each genetic subtypes; 6) financial costs of the highly personalized treatments. Recently applied therapeutic strategies foresee the use of antisense oligonucleotides (AONs), small and flexible RNA molecules able to alter pre-mRNA splicing by specifically binding to a target region in the pre-mRNA, thereby inhibiting aberrant splicing events

determined by specific mutations (Garanto & Collin, 2018), and genome editing, frequently using the CRISPR/Cas9 system. Just cited technique is based on a highly precise double-strand break introduction in the genomic DNA at the specific site of the mutation, and can be used to repair a primary genetic defect directly within the patient's genome (Yanik, Wende, & Stieger, 2017). Another emerging class of highly useful therapeutic compounds that can serve in a gene-specific and/or mutation-specific way is represented by the small-molecule compounds. Early onset RP patients with LRAT or RPE65 mutations present a disruption of visual cycle. In these patients, an oral treatment with 9-cis-retinoid, an analog of 11-cis-retinal, was well tolerated and quite effective during early-phase clinical trials, and treatment efficacy was correlated with residual retinal integrity (Scholl et al., 2015). Furthermore, diet-based treatment can prevent or reduce disease progression in several syndromic RP forms, such as Bassen-Kornzweig syndrome, adult Refsum disease and α -tocopherol transfer protein.

- Mutation-independent approaches: during last years, different dietary supplements (e.g., vitamin E and vitamin A) and dietary changes have been suggested RP treatment (Brito-Garcia et al., 2017), even if there is no clear evidence that vitamin A and/or the fish oil docosahexaenoic acid has beneficial effects in RP patients (Rayapudi, Schwartz, Wang, & Chavis, 2013). A most powerful technique is represented by cell replacement therapy, consisting of the administration of ocular-derived retinal progenitor cells (RPCs) or non-ocular-derived stem cells (e.g. embryonic stem cells -ESCs- and induced pluripotent stem cells -iPSCs-) into the subretinal space or vitreous body. Each of these cell types has specific advantages and disadvantages (Z. Tang et al., 2017). Rather than stem cells, RPCs have the advantage to be relatively easy to process, and the recipient does not need immunosuppression therapy; on the other hand, obtaining sufficient donor cells is very difficult. Moreover, iPSCs permit the autologous transplantation of iPSC-derived photoreceptor or RPE cells, preceded by the possibility to correct underlying genetic defect using genome editing (Chakradhar, 2016). Phase I/II trials using RPCs are currently

being performed in RP patients, and this technique represents a promising future for them. One more recent approach regards the use of electronic retinal implants for end-stage RP patients with reduced light perception. The two existing retinal implants, the Alpha AMS subretinal implant (produced by Retina Implant AG in Reutlingen, Germany) and the Argus II epiretinal implant (produced by Second Sight Medical Products Inc. in Sylmar, CA) stimulate the inner retinal layers, and therefore require an intact inner retinal architecture. While a subretinal implant consists of a light-sensitive microphotodiode array that stimulates the bipolar cells, an epiretinal implant stimulates the residual retinal ganglion cells directly. Despite the promised possibility to restore basic visual function (Stingl et al., 2017), visual rehabilitation for patients with such devices is difficult, mainly do to device longevity, resolution, and other several adverse effects (Cheng, Greenberg, & Borton, 2017). The most innovative approach able to provide therapeutic benefits in patients with photoreceptor and/or RPE cells loss is optogenetics, which applies gene therapy to express light-activated ion channels in the residual retinal neurons, trying to recover photo-sensitivity (Swiersy, Klapper, & Busskamp, 2017). Although promising results in experimental models, such approach need to be fully validated by clinical setting. Interestingly, the reduction of photoreceptor death in animal models was related to various neuroprotective factors, such as glial cell-derived neurotrophic factor (GDNF) (Dalkara et al., 2011), rod-derived cone viability factor (rdCVF) (Byrne et al., 2015), brain-derived neurotrophic factor (BDNF) (Okoye et al., 2003), basic fibroblast growth factor (bFGF) (Faktorovich, Steinberg, Yasumura, Matthes, & LaVail, 1990), nerve growth factor (NGF) (Lenzi et al., 2005) and ciliary neurotrophic factor (CNTF) (Liang et al., 2001). Finally, a novel approach consists in Transcorneal electrical stimulation (TES), seems to exert its effect through the release of neurotrophic factors after corneal electrostimulation (Wagner et al., 2017).

3. MATERIALS AND METHODS.

3.1 GENOMICS.

3.1.1. Patients' clinical features.

A total of 80 RP patients (56 female and 24 male) were recruited from Messina and province. For each patient, a full medical and family history was taken and an ophthalmological examination (including dark adaptation and color vision, visual acuity testing by Snellen chart and computerized visual field measurement) was performed. Moreover, each patient underwent a deep ophthalmic examination: fundus analysis, autofluorescence (FAF), OCT, visual field (VF), ISCEV Electroretinography (ERG), pattern electroretinogram (PERG), flash electroretinogram (FERG), pattern evoked potential (PEP) and flash evoked potential (FEP), whose response confirms the typical clinical picture of retinitis pigmentosa. The mean age of patients was 39 ± 6.3 years (range: 30-80 years). This study was approved by the Ethics Committee of "Azienda Policlinico Universitario of Messina" and conformed to the tenets of the Declaration of Helsinki. All subjects had given written informed consent prior to participation in the study. Among all, several familial cases and several particular patients, negative to already known causative genes mutations, were deeply investigated to find new potential causative genes (Fig. 11).

1. One object of the study was a Sicilian family with three members. The proband, 54-year-old father, showed a symptomatology common to syndromic retinitis pigmentosa and Stargardt disease: high myopia and myopic chorioretinitis, irregular astigmatism, incipient cataract and retinal dystrophy. All these diseases have left the patient severely visually impaired, with a useful visual acuity of 1/20 in both eyes and short perceptions of light and colors since pediatric age. Fundus examination showed peripheral degeneration, an area of vitreous traction and macular thickness reduced in the right eye. The left eye showed degenerative myopia. Pattern evoked potential (PEP) and flash evoked potential (FEP) confirm typical signs of retinitis pigmentosa. The proband's wife, 65 years old, showed only a slight reduction of sensitivity on left eye

peripheral areas. Their 29-year-old daughter, instead, reveals no ophthalmologic symptoms (Fig. 11b).

2. A Sicilian female patient of 70 years, affected by an unknown form of RP, was recruited by Policlinico Universitario of Messina. Fundus examination revealed rounded macular and perimacular pigment deposits with sharp edges, confirmed by IR and FAF. ERG revealed a generalized rods impairment with cones involvement (reduced photopic and scotopic responses), with a delay in visual response (PERG with hypovolted P50 wave and increased latency). VF showed central scotoma correlating with outer retinal subfoveal atrophy observed on FAF and OCT (Fig. 11d).
3. Another interesting case was the one of a 31-years old woman, born in Fiumedinisi, a small Sicilian town. Her parents, also native of Fiumedinisi, are not consanguineous. About the proband, at the age of 5, myopia was diagnosed; two years later, she began suffering from night vision disturbance. Fundus revealed the typical “salt and pepper” aspect, without macula involvement; additionally, optical coherent tomography (OCT) examination showed the presence of numerous well – demarcated homogenous dome – shaped lesions, originating from the RPE layer. One year later, fundus analysis confirmed the progressive kind of phenotype, so RPA was diagnosed. Thereafter she has report continuous worsening with also reduction of the visual field due to “retinal-tapetum” degeneration. No evidences of eye diseases were reported neither for her parents nor for younger sister (Fig. 11f).
4. A family from Messina with ocular pathology showing a dominant inheritance pattern was studied (Fig. 11h). A total of nine family members, including four affected and five unaffected individuals, were examined. Deep ophthalmological tests, including ISCEV ERG, PERG, OCT, EP and fundus autofluorescence were performed on four affected individuals. Clinical history of the four affected individuals was also obtained focusing on: subjective degree of vision loss, age at onset, evolution, medication, and other

RP specific clinical manifestations (such as night vision impairment, loss of peripheral vision and color perception). Clinical features of the four affected family members were typical of those associated to RP, such as night blindness from birth, and progressive loss of visual field and visual acuity. The proband became completely blind at 50 years of age, and fundus examination showed tapetal retinal degeneration, macular pigmentary dystrophy, pale disc and retinal pigmented epithelium atrophy, OCT showed a relevant ellipsoid band loss in outer retina, choroid thickness and a thinning of retinal pigment epithelium (RPE) in both eyes. Additionally, ERGs revealed a generalized cone dysfunction with rod involvement (photopic extinct ERG and scotopic hypovolted ERG), with a delay in visual response (hypovolted scotopic b wave and increased latency). The remaining five unaffected individuals, instead, showed normal phenotype in all ophthalmological examinations.

5. The proband, a 42-year old Caucasian man, came with a diagnosis of Stargardt disease, claiming that he started to show visual problems at young age. His visual acuity was 1.6/10 in the right eye and 2/10 in the left eye; his peripheral visual field was well represented, while the central one was almost absent. Moreover, he also showed an initial loss of color vision, photophobia and a slow dark adaptation. Diagnosis was the result of the following evaluations: fundus analysis, fundus autofluorescence (FAF), infrared reflectance imaging (IR), optical coherent tomography (OCT), visual field (VF), ISCEV electroretinography (ERG) and pattern electroretinogram (PERG). Fundus examination revealed bilateral anatomic, rounded maculopathy with sharp edges, surrounded by pisciform flecks, confirmed by IR and FAF. Furthermore, FAF showed mottled areas of hyperautofluorescence and hypoautofluorescence, corresponding to areas of lipofuscin accumulation and RPE atrophy, respectively. ERG revealed a generalized rods dysfunction with cones involvement (photopic and scotopic hypovolted ERG), with a delay in visual response (PERG with hypovolted P50 wave and increased latency). VF showed central scotoma correlating with outer retinal subfoveal atrophy

observed on FAF and OCT. In details, OCT highlighted disruption of both inner and outer photoreceptor segment layers, combined with the loss of the inner segment – outer segment junction and thinning of other retina layers. The patient's family, composed of father and mother, was evaluated by the same clinical and instrumental analyses, and resulted healthy. Both parents did not manifest bilateral central visual loss, photophobia, color vision abnormalities, central scotomas or slow dark adaptation. Moreover, they showed a visual acuity of 20/20, a normal visual field and a clean fundus. All 3 known Stargardt disease causative genes (*ABCA4*, *ELOVL4* and *PROM1*) were screened, and no associated or causative variants were found (HGMD Professional was the most important and updated database we considered), except those analyzed in this paper (Fig. 9l).

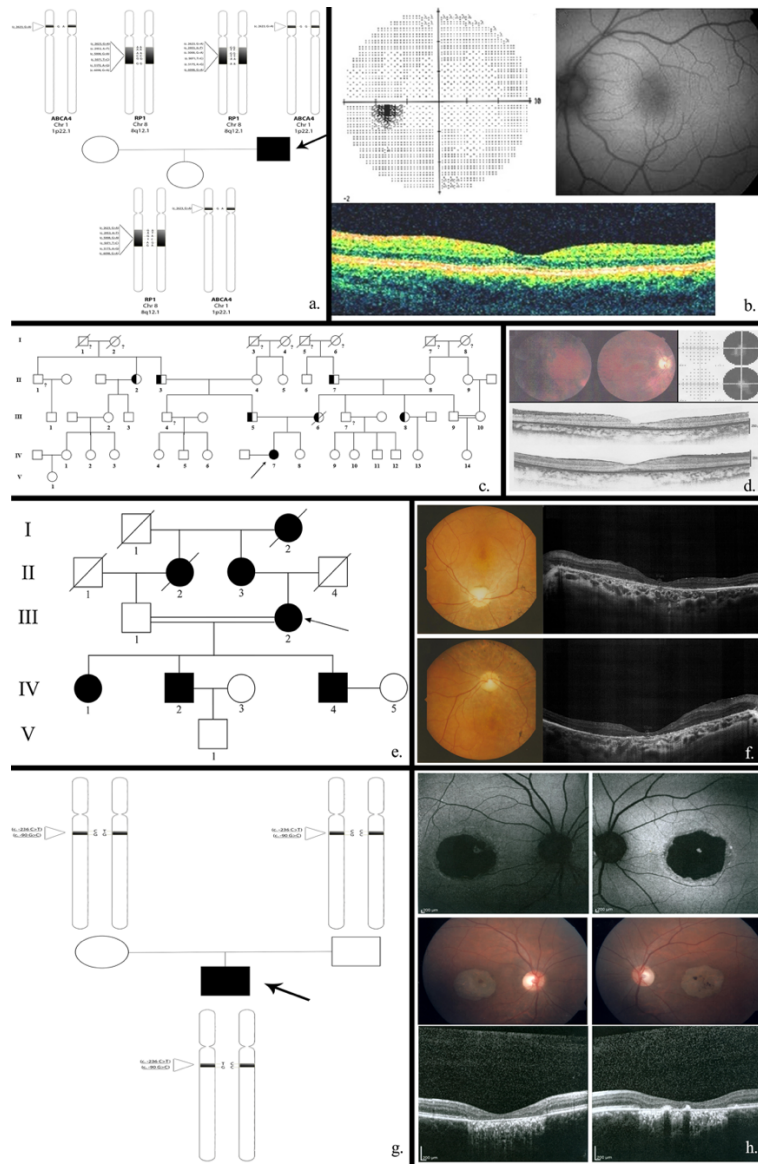


Fig. 11. Pedigrees and clinical exams of analyzed familial cases. Black arrow indicates the proband. Mutated condition, due to present polymorphisms, is underlined. Empty squares and circles symbolize wild-type men and women, respectively. Half fill indicates the heterozygous condition for a given mutation. Question mark indicates the unknown genotype due to unavailability of the sample. Slash indicates died individuals. (a, b). N°1 family tree genotypes for RPI and ABCA4. Clinical examination of the proband's daughter (visual field, fundus and OCT) highlight a healthy condition. (c, d). N° 3 Familial pedigree. Fundus photograph of proband's both eyes shows papillary pallor, fundus albipunctatus, narrowed retinal arteries and temporal displacement of the papilla opaque vessels. A horizontal SD-OCT scan shows numerous well-demarcated homogenous dome-shaped lesions originating from the RPE layer and diffused to the IS/OS junction of the photoreceptors, external limiting membrane, and into the outer nuclear layer. Visual field of both eyes shows a deep impairment of visual field from tapeto-retinal degeneration; GHT's 30° Threshold Test denotes annular scotom in the explored area with central vision islands. (e, f). N° 4 familial pedigree. Fundus examination demonstrated mild changes typical of RP in the left and the right eyes, including slightly pale optic discs with almost normal retinal vessels, generalized pigmentary granularity, and moderate bone-like spicules in peripheral areas. The OCT scans of the left eye and the right eye revealed decreased macular thickness. (g, h). 5° family tree. Infrared images, FAF and OCT of proband. Both eyes show absence of FAF in the fovea, corresponding to geographic atrophy. Moreover, it is evidenced a central, bright, hyperreflective area, which corresponded to the atrophic macular lesion, surrounded by a darker, hyporefective zone with distinct borders. This area is consistent with a zone where there is thinning and hypopigmentation of the RPE. Proband's right eye OCT depicts the extent of the transverse loss of the junction between the inner and outer segment of the photoreceptors in the foveal region. Furthermore, his left eye showed abnormal pigmentation in the RPE layer, due to macular degeneration.

SIGN, SYMPTOMS, OTHER FEATURES	PATIENT			
	III2	IV1	IV2	IV4
NIGHT BLINDNESS	Yes	No	No	Yes
NARROWING OF VISUAL FIELD	No	No	No	No
PHOTOPHOBIA	Yes	Yes	Yes	Yes
AGE OF ONSET	Newborn	Newborn	Newborn	Newborn
PHOTOPHOBIA (Scholastic Age)	Yes	Yes	No	No
DARK ADAPTATION (Scholastic Age)	Yes	No	No	No
NEAR VISION (Scholastic Age)	Yes	No	Yes	Yes
DISTANCE VISION (Scholastic Age)	No	Yes	Yes	Yes
TUNNEL VISION	No	No	No	No
PERIPHERAL VISION	Yes	Yes	Yes	Yes
GREEN->LIGHT BLUE (Altered colour perception)	Yes	Yes	No	No
BLACK->BLUE (Altered colour perception)	No	Yes	No	Yes
WHITE PERCEPTION (Altered colour perception)	No	Yes	No	No
RED->ORANGE (Altered colour perception)	No	No	Yes	Yes
YELLOW (BY COMPARISON) (Altered colour perception)	No	Yes	Yes	No
COMPROMISED OPTICAL NERVE	No	Yes (marked ischemia)	No	Yes (subatrophy and pale)
BILATERAL AND HORIZONTAL NYSTAGMUS	Yes	Yes	Yes	Yes
MACULAR DEGENERATION	Macular and perimacular	Macular	Macular	Macular
BEST CONDITION OF VIEW	Penumbra (Darkness until 50 years)	Penumbra	Darkness	Penumbra
HEAD MOVEMENT (TO IMPROVE FOCUS)	Yes	No	Yes	No
PHOTOPSIA	Yes	Yes	No	No
EVOLUTION	Up to 15 years walking well in the dark; gradual reduction of vision, up to only light perception by 45 years; today blindness in the dark	Normal vision up to high school, then lack of focus; at university did not read any more, high photophobia; today more difficulty in vision, much more photophobia, blurred vision	Gradually worsening of vision until present day	From 12 years onwards, significant photophobia and following worsening of vision
CURRENT THERAPY	Antioxidants	/ ^b	/	Antioxidant (astaxanthin)
OTHER OCULAR DISEASES	Bilateral cataracts	Astigmatism, Myopia	/	Astigmatism, Myopia
OTHER DISEASES	Bilateral hearing loss, Hypertension, Diabetes mellitus type 2, Allergies, Appendectomy	Multinodular goiter, Chronic otitis, adrenocortical hypertrichosis, Appendectomy	/	Appendectomy

Tab. 3. Clinical features of the four affected members of the reported Sicilian family. The signs, symptoms, and clinico-pathological features listed are those most frequently observed in RP, as well as those observed in the reported cases. *b*/, indicates the absence of specific feature in exam.

3.1.2. Genotyping (*Sanger sequencing*) (Fig. 12)

- *Selected gene genotyping*: genomic DNA was extracted from heparinized peripheral blood using the salting out method and then stored in TE buffer (10 mM Tris–HCl, 1mM EDTA, pH 8.0) until analysis. Coding exons, intron–exon boundaries and promoter regions of the selected genes were screened using primers designed according to the published nucleotide sequences of GenBank.
- *Polymerase Chain Reaction (PCR)*: PCR amplifications were carried out in a 50 µl solution containing MgCl₂ (2.5 mM), dNTPs (0.2 mM), 0.2 µl, (of each primer, 10 µM) 0.8 µg of genomic DNA and 1 U of Euro Taq polymerase (Euroclone Spa Life Sciences Division, Italy). DNA amplification was performed on a thermal cycler Gene Amp PCR System 2700 (PE Applied Biosystems, Foster City, CA) as follows: after an initial denaturation step at 94°C for 5 min, samples were subjected to 35 cycles of amplification consisting of 40 sec of denaturation at 95°C, 35 sec of annealing and 45 sec of extension at 72°C. The annealing temperature was optimized for each primer set. A final extension at 72°C was carried out for 10 min. Following PCR, 5 µl of amplified product was examined by electrophoresis on a 2% agarose gel.
- *Sanger sequencing and Data Analysis*: all PCR products were analyzed also by direct nucleotide sequence analysis by the dideoxynucleotide method with the BigDye Terminator 3.1 Cycle Sequencing kit on the 3500 Genetic Analyzer (Applied Biosystems, Foster City, CA). Obtained electropherograms were analyzed by 4Peaks software (<https://nucleobytes.com/4peaks/index.html>).

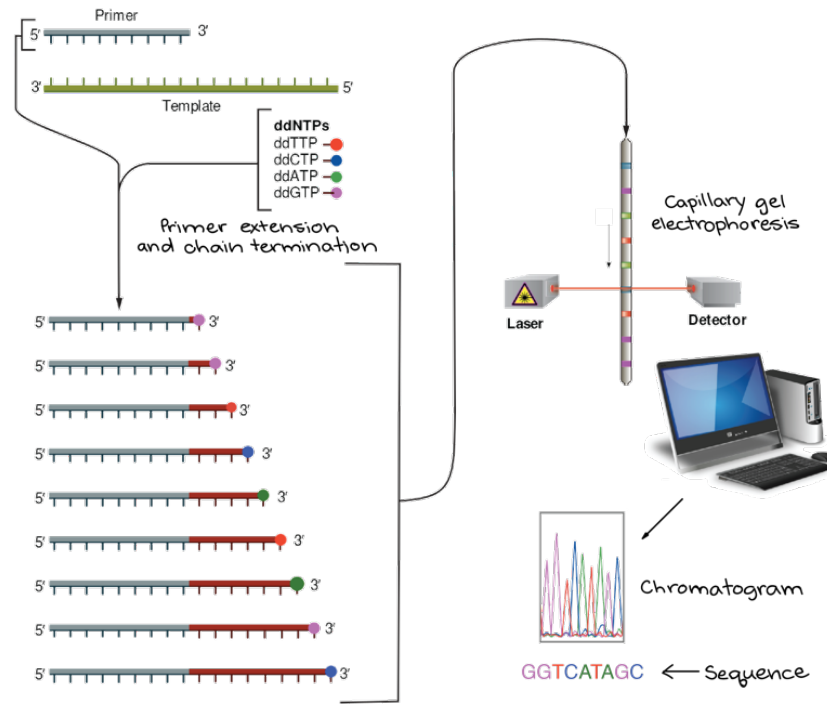


Fig. 12. Sanger sequencing workflow. In Sanger sequencing, the target DNA is copied many times, making fragments of different lengths. Fluorescent “chain terminator” nucleotides mark the ends of the fragments and allow the sequence to be determined.

3.1.3. Whole Genome Sequencing (WGS) (Fig. 13)

- NGS experimental design DNA extraction: genomic DNA was extracted from peripheral blood using QIAamp[®] DNA Mini Kit (Qiagen) then quantified by NanoPhotometer P-330 (Implen). DNA integrity was evaluated by visual inspection on a 1% agarose gel.
- WGS Ion Proton Sequencing: workflow for Ion Proton Sequencing can be outlined in three different steps: fragment library preparation, library clonal amplification, and sequencing.
 1. Fragment library preparation: 1,2 µg of gDNA were fragmented by Ion Xpress[™] Plus Fragment Library Kit (ThermoFisher Scientific), for 10 min digestion time and, then, purified by Agencourt[®] AMPure[®] XP Reagent (Beckman Coulter); fragmentation status was tested by Bioanalyzer, using the Agilent[®] High Sensitivity DNA Kit. A no-barcoded library was obtained, using Ion Plus Fragment Library Kit

(ThermoFisher Scientific), according to manufacturer's instructions. The library was again purified and size selection was performed with an E-Gel®SizeSelect™ Agarose Gel (ThermoFisher Scientific), using 50-bp DNA Ladder: 150 bp and 200 bp fragments were captured. The two libraries were individually quantified by Real-time StepOne™ Plus System, with Ion Library Quantitation Kit (ThermoFisher Scientific). No library amplifications were performed.

2. *Library clonal amplification*: an equimolar 11pM quantity of both libraries was amplified by Ion PI™ Template OT2 200 Kit v3 at Ion OneTouch™ 2 Instrument (ThermoFisher Scientific). Emulsion PCR occurs on microbeads, called ion sphere particles (ISPs). To evaluate presence of amplification of polyclonal sequences, obtained ISPs were qualitatively checked by Ion Sphere Quality Control kit on a Qubit® 2.0 instrument. ISP enrichment was performed on an Ion OneTouch™ ES instrument (ThermoFisher Scientific).
 3. *Sequencing*: two Ion PI Chip v2 were run on an Ion Proton™ System (ThermoFisher Scientific); sequencing run was performed using the Ion PI Sequencing 200 Kit v2.
- *WES Illumina Hi-Seq Sequencing*: genomic DNA of affected individuals was subjected to whole exome paired-end sequencing analysis with 100X coverage by generating 51 Mb SureSelectXT Human All Exon V6 libraries (Agilent Technologies, USA). Shearing, hybridization using RNA-based Library Baits, Target capture and bridged amplification were subsequently carried out. The imaging and extension were achieved in automated cycles by mounting the clusters-bearing flow cell onto the Illumina HiSeq 2000/2500 sequencer (Illumina, San Diego, CA, USA).
 - *Read Mapping*: generated sequences were processed in-house using the bioinformatics software CLC Genomics Workbench 10.0.1 ("CLC Genomics Workbench 9.5.3," 2016). In CLC workflow, the generated FASTQ files were imported and processed through a sequential workflow: 1) Sequence

quality trimming based on Phred quality scores (“minimal score = 27”) and removal of ambiguous base-calls; 2) Read Mapping (human reference sequence hg19) with <3 mismatches/100 bp per alignment; 3) Read Mapping coverage analysis, designed to identify regions indicative of a deletion or an amplification in the sample. The algorithm fits a Poisson distribution to the observed coverage in the positions of the mapping (“Minimum length = 50” and “P-value threshold = 0.0001” were set).

- *Variant calling*: variant calling using the fixed ploidy variant detection was performed, reporting variants with >90% probability. Pyro-error variants were removed through specific filtering (parameters set: “in homopolymer regions with minimum length=3”; “with frequency below=0.8”). This process detects variants whose representation in the reads is in accordance with the assumed ploidy, discarding sequencing errors or mapping artefacts. The algorithm behind the Fixed Ploidy Variant Caller combines a Bayesian model (examining posterior probabilities) with a maximum likelihood approach.
- *Annotations from known variants*: to determine if newly-identified variants had already been associated to RP, comparison with known variants in reference databases (dbSNP, 1000 genomes, HapMap) was performed.
- *Functional consequence prediction*: to assess the potential impact of variants on gene function, the following steps were realized:
 1. Annotation of variants with aminoacid changes;
 2. Determination of variants potentially involved in splice site alterations (e. g., variants falling within two base pairs of an intro/exon boundary, are annotated as a possible splice site disruption);
 3. Investigation on genes presenting candidate variants to disclose common functional roles, by Gene Ontology (GO) (Gene Ontology, 2015) enrichment analysis;

4. Annotation with conservation score. This quantifies to what extent a particular position is conserved across different species, as conserved bases are expected to be functionally important. If a variant is found at a position that is otherwise well conserved, it is an indication that the variant may have functional impact.
- *Filtering candidate variants*: the first criterion used to select candidate variants was based on involvement of affected genes in eye biological processes and/or ocular diseases. This filtering was applied with the help of GO and Kyoto Encyclopedia of Genes and Genomes (KEGG) (Kanehisa, 2002), and relevant literature analysis. The second filtering step opted-out deep intron variants in previously selected genes.
 - *Preliminary pathway analysis*: to determine related effects of selected variants, it was fundamental to establish functional connections between analyzed genes. This was carried out by Cytoscape (v3.4) (Shannon et al., 2003) and its plugin GeneMANIA (v3.4.1) (Warde-Farley et al., 2010). The latter was set to find the top 100 related genes and the 100 most significant attributes, using automatic weighting.
 - *Data mining and statistical analysis*: qualitative association analysis was performed by means of MatLab software package (R2018, The MathWorks Inc., Natick, MA, 2000); for statistical analysis we made use of IBM SPSS software package (IBM Corp. Release 2016. IBM SPSS Statistics for Macintosh, Version 25.0. Armonk, NY: IBM Corp). To investigate the complex patterns between disease symptoms and genome, and due to the relatively low sample size investigated, we adopted a qualitative approach: for each genotype v , we clustered patients showing a given symptom s from those who did not. By considering an additive model (1=wild-type, 2=heterozygous, 3=homozygous mutated), we extracted and averaged genotype from each group and calculated the difference $\overline{a_v^s}$. A positive sign indicates that affected patients showed a genotype more directed towards homozygous mutation if

compared to unaffected patients; vice versa, a negative sign indicates that unaffected patients showed a genotype preferentially directed towards heterozygous mutation. Positive values may therefore appear in variants involved in symptom manifestation, whereas negative differences may highlight variants whose presence may have a protective role in symptom arousal. A weight p_v^s was subsequently created to better define the magnitude of the difference d_v^s : p_v^s was assigned a value of 0 when $\text{abs}(d_v^s) < 0.5$, alternatively a value of 1 was considered when $0.5 \leq \text{abs}(d_v^s) < 1$. If $\text{abs}(d_v^s) \geq 1$, p_v^s was set to 2. By gathering the weights obtained from each genotype v and symptom s , we therefore obtained a matrix vector $P_{s,v} = [p_v^s]$, with row elements s representing symptom s , while columns v represent scores for genotypes. The usefulness of the matrix consists in the fact that by summing over the v -th column we are able to obtain a score SC_{pol}^v whose magnitude is proportional to its relevance in clustering both affected and unaffected patients given the whole patterns of symptoms.

- *Pathway functional enrichment*: pathway enrichment analysis was performed by Cytoscape, based on GO, KEGG, and Reactome (Fabregat et al., 2016). The statistically enriched GO categories for the identified protein interactome were established by Cytoscape plugin ClueGO (v2.2.6) + CluePedia (v1.2.6) (Bindea, Galon, & Mlecnik, 2013). Subcellular locations, biological processes, molecular function, and KEGG pathways, which were inferred from electronic annotation and experimental data, were all in the identified GO categories. A minimum level of 3 and a maximum level of 8 were set as the GO level interval with a minimum of two genes per category. Obtained experimental data were directly compared and enriched with publicly available information from STRING (Szklarczyk et al., 2015), IntAct (Orchard et al., 2014), MiMI (Tarcea et al., 2009), miRBase (Kozomara & Griffiths-Jones, 2014), and miRecords (F. Xiao et al., 2009). miRNAs target sites analysis was performed using the PolymiRTS Database (v3.0) (Bhattacharya, Ziebarth, & Cui, 2014).

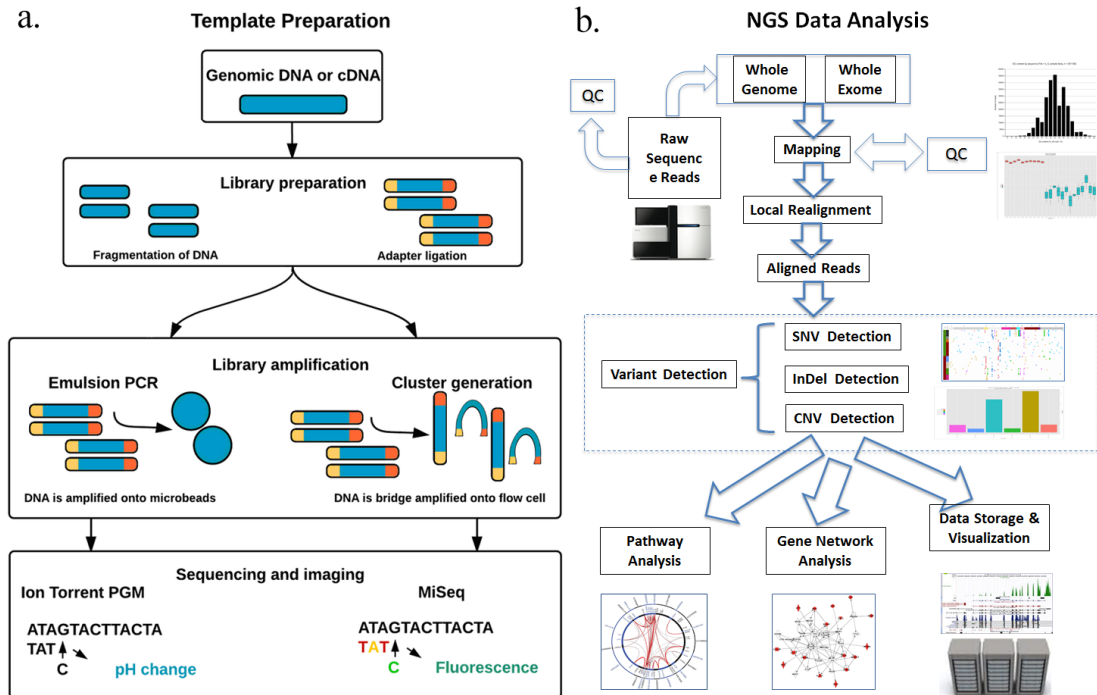


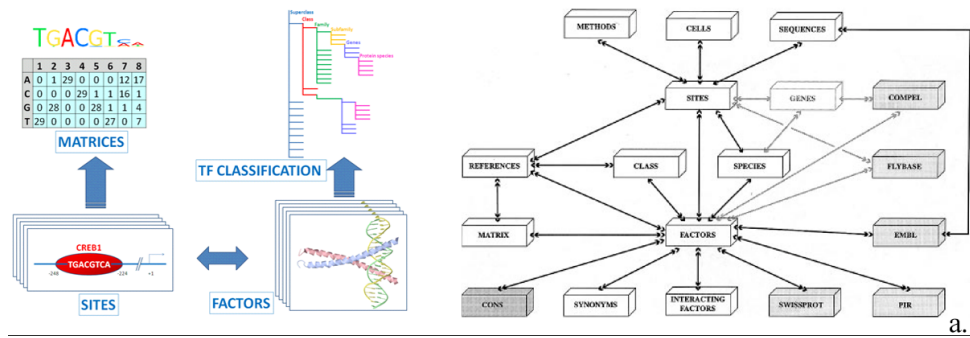
Fig. 13. Ion Torrent and Illumina sequencing (WGS and WES) workflows (a), with following data analysis (b). Illumina amplifies individual library molecules on a solid surface to form colonies Ion Torrent uses emulsion PCR on beads. Illumina uses reversible terminated nucleotides delivered as pools of all four. Detection is via imaging. Newer systems use a two-color scheme with G nucleotides unlabeled. Since each color is a separate scan (monochrome imaging is always higher resolution than multicolor), two-color labeling halves imaging time. Ion Torrent uses natural nucleotides presented as pure sets of individual nucleotides. Detection is via the H⁺ Ion generated during nucleotide incorporation, using electronic sensors in each well of the sequencing plate. Illumina reads in a run will all have the same untrimmed length. Ion Torrent reads have variable lengths due to homopolymers and the correspondence of flow order to sequence - if the flow order was A, T, C, G and the sequence of two fragments ATCG and GCTA, the former will read in all four flows but the latter only in the fourth flow. Data analysis was mainly realized by CLC Genomics Workbench and Cytoscape software, with their own plugins,

3.1.4. In silico functional prediction analyses of variant effects (Fig. 14)

- In silico transcription factor predictive analysis: in silico transcription factor analysis was performed using two transcription factors (TF) prediction tools, individually and in pairs: BioBase TRANSFACTM Professional (Matys et al., 2006) and Alggen PROMO (Farre et al., 2003). These tools were used to identify potential TF binding sites in the region where the variants in selected gene promoter were found. TRANSFAC was set to use the profile matrix for Vertebrates, with a cut-off to minimize false positives (minFP). This is defined as the score that gives one percent of hits in the used sequences relative to the number of hits received at the minimum false negative (minFN) cut-off (the score at which at least 90% of the positive test set are recognized, i.e. it equals a false negative rate of 10%). The false positive rate is estimated by applying

the MatchTM algorithm to upstream sequences. PROMO, instead, involves the dissimilarity threshold, a parameter that controls how similar a sequence must be to the matrix to be reported as a hit. It was set at 15% (85% similarity). Random expectation (RE) gives the number of expected occurrences of the match, in a random sequence of the same length as the query sequence, according to the dissimilarity index. Two models are considered: (1) Equiprobability for the 4 nucleotides (RE equally), (2) Estimate the nucleotide probability as the nucleotide frequencies in the query sequence (RE query). Furthermore, Cytoscape software and its MCODE plug-in were used to analyze pathways between involved TFs, in order to predict possible interactions among them.

- *In silico analysis of mutation effects on protein structures*: to clarify the hypothetical effects of examined variants, a deep bioinformatic analysis with CLC Genomics workbench 10.0.1 for primary structure details, followed by PSIPRED secondary structure prediction (<http://bioinf.cs.ucl.ac.uk/psipred/>) was performed. Finally, RaptorX (<http://raptorx.uchicago.edu>) and Chimera software (<http://www.cgl.ucsf.edu/chimera/>) were used to highlight third structure aspects of mutated and wild-type predicted proteins.
- *Splicing variant effect predictions*: finally, we assessed the potential negative effects of intronic variants emerged from NGS and then resisted the various filtering and pathways analyses. The possible creation of ESS sequences, the abolition of ESE sequences, as well as the abolition and creation respectively canonical sites and cryptic splice sites, were analyzed through an in silico approach with the help of Human Splicing Finder web – based software (Desmet et al., 2009).



Section II. Summary Prediction Results

The predicted model for the whole sequence. Left click for an image of higher quality; right click to save.

Summary (help)

- The input predicted as **1** domain(s)
- Best template: **3b4yA**, p-value **2.90e-10**
- Overall uGDT (GDT): **319 (95)**
- 336(100%)** residues are modeled
- 5(1%)** positions predicted as disordered
- Secondary struct: **43%**H**, 17%**E**, 38%**C****
- Solvent access: **30%**E**, 29%**M**, 40%**B****

Download

[Download](#) the predicted model as PDB file.

[Download](#) detailed prediction results.

To open zip files, you may use [7-zip](#) for Windows or unzip for Linux/Unix/MacOS.

Status

Current status: Complete
Submitted on: 2017-07-12 03:43
Scheduled on: 2017-07-12 05:37
Finished on: 2017-07-12 05:50

Predicted signal	Prediction algorithm	cDNA Position	Interpretation
New Acceptor Site	1 - HSF Matrices	<pre> ATCCAAATCTGATTAGACAAGTCAATGAGN ----- ----- 5 10 15 20 25 30 </pre>	Activation of an exonic cryptic acceptor site, with presence of one or more cryptic branch point(s). Potential alteration of splicing.
New ESS Site	1 - Fas-ESS hexamers	<pre> T C T G A T T A G A C A A G T ----- ----- 10 12 14 16 18 20 22 24 </pre>	Creation of an exonic ESS site. Potential alteration of splicing.
	2 - HSF Matrices - hnRNP A1	<pre> T C T G A T T A G A C A A G T ----- ----- 10 12 14 16 18 20 22 24 </pre>	
ESE Site Broken	1 - ESR Sequences from Goren et al.	<pre> T G A T T T G A C A A G ----- ----- 12 14 16 18 20 22 </pre>	Alteration of an exonic ESE site. Potential alteration of splicing.
	2 - EIEs from Zhang et al.	<pre> T G A T T T G A C A A G ----- ----- 12 14 16 18 20 22 </pre>	

Fig. 14. In silico functional predictions. TF predictive analyses were realized by *Alggene PROMO* and *TRANSFAC* (a) software and their related databases. Analyses of mutation effects on protein structure were carried out by *CLC Genomics Workbench*, *PSIPRED* and *RaptorX* softwares (b), while splicing variant consequences were analyzed by *Human Splicing Finder* (c).

3.2. TRANSCRIPTOMICS (Fig. 13)

3.2.1. Cell culture

Human RPE-derived Cells (H-RPE – Human Retinal Pigment Epithelial Cells, Clonetics™, Lonza) were maintained at 1x10⁶ cells/ml culture in T-75 flasks containing RtEGM™ Retinal Pigment Epithelial Cell Growth Medium BulletKit® (Clonetics™, Lonza) with 2% FBS, 100 units/mL of penicillin and 100 µg/mL of

streptomycin and incubated at 37 °C with 5% CO₂. After 24 hours, 100 µg/ml of oxLDL was added to the treated group.

3.2.2. Total RNA sequencing

RNA was isolated by TRIzol™ Reagent (Invitrogen™, ThermoFisher Scientific), following manufacturer's protocol and quantified at Qubit 2.0 fluorimeter by Qubit® RNA assay kit (Invitrogen, Life Technologies). Expression analysis was tested by comparison of Human RPE cells treated with 100µg/ml of oxLDL and not-treated, both at the moment of treatment and for four different time points (1h, 2h, 4h, 6h). Libraries were generated using 1 µg of total RNA and the Ion Total RNA-Seq Kit v2 (ThermoFisher Scientific) then purified by Dynabeads® Magnetic Beads and quantified at Qubit® 2.0 fluorimeter with Qubit® dsDNA HS Assay Kit. Appropriate libraries amount was used for clonal amplification performed with Ion PI™ Template OT2 200 Kit v2 (ThermoFisher Scientific) on Ion One Touch™ 2 System; template-positive Ion Sphere Particles were enriched at Ion One Touch™ Enrichment System. Sequencing runs were performed on an Ion Proton™ Sequencer (Ion Torrent technology, ThermoFisher Scientific), using the Ion PI™ Sequencing 200 Kit v2 and the Ion PI™ Chip Kit v2 (ThermoFisher Scientific). The experiment was thrice repeated.

3.2.3. Quality validation and read mapping

Sequence reads were generated from RPE specific cDNA libraries on the Ion Torrent Proton. Obtained raw data was filtered to remove low quality reads (average per base Phred score < 28). Moreover, the reads containing adaptor sequences and low-quality sequences (reads presenting ambiguous bases denoted as “N”) were also trimmed from the raw data. The quality of analyzed data was checked using the FastQC v.0.11.5 (Andrews, 2014) and QualiMap v.2.2.1 (Okonechnikov, Conesa, & Garcia-Alcalde, 2016) softwares. The filtered data was, then, aligned by the spliced read mappers CLC Genomics Workbench v.11 (<https://www.qiagenbioinformatics.com/products/clc-genomics-workbench/>), STAR v2.5.3a (Dobin et al., 2013) and TopHat v.2.1.1 (Kim et al., 2013), using Homo sapiens genome hg19 and Ensembl RNA database v.74 as

references. CLC Genomics Workbench alignment was conducted using the following settings: quality trim limit=0.01, ambiguity trim maximum value=2, Map to annotated reference: minimum length fraction and minimum similarity fraction=0.8, maximum number of hits/read=2, type of organism=eukaryote, paired settings=default. TopHat2 alignment, instead, foresaw these parameters: Max realign edit distance=1000, Max edit distance=2, Library Type FR=Unstranded, Final read mismatches=2, Use bowtie -n mode=No, Anchor length (at least 3)=4, Maximum number of mismatches that can appear in the anchor region of spliced alignment=0, The minimum intron length=40, The maximum intron length=2000, Allow indel search=Yes, Max insertion length=3, Max deletion length=3, Maximum number of alignments to be allowed=20, Minimum intron length that may be found during split-segment (default) search=40, Maximum intron length that may be found during split-segment (default) search=2000, Number of mismatches allowed in each segment alignment for reads mapped independently=2, Minimum length of read segments=25, Output unmapped reads=True, Do you want to supply your own junction data=No, Use coverage-based search for junctions=Yes, Minimum intron length that may be found during coverage search=40, Maximum intron length that may be found during coverage search=2000, Use Microexon Search=Yes, Do Fusion Search=Yes, Set Bowtie2 settings=No, Specify read group=No, Job Resource Parameters=No. Finally, STAR alignment was realized following these settings: outFilterMismatchNoverLmax=0.05, outFilterMatchNmin=16, outFilterScoreMinOverLread=0, outFilterMatchNminOverLread=0, alignIntronMax=1, chimSegmentMin=10.

3.2.4. Differential gene and non – coding RNA expression and statistical analysis

From previous mapping, the paired end reads were categorized and assigned to the genes, according to their abundances, using the expectation-maximization (EM) algorithm (B. Li, Ruotti, Stewart, Thomson, & Dewey, 2010), in order to determine expressions even in cases where the majority of reads map equally well to multiple genes or transcripts. Soon after, the differential expression analysis between untreated and treated samples, after 1h, 2h, 4h and 6h, was realized applying the Empirical analysis of DGE (EDGE) statistical algorithm (Robinson, McCarthy, & Smyth, 2010),

by an internal routine of CLC Genomics Workbench. It assumes that the count data follows a Negative Binomial distribution, and accounts for overdispersion caused by biological variability. Such situation fits perfectly with our data, consisting of few biological replicates available for each of the experimental group studied (only 3 replicates for each considered time point), but with many features to be studied simultaneously (genes in a genome). The genes uniquely identified in the RPE cells with at least 5 unique gene reads, showing a fold change (FC) greater than 1 (up-regulated) or between 0 and 1 (down-regulated), with Bonferroni – adjusted p-values lower than 0.05, were selected for functional categorization of differentially expressed genes. Furthermore, because the fold changes are linear, they were replaced by \log_2 values in order to make the variation more noticeable (for instance, 2-fold downregulation is indicated by a value of -1 instead of 0.5).

3.2.5. Functional gene annotations

The up- and down- regulated genes were analyzed by gene ontology (GO) (The Gene Ontology, 2017) and Kyoto Encyclopedia of Genes and Genome (KEGG) (Kanehisa, Furumichi, Tanabe, Sato, & Morishima, 2017) frameworks, and then categorized based on enrichment of CLC Genomics Workbench with InterPro (Finn et al., 2017), Reactome (Fabregat et al., 2016), Human Protein Atlas (Uhlen et al., 2017), UniProt (The UniProt, 2017), IntAct (Orchard et al., 2014), Ensembl (Aken et al., 2016) and HGNC (Wain et al., 2002) databases, which provided hierarchical relationships for the gene products distinguishing biological process, molecular function and cellular component.

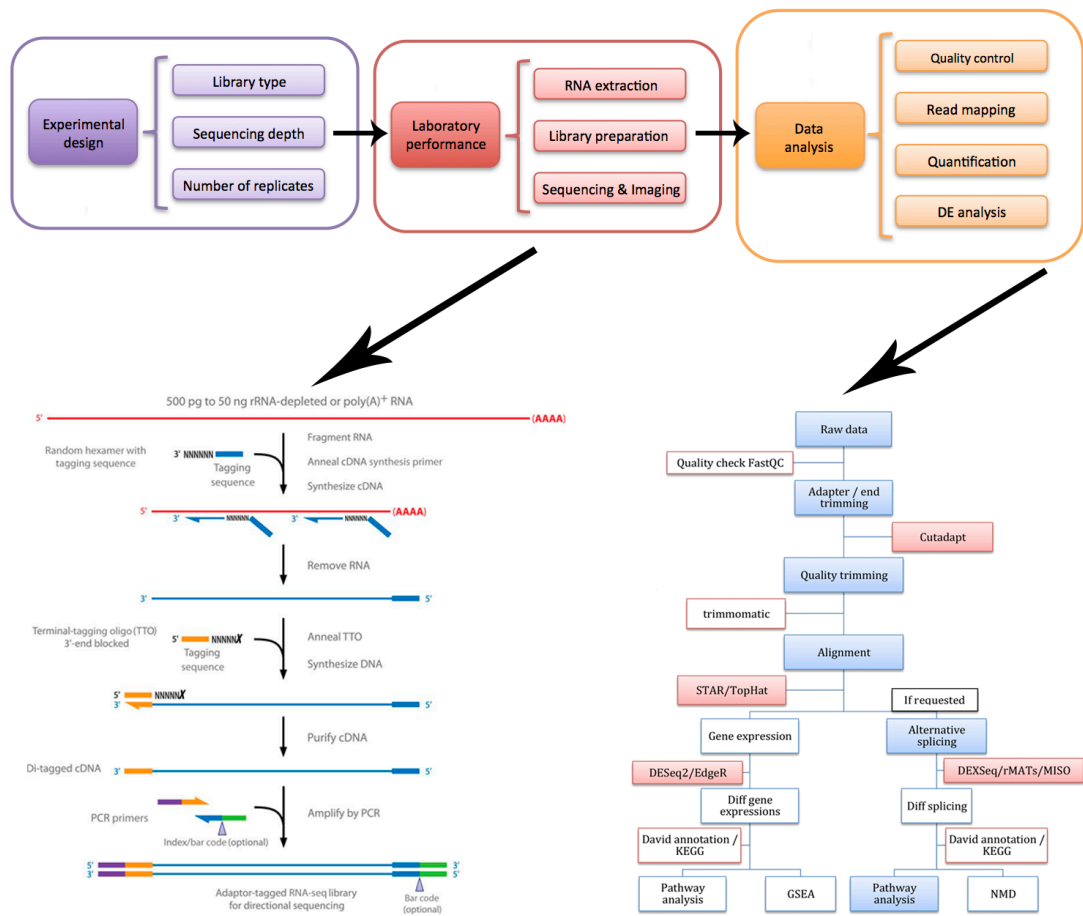


Fig. 15. RNA – Seq workflow. After “wet laboratory” phase, a huge data analysis was performed to obtain expression data. Such data analysis used also CLC Genomics Workbench software (not shown). The whole data was, finally, subjected to statistical analyses.

3.2.6. Filtering and annotation of non – coding RNAs (Fig. 14)

The applied approach counted the different types of collected non – coding RNAs and compared them to several RNA annotation databases. Once imported whole RNA – Seq data, the ncRNAs were extracted and counted, in order to create a small RNA sample that could be used for further steps. Sequences were filtered basing on length (reads between 18 bp and 200 bp were considered for small ncRNAs, reads >200 bp for long ncRNAs) and on minimum sampling count (set at 1). Subsequently, the number of reads mapping to each transcript sequence was counted by Cufflinks (Trapnell et al., 2013) and, then, normalized using either the Trimmed Mean of M-values (TMM) method (Robinson & Oshlack, 2010) or reads per million (CPM). Finally, filtered RNA pool produced when counting the tags was, then, enriched by

comparing the tag sequences with the annotation resources UCSC non-coding(Casper et al., 2018), Ensembl non –coding RNA database v.91 (Zerbino et al., 2018), iGenomes (Illumina), GENCODE v. 27 (Harrow et al., 2012), Database of small human noncoding RNAs (DASHR) v. 1.0 (Leung et al., 2016) and LNCipedia v. 5.0 (Volders et al., 2015).

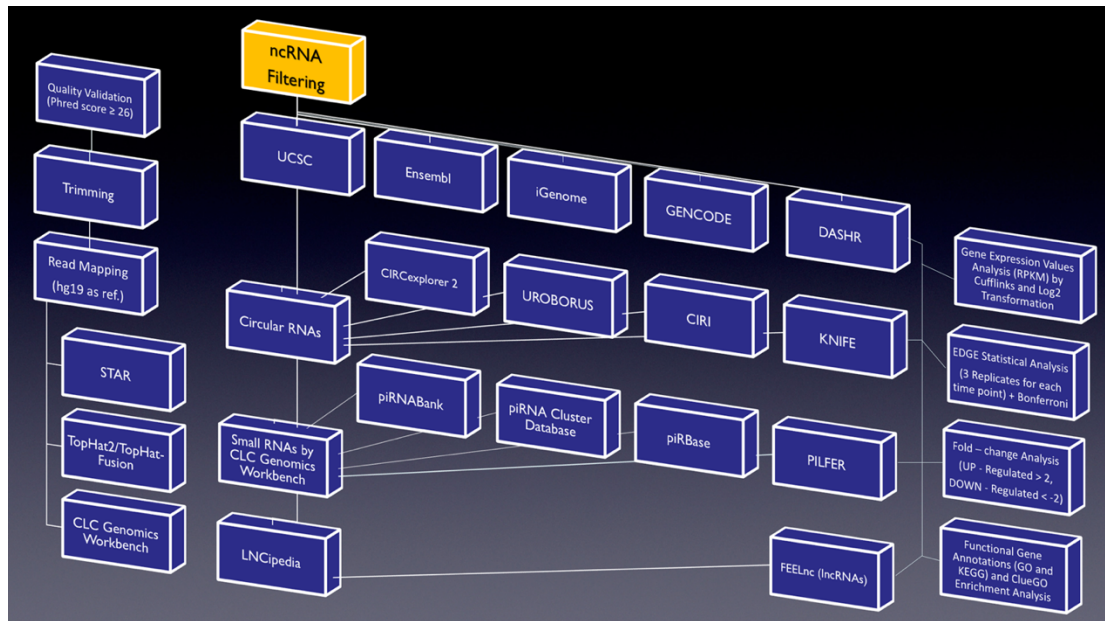


Fig. 16. Graphical workflow of RNA – Seq data analyses. The whole data analysis followed each phase represented in figure. In details, on the left is illustrated the initial transcriptome quality check, following by alignment and annotation steps. Non – coding RNA filtering and analytic pipelines, specific for circular RNAs, PIWI – interacting RNAs and long non – coding RNAs, can be found in the central block. The differential expression analysis, followed by pathway enrichment, is represented on the right side.

- Long non – coding RNA specific algorithms of analysis: reliable identification of lncRNAs interfaces are critical to understand the structural bases, functional implications and for developing effective computational methods that offers a fast, feasible as well as cost-effective way to recognize putative lncRNAs. We used the alignment-free program FEELnc (Wucher et al., 2017) that accurately annotates lncRNAs based on a Random Forest model trained with general features such as multi k-mer frequencies and relaxed open reading frames. One of the main features is given by the length of the longest open reading frame (ORF) since a transcript harboring a long ORF will most likely be translated into a protein. A complementary feature to discriminate mRNAs from non-

coding RNAs is the relative frequency of oligonucleotides or k-mer (where k denotes the size of the oligonucleotide). Some tools already use k-mer frequencies but are often limited to one and/or small k-mers (generally $k \leq 6$), whereas longer k-mers could help resolve ambiguities by considering lncRNA-specific repeats or spatial information. Based on a relaxed definition of ORFs and a very fast analysis of small and large k-mer frequencies (from $k = 1$ to 12), the program implements an alignment-free strategy using Random Forests to classify lncRNAs and mRNAs.

- ◇ Circular RNAs specific pipelines: circRNA detection from RNA-seq data is based on the analysis of sequence reads spanning the back-splice junctions generated in circRNAs biogenesis. Back-splice reads map to the genome in chiasitic order, so circRNA detection from RNA-seq reads needs specific methods for non-collinear read alignment and analysis. In order to extend and improve the quality of resulting circRNAs, we compared data from four different algorithms, each one using different approaches for circRNA identification. These strategies employ different read aligners, require variable inputs, as genome and gene annotation, and provides software-related output in term of predicted back-splice junction annotation. Specifically, in the “pseudo-reference-based”, also known as “candidate-based” approach, the putative circRNA sequences to be constructed with gene annotation data have to be provided in order to detect circRNAs. This strategy is used by KNIFE (Szabo et al., 2015), which directly constructs all the potential out-of-order exon–exon junction sequences from gene annotation information before alignment. Two other exploited algorithms, CIRCexplorer (X. O. Zhang et al., 2016) and UROBORUS (X. Song et al., 2016), followed the “fragmented-based” or “segmented read” approach, which identified backsplicing junctions from the mapping information of a multiple-split read’s alignment to the genome. In details, CIRC explorer takes advantage of spliced alignment algorithms to detect and parse the backsplicing events, while UROBORUS collects the unmapped reads after their alignment to the genome, extract the

first and last 20 bp anchors from the unmapped reads, and then obtain the backsplicing events from the mapping information of these anchors. Finally, the last used tool called CIRI (Y. Gao, Wang, & Zhao, 2015), exploited an own unique method, based on paired chiastic clipping (PCC) signals detection. Such signals come from the mapping information of reads by local alignment with STAR and are, then, systematically filtered to discharge potential false positives. We followed the instructions provided in each tool manual and focused on output circRNAs with ≥ 2 backspliced junction reads.

- Small non – coding RNA specific algorithms of analysis

- ◇ miRNAs: the aligned and selected reads were grouped on the sequence of the mature miRNAs allowing up to two mismatches within the exact length of the reference mature sequence (i.e. excluding trimming or extension variants). Subsequently, the number of reads mapping on each mature miRNA was counted and then normalized using either the already cited TMM method or CPM. Finally, the small RNA sample produced when counting the tags was, then, enriched by comparing the tag sequences with the annotation resources miRBase (v. 21), Ensembl non – coding RNA database (v.74), Genecode Release 27 and Database of small human noncoding RNAs (DASHR).
- ◇ piRNAs: reads from the samples were matched against piRNABank 84 and piRNA Cluster Database 85. The reads which mapped with at most two nucleotides short to the piRNA sequence and with at most one edit distance were filtered and annotated as canonical piRNAs. Moreover, the 26-33 nt mapped reads and all the other non-coding RNAs annotated in Ensembl were filtered out, leaving only predicted piRNAs, annotated as putative piRNAs. These piRNAs were further matched against piRBase. Finally, we used the recent cluster prediction tool PILFER (PIrnacLusterFindER) 86 to

accurately predict piRNA clusters from small RNA sequencing data, using a sliding-window mechanism by integrating the expression of the reads along with the spatial information.

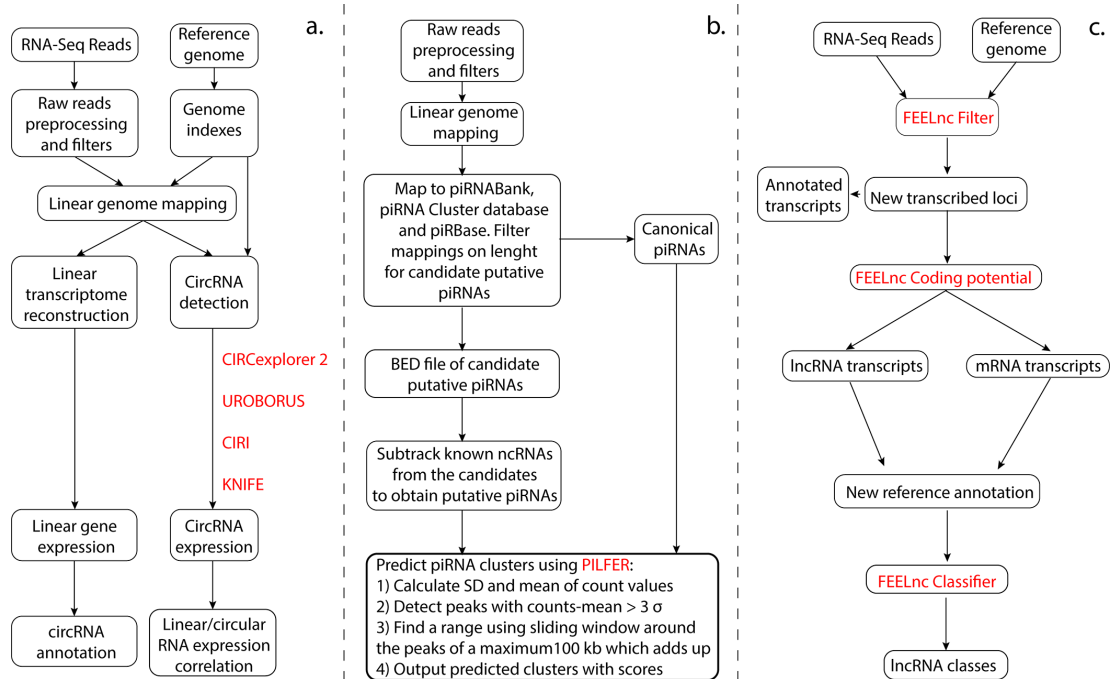


Fig. 17. Data analysis specific pipelines for considered non – coding RNAs. Each investigated non – coding RNAs was analyzed by specific bioinformatic tools (red text), each one with own selective pipelines for circular RNAs (a), PIWI – interacting RNAs (b) and long non – coding RNAs (c).

3.2.7. Coding and non – coding genes pathway analyses

- Coding gene pathway analysis.
 - ◇ Gene set enrichment analysis (GSEA): a Gene Set Enrichment Analysis (GSEA) was applied (Tian et al., 2005) to identify classes of over-represented genes, which may have an association with particular biological annotations in a large set. This algorithm considers a measure of association between the genes and phenotype of interest (e.g. test statistic for differential expression) and rank the genes according to this measure of association.

- ◇ Identification and classification of most altered pathways: our aim was to quantify the relevance of each pathway based on the evidence emerged from the folding analysis, whose information were gathered with respect to the baseline condition after one hour (1h), two hours (2h), four hours (4h) and six hours (6h) from the beginning of the experiment respectively. Subsequently, we separately considered folding distribution at each time point for all the involved genes. In order to highlight only genes whose expressions mostly changed, as realized by other authors in similar experiments (Bennis et al., 2015; S. F. Janssen et al., 2013; Y. Lin et al., 2016), a customized choice was performed. We selected those falling in the extremal 5-percentile of the distribution. By using a fixed percentage for all time-points we attempted to obtain a more robust choice that may consider both the folding magnitude and the dimensionality of the genes involved into the analysis. In the following, the 5% most changing genes at each time point were referred to as *survived*. Subsequently, for each pathway, we counted the number of survived genes at a given timepoint, thus obtaining the so-called percentage of survival. We used such percentage to rank the pathways from the most “changed” to the lowest one. A score was therefore assigned based on the ranking: for instance, if a given pathway ranked as first, since we investigate 14 pathways, a score of 14 points was assigned.

- ◇ Selection of “Master sub-pathways”: after the previous clustering based on number of genes with altered expression, which gave rise to 14 “macro – pathways”, we analyzed sub – pathways, in order to discover a more specific role of selected genes.

- ◇ Selection of single pathway “Master genes”: in order to highlight new candidate genes involved into Retinitis pigmentosa, basing on oxidative-related candidate pathways, we chose the 20 most altered genes for each one. Firstly, we considered them for each time point, then we chose the commons in all time points.

- ◇ “Master genes” functional enrichment and selection of Retinitis pigmentosa candidate genes: finally, we firstly enriched unique most altered genes (filtered in “Functional gene annotations” section) for all pathways with Cytoscape (Shannon et al., 2003) and CluePedia (Bindea et al., 2013), in order to highlight possible interactions between them and, then, intersected them with genes already known to be associated or causative of Retinitis pigmentosa (<https://sph.uth.edu/retnet/>).
- ncRNA host gene pathway analysis: GO term enrichment analysis for the most altered ncRNA host genes was performed using the ClueGO (v. 2.5.0) (Bindea et al., 2009), CluePedia (v. 1.5.0) (Bindea et al., 2013) and ncINetView (v. 1.0.2) (Bonnici, Russo, Bombieri, Pulvirenti, & Giugno, 2014) plugins in Cytoscape (ver. 3.6.1)(Shannon et al., 2003). Default parameters were used, and only GO terms with $P < 0.01$ were selected.
 - ◇ snRNA target identification and host genes pathway analysis: obtained snRNAs were firstly analyzed by the experimentally validated snRNAs database snRNABase (Lestrade & Weber, 2006), and then investigated by snRNA Orthological Gene Database snOPY web – based archive (Yoshihama, Nakao, & Kenmochi, 2013) and by Ingenuity Target Explorer (<https://targetexplorer.ingenuity.com/index.htm>), in order to define specific targets and host genes. Once obtained them, a pathway analysis of selected host genes was performed by Cytoscape and its plug in ClueGO.
 - ◇ microRNA targeting to most altered RPE expressed circRNAs: to evaluate the only characterized biological function for a neural circRNA as microRNA sponge when exogenously expressed, the computational resource CircInteractome (Dudekula et al., 2016) with most dysregulated circRNAs was exploited. This bioinformatic platform helped to search systematically for possible interactions of circRNAs with RNA – binding proteins (RBPs) and miRNAs.

3.3. FUNCTIONAL AND VALIDATION ASSAYS

3.3.1. Sanger validation and family member genotyping

Variants detected in the proband were validated by Sanger sequencing. Amplification of gene fragments with selected variants was performed using primer pairs designed according to corresponding nucleotide sequences in GenBank (the full sequence set is available upon request). The PCR mix was prepared adding 1 µg of genomic DNA to 50 µl reaction mixture containing a 0.2 µM concentration of each primer and 1 U ACCUZYME™ DNA Polymerase (Bioline).

3.3.2. Population screening

To validate the analyzed variants as disease-related, their occurrence in a group of 500 healthy subjects from Messina was defined.

3.3.3. Data validation by qRT – PCR

To confirm the transcriptome results, we selected twenty most dysregulated mRNAs, ncRNAs and miRNAs to be validated by qRT-PCR. Reverse transcription was carried out according to the manufacturer's protocol of GoScript™ Reverse Transcription System (Promega, USA). The obtained cDNA was subjected to the RT-PCR in the ABI 7500 fast sequence detection system (Applied Biosystems, Foster, USA), using BRYT-Green based PCR reaction. PCR amplification was performed in a total reaction mixture of 20 µL, containing 20 ng cDNA, 10 µL 2 × GoTaq1qPCR Master Mix (Promega, USA) and 0.2 µM of each primer. PCR was run with the standard thermal cycle conditions using the two-step qRT-PCR method: an initial denaturation at 95°C for 30 s, followed by 40 cycles of 30 s at 95°C and 30 s at 60°C. A little difference has to be highlighted about predicted circRNAs, whose expression was accessed by using divergent primers in qPCRs, amplifying the circle without amplifying the genomic regions. Additionally, samples were treated with RNase R to

decrease the amount of linear RNAs. Each reaction was run in triplicate, considering all selected time points (1h, 2h, 4h, 6h), and the average threshold cycle (Ct) was calculated for each replicate. The expression of mRNA was calculated relative to expression level of endogenous control β -actin (Glyceraldehyde3-phosphate dehydrogenase -GAP DH- for ncRNAs and U6 for miRNAs), and the relative expression of gene was calculated using the $2^{-\Delta\Delta Ct}$ method. The correlation of the fold change of the gene expression ratios between qRT-PCR and RNA-Seq was checked by linear regression analysis in IBM SPSS 25.0 software.

3.3.4. Dual luciferase assay (Fig. 15)

- *Cell culture*: U373 MG (human, Caucasian, glioblastoma-astrocytoma) cells (Sigma – Aldrich) were cultured in Dulbecco’s modified Eagle’s medium (DMEM) supplemented with 10% fetal bovine serum (FBS), 100U/ml penicillin and 1mg/ml ampicillin (Lonza) at 37°C in a water-saturated atmosphere with 5% CO₂. The essential feature that led us to choose this cell line was the acquisition of infinite growth potential, which set the stage for multiplication of genetic variants with an ever-increasing fitness for proliferation and spread. A glioblastoma cell line was used to perform another dual luciferase assay, involving cerebral cavernous malformations (Scimone et al., 2016). This cell line can be useful because the retina has a nervous derivation as glia. Despite this, the tumoral nature of glioblastoma cells could correctly lead to think that the whole transcription factors set is totally different from that normal cells. In order to clarify this point, several supporting evidence could be addressed: almost all TFs coming from our in silico analysis result expressed both in glioblastoma cells and retina cells, as evidenced by DPRP database (Tzeng et al., 2014), based on expression and ChIP-Seq experimental data, and TiGER (X. Liu, Yu, Zack, Zhu, & Qian, 2008). Moreover, description of common TFs was reported among others also by Rheinbay E. et al 2013 and Mysickova A. et al. 2012 (Rheinbay et al., 2013).

- Construction of the reporter gene plasmids: in order to highlight if the variants could affect *ELOVL4* expression, the effects of two combined genotypes, c.-236T/c.-90C (T-C) and c.-236C/c.-90C (C-C), were studied on promoter activity. 805 bp promoter sequence was amplified by PCR using genomic DNA from the proband and one donor, selectively carrying each haplotype, using the primers shown in Table 3, under the following conditions: 1 cycle of 95°C for 1 min; 35 cycles of 95°C for 15 secs, 49.5°C for 15 sec, and 72°C for 10 sec; and 1 cycle of 72°C for 7 min. Each PCR product, as well as pGL4.10 (*luc2*) was digested by *BglIII* and *HindIII* (Promega) and then purified (PureLink™ PCR Purification Kit, Life Technologies). Each promoter and pGL4.10 (*luc2*), digested and purified, was incubated overnight in appropriate concentrations, in order to execute ligation. The efficiency of promoter insertion upstream of the luciferase gene, cloned into the pGL4.10 (*luc2*), was verified by agarose gel electrophoresis. Novel constructs were subcloned into E. coli Top 10 cells (Life Technologies) and single colonies were miniprep. The correct sequence of all the clones was verified by DNA sequencing, using the Sanger method, and then selected for transient transfection.
- Transient transfection and promoter assays: cells were first seeded in 96-well culture plates at a density of 2×10^4 cells per well. Then, a transient transfection was performed with following modality: 1) in 1/4 of wells (16), cells were co-transfected with 0.05 µg of the pGL4.10 [*luc2*] promoter construct containing the only c. -90 G>C variant, and with 0.05 µg of the pGL4.10 [*luc2*] promoter construct containing the ELOVL4 wild-type promoter; 2) in a second 1/4 of wells (16), cells were co-transfected with 0.1 µg of the pGL4.10 [*luc2*] promoter construct containing only the c. -236 C>T variant, and with 0.05 µg of the pGL4.10 [*luc2*] promoter construct containing the ELOVL4 wild-type promoter; 3) in another 1/4 of wells (16), cells were co-transfected with 0.05 µg of two pGL4.10 [*luc2*] promoter constructs containing, respectively, the c. -90 G>C and the c. -236 C>T variants; 4) in the final quarter of wells (16), cells were transfected with 0.1 µg of the pGL4.10 [*luc2*] promoter construct containing the ELOVL4 wild-type promoter. Finally, the remaining 32 wells were filled with not transfected cells (16) and with the luciferase substrate only

(16). In each well, besides cells, the mixture included 0.2 μ l of Lipofectamine™3000 Reagent (ThermoFisher Scientific) and 0.2 μ l of P3000™Reagent, in a serum-free medium and then incubated for 24 h at 37°C in a humidified atmosphere of 5% CO₂ in air. After incubation, cells were washed twice with PBS and lysed by Passive Lysis Buffer (Promega). Luciferase activity was measured using Dual-Luciferase assay kit (Promega) and GloMax-Luminometer (Promega). Reporter construct activity was normalized by comparison with activity from the *Renilla* luciferase construct. Luciferase activities are representative of at least six independent experiments, with each construct tested 16 times per experiment. All data analyses were performed using the IBM SPSS 25 software. A one-way analysis of variance (one-way ANOVA) was performed to compare between the sample groups. All p-values were Bonferroni's corrected and considered significant if $p < 0.05$.

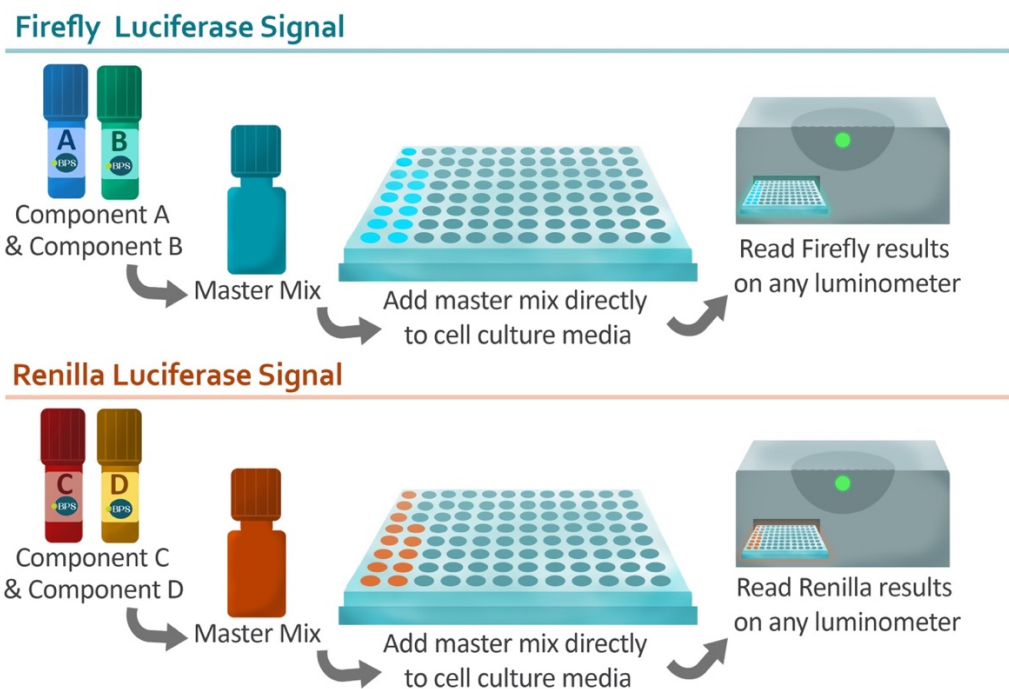


Fig. 18. Dual luciferase assay workflow. In the Dual-Luciferase® Reporter (DLR™) Assay System, the activities of firefly (*Photinus pyralis*) and Renilla (*Renilla reniformis*, also known as sea pansy) luciferases are measured sequentially from a single sample. The firefly luciferase reporter is measured first by adding Luciferase Assay Reagent II (LAR II) to generate a stabilized luminescent signal. After quantifying the firefly luminescence, this reaction is quenched, and the Renilla luciferase reaction is simultaneously initiated by adding Stop & Glo® Reagent to the same tube. The Stop & Glo® Reagent also produces a stabilized signal from the Renilla luciferase, which decays slowly over the course of the measurement.

4. RESULTS

4.1. GENOMICS

4.1.1. Combined effects of known variants in genes still not associated to RP

Affected members of the fourth family described in 3.1.1 underwent whole genome sequencing analyses. WGS was initially performed on the proband (Fig. 1, II3), then on her 3 sons, using 3 chips for each one on an Ion Torrent Proton instrument. In total, 72,372,728 single-end reads (mean read length ~ 118 bp) were generated for proband's genome, and a mean of 79,001,234 for her sons. About 99% of all genome reads mapped, reaching an average depth of ~259 fold for mitochondria (MT) and an average quality score (Phred score) per read near 30, which allowed us to identify SNPs and new mutations. A total of 20,306 variants, including 17,501 SNVs and 2,805 InDels were identified throughout the whole proband's analyzed genome, while a mean of 21,822 variants, of which 19,231 and 2,591 InDels, were detected in sons' genomes, all resisting quality and homopolymeric filters. According to functional effects, eye localization and ocular disease affinity, 32 candidate pathogenic variants, distributed within 8 genes, were categorized as new missense and UTR mutations (Group 1); missense, nonsense, and inframe SNPs (Group 2); splice-site and UTR regulation site SNPs (Group 3); and synonymous SNPs (Group 4). All the identified variants were validated by Sanger sequencing and genotyped in all family members. Afterwards, several filtering pipelines were applied to obtain the final candidate variants (represented in Table 4):

- *Preliminary pathway analysis:* a preliminary pathway analysis conducted by Cytoscape and its GeneMANIA plug-in revealed that relevant genetic and physical interactions connect almost the entire set of analyzed genes, suggesting a common involvement in multiple pathways. To determine to which pathways the selected eight genes belong to, we examined the GO, KEGG, Reactome, and WikiPathways annotations, using the ClueGO plug-in. The results were then clustered with STRING interaction categories. Subsequently, the analyzed genes were grouped into four hierarchically

structured GO terms: Biological Process, Cellular Component, Molecular Function, and Immune System Process; this was in addition to the already mentioned KEGG, Reactome, and WikiPathways. Then, the same genes, based on eye and vision relationship of related encoded proteins, were subcategorized into 87 main hierarchically structured GO classifications, including 59 biological processes, 13 cellular components, 4 immune system processes, and 11 molecular functions. Two KEGG pathways, 12 Reactome pathways, and 2 WikiPathways emerged from analysis. The overall results indicated that the identified genes belonging to these GO categories may play the most important roles in regulation of eye/retina development, homeostasis and functionality, especially in synaptic activities and ciliary transport.

- *Data mining and statistical analysis*: once established that the analyzed genes were involved in common eye related pathways, it was necessary to determine the genotype – phenotype association with the pathology. Additive, dominant, and recessive genetic models were compared. The additive model implies that the risk conferred by an allele is increased 1r-fold for heterozygotes and 2r-fold for homozygotes; the recessive model compares groups with homozygous genotypes vs the rest, combining heterozygotes for the variant and homozygotes for the wild-type allele; and the dominant model, compares wild-type homozygous genotypes vs allele positivity, combining heterozygotes and homozygotes for the variant. Variant genotypes in all family members were, then, analyzed and the only variant with different distribution between healthy and sick subjects was *CACNG8* rs66507429:A>T. This observation was statistically confirmed by Fischer exact test, which associated the variant to disease (p-value=0.040). However, these data did not suffice to explain the wide spectrum of different RP phenotypes. Therefore, it could be reasoned that additional variants may play a role in the unknown RP form described here. To discriminate phenotypes, variants were associated to clinical symptoms, which were quite varied in the affected family members:

- I. irrelevant differences between affected and unaffected groups ($-0.05 \leq d < 0.05$);

- II. low differences between groups, likely having a pathogenic, causative role ($0.05 \leq d < 1$), or a protective role ($-1 < d \leq -0.05$) against symptom manifestation;
- III. big differences between groups, linked to stronger evidence of a pathogenic, causative ($d \geq 1$) or protective ($d \leq -1$) role against symptom manifestation.

According to these analyses, it resulted that *CACNG8* rs66507429:A>T departs two standard deviations from the median, while the other eight genes (*PAX2* rs7094977:C>A, *RXRG* rs283696:A>G, *CCDC175* rs7141565:C>G and c.76 C>T, *PDE4DIP* rs141564171:G>A and c.*105 G>A, *LTF* rs1126477:G>A and rs1126478:A>G) fall between one and two standard deviations from the median. No other significant differences were observed for the other variants. These results led to the idea that the heterogeneity of the phenotypes could be determined by the above variants, differently distributed amongst the family patients. Moreover, to highlight the similarity of family components, a clustering based on all variant genotypes and symptom distribution was performed, with a cut-off of 70% and 80% respectively, which revealed that the proband and two sons (IV1 and IV2) cluster together genetically, as (IV3 and V1), while common clinical findings are found for II3, III1, IV3, IV5 and V1, who appear healthy.

- Population screening: based on Exome Variant Server (<http://evs.gs.washington.edu/EVS/>), for all the variants identified, minor allele frequency (MAF) was at least 5% in all populations assayed. To determine the frequency of selected variants within the population of Messina, a population screening was performed, considering an unrelated healthy donor group (n = 100) born and living in Messina for at least two generations. In detail, especially for *CACNG8* rs66507429:A>T and *CCDC175* c.76 C>T, the survey revealed a very low frequency distribution, with the latter was totally absent in unaffected people.
- Pathway functional enrichment: finally, to clarify the interaction between the 10 analyzed markers, and to determine their role in as yet undescribed “eye-

related” pathways, a CluePedia enrichment analysis, based on public available data from STRING and miRANDA, was performed. Ninety-three terms were connected by 247 edges (activation, binding, catalysis, expression, inhibition, ptmod, reaction) with the kappa scores, and showed relevant enrichment ($p < 0.05$) in the identified protein interactome. By CluePedia Cerebral plug-in layout (Barsky, Gardy, Hancock, & Munzner, 2007), which automatically extracts the cellular location of markers from GO terms and maps it on pre-defined cellular compartments, it was possible to establish that most of the protein encoded in the 8 genes are located in intracellular compartments, with only one (LTF) that could be extracellular and one (CACNG8) that could act at the plasma membrane level. By using the miRANDA database we showed that from 2 to 9 miRNAs could regulate gene expression of each analyzed gene. These data were supported by the PolymiRTS Database, which indicates that the presence of *CACNG8* rs66507429:A>T and *PDE4DIP* rs141564171:G>A could create or disrupt several miRNAs target sites.

or associated variants were found. According to pathway analyses conducted by Cytoscape and its plugins GeneMANIA and ClueGO, which highlighted functional effects, eye localization and ocular disease affinity, 15 candidate pathogenic variants, distributed in 6 genes (*EYS*, *PPEF2*, *RNF144B*, *RDH13*, *FLT3* and *MYO7A*), were selected. These genes resulted linked to each other in co-expression, co-localization, genetic and physical interactions networks, suggesting a possible involvement into common pathways. The ClueGO analysis permitted to discover these metabolic and biochemical ways, principally represented by photoreceptor cell development and detection of light stimulus involved in visual perception, then subcategorized into 37 hierarchically structured GO classification. Corroborated by these data, all chosen variants were validated by Sanger sequencing. Finally, because all analyzed variants consisted of intronic polymorphisms, we predicted a possible involvement into splicing, due to a potential alteration determined by their presence into corresponding genes. The bioinformatics web – based platform Human Splicing Finder highlighted the alteration of several ESE (exonic splicing enhancer) and ESS (exonic splicing silencers) sites, as well as of branch points hypothesizing, therefore, a possible modifying role in the splicing process (Table 5). This strategy was realized in order to support an involvement that can appear risky but which could be decisive.

GENE		EYS				RNF144B				RDHL3				POTENTIAL SPLICE SITES		BRANCH POINTS		ENHANCERS MOTIFS (ESS)	SILENCERS MOTIFS	OTHERS
VARIANT		rs149849078		rs71638759		rs112160251		rs1886248		rs2569514		rs2569513		Splicing Site Type (HFS)		N° of Potential Altered Branch Points		ESE Variations for SRP40, SC35, SF2/ASF and SRP55 proteins (%) and New/Broken ESE Sites	PESS Octamers, Fas and IIIEs from Zhang Algorithms	Exonic Splicing Regulatory Sequences from Goren et al.
		2 Acceptors (+)		2 Acceptors (+) 2 Donors (-)		/		2 Acceptors (-) 2 Donor (+)		/		/		1 Donor (-)		Average Variation (%)				
		9.37		+16 and -62		/		+62 and -1		/		/		-3.6		250/-55				
		-616		-400		/		-397		/		/		-397						
		3' Motif = 4 Changed		5' Motif = 1 Changed		/		5' Motif = 2 Changed		/		/		3' Motif = 1 Changed						
		-468.82		-488.11		/		-234.71		/		/		-3128.13						
		19 New 17 Broken		14 New 12 Broken		9 New 9 Broken		/		/		/		16 New 16 Broken						
		350/-70		450/-75		350/-55		/		/		/		250/-55						
		+13 and 1 Site Broken		+12 and 3 Broken/3 New Sites		-9 and 1 Broken Site		-13 and 1 Broken/3 New Sites		+8 and 1 Broken Site		/		+10						
		7 New/3 Broken Sites		4 Broken Sites		/		4 New Sites		1 New Site		/		3 New/14 Broken Sites						
		1 Broken Site		1 New/3 Broken Sites		1 New/3 Broken Sites		3 New Sites		/		/		3 Broken Sites						

Tab. 5. Splicing motifs prediction of deep intronic variants. Scores from algorithms applied to deep intronic variants splicing analysis.

Furthermore, a case-control study on the 80 RP patients came to our attention and 120 healthy controls from Sicilian population was performed, in order to evaluate the

possible association between several polymorphisms in *GLO1* (already studied in association with autism, multiple sclerosis, cerebral cavernous malformations and type 2 diabetes complications, like retinopathy) and RP disease (still uninvestigated). Analyzed polymorphisms in *GLO1* gene (rs2736654, rs1049346 and rs1130534), resulting in differences in antioxidant activity, could contribute to increase the damage from oxidative stress observable in the cones in the retina after rod degeneration. Genotypic and allelic frequencies of *GLO1* c.A372T, c.A332C and c.-7C>T gene polymorphisms in control subjects and RP patients are given in Table 2. All polymorphisms were in Hardy Weinberg equilibrium (cut off= $p < 0.05$), and following results consider the Bonferroni corrected p – value cutoff of 0.017. With regard to rs1130534 polymorphism (c.372A>T), frequency of T allele was 112 (70.0%) and 136 (60.0%) in the RP patients and control population respectively, which is near to be significantly different ($p=0.0213$; $\chi^2= 7.2439$; CI 95%= 1.17 - 2.73). Conversely, the genotypic frequencies of c.372A>T was not found significantly different ($p= 0.2877$; $\chi^2= 4.6886$). In rs2736654 (c.A332C) polymorphism genotypic and allelic frequencies were not significant among patients and controls. Different trend was observed for rs1049346 (c.-7 C>T) polymorphism. The prevalence of -7T allele was significantly higher in controls (70%; $\chi^2=51.7094$; $p=1,931e-12$) than in patients. Moreover, CT (53%) and TT (40%) genotype frequencies in controls were found to be higher in comparison to patients showing significant difference ($\chi^2=68.0952$; $p=4.902e-15$). Linkage disequilibrium (LD) calculations revealed strong linkage disequilibrium between the rs1130534 (c.372A>T) and rs2736654 (c. A332C) polymorphisms. A total of six haplotypes resulting from the three *GLO1* polymorphisms was observed in both RP patients and healthy controls (Table 6). The frequency of AAT (++-) (rs1130534- rs2736654-rs1049346) haplotype was significantly higher in controls (30%) than in RP patients (15%). Same trend was observed for TCT (---) and TAT (-+-) haplotypes. In particular this last was absent in patients and its frequency in controls group was 3%.

Haplotype	Controls	Patients	p-value	ODDS Ratio	CI 95%	P-Fisher
AAT (++-)	36 (30%)	12 (15.0%)	2.691e-7	0.2222	0.12 - 0.40	2.761e-7
AAC (+++)	16 (13.3%)	12 (15%)	0.0334	0.5000	0.26 - 0.95	0.0362
TCC (--+)	24 (20%)	36 (45%)	1.0000	1.0000	0.60 - 1.68	1.0000
TCT (---)	40 (33.3%)	12 (15%)	2.560e-8	0.2000	0.11 - 0.36	2.238e-8
TAT (-+-)	4 (3%)	0	0.0009	0.0394	0.00 - 0.70	0.0010
TAC (-++)	0	8 (10%)	0.0017	22.0759	1.29 - 376.69	0.0006

Tab. 6. Haplotype frequencies of *GLO1* polymorphisms in healthy controls and RP patients.

4.1.2. Combined effects of known variants and haplotypes in Stargardt disease causative genes

The entire genotype tree of the first analyzed family in 4.1.1 is reported in Fig. 11. Regarding the proband, a wild-type condition for rs444772 (c. 2623, G>A) and for three SNPs of *RPI* “hot-spot” region in exon 4 was reported (El Shamieh et al., 2015): rs446227 (c. 5008 G>A), rs414352 (c. 5071, T>C) and rs441800 (c. 5175, A>G). In contrast, there is a homozygous mutated condition regarding the other two *RPI* SNPs, rs2293869 (c. 2953 A>T) and rs61739567 (c. 6098, G>A). The proband’s wife, instead, shows an opposite situation, a homozygous mutated condition for the first four SNPs analyzed in her husband, while the last two were wild-type. Their daughter, as expected from parents’ genotypes, shows a heterozygous condition for all examined SNPs. Regarding the *ABCA4* gene, the proband shows a wild-type condition for rs3112831 (c. 1268, A>G), while his wife and daughter are both heterozygous. A search for Pfam domains on a *Abca4* mutated protein sequence was performed, against a wild sequence using CLC Genomics Workbench. The Pfam database, a large collection of protein families, each represented by multiple sequence alignments and hidden Markov models (HMMs), was used to obtain the results. The rs3112831 implies that one of two TMD domains starts from aa 515 instead of 513 of the wild type, altering the recognition site of protein substrate (ATR or NR-PE). The hypothesis was that *RPI* homozygous mutations found in the proband could be responsible for his phenotype. His wife, instead, although carrying a triple homozygous in the “hot-spot” region of *RPI*, normally associated with retinitis pigmentosa pathology (El Shamieh et al., 2015), is only mildly affected. Regarding *ABCA4*, she is carrying the c. 1268, A>G in heterozygosity. The non-affected daughter, inherited a condition of

heterozygosity for all analyzed variants of both genes, manifesting no typical symptoms of retinal pathologies in exam. Online genetic databases (EMBASE, ENSEMBL and PUBMED) report found mutations as polymorphisms. The Human Gene Mutation Database (HGMD) classifies two of them (c. 5008G>A for *RPI* and c. 1268A>G for *ABCA4*) as disease-causing mutations with a question mark (DM?), denoting a probable/possible pathological mutation, reported to be pathogenic in the corresponding report, but where the author has indicated that there may be some degree of uncertainty. The c. 5008G>A, present in wild type condition in the proband, implies the change of an alanine in position 1670 with a threonine implemented by this variation and represents a regulatory region modification, due to its location in a promoter flanking region. As with other *RP1* analyzed SNPs, it would appear to be implicated in retinitis pigmentosa phenotype of Chinese (Sheng et al., 2008; D. Y. Wang, B. J. Fan, et al., 2005; X. Zhang et al., 2010; X. Zhang, Yeung, Pang, & Fu, 2002) and Indian (Gandra et al., 2008) populations, as well as associated as a member of the “hot-spot” high causative region of *RP1* (Schwartz et al., 2003). The c. 1268A>G, also found in the wild type condition in the proband, represents a missense variation, which changes the histidine in position 423 with a proline, is located within a regulatory region, showing enhancer features, involving one of two transmembrane domains (TMD). It was regarded as a polymorphism found in heterozygosity in 101/440 controls in a comprehensive survey of sequence variation in the *ABCA4* of a German population (Rivera et al., 2000). The same variant results as a high-penetrance disease-causing mutation in a cohort of patients with Stargardt disease in a study from 2004 (Oh et al., 2004), and as a reducing risk factor more recently, also in a heterozygous model (Aguirre-Lamban et al., 2011; Brion et al., 2011; Webster et al., 2001). Bioinformatic software predictions (Sift, PolyPhen 2, PROVEAN), analyzing non-synonymous coding SNPs effects on protein function, give this mutation the status of tolerated or neutral. Furthermore, literature reports the c. 1268, A>G as associated to late-onset Stargardt disease (Yatsenko, Shroyer, Lewis, & Lupski, 2001), to macular degeneration (Baum et al., 2003) and to retinitis pigmentosa (Valverde et al., 2007), depending on severity of symptoms manifested. Despite all these studies, the phenotype associated with this *ABCA* variant is not clear. According to our hypotheses, the c. 1268A>G missense variant may play a protective role against the damaging *RP1*

“hot–spot” region variants in syndromic retinitis pigmentosa. These findings suggest that, in this family case, the variant examined leads to an asymptomatic visual phenotype, without any typical features of Stargardt disease or syndromic retinitis pigmentosa. Our data are corroborated by the genetic and phenotypic (only a slight reduction of sensitivity on peripheral areas) condition of the proband’s wife and daughter (the latter without any typical or atypical symptomatology), suggesting the likely delaying effect of analyzed polymorphisms regarding pathology onset. Obtained results suggest that *Rp1* and *Abca4* could interact, directly or indirectly, in order to extend the half–life of photoreceptors. In particular, it could be speculated that the missense variant 1268A>G of *ABCA4* induces a misfolding into encoded protein, which decreases the transport of ATR/NR-PE and, consequently, a lower quantity of PE from disc membranes is consumed in spontaneous adduct formation with ATR. This renewed stability of disc membrane lipids could compensate for the lack due to *RPI* homozygous mutation in the “hot–spot” region, which results in a misfolded protein unable to guarantee the correct stacking of discs and, above all, proper lipid transport from the inner to the outer segment, in order to build new functional discs.

Furthermore, genotyping of *ELOVL4* promoter in the whole components of the fifth family in 4.1.1 section highlighted that the proband’s mother and father present an alternate heterozygosity for each variant in exam (Fig. 11), indicating that the proband has inherited both variants in trans. The predictive analysis of the proband’s *ELOVL4* promoter by TRANSFAC Professional evidenced the loss of one group of TF binding sites (ETF, ZF5, E2F-6, FBI-I, HDAC2 and TAFII250) in the double heterozygous genotype, due to the presence of c. -90 G>C for most of them. The exception was represented by FBI-I and the complement 666...679 binding sites for TAFII250, whose deprivation was attributable to c. -236 C>T. A second group analysis, resulting from the combined predictions of TRANSFAC and PROMO, revealed the appearance of new possible binding sites of different TFs (CPB, BCL6B secondary motif, Spi-B, Pax-4, RXR-alpha, GKLF, POLR3A, TFII-I, Pax-5, p53, SP1 and GR-alpha), determined by c. -236 C>T for Spi-B, Pax-4 and RXR-alpha, and by c. -90 G>C for others. This data suggest a probable transcription variation, due to the altered balance of TF binding properties. Furthermore, it is important to understand the relationship between the analyzed TFs, and how each one could influence the others. This was

examined by Cytoscape pathway analysis, along with its MCODE plug-in, from which arose a 4-cluster division that highlighted a relevant network involving most of the TFs in exam. The confirmation of this data has been demonstrated by the experimental study with the Dual-Luciferase® Reporter Assay, involving the proband's *ELOVL4* promoter, compared in its wild form, versus both variants and c. -90 G>C and c. -236 C>T only samples. Results from this experiment showed an expression reduction of about 14% in the c. -90 G>C sample and of about 18% in the c. -236 C>T one (compared to a healthy control), but a strong decrease (about 97%) arose from the promoter carrying the combination of above variants (Fig. 19). The one-way ANOVA, after Bonferroni's correction, confirmed the statistical significance of analysis ($p < 0.05$). Examined results play an even more important role because both analyzed variants showed a very low frequency distribution in Messina healthy population (c. -90 G>C: G frequency = 0.94, C frequency = 0.06; c. 236 C>T: C frequency = 0.95%, T frequency = 0.05), in contrast to what has been analyzed in the European population (http://www.ensembl.org/Homo_sapiens/Variation/Population?db=core;r=6:7994686-9-79947869;v=rs62407622;vdb=variation;vf=12792675; http://www.ensembl.org/Homo_sapiens/Variation/Population?db=core;r=6:79947015-79948015;v=rs240307;vdb=variation;vf=129670).

SAMPLE	c. -90 G>C	C. -236 C>T	c. -236 C>T c. -90 G>C	Control	Not Transf. Cells.	Substrate only
MEAN	2,262	2,040	0,810	2,502	0,773	0,772
SD	0,045	0,040	0,063	0,049	0,046	0,010
SEM	0,011	0,010	0,016	0,012	0,011	0,002

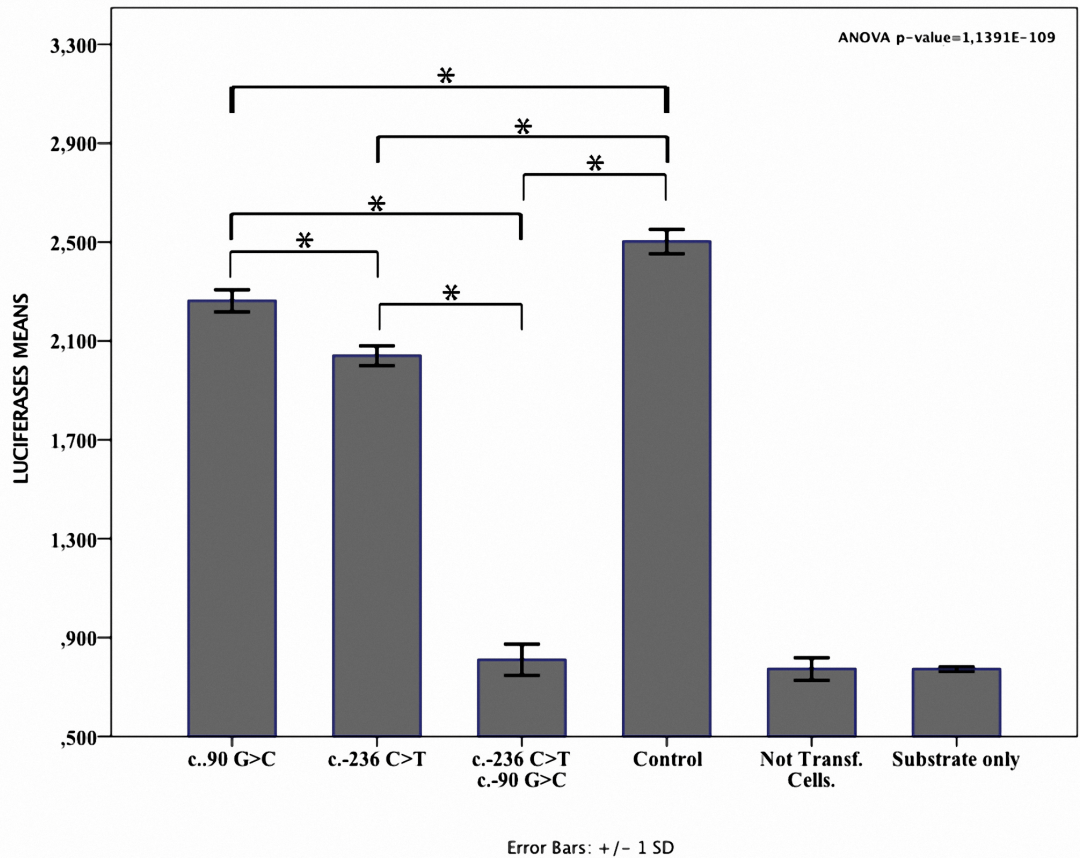


Fig. 19. Dual luciferase assay results. The histogram shows the means coming from luciferase ratios between Firefly and Renilla bioluminescence measurements (in relative luminescence units - LRU) for each sample. As reported, ANOVA test resulted significant ($P = 1.1391 \times 10^{-109}$), also for multiple comparisons (highlighted with pairwise lines on bars and asterisk). The presence of only the c.-90 G>C or the c. 236 C>T variant determines an ELOVL4 expression reduction, respectively, of approximately 14% or 18%, compared with the healthy control, while the heterozygous condition for both examined variants drastically lowers it (~97%).

4.1.3. Novel mutations in already known RP causative genes

Direct sequencing of all known RPA causative genes *LRAT*, *RDH5* and *RHO* in 4.1.1 third family showed no significant variants. Two SNPs rs390659 (c.910C>G, p.Q304E) and rs434102 (c.1013A>G, p.D338G) were detected in *PRPH2*; however, in ClinVar database these are reported as benign (<http://www.ncbi.nlm.nih.gov/clinvar/variation/138904/>, <http://www.ncbi.nlm.nih.gov/clinvar/variation/138906/>). A novel single base-pair frameshift deletion, the c.398delC (p.P133Qfs*258), was detected in exon 6 of *RLBP1* gene in a homozygous

condition. It is not present in mutations and SNPs databases as HGMD, dbSNPs, ClinVar, ExAC, Ensembl. The variant leads to substitution of proline 133 in glutamine and results in a frameshift with consequent premature termination at the 258th codon, in exon 8, causing the loss of the last 60 amino acids at the C-terminus of the protein. As evident by in – silico prediction, the c.398delC results in total disruption of functional domain as well as in an altered folding. About other family’s members, the novel mutation was observed in both parents, in heterozygous condition and was absent in the sister. Moreover, mutated allele was found both in paternal and in maternal relatives. Moreover, as previously described, *RLBPI* mutations are very uncommon and founder mutations were reported. Frequency of c.398delC allele was assessed in both Fiumedinisi and Sicilian population. In the first group the mutated allele was detected in 0.01%, while none of screened samples of general Sicilian population showed the variant. Table 7 shows distribution of alleles frequencies in Fiumedinisi population; χ^2 test results in a p-value = 0.9306 showing the condition of HWE (HWE not consistent for p<0.05).

	Samples	Allele +	Allele -	Observed Frequency	%	HW - Expected Frequency	%	Chi-square	p-value
+/+	297	594	0	297	99.00	297.01	99.00	0.000	
+/-	3	3	3	3	1.00	2.99	1.00	0.000	
-/-	0	0	0	1	0.00	0.01	0.00	0.008	
Total	300	597	3	300	100.00	300.00	100.00	0.008	0.9306
	600	1.00	0.01	600				(p-value) Chisq w 1 df	

Tab. 7. Wild-type (+) and c.398delC (-) alleles frequencies in Fiumedinisi population. A total of 300 samples were genotyped. Only 0.01% of screened population carries the mutated allele. Chi-square test exhibits a p-value = 0.9306 suggesting the presence of the equilibrium’s condition between wild-type and mutated allele in Fiumedinisi population.

4.2. TRANSCRIPTOMICS

4.2.1. *Expression changes in RP candidate genes caused by oxidative stress*

RNA sequencing of RPE stressed cells described in 4.2 section carried out on Ion Proton™ Torrent yielded an average of 11,214,300 quality reads (mean mapping quality=32.92) with mean read length of 155.03 nt. Out of 7,569,891 counted fragments, 6,518,196 reads mapped uniquely whereas 1,051,695 reads mapped nonspecifically with reference genome. A total of 16,799 genes were identified out of 20,805 reference coding genes of human transcriptome. The annotated reference assembly (GRCh37/hg19) was downloaded from Ensembl genome browser (http://grch37.ensembl.org/Homo_sapiens/Info/Annotation). All previous mapping statistics were based on average values calculated for all three replicates in each time point.

- *Analysis of gene expression profile of RPE cells:* in analyzed transcriptome study, 16,799 genes were expressed with RPKM values ≥ 0.50 , considered as average value per sample. The original expression values were normalized in order to ensure that samples were comparable (Allison, Cui, Page, & Sabripour, 2006). Up – regulated genes number raises from 2010 after the first hour of treatment to 3276 at 6h, while down – regulated ones decrease from 900 in the first observation time point to 526 at final observation stage. As evidenced by hierarchical clustering of features (Fig. 20), several groups of genes changed their expression profiles between untreated and treated ones, exhibiting a strong statistical significance.

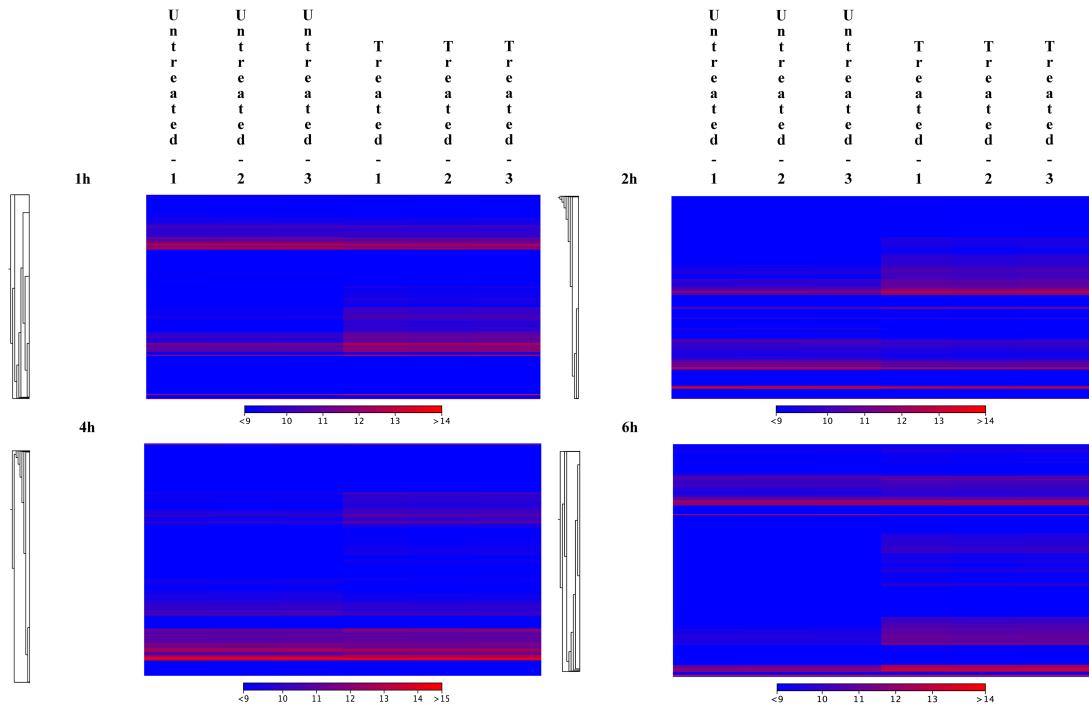


Fig. 20. Hierarchical clustering of features (all significant genes). Fig. 20 represents a hierarchical tree view with associated heatmap, a representation of the similarity in expression profiles of selected genes (rows) over a set of untreated and treated groups (columns), based on Euclidean distance and single cluster linkage. The color in the i 'th row and j 'th column reflects the expression level of feature i in sample j (the color scale is shown under each plot). The order of the rows in the heatmap are determined by the hierarchical clustering, while the order of the columns (that is, samples) is determined by their experimental grouping. As evidenced by all heatmaps in this fig., almost all pathways (taken together or individually) show many different patterns, represented by rectangular areas of about the same color. That suggests a group of genes that is correlated for the corresponding group of samples, changing in their expression profiles.

- Functional annotation of RPE expressed genes (GO + GSEA Analysis): gene annotation of GO terms, combined with statistical analysis of GSEA, resulted significant (p value < 0.01) for all 569 analyzed categories. The most relevant functional categories dealt with “regulation of transcription, DNA dependent” (GO_REF:0000019), “signal transduction” (Adams & Zhang, 1999), “positive and negative regulation of transcription from RNA polymerase II promoter” (Denecker et al., 2014), “oxidation-reduction process” (GO_REF:0000002), “protein phosphorylation” (Raya, Revert, Navarro, & Saus, 1999) and “protein transport” (GO_REF:0000037).
- Most altered pathways: in order to focus attention on most altered pathways, it was chosen to derive them from GSEA annotations clustering. In Table 8 are

reported the 14 “macro-pathways”, showed the highest number of genes with the highest alteration of expression, classified by selection of 5271 genes together with the percentage of survived genes at each time point as well as the obtained score, based on its ranking. In details, five pathways highlighted the widest differences in gene expression: Cytoskeleton & Trafficking, Signal Transduction, Proteostasis, Fatty Acids Metabolism and Phototransduction. Data are summarized in Table 9. Moreover, as evidenced by Volcano plots (Fig. 21), every pathway showed a remarkable and statistically significant fold-change in many involved genes and throughout all time points.

PATHWAY	Number of involved genes	PERCENTAGE OF SURVIVAL AT A GIVEN TIMEPOINT				SCORE AT A GIVEN TIMEPOINT			
		1H	2H	4H	6H	1H	2H	4H	6H
APOPTOSIS & CELL DEATH	626	4.95	2.56	5.11	3.51	10	2	11	9
OXIDATIVE STRESS	387	4.39	3.10	4.91	3.62	9	5	10	10
FATTY ACIDS METABOLISM	1047	3.92	3.92	3.92	4.68	6	11	3	12
PHOTOTRANSDUCTION	659	3.64	2.58	4.25	2.12	3	3	6	3
SIGNAL TRANSDUCTION	2057	3.94	3.31	4.08	3.31	7	6	5	8
CYTOSKELETON AND TRAFFICKING	2164	3.84	3.56	4.62	3.19	4	10	9	6
RNA PROCESSING	296	5.74	4.39	6.42	4.39	13	13	13	11
SPLICING	200	3.00	2.50	2.50	2.00	2	1	2	2
PROTEOSTASIS	1600	3.88	3.50	4.25	3.25	5	9	7	7
MITOCHONDRION	686	5.39	4.81	6.56	5.39	11	14	14	13
INFLAMMATION	269	5.95	3.35	4.46	6.32	14	7	8	14
NEURON	622	2.73	2.89	4.02	2.73	1	4	4	4
EPIGENETIC	526	5.51	3.42	5.32	2.85	12	8	12	5
CIRCADIAN RHYTHMS	76	3.95	3.95	1.32	1.32	8	12	1	1

Tab. 8. Percentages and scores of survived genes at a given time point. In this table are reported the 14 “macro-pathways”, showed the highest number of genes with the highest alteration of expression, classified by selection of 5271 genes together with the percentage of survived genes at each time point as well as the obtained score, based on its ranking.

PATHWAY	1h		2h		4h		6h		Average UP	Average DOWN
	UP	DOWN	UP	DOWN	UP	DOWN	UP	DOWN		
APOPTOSIS	314	145	67	45	286	143	101	14	192	86,75
OXIDATIVE STRESS	159	79	158	114	149	78	227	44	173,25	78,75
FATTY ACIDS METABOLISM	255	108	436	326	226	139	692	119	402,25	173
PHOTOTRANSDUCTION	295	97	284	168	281	172	382	53	310,5	122,5
SIGNAL TRANSDUCTION	869	300	899	547	818	323	1291	157	969,25	331,75
CYTOSKELETON AND TRAFFICKING	930	339	899	626	834	406	1351	205	1003,5	394
RNA PROCESSING	122	69	120	95	103	76	185	33	132,5	68,25
SPLICING	75	40	82	56	71	46	140	13	92	38,75
PROTEOSTASIS	711	240	653	394	625	279	1048	127	759,25	260
MITOCHONDRION	250	146	263	221	225	166	400	106	284,5	159,75
INFLAMMATION	97	53	98	81	87	56	148	35	107,5	56,25
NEURON	277	85	269	178	248	108	390	45	296	104
EPIGENETIC	231	77	220	121	210	80	352	22	253,25	75
CIRCADIAN RHYTHMS	32	9	39	17	32	11	43	3	36,5	10
TOTAL	4617	1787	4487	2989	4195	2083	6750	976	5012,25	1958,75

Tab. 9. Number of dysregulated genes for 14 selected pathways, in each time point. In this table is highlighted the exact number of up - and down - regulated genes in each of 14 selected "macro - pathways", for each time point is highlighted. The average value for each pathway, considering all time points, is also shown. UP. Up-regulated. DOWN. Down-regulated.

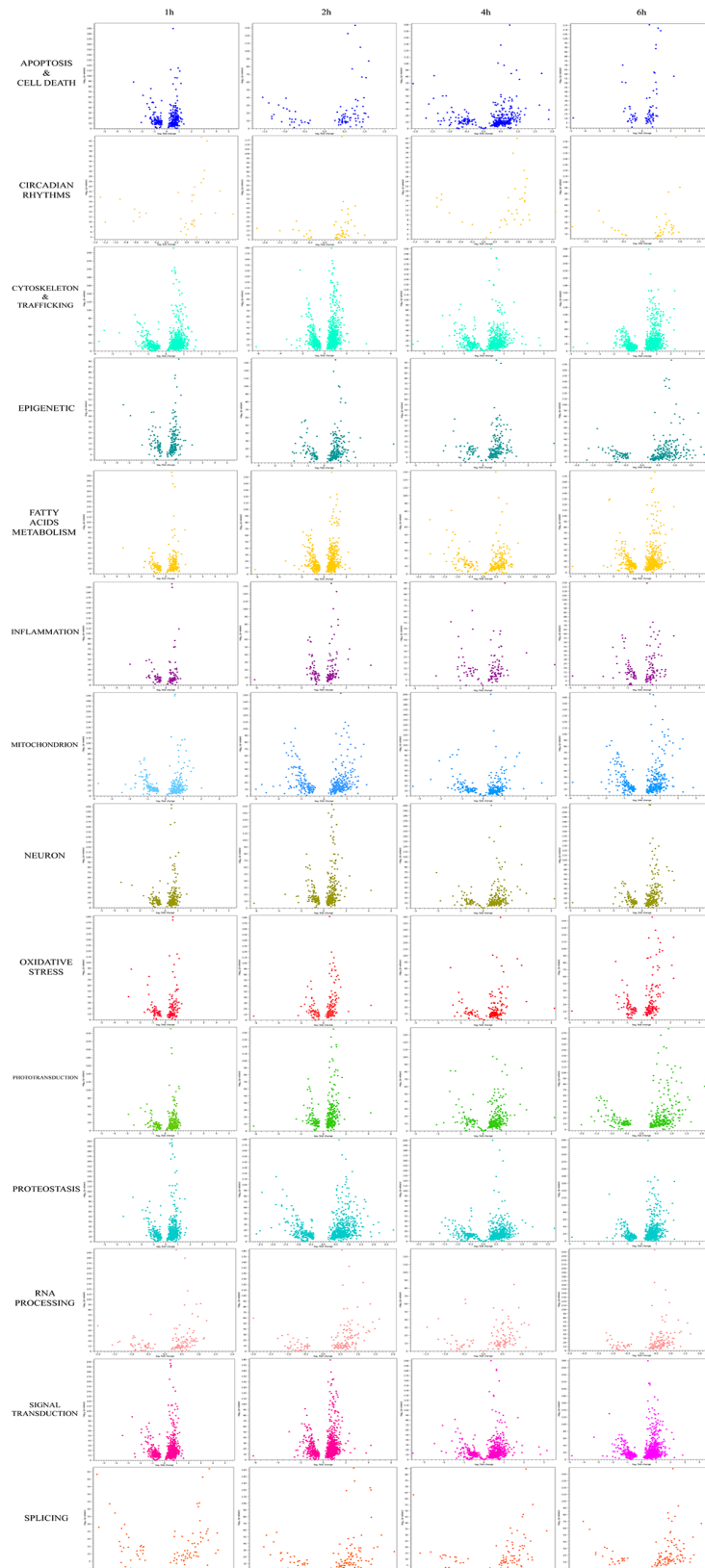


Fig. 21. Volcano plots for all genes involved in each of the 14 clustered “macro-pathways”. Represented volcano plots are based on p -values and fold-changes, produced by the EDGE test, for all genes involved in each of 14 clustered “macro-pathways”. It is highlighted how the most of analyzed genes differ between treated and untreated samples.

- Selection of “Master sub-pathways”: the most specific involved sub-pathways, with corrected GSEA statistic test p-values < 0.01, resulted “Negative regulation of apoptotic process” (Apoptosis and cell death), “Oxidation – reduction process” (Oxidative stress), “Lipid metabolic process” (Fatty Acids Metabolism), “Visual perception” (“Phototransduction”), “Small GTPase mediated signal transduction” (Signal transduction), “Protein transport” (Cytoskeleton and trafficking), “Translational initiation” (RNA processing), “mRNA splicing, via spliceosome” (Splicing), “Protein phosphorylation” (Proteostasis), “Mitochondrial translational elongation” (Mitochondrion), “Inflammatory response” (Inflammation), “Neuron projection development” (Neuron), “Chromatin modification” (Epigenetic) and “Circadian regulation of gene expression” (Circadian rhythms). Detailed results of most significantly enriched sub-pathways are reported in Fig. 22.

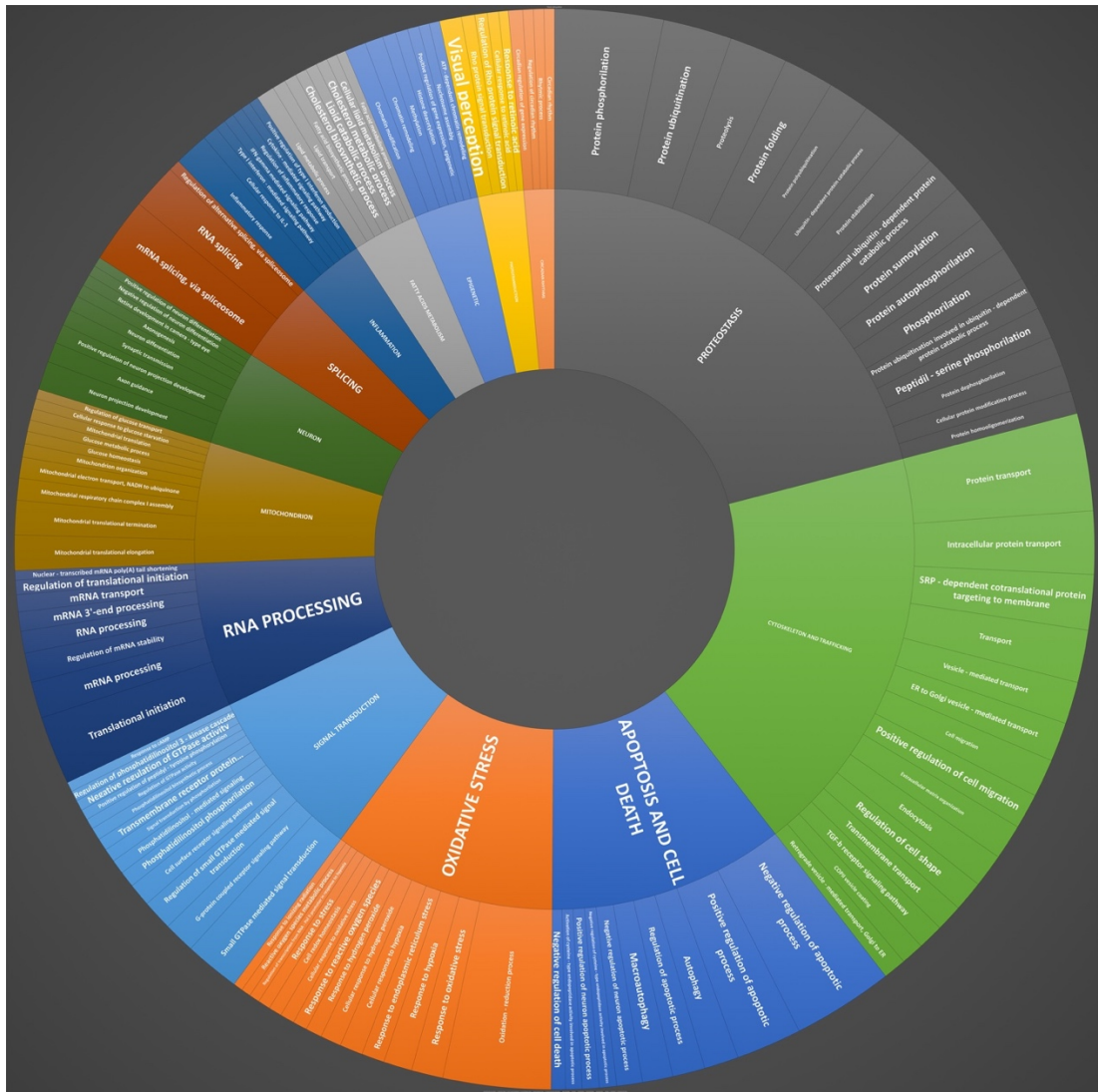


Fig. 22. Circular chart of most enriched sub – pathways. This type of visualization shows hierarchy through a series of rings, representing each category node. Each ring corresponds to a GO level in the hierarchy, with the central circle representing the root node made of 14 most altered pathways, and the hierarchy moving outwards from it. The angle of each slice is either divided equally under its parent node or made proportional to the percentage of most altered genes involved in each GO categories. Different colors highlight hierarchal groupings, while font dimension is proportional to up – regulated pathway and sub – pathways (bigger font) and down – regulated ones (smaller font).

- Selection of single pathway “Master genes”: among the 20 most altered genes for each considered time point, several genes could act as “master genes” (Table 10). In details: 16 for *Apoptosis and Cell Death*, 17 for *Oxidative Stress*, 20 for *Fatty Acids Metabolism*, 18 for *Phototransduction*, 30 for *Signal transduction*, 27 for *Cytoskeleton and Trafficking*, 10 for *RNA Processing*, 12 for *Splicing*, 21 for *Proteostasis*, 23 for *Mitochondrion*, 15 for *Inflammation*, 19 for *Neuron*, 20 for *Epigenetic*, and 10 for *Circadian Rhythms*.

		Apoptosis and Cell Death		Oxidative Stress		Fatty Acids Metabolism		Phototransduction		Signal transduction							
		p-value		p-value		p-value		p-value		p-value							
1b	DOWN	EGR1	38.10	1.98491E-22	FOS	30.42	2.3417E-188	EGR1	38.10	3.56921E-19	FOS	30.42	1.71519E-09	EGR1	38.10	8.59864E-06	
		DUSP1	-4.38	1.74824E-36	KLF2	-5.12	0	HES1	-7.58	1.9737E-202	KLF2	-5.12	1.22398E-65	FOS	30.42	3.32565E-19	
		ZNF830	-2.88	3.74505E-11	DUSP1	-4.38	1.5725E-26	PIGC	-2.34	3.24751E-10	TBX2	-3.86	3.20997E-06	HES1	-7.58	9.02421E-47	
		IER3	-2.66	2.2837E-22	DOHH	-2.14	2.64317E-14	NME1	-2.24	0.052582776	ATF3	-2.62	1.14607E-09	DUSP1	-4.38	7.05591E-06	
		LAMTOR2	-2.57	2.59133E-42	PFN1	-1.95	4.45311E-28	PTRH1	-2.16	5.51916E-06	BCL3	-2.05	2.3052E-107	TBX2	-3.86	4.46274E-08	
		NME1	-2.24	1.3617E-09	NDUFA13	-1.82	1.50285E-12	RARRS2	-2.04	0	ZFPM1	-2.02	3.69815E-14	VASN	-3.71	1.5926E-05	
		BCL3	-2.05	1.33097E-10	ZFP36	-1.81	3.69516E-09	ATP5G2	-1.89	9.0727E-15	PFN1	-1.95	4.89108E-08	IER3	-2.66	2.86556E-27	
		SDFL1	-1.84	7.7527E-33	ROMO1	-1.79	0	ZC3H12A	-1.75	0	GADD45GPI1	-1.86	2.7384E-05	ATF3	-2.62	1.32138E-16	
		NDUFA13	-1.82	8.70124E-14	ZC3H12A	-1.75	4.1486E-26	SI00A13	-1.73	1.49961E-21	ZFP36	-1.81	2.09184E-09	CDKN2B	-2.58	4.39597E-39	
	UP	FIS1	-1.76	0.029539984	RPS3	-1.69	5.73312E-16	EDF1	-1.70	1.25228E-12	ZC3H12A	-1.75	9.66744E-24	LAMTOR2	-2.57	8.99159E-05	
		VTAI	3.05	0	DNAJC10	2.76	5.86058E-13	ABHD10	2.87	0	LEPR	2.95	1.85688E-98	CLIC4	3.32	8.82764E-17	
		GCLM	3.13	1.25001E-11	PLOD2	2.77	9.54812E-13	CLINT1	2.92	0	SNX2	3.00	5.43623E-29	EPHA5	3.33	1.20713E-11	
		RRAGD	3.22	3.41872E-06	RFK	3.20	1.29231E-10	SPRED1	3.00	0	UBE3A	3.02	0	RAB32	3.43	0	
		TOMM7	3.23	2.67361E-12	SIRT1	2.83	3.55209E-12	RARS	3.00	6.91908E-15	IL6ST	3.02	6.58819E-26	CAPZB	3.46	1.90092E-17	
		CHM	3.25	3.37746E-10	TMX1	2.87	0	NIPBL	3.04	1.74132E-18	NIPBL	3.04	2.49221E-13	KITLG	3.46	1.04242E-11	
		MAD2L1	3.26	2.63847E-11	RRM2B	2.90	2.00491E-07	ATP11B	3.05	0.000380418	ARHGAP29	3.09	2.29737E-14	MYL12B	3.51	5.32856E-47	
		CDK1	3.27	0	OGFOD1	3.03	0	DBI	3.16	1.89425E-16	GCLM	3.13	1.08604E-12	CERKL	3.77	0	
		CLIC4	3.32	8.96145E-30	COX2A2L	3.07	8.60358E-07	AASDHPTT	3.32	2.98342E-11	RRAGD	3.22	1.22106E-28	GF2H2	3.96	5.05053E-38	
UP	KITLG	3.46	0	GCLM	3.13	4.5167E-16	C1GALT1C1	3.52	0	CHM	3.25	1.07806E-20	RAB30	4.03	1.47934E-07		
	CERKL	3.77	2.4429E-18	MYL12B	3.51	2.04662E-13	ESCO2	4.43	0.000277112	CLIC4	3.32	2.8724E-178	SNX15	4.33	2.11247E-07		
	RPS3	-2.48	1.86293E-09	EGLN2	-3.58	1.05544E-75	TPCS1	-8.38	2.80048E-30	TGF2	-4.04	9.75512E-13	CDKN2B	-6.10	4.59347E-09		
	BBC3	-2.22	1	DOHH	-3.03	2.53097E-06	ABHD14A	-4.80	2.89176E-13	HIST3H2A	-2.72	6.00145E-24	SDHA2	-4.44	0		
	BAD	-2.00	2.19654E-13	RPS3	-2.48	7.13065E-52	EGLN2	-3.58	0	TFPT	-2.54	9.19107E-07	TGF12	-4.04	0		
	CDKN2D	-1.90	3.47324E-11	ALKBH7	-2.40	0	TMEM86B	-2.03	2.38762E-44	IRE7	-2.16	0	ID1	-3.66	8.16523E-12		
	TSPO	-1.89	9.75738E-07	NDUFA13	-1.82	0	LDLR	-1.88	1.39993E-10	PHLHF40	-2.14	4.86932E-21	EGLN2	-3.58	0		
	DDIT4	-1.88	3.59072E-12	BBC3	-2.22	2.33726E-21	DEC2	-2.80	1.51924E-16	REEP6	-2.10	3.49304E-06	SPSB2	-3.18	3.21984E-69		
	ING1	-1.83	3.45268E-38	ROMO1	-2.13	3.27302E-17	LAMTOR2	-2.79	3.32572E-08	CYBA	-2.00	1.13157E-08	SERTAD1	-3.14	4.14894E-09		
DOWN	BAX	-1.81	3.599E-59	PRDX2	-2.02	1.72226E-07	RARRS2	-2.70	4.311E-16	BAD	-2.00	9.76865E-23	RPS19	-2.96	6.21146E-26		
	SIVA1	-1.68	2.998E-110	CYBA	-2.00	1.00719E-08	TUT1	-2.66	1.873E-32	SOD1	-2.00	2.66413E-13	LDLR	-2.88	0		
	HSPA1A	-1.67	5.11176E-23	SOD1	-2.00	3.10132E-06	HIC1	-2.48	9.34139E-18	RDH5	-1.94	5.02615E-11	LAMTOR2	-2.79	3.61557E-17		
	HMOX1	2.52	2.09888E-15	PLOD2	2.92	0	DHX40	3.61	2.76069E-08	ABCE1	3.31	5.21509E-17	SRPRB	4.23	5.72053E-31		
	CASP8A2	2.57	1.62792E-10	E1F2AK2	2.94	1.2834E-102	SVT1	3.61	1.50359E-13	GCLM	3.35	2.6779E-25	TRIM59	4.38	9.81512E-19		
	ROCK1	2.57	0	RRM2B	2.96	2.19325E-07	CLIC4	3.63	1.19135E-32	TNLNG	3.42	1.22679E-24	KRAS	4.83	7.31201E-15		
	TRIM13	2.57	2.93695E-13	PKD4	2.98	4.8979E-23	ZNF845	3.75	0	FAM73A	3.45	0	FBX7	5.23	5.8767E-20		
	RARS2	2.61	0	XBP1	3.21	9.07227E-15	PEX19	3.84	1.00745E-13	CHM	3.51	2.3223E-10	EGR1	6.02	3.12757E-12		
	FAS	2.63	4.71113E-29	GCLM	3.35	1.45751E-30	ZNF700	4.15	0	CLIC4	3.63	2.78763E-09	INHBA	6.49	2.6457E-191		
UP	PDCD10	2.69	0	COX2A2L	3.40	7.84733E-14	ZNF12	4.86	1.32814E-12	TPD52	4.17	0	SMG8	7.05	0		
	FGF2	2.71	8.37438E-10	MYL12B	3.79	4.28017E-09	MAK16	5.00	0	KRAS	4.83	4.02803E-08	Ctorf44	9.17	8.05183E-29		
	KITLG	2.81	0.00052549	SERP2	6.17	3.48667E-22	EGR1	6.02	2.00952E-09	INHBA	6.49	1.06107E-08	LRRRC8	19.50	2.0927E-11		
	PAK2	2.84	5.33307E-17	FOS	25.50	5.82743E-13	ZNF585A	6.57	1.55465E-13	FOS	25.50	0	FOS	25.50	1.16542E-07		
	4b	DOWN	NME1	-3.19	1.38794E-08	ROMO1	-2.28	8.41303E-08	LDLR	-4.99	1.41853E-13	ZNF580	-3.24	9.83532E-15	SGSM1	-9.43	1.3256E-100
			C19orf68	-2.47	6.21629E-09	NDUFA13	-2.16	7.25521E-08	NME1	-3.19	0.009912479	HIST3H2A	-2.59	4.35505E-09	LDLR	-4.99	1.34331E-15
			LAMTOR2	-2.32	3.81482E-14	HMGCR	-2.08	1.1065E-11	HMGCS1	-3.16	0	GADD45GPI1	-2.14	1.9659E-139	VASN	-4.23	1.61783E-11
			NDUFA13	-2.16	2.32093E-12	BBC3	-1.93	2.04533E-10	INSIG1	-3.08	4.30133E-09	HMGCR	-2.08	0	CDKN2B	-3.32	3.7494E-20
			SDFL1	-2.11	6.07233E-21	EGLN2	-1.84	6.97266E-10	HSD17B7	-2.19	0	REEP6	-1.93	1.68828E-29	NME1	-3.19	1.48741E-16
HMGCR			-2.08	7.13164E-06	DDIT4	-1.81	5.81496E-21	DOK7	-2.06	7.66624E-08	TFPT	-1.81	0.000045802	INSIG1	-3.08	7.08156E-12	
BBC3			-1.93	1.25591E-05	SOD1	-1.79	1.28469E-11	SI00A13	-2.04	5.74001E-46	POLR2L	-1.81	2.73461E-07	SHC3	-2.85	2.94054E-07	
TOMM6			-1.92	6.38179E-05	SOLE	-1.78	1.61828E-16	MIDH1P1	-1.94	2.66413E-11	NDUFS6	-1.80	6.44834E-11	LAMTOR2	-2.32	0	
EGLN2			-1.84	7.9001E-08	RPS3	-1.78	0	NDUFS6	-1.80	1.28024E-26	SOD1	-1.79	4.6159E-15	RPS19	-2.30	1.36378E-35	
UP		DDIT4	-1.81	1.53269E-41	PFN1	-1.74	3.344E-163	EDF1	-1.79	2.83965E-21	RHOD	-1.75	3.20132E-13	NDUFA13	-2.16	3.8809E-12	
		MALT1	2.72	4.07304E-12	DIABLO	2.45	3.7965E-06	STXBP5	2.57	5.50741E-06	AKR1C3	2.71	1.49464E-12	RAB30	3.57	1.1146E-249	
		NOO1	2.73	7.51451E-05	BRAF	3.55	1.45553E-09	PKN2	2.64	0	GABPA	2.71	0.003833306	PI4KB	3.69	0	
		LEPR	2.74	6.94304E-08	DDX6	2.62	2.15759E-13	ESCO2	2.69	2.16725E-09	MALT1	2.72	3.68003E-18	PIPSKB	3.75	0	
		TOMM5	2.77	0	GCLC	2.63	5.84664E-16	AKR1C3	2.71	9.11109E-22	LEPR	2.74	0	APC	4.05	1.61137E-14	
		CHM	2.99	0	AKR1C3	2.71	5.88649E-14	ARID4A	2.76	1.1973E-11	CHM	2.99	1.77362E-44	GCLM	4.23	6.10702E-09	
		CDK1	3.06	0	RRM2B	2.75	8.80572E-15	KANSL1L	2.77	2.76292E-06	DENND1B	3.42	2.51257E-09	HMOX1	4.90	3.44567E-11	
		APC	4.05	1.09463E-21	SLC7A11	3.72	1.29578E-09	ZNF451	2.78	4.82188E-13	APC	4.05	1	MLLT11	4.90	5.22345E-14	
		GCLM	4.23	1	GCLM	4.23	2.8927E-75	SVT1	2.81	2.4015E-15	GCLM	4.23	0	SRP19	8.88	2.22934E-12	
UP	HMOX1	4.90	6.07453E-10	HMOX1	4.90	3.26212E-09	ESCO1	2.88	4.34087E-06	HMOX1	4.90	0	SNX15	9.31	1.94202E-13		
	MLL11	4.90	5.25098E-12	FOS	11.79	1.57166E-17	AASDHPTT	3.32	7.87104E-95	FOS	11.79	5.23398E-12	FOS	11.79	3.92081E-42		
	6b	DOWN	APOE	17.00	9.06353E-15	APOE	17.00	2.88156E-05	APOE	17.00	7.11506E-17	TRIM32	-2.15	0.053694339	APOE	17.00	0
			RPS3	-1.62	6.66878E-15	ROMO1	-1.85	3.16095E-39	ACOT1	-3.43	6.7041E-08	HMGCR	-1.69	5.68991E-21	CDKN2B	-5.26	7.32845E-13
			BAD	-1.42	2.55987E-08	NDUFA13	-1.81	3.95471E-43	LDLR	-3.39	9.00107E-09	PFN1	-1.59	6.54775E-15	IL11RA	-3.49	9.33667E-40
			TSPO	-1.40	2.81496E-13	HMGCR	-1.69	9.05021E-22	ZFP1	-2.84	7.99021E-27	ZFPM1	-1.58	0	LDLR	-3.39	2.7293E-06
			SIVA1	-1.37	3.91277E-22	RPS3	-1.62	1.6468E-09	HSD17B7	-2.62	4.79138E-17	GADD45GPI1	-1.50	1.00407E-05	ZFP1	-2.84	9.27201E-08
			BAX	-1.33	8.21511E-19	DOHH	-1.60	5.5481E-06	LAMTOR2	-2.52	2.05725E-10	SOD1	-1.49	7.04469E-24	LAMTOR2	-2.52	9.8228E-38
			EMP2	-1.31	9.24508E-07	PFN1	-1.59	2.78763E-09	ZNF830	-2.58	1.05445E-17	RHOD	-1.44	4.8947E-11	RPS19	-2.47	1.22382E-07
CDKN2D			-1.30	4.51641E-13	EGLN2	-1.57	0	HMGCS1	-2.29	0	NDUFS6	-1.44	9				

		Cytoskeleton and Trafficking		RNA Processing		Splicing		Prokaryosis		Mitochondrion						
		p-value		p-value		p-value		p-value		p-value						
1h	DOWN	NDUFC2	-9.41	1.56572E-69	ZFP36L2	-2.74	4.52291E-21	POLR21	-1.84	3.16305E-25	EGRI	-38.10	4.05872E-09	NDUFC2	-9.41	1.40375E-19
		HESI	-7.58	5.14469E-27	RPS27	-2.26	6.99442E-08	SNRPF	-1.79	4.05025E-07	HESI	-7.58	9.68163E-15	VASN	-3.71	7.65968E-15
		IER2	-4.20	3.5372E-07	RPS19	-2.07	1.24888E-13	UBL5	-1.65	2.2767E-115	DUSP1	-4.38	1.63749E-15	MRPL53	-3.24	0
		MZT1A	-2.30	0	RPL37	-2.06	0	POLR2F	-1.53	1.53232E-09	LAMTOR2	-2.57	5.15521E-39	COMTD1	-2.64	2.86753E-26
		RPS27	-2.26	8.33881E-14	RPL36A	-2.04	3.65859E-08	SLGIP1	-1.41	1.73363E-11	EMC6	-2.35	1.06563E-18	GLYCTK	-2.25	0
		NME1	-2.24	7.71116E-13	RPL30	-1.98	3.77228E-08	NOL3	-1.32	0.20891795	RPS27	-2.26	3.20222E-07	NME1	-2.24	7.3824E-12
		KRT181	-2.20	1.85274E-08	RPL35	-1.88	9.07227E-15	SNRPB	-1.32	7.47097E-07	ANAPC11	-2.11	1.62234E-29	MRPL54	-2.20	3.96635E-22
		MZT2B	-2.11	1.67117E-07	RPL29	-1.85	1.86521E-25	U2AF1	-1.32	2.2344E-21	RPS19	-2.07	0	PTRH1	-2.16	6.426E-15
		RPS19	-2.07	5.46113E-22	ZFP36	-1.81	4.23611E-11	GPKOW	-1.30	0.008046577	RPL37	-2.06	1.56157E-35	GMPFB	-1.89	4.34776E-10
	UP	RPL37	-2.06	2.47606E-12	ZC3H12A	-1.75	0	PCBP1	-1.29	5.74161E-13	BCL3	-2.05	5.36092E-17	ATP5G2	-1.89	0
		SLBP	-3.42	1.9725E-10	BTBD1	2.70	2.88815E-05	NCBP1	2.61	3.49439E-07	RCPD8	3.32	2.56422E-90	TOMM7	3.23	2.67231E-14
		RAB32	3.43	8.11186E-37	CNOT6	2.71	9.139E-07	AAR2	2.74	0.063681932	UBE2T	3.34	0	CDK1	3.27	4.67419E-16
		DHX40	3.45	1.6633E-110	E1F2AK2	2.76	3.08304E-07	CWC15	2.77	7.67685E-08	SLGT1	3.36	0	PLGRKT	3.31	5.66701E-09
		CAPZB	3.46	9.82834E-42	E1F2S3	2.79	2.77039E-09	SRSF3	2.79	2.54938E-11	SLBP	3.42	1.2135E-19	CLIC4	3.32	1.58513E-08
		KITLG	3.46	1.13562E-05	PTBP3	2.83	2.85303E-09	DHX32	2.81	2.5321E-08	CAPZB	3.46	2.28428E-18	TCAM1	3.34	1.86671E-10
		MYL12B	3.51	1.68677E-14	UHMK1	2.87	2.51765E-06	PTBP3	2.83	1.9054E-11	SNAPC1	3.48	3.0441E-38	RAB32	3.43	1.02712E-06
		DNT1P2	3.96	8.36116E-13	E1F3E	3.03	1.09076E-18	UHMK1	2.87	6.52497E-45	HLA-DMA	4.24	1.12173E-07	C7orf73	3.66	0
		SNX15	4.33	0	PPP4R2	3.22	1.61747E-05	GCFC2	3.16	1.57166E-17	CIGAL1TC1	4.32	2.7851E-10	MRPL13	3.91	1.7704E-10
UP	TMEF7	4.57	4.14607E-11	E1F3I	3.26	1.6418E-80	PPP4R2	3.22	2.35651E-44	ESCO2	4.43	1.57495E-10	TMEM126A	4.28	3.03571E-15	
	HOOK3	4.69	1.32086E-19	SLBP	3.42	6.81891E-07	SNRP27	3.27	4.83184E-07	HOOK3	4.69	0	MYCBP	5.94	5.54184E-29	
	TPGS1	-8.38	0	RPS27	-3.05	0	UBL5	-3.25	4.47997E-12	ABHD14A-ACY1	-4.80	1.94114E-13	NDUFC2-KCTD14	-6.10	3.54549E-12	
	NDUFC2-KCTD14	-6.10	3.15074E-07	ZFP36L2	-3.01	5.21201E-06	SNRPF	-2.08	1.18605E-07	GET4	-4.35	0	NDT18	-5.11	7.65039E-10	
	SDHA2	-4.44	5.16474E-12	RPS19	-2.96	3.14893E-13	POLR21	-1.99	2.37585E-09	EMC6	-4.09	3.3778E-07	SDHA2	-4.44	1.52471E-08	
	GET4	-4.35	3.47996E-07	RPL37	-2.80	0	LSM10	-1.86	4.85442E-13	SPSB2	-3.18	2.52037E-09	YJEFN3	-3.57	4.38297E-10	
	IDI	-3.66	4.21963E-13	RPL35	-2.65	2.62184E-11	FASTK	-1.76	8.38699E-08	RPS27	-3.05	1.97107E-07	COMTD1	-2.90	8.66089E-51	
	EGLN2	-3.58	0.000226928	RPL30	-2.58	1.5281E-113	POLR2F	-1.67	8.19803E-12	RPS19	-2.96	7.77558E-11	MRPL54	-2.54	0	
	KRT181	-3.57	3.4233E-13	RPS3	-2.48	1.01283E-05	POLR2L	-1.63	2.97741E-06	RPL37	-2.80	4.45626E-17	MRPS24	-2.50	7.66349E-76	
2h	DOWN	MZT1A	-3.50	0	RPL29	-2.22	7.94939E-12	LSM4	-1.59	2.4338E-09	LAMTOR2	-2.79	1.83283E-08	RPS3	-2.48	2.27403E-08
		MZT2B	-3.18	0	RPL14	-2.03	7.62078E-24	THOC3	-1.56	0	JOSD2	-2.77	0	ALKBH7	-2.40	7.60309E-13
		RPS27	-3.05	6.62632E-07	RPS28	-1.99	5.04104E-31	CACTIN	-1.55	8.58729E-20	RPL35	-2.65	0.03208312	AURKAIP1	-2.38	3.98852E-09
		RPS17	4.02	6.6939E-23	UHMK1	2.92	1.46044E-09	SNRP27	2.85	1.02398E-07	RPS17	4.02	0.291889694	FAM73A	3.45	2.65526E-14
		HOOK3	4.10	9.60805E-09	E1F2AK2	2.94	3.17019E-46	UHMK1	2.92	1.16158E-22	HOOK3	4.10	1.11072E-22	CDC58	3.54	3.59479E-09
		SRPBB	4.23	0	E1F1AY	2.99	1.177E-21	IVNS1ABP	2.96	1.26458E-08	SRPBB	4.23	4.71057E-09	MLLT11	3.62	4.36063E-13
		TRIM59	4.38	2.09123E-08	ZRANB2	3.10	4.74481E-20	TXNL4B	2.96	3.70716E-21	ARRDC4	4.47	0	CLIC4	3.63	0
		ARRDC4	4.47	5.54488E-24	E1F3	3.24	1.80705E-12	SRSF3	2.98	1.07305E-12	KRAS	4.83	6.94313E-24	TRMT10C	3.73	3.08405E-44
		KRAS	4.83	1.27666E-10	PTBP3	3.32	0	C2orf49	3.03	7.63582E-14	RNF169	4.92	0	TRMT5	3.73	0.00245442
	UP	FKBP1B	5.23	8.9775E-15	ANP32A	3.36	1.13017E-09	ZRANB2	3.10	1.84619E-10	FKBP1B	5.23	8.07842E-13	MRPL1	3.75	0
		DNT1P2	5.59	1.05384E-08	PPP4R2	3.53	5.60273E-07	PTBP3	3.32	9.20422E-25	EGRI	6.02	8.40003E-27	TMEM126A	4.09	4.43408E-11
		SERP2	6.17	2.6514E-16	SLBP	3.68	4.45336E-10	PPP4R2	3.53	0.182161949	SERP2	6.17	0	MRPL13	4.41	9.30390E-16
		LRRRC8C	19.50	0	RPS17	4.02	0	GCFC2	4.40	0	C2orf44	9.17	4.18795E-11	KRAS	4.83	1.18089E-39
		SGSM1	-9.43	5.3254E-16	RPS27	-3.78	6.23285E-08	POLR21	-1.89	3.30813E-06	RPS27	-3.78	1.23564E-10	NDUFC2-KCTD14	-7.63	3.49579E-44
		NDUFC2-KCTD14	-7.63	3.35661E-15	RPS28	-2.65	0	POLR2L	-1.81	1.38794E-18	RPS28	-2.65	6.04347E-18	VASN	-4.23	2.41979E-06
		LDLR	-4.99	8.58923E-13	RPS19	-2.30	5.67242E-10	POLR2F	-1.75	0	C19orf88	-2.47	2.06176E-74	NME1	-3.19	2.03008E-16
		ZNF580	-3.24	0	RPL30	-2.30	2.03096E-07	LSM10	-1.74	2.77702E-07	LAMTOR2	-2.32	4.02575E-64	COMTD1	-2.42	0.001607016
		NME1	-3.19	4.97584E-26	RPL29	-2.15	4.60732E-12	UBL5	-1.67	5.60656E-17	RPS19	-2.30	5.5966E-09	ROMO1	-2.28	6.91664E-09
4h	DOWN	INSIG1	-3.08	3.76419E-35	RPL35	-2.15	1.9784E-27	SNRPF	-1.51	1.08018E-14	RPL30	-2.30	2.40063E-09	MRPL54	-2.25	0
		RPS27	-2.78	2.34065E-05	RPL36A	-2.13	1.16244E-19	U2AF1	-1.48	1.91282E-15	NDUFA13	-2.16	9.88658E-09	NDUFA13	-2.16	1.61428E-50
		RPS28	-2.65	0	RPL37	-2.12	2.04739E-19	SNRPB	-1.38	2.94032E-32	RPL29	-2.15	6.47601E-31	MRPL53	-2.14	0
		KRT181	-2.53	1.89632E-09	RPS3	-1.78	4.64459E-87	PQBPI	-1.36	2.52095E-09	RPL35	-2.15	0	GADD45GPI1	-2.14	6.52624E-07
		MZT2B	-2.50	2.33628E-05	RPS11	-1.78	4.35101E-16	THOC3	-1.33	2.53285E-27	RPL36A	-2.13	3.84507E-08	HMGCR	-2.08	8.68702E-13
		ZNF174	3.58	6.21708E-19	E1F2AK2	2.29	8.72892E-41	ZNF68	2.23	3.78884E-16	RNF169	2.96	2.93937E-10	MRP2B	2.75	4.22199E-15
		HAUS2	3.70	4.32406E-15	PTBP3	2.33	3.72384E-11	SRSF10	2.26	2.77039E-09	CHM	2.99	2.67535E-10	TOMM5	2.77	1.12957E-14
		SCT1A11	3.72	2.26481E-23	SREK1IP1	2.35	4.81395E-10	SON	2.28	2.02594E-08	CDK1	3.06	1.1189E-09	MRPL47	2.79	5.21441E-22
		HOOK3	3.73	3.88693E-12	ZRANB2	2.42	1.06352E-10	PTBP3	2.33	3.65165E-08	ASFA1	3.11	2.40529E-19	CDK1	3.06	4.89148E-49
	UP	APOC	4.05	6.59985E-12	UHMK1	2.49	4.49236E-08	SREK1IP1	2.35	1.32286E-28	MIMR6	3.19	0	MRPL1	3.14	0
		HMOX1	4.90	5.15723E-08	RPS6KB1	2.53	5.2072E-20	ZRANB2	2.42	0	KLHL4	3.35	1.41914E-55	TMEM126A	3.63	9.07237E-15
		MLLT11	4.90	1.2167E-37	DDX6	2.62	3.97176E-12	CWC22	2.47	6.20518E-09	HOOK3	3.73	1.59673E-10	MRPL13	3.90	1.18728E-09
		SLC30A4	5.59	3.0181E-22	SLBP	2.75	9.11848E-25	RNP3	2.48	7.52335E-22	APC	4.05	1.16983E-08	GCLM	4.23	4.83314E-73
		SRP19	8.88	1.93968E-09	E1F3CL	2.84	1.5084E-11	UHMK1	2.49	6.06112E-24	HMOX1	4.90	8.57351E-41	MLLT11	4.90	8.10585E-17
		SNX15	9.31	2.32263E-06	PPP4R2	2.99	0	PPP4R2	2.99	2.70612E-10	SRP19	8.88	8.88	8.88	8.88	
		APOE	17.00	1.34452E-11	RPS27	-2.82	7.24542E-06	POLR21	-1.54	1.65505E-10	APOE	-17.00	6.97184E-12	NDUFC2-KCTD14	-7.78	7.2596E-14
		NDUFC2-KCTD14	-7.78	4.23638E-08	RPS19	-2.47	4.45914E-10	UBL5	-1.42	3.90283E-11	ZFP91	-2.84	3.29721E-14	MRPL53	-2.56	8.13272E-12
		LDLR	-3.39	7.84366E-19	RPL37	-2.10	1.52316E-41	POLR2L	-1.39	9.23315E-08	RPS27	-2.82	0	YJEFN3	-2.17	0
RPS27	-2.82	0.015176085	RPL35	-1.96	1.00688E-46	POLR2F	-1.38	4.86773E-06	LAMTOR2	-2.52	1.67692E-37	MRPL54	-2.09	3.00931E-10		
RPS19	-2.47	6.0373E-23	RPS28	-1.94	7.13912E-13	SNRPF	-1.23	1.793E-09	RPS19	-2.47	4.47875E-21	NME1	-1.94	0		
TRIM32	-2.15	1.59235E-08	RPL30	-1.94	3.10871E-05	LSM10	-1.23	3.98974E-06	TRIM32	-2.15	2.96327E-10	PTRH1	-1.92	2.33174E-12		
6h	DOWN	P2RY6	-2.10	8.97727E-09	RPL29	-1.72	0	THOC3	-1.08	5.07218E-1						

		Inflammation	p-value	Neuron	p-value	Epigenetic	p-value	Circadian Rhythms	p-value				
1h	DOWN	EGRI	-38.10	0	FOS	-30.42	4,32179E-60	EGRI	-38.10	9,57883E-12	IDI	-1.69	5,84527E-08
		FOS	-30.42	0	HES1	-7.58	3,95527E-20	FOS	-30.42	3,26906E-07	JUN	-1.58	6,00168E-13
		KLF2	-5.12	1,21074E-08	IER2	-4.20	8,70745E-05	HES1	-7.58	6,03317E-09	BHLHE40	-1.41	9,81993E-16
		RPS19	-2.07	9,58196E-12	NME1	-2.24	6,2336E-18	KLF2	-5.12	0,526563681	CDK5	-1.29	0
		BCL3	-2.05	2,55835E-09	PFN1	-1.95	1,99556E-11	COMTD1	-2.64	0	SIK1	-1.20	1,62219E-10
		RARRES2	-2.04	5,41339E-26	IDI	-1.69	3,57578E-09	HIFX	-1.99	1,35074E-05	JUND	-1.18	0
		ZFPMI	-2.02	1,57965E-21	SOD1	-1.65	0	SNRPF	-1.79	4,19067E-05	RAI1	-1.08	1,59159E-22
		NDUFA13	-1.82	0	CDC34	-1.62	1,57606E-12	TUT1	-1.76	0	PPP1CA	-1.07	2,54968E-05
	UP	ZFP36	-1.81	1,36674E-08	JUN	-1.58	7,81949E-06	ZC3H12A	-1.75	0	NR2F6	-1.06	3,11041E-14
		METRNL	-1.75	2,89823E-07	PNKD	-1.56	2,62515E-06	EDF1	-1.70	5,66971E-11			
		ITGA2	2.61	1	PIA2	2.92	4,88362E-11	CDK1	3.27	1,31329E-05	ROCK2	2.19	1,48974E-06
		AZ12	2.64	7,80239E-34	NOO1	2.94	1,4306E-08	IFT74	3.28	8,52683E-24	AHR	2.33	7,46405E-08
		IL7R	2.65	0	IL6ST	3.02	3,60092E-12	ASF1A	3.28	6,61603E-11	NR1P1	2.33	4,74776E-11
		XBP1	2.65	0	COPS2	3.12	8,57615E-28	TIPIN	3.32	2,20673E-11	TOP2A	2.34	1,19521E-21
		INHBA	2.68	1,19063E-09	GCLM	3.13	3,42695E-10	UBE2T	3.34	0	GNAQ	2.41	6,9532E-15
		E1F2AK2	2.76	2,85498E-18	LIN7C	3.19	3,04799E-12	SLBP	3.42	1,33163E-11	NAMPT	2.44	1,61456E-07
UP	PARP9	2.79	0	CDK1	3.27	1,73573E-06	SUV39H2	3.60	0	GFPT1	2.53	3,48628E-22	
	LXN	2.92	0	EPHA5	3.33	2,63619E-07	METTL23	4.02	7,96234E-13	SIRT1	2.83	0	
	IL6ST	3.02	0,103373054	CAPZB	3.46	2,71665E-10	ESCO2	4.43	0	UBE3A	3.02	9,25312E-14	
	PLGRKT	3.31	0	HOOK3	4.69	2,38063E-21	NNMT	6.48	5,03041E-08	SUV39H2	3.60	1,35089E-11	
2h	DOWN	RPS19	-2.96	0,012218456	TPGS1	-8.38	0	COMTD1	-2.90	1,99255E-11	IDI	-3.66	0
		RARRES2	-2.70	9,47969E-10	TGIF2	-4.04	2,36775E-21	HIST3H2A	-2.72	1,48253E-07	BHLHE40	-2.14	6,81754E-40
		NDUFA13	-2.28	2,73031E-12	IDI	-3.66	5,93889E-23	TUT1	-2.66	1,49643E-05	JUND	-1.65	2,855E-06
		IRF7	-2.16	1,6941E-110	EGLN2	-3.58	1,0233E-06	HIFX	-2.56	7,99583E-12	SIK1	-1.64	2,60313E-09
		ELF3	-2.11	1,6163E-43	RABAC1	-2.50	1,19005E-08	HIC1	-2.48	0	ATF5	-1.58	8,5532E-105
		MT2A	-2.03	4,63393E-17	NME1	-2.24	5,63288E-18	SNRPF	-2.08	8,32308E-98	CDK5	-1.46	1,68921E-19
		CYBA	-2.00	9,59763E-19	BBC3	-2.22	2,5767E-09	HDAC10	-2.04	3,52362E-29	PPP1CA	-1.41	7,82136E-13
		SI00A13	-1.84	3,52932E-14	METRNL	-2.17	0	KIF22	-1.95	8,93593E-12	ADORA1	-1.38	7,0904E-11
	UP	PN1	-1.81	1,22792E-08	CTF1	-2.03	1,6097E-42	RFXANK	-1.95	3,19505E-40	JUN	-1.29	3,04699E-16
		TREX1	-1.78	0	PRDX2	-2.02	3,14991E-47	LSM10	-1.86	2,70065E-30	NR2F6	-1.22	3,77511E-07
		IL6ST	2.92	3,0309E-43	GCLM	3.35	2,98955E-23	NNMT	3.45	1,20602E-05	NAMPT	2.25	7,54318E-08
		E1F2AK2	2.94	0	HOMER1	3.58	2,10114E-11	ESCO1	3.47	7,43793E-08	SYNCRIP	2.25	2,8173E-32
		ERAP1	3.01	5,5473E-17	SYT1	3.61	2,54894E-67	MYOCD	3.59	7,56658E-63	CBX3	2.25	9,29164E-19
		ITGA2	3.19	5,49319E-10	CAPZB	3.73	0	SLBP	3.68	0	AHR	2.25	2,15705E-05
		IL7R	3.20	3,7071E-13	FBXO45	3.92	8,82192E-17	TRMT10C	3.73	3,62736E-11	SIRT1	2.28	7,0377E-09
		XBP1	3.21	0	HOOK3	4.10	1,62562E-07	TRMT5	3.73	8,08053E-11	GNAQ	2.42	1,36813E-08
UP	CLOCK	3.33	4,97314E-11	KRAS	4.83	3,27988E-39	CENPK	4.56	3,7526E-10	FAS	2.63	4,87692E-11	
	EGRI	6.02	0,000166516	FKBP1B	5.23	1,24397E-07	RNF169	4.92	1,94444E-18	GFPT1	2.66	9,70193E-05	
	INHBA	6.49	6,51477E-08	INHBA	6.49	7,49547E-10	EGRI	6.02	0	SUV39H2	2.83	3,40937E-45	
	FOS	25.50	3,62946E-18	FOS	25.50	2,64786E-34	FOS	25.50	2,52874E-14	CLOCK	3.33	0	
4h	DOWN	ZNF580	-3.24	0	NME1	-3.19	1,42308E-34	HIST3H2A	-2.59	6,94794E-14	JUND	-1.38	2,04435E-35
		RPS19	-2.30	3,0116E-15	SHC3	-2.85	1,23256E-21	COMTD1	-2.42	1,33101E-06	BHLHE40	-1.37	5,13594E-11
		NDUFA13	-2.16	3,86678E-07	BBC3	-1.93	4,11331E-29	HIFX	-1.99	1,30276E-07	ADA	-1.34	3,04234E-29
		MT2A	-2.11	2,41508E-21	EGLN2	-1.84	1,07023E-35	HIST1H1C	-1.90	1,23117E-10	DBP	-1.34	0
		SI00A13	-2.04	2,5186E-10	DDIT4	-1.81	1,38589E-14	KIAA0101	-1.83	4,97329E-09	CDK5	-1.27	7,85834E-09
		POLR2L	-1.81	7,03187E-10	SOD1	-1.79	1,42957E-24	POLR2L	-1.81	7,87313E-14	NR2F6	-1.27	5,3461E-11
		RARRES2	-1.79	9,4876E-108	RABAC1	-1.74	3,00491E-39	EDF1	-1.79	5,46405E-26	PPP1CA	-1.24	0
		POLR2F	-1.75	5,19344E-29	PFN1	-1.74	5,81883E-17	POLR2F	-1.75	4,78643E-14	RAI1	-1.16	2,02383E-11
	UP	MVK	-1.66	0	TSPO	-1.70	5,11818E-21	LSM10	-1.74	9,07927E-07	SIK1	-1.10	2,71283E-22
		IFI27L1	-1.65	1,81788E-09	CYBA	-1.62	3,08756E-10	TUT1	-1.59	0	SIX3	-1.08	0,000232797
		PAWR	2.28	2,44864E-06	NOO1	2.73	0	UBE2T	2.88	7,46458E-06	NFYA	2.10	0,000220364
		E1F2AK2	2.29	2,15074E-22	SYT1	2.81	8,43959E-14	ESCO1	2.88	0,002736309	PPP1CC	2.13	0
		XBP1	2.35	1,51259E-06	MPP5	2.86	7,15824E-52	RNF169	2.96	6,12585E-18	PRKAA1	2.15	4,29153E-21
		SCN9A	2.37	1,94875E-14	CDK1	3.06	8,435E-39	SMCHD1	2.98	2,08889E-34	GNAQ	2.15	2,10654E-38
		R1CTOR	2.45	0,000104462	EPHA5	3.16	9,52604E-62	CDK1	3.06	0	AHR	2.15	1,33917E-19
		IL6ST	2.54	1,63037E-25	HOOK3	3.73	4,85379E-10	ASF1A	3.11	2,0195E-09	NR1P1	2.16	0,000153384
UP	MALTI	2.72	2,67803E-09	APC	4.05	2,62977E-05	SUV39H2	3.11	8,51631E-12	GFPT1	2.20	4,15119E-07	
	LXN	2.79	0	GCLM	4.23	2,31954E-11	FANCM	3.20	1,68126E-11	ARNTL2	2.26	0	
	HMOX1	4.90	5,71871E-18	HMOX1	4.90	1,28984E-06	NNMT	3.65	3,26188E-11	SIRT1	2.28	0,005839373	
	FOS	11.79	5,18964E-08	FOS	11.79	2,01474E-08	FOS	11.79	1,82382E-14	SUV39H2	3.11	1,02504E-28	
6h	DOWN	APOE	-17.00	3,1345E-10	APOE	-17.00	9,07227E-35	TUT1	-1.73	9,67769E-07	IDI	-1.93	1,82438E-06
		IL11RA	-3.49	2,53871E-16	TRIM32	-2.15	0	HIFX	-1.65	1,3697E-15	CDK5	-1.18	1,6755E-12
		RPS19	-2.47	2,22467E-36	NME1	-1.94	1,1847E-12	EDF1	-1.50	0	RAI1	-1.09	8,23732E-13
		MVK	-2.16	2,03025E-13	IDI	-1.93	2,21896E-08	POLR2L	-1.39	4,60859E-18			1,39266E-70
		TRIM32	-2.15	5,79407E-20	PFN1	-1.59	2,4838E-13	POLR2F	-1.38	1,1029E-26			3,32922E-11
		MT2A	-1.88	3,04335E-14	EGLN2	-1.57	1,858E-06	NUPR1	-1.35	2,30568E-21			6,10295E-10
		NDUFA13	-1.81	5,43659E-10	P2RY11	-1.56	0	HIST1H1C	-1.34	2,84621E-08			1,30965E-07
		IFI27L1	-1.78	1,55837E-11	SOD1	-1.49	8,00502E-16	SNRPF	-1.23	1,68891E-17			3,59662E-24
	UP	FASN	-1.60	3,37244E-10	KCNN4	-1.43	0	LSM10	-1.23	2,33107E-09			4,09651E-35
		RARRES2	-1.59	4,18144E-17	BAD	-1.42	3,27171E-25	KIF22	-1.20	2,32831E-10			9,35754E-06
		PLGRKT	4.46	8,45281E-22	NOO1	4.75	6,51581E-11	ASF1A	5.08	0	GFPT1	3.21	1
		XBP1	4.50	6,24307E-10	KCTD8	4.77	8,80692E-09	METTL23	5.19	0	CBX3	3.24	2,27038E-18
		RBMX	4.54	2,43223E-06	MCPHI	4.88	3,5723E-136	SMCHD1	5.22	0	KLF9	3.24	0
		AZ12	4.82	5,95311E-11	BNIP2	4.90	0,000592169	TIPIN	5.43	1,80871E-22	FAS	3.25	7,92608E-34
		MCPHI	4.88	2,10964E-83	PAQR3	4.93	5,63831E-13	CENPK	5.58	1,84918E-11	AHR	3.30	4,38303E-10
		TRIM34	5.56	2,12205E-06	SI00A4	5.71	0	GLMN	5.83	9,24322E-07	UBE3A	3.33	6,6904E-10
ZNF675	5.73	1,06045E-59	CDK1	6.19	7,38651E-10	CDK1	6.19	8,54531E-39	PRKAA1	3.35	4,67748E-18		
UP	GLMN	5.83	5,19066E-21	HOOK3	6.82	0	ESCO2	6.56	2,65526E-14	TOP2A	3.49	5,21477E-14	
	GBPI	5.87	5,10311E-43	GCLM	8.05	2,64317E-34	NNMT	7.02	8,5981E-17	SIRT1	3.68	3,04045E-11	
	HMOX1	8.73	0,000126539	HMOX1									

- “Master genes” functional enrichment and selection of Retinitis pigmentosa candidate genes: the whole RNA-seq analysis revealed expression changes for 23 already known RP causative genes (15 over-expressed and 8 down-expressed), whose enrichment highlighted 77 candidate related genes (49 over-expressed and 28 down-expressed). Many of 77 discovered were, finally, ordered basing on the number of STRING CluePedia interaction pathways involved in, giving us the final number of 31 as new candidate associated or causative RP genes (Table 11). Additionally, a plot with cerebral layout was represented, in order to establish cellular localization of proteins encoded by altered genes (Fig. 27).

RetNet genes linked to most 20 altered genes	1h	2h	4h	6h	ABSOLUTE MEAN	SD	CV	Candidate genes (linked to RetNet ones)	1h	2h	4h	6h	ABSOLUTE MEAN	SD	CV
ATF6	2.12	1.91	1.62	2.69	2.08	0.45	0.22	CDK5	-1.29	-1.46	-1.27	-1.18	1.30	0.11	0.09
BBS10	2.83	2.62	1.00	1.00	1.86	1.00	0.54	CDK1	3.27	3.00	3.06	6.19	3.88	1.55	0.40
CERKL	3.77	1.00	1.00	4.50	2.57	1.84	0.71	RRAS2	2.66	2.61	1.91	3.63	2.70	0.70	0.26
CRM	3.23	3.51	2.99	3.91	3.42	0.39	0.11	ANAPC1	-2.11	-2.38	-1.84	-1.80	2.04	0.26	0.13
COL11A1	1.93	1.93	1.85	2.81	2.13	0.45	0.21	RHOD	-1.56	-1.76	-1.75	-1.44	1.63	0.15	0.09
DHDDS	2.13	2.09	1.99	2.60	2.20	0.27	0.12	KRAS	1.00	4.83	1.00	1.00	1.96	1.92	0.98
INVS	1.00	1.00	1.00	3.12	1.53	1.06	0.69	HSPA1A	-1.33	-1.67	1.00	-1.07	1.27	1.20	0.95
KIF11	2.66	2.24	1.98	3.21	2.52	0.54	0.21	BCL3	-2.05	-1.70	-1.60	-1.07	1.60	0.41	0.25
KLHL7	1.00	1.00	1.00	2.78	1.45	0.89	0.62	SUV39HE	3.60	2.83	3.11	1.00	2.64	1.14	0.43
MVK	1.00	-1.28	-1.66	-2.16	1.53	1.40	0.92	XBPI	2.65	3.21	2.35	4.50	3.18	0.95	0.30
MYO7A	-1.20	-1.24	1.00	1.00	1.13	1.31	1.16	ZNF708	1.00	1.00	1.00	7.20	2.55	3.10	1.22
NPHF3	1.00	1.00	1.00	2.77	1.44	0.89	0.61	ZNF80	1.00	1.00	-3.24	1.00	1.56	-3.12	1.36
NR2F1	1.06	-1.24	-1.18	1.18	1.16	1.34	1.16	ZNF85	1.00	6.57	1.00	1.00	2.39	2.79	1.16
PLK4	1.00	1.00	2.56	3.44	2.00	1.21	0.60	ZNF700	1.00	4.15	1.00	1.00	1.79	1.58	0.88
PNPLA6	1.05	-1.36	-1.12	1.05	1.15	1.33	1.16	SIRT1	2.83	2.28	2.28	3.68	2.77	0.67	0.24
PRPF8	1.72	1.57	1.00	1.00	1.32	0.38	0.29	EGR1	-38.10	6.02	1.00	1.00	11.53	20.52	1.78
RBI	2.48	2.62	2.57	3.80	2.82	0.66	0.24	NFYA	1.00	2.10	1.00	1.00	1.28	0.55	0.43
RDH5	1.00	-1.94	1.00	1.00	1.23	1.47	1.19	ASB1A	3.28	3.22	3.11	5.08	3.67	0.94	0.26
SNRPB200	1.72	1.00	1.55	1.00	1.32	0.37	0.28	ITGA2	2.61	3.19	1.00	1.00	1.95	1.12	0.57
TIMP3	1.00	1.00	1.00	2.24	1.31	0.62	0.47	INHBA	2.68	6.49	1.00	1.00	2.79	2.59	0.93
TOPORS	1.00	2.68	2.38	3.19	2.31	0.94	0.40	ZNF174	1.00	2.79	3.58	1.00	2.09	1.30	0.62
WFS1	-1.02	-1.09	-1.07	1.27	1.11	1.17	1.05	CDKN2D	1.00	-1.90	-1.54	-1.30	1.43	1.31	0.92
ZNF513	-1.33	1.00	1.00	1.00	1.08	1.17	1.08	MAD2L1	3.26	3.05	2.49	3.77	3.15	0.53	0.17
								CDKN2B	-2.58	-6.10	-3.32	-5.26	4.31	1.64	0.38
								CDK6	2.52	2.09	2.02	3.05	3.42	0.88	0.20
								JUN	-1.58	-1.29	1.00	1.38	1.31	1.53	1.16
								JUND	-1.18	-1.65	-1.38	1.09	1.33	1.26	0.95
								CDKN1B	2.47	2.27	1.89	3.80	2.61	0.83	0.32
								HDAC10	-1.41	-2.04	1.00	1.05	1.38	1.61	1.17
								ZFPM	-2.02	1.00	1.00	-1.58	1.40	1.63	1.16
								ZNF12	1.00	4.86	4.18	8.61	4.66	3.12	0.67
								ZNF845	1.00	3.75	1.00	1.00	1.69	1.38	0.82
								ATP11B	3.05	2.67	2.43	3.42	2.89	0.43	0.15
								DUSP1	-4.38	-1.16	1.00	1.36	1.97	2.64	1.33
								PAK2	2.44	2.84	2.32	4.07	2.92	0.80	0.27
								FOX	-30.42	25.50	11.79	1.00	17.18	23.81	1.39
								PKC2	2.62	2.97	2.64	3.70	2.98	0.50	0.17
								CNO16	2.71	2.62	1.93	3.41	2.67	0.60	0.23
								VASN	-3.71	-1.66	-4.23	-1.86	2.86	1.29	0.45
								LRRCS	1.00	19.50	1.00	1.00	5.63	9.25	1.64
								ZNF675	1.00	1.00	1.00	5.73	2.18	2.36	1.08
								RP66B1	1.00	1.00	2.53	1.00	1.38	0.77	0.55
								ARHGAP29	3.09	2.44	1.95	3.15	2.66	0.57	0.22
								RFXANK	-1.24	-1.95	-1.32	1.10	1.40	1.34	0.85
								CDKN2A	2.53	1.00	1.00	1.00	1.38	0.77	0.55
								CDK4	1.00	1.00	1.00	1.32	1.08	0.16	0.15
								PLD2	2.77	2.92	2.30	4.04	3.01	0.74	0.25
								MCPH1	1.00	2.71	1.00	4.88	2.40	1.84	0.77
								CLINT1	2.92	3.03	2.26	4.18	3.10	0.80	0.26
								BRAF	1.00	1.00	2.55	1.00	1.39	0.78	0.56
								ARID1A	1.00	1.00	2.76	5.05	2.45	1.91	0.78
								TOP2A	2.34	1.95	1.96	3.49	2.44	0.73	0.30
								GLMN	1.00	1.00	1.00	5.83	2.21	2.42	1.09
								IVNS1ABP	2.60	2.96	2.23	3.46	2.81	0.53	0.19
								GPXOW	-1.30	1.00	-1.31	1.15	1.19	1.38	1.16
								MZT2A	-2.30	-3.50	-2.10	-1.45	2.34	0.85	0.37
								MZT2B	-2.11	-3.18	-2.50	-1.91	2.43	0.56	0.23
								RAB32	3.43	3.42	2.59	5.16	3.65	1.08	0.30
								SGSM1	1.00	1.00	-9.43	1.00	3.11	5.21	1.68
								PPP1CA	-1.07	-1.41	-1.24	1.04	1.19	1.15	0.97
								PPP1CC	2.13	1.91	2.13	2.82	2.25	0.40	0.18
								HAUS2	1.00	2.54	3.70	4.04	2.82	1.37	0.49
								DNAJC10	2.76	2.61	2.30	3.38	2.74	0.41	0.15
								SNRP	-1.79	-2.08	-1.51	-1.23	1.65	0.36	0.22
								POLR21	-1.26	-1.63	-1.81	-1.39	1.52	0.24	0.16
								POLR21	-1.84	-1.99	-1.89	-1.54	1.82	0.19	0.11
								SRSF3	2.79	2.98	2.20	4.59	3.14	1.02	0.33
								PCBP1	-1.29	-1.32	-1.19	-1.00	1.20	0.14	0.12
								DHX40	3.45	3.61	2.50	4.59	3.54	0.86	0.24
								RNRC3	1.00	1.00	2.48	3.81	2.07	1.35	0.65
								NCBP1	2.61	2.11	1.96	3.90	2.39	0.44	0.18
								SRSF6	1.79	2.24	1.90	3.67	2.40	0.87	0.36
								DHX38	-1.08	-1.05	-1.03	1.10	1.07	1.08	1.01
								CD2BP2	-1.20	-1.30	-1.25	-1.02	1.19	0.12	0.10
								TXNL4B	1.00	2.96	1.00	4.02	2.25	1.50	0.67
								SNRPB	-1.32	-1.46	-1.38	-1.02	1.30	0.19	0.15
								SLBP	3.42	3.68	2.75	4.50	3.59	0.72	0.20

Tab. 11. Known RP causative/associated altered genes and candidate ones. The whole RNA-seq analysis revealed expression changes for 23 already known RP causative genes, whose enrichment highlighted 77 candidate related genes. Many of 77 discovered were, finally, ordered basing on the number of STRING CluePedia interaction pathways involved in, giving us the final number of 31 as new candidate associated or causative RP genes. DV. Standard deviation. CV. Coefficient of Variation.

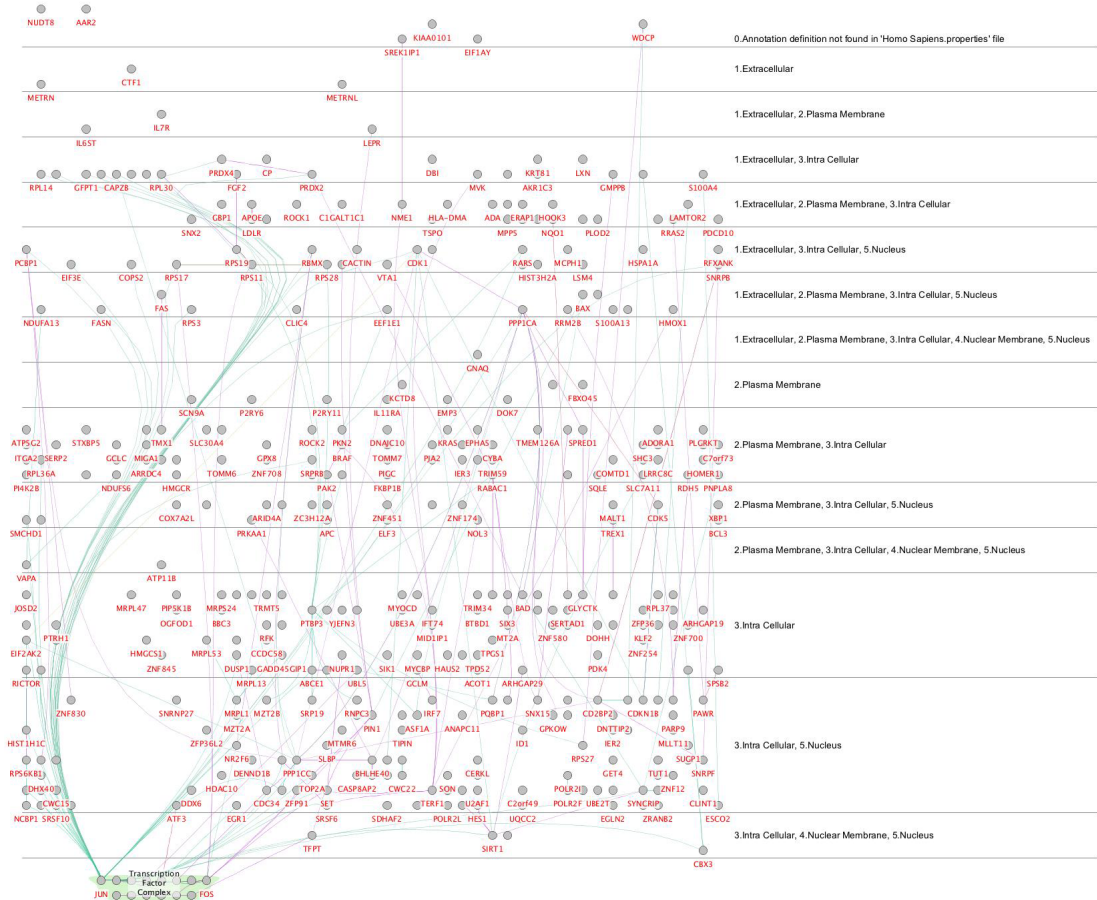


Fig. 23. Cerebral layout for 20 most altered genes networks. Thanks to CluePedia cerebral layout plugin, we extracted the cellular location of 20 most altered genes and related gene networks from GO terms and mapped it on pre-defined cellular compartments. Most of the proteins encoded by 20 genes are located in intracellular compartments or at membrane level.

4.2.2. Discovery of new regulative “hot – spot” within new found biochemical pathways

About ncRNA mapping statistics, CLC and STAR consistently resulted the most accurate performers, with STAR highlighting the best recalling abilities and CLC resulting the best algorithm to detect alternative splice sites at annotated junctions (Fig. 24). Soon after, previously mapped reads were annotated and filtered by those transcript databases and circularRNAs and piRNAs algorithms.

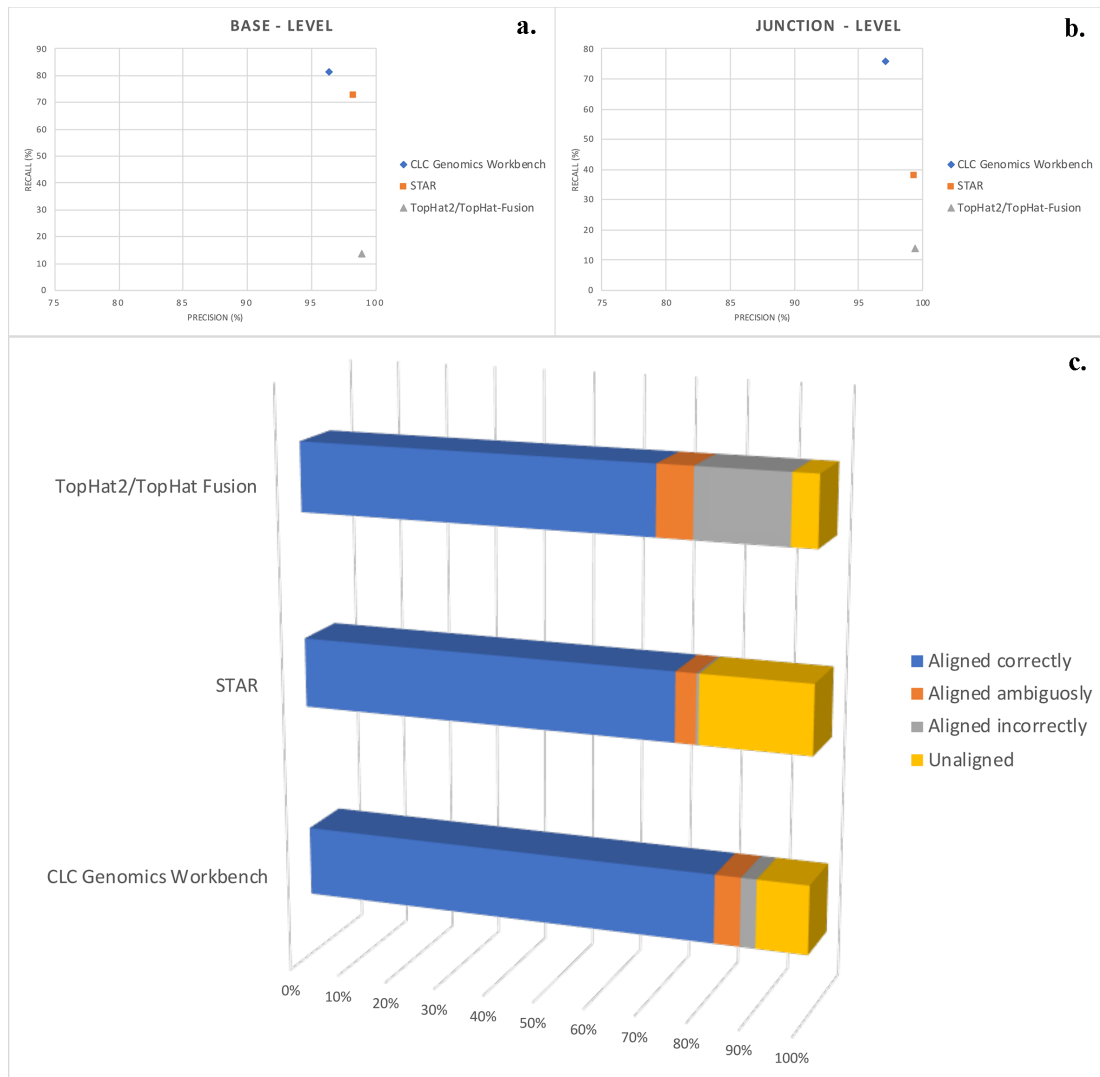


Fig. 24. Alignment algorithm comparison. Exploited alignment algorithms showed significant differences in several parameters. The most important are recall, which measures the fraction of all bases that were aligned correctly, and precision, which determines the fraction of all aligned bases that were aligned correctly. Precision was high for most aligners, while the greatest variance in performance was seen in recall. Both parameters were evaluated at base – (a) and junction – level (b), in which the “event” considerable right or wrong was each base of each read in the first, and a single read crossing a single splice junction the second. CLC Genomics Workbench algorithm showed the best performance, as confirmed by the highest percentage of correctly aligned reads (c).

- Differential expression analysis: about 8,500 lncRNAs, including about 4,900 circRNAs detected by the four specific tools, and 68 piRNAs were founded in all samples, with the highest average expression level of about 5 FPKM for Antisense and Intronic lncRNAs across all considered treated and untreated RPE cells cultures. The variability was significant across samples, with an interesting higher trend for piRNAs expressed at lower levels. Additionally, 3,210 between lncRNAs and piRNAs showed expression alterations in

analyzed time points. In details, 2,900 lncRNAs (1,955 Antisense lncRNAs, 85 Intronic lncRNAs and 860 Sense lncRNAs, 150 lincRNAs, 105 circRNAs) and 55 piRNAs resulted over – or under – expressed (Figg. 25 and 26). All previous mapping statistics were based on average values calculated for all three replicates in each time point. Then, most altered expressed ncRNAs were filtered by setting a minimum fold change cutoff of 2 for significant up – regulated and -2 for relevant down – regulated ones (Table 8). Moreover, there are few values of fold – change that repeat during analyzed time points, with the highest value of 11 reached by CTD-2384B11,2 and the lowest value of -12 reached by AP4B1-AS1, both Sense lncRNAs. Interestingly, fourteen clusters of circRNAs showing particular trends through all analyzed time points were found: *Cluster 1*, consisting of *FNDC3B* derived circRNA, showed an increased fold change (+2.87) after 1h of treatment, bigger if compared to 1h untreated samples (+3.46). A similar trend was highlighted by the high fold change (+2.32) of 1h – Treated samples for Cluster 2. Cluster 3 and Cluster 4, instead, showed an increasing after 1h of culturing (+4.95 and +2.17, respectively), with a huge decrease (-3.95) after 1h of treatment for the first, and a minor one (-2.54) after 2h of exposure versus unexposed samples. Very curiously, all other clusters could be grouped in pairs with opposite trends. In details, Cluster 5 and 6 only to 1h – Untreated samples, with the first showed a great increased of fold change (about +3.13), while the second a relevant decrease (about -2.32). Then, Cluster 7 and Cluster 8 highlighted, respectively, a growing fold change (+2.81) and a remarkable decrease (about -3.81), in 1h – Treated cells compared to untreated ones. Such trends are evidenced by Cluster 9 (about +2.81) and Cluster 10 (-2.38) in 2h Treated vs Untreated samples, by Cluster 11 (about +2.58) and Cluster 12 (-2.32) in 4h Treated vs Untreated samples, and by Cluster 13 (about +2.63) and 14 (about -2.81) in 6h Treated vs Untreated samples. Afterwards, due to the absence of repetitive values of fold change, a different clustering criterion was applied. All other significantly altered ncRNAs were grouped by the presence of increased fold changes in more than two times points (“totally positive”), in a single time point (“positive in 1 time point only”) or with a prevalence of raised fold

changes than decreased ones (“globally positive”) throughout all analyzed time points. The same approach was, then, considered for down – regulated ncRNAs (“totally negative”, “globally negative” and “negative in 1 time point only”). A final cluster was, then, created basing on a perfect balance between up – regulated and down – regulated time points (“50%”). Such clustering evidenced a global up – regulation trend for long – non coding RNAs, in contrast with the high down – regulation expressed by little piRNAs. In details: the “totally positive” cluster showed 19 lincRNAs, 86 Antisense lincRNAs, 4 Intronic lincRNAs, 31 Sense lincRNAs and 2 piRNAs; the “globally positive” cluster showed 1 lincRNAs, 18 Antisense lincRNAs, 1 Intronic lincRNAs, 20 Sense lincRNAs and nopiRNAs; the “positive in 1 time point only” cluster showed no lincRNAs, 142 Antisense lincRNAs, 3 Intronic lincRNAs, 54 Sense lincRNAs and 5 piRNAs; the “totally negative” cluster showed 12 lincRNAs, 51 Antisense lincRNAs, 2 Intronic lincRNAs, 32 Sense lincRNAs and 4 piRNAs; the “globally negative” cluster showed 4 lincRNAs, 25 Antisense lincRNAs, 1 Intronic lincRNAs, 17 Sense lincRNAs and no piRNAs; the “negative in 1 time point only” cluster showed no lincRNAs, 81 Antisense lincRNAs, 3 Intronic lincRNAs, 12 Sense lincRNAs and 7 piRNAs; the “50%” cluster showed 6 lincRNAs, 50 Antisense lincRNAs, no Intronic lincRNAs, 23 Sense lincRNAs and no piRNAs.

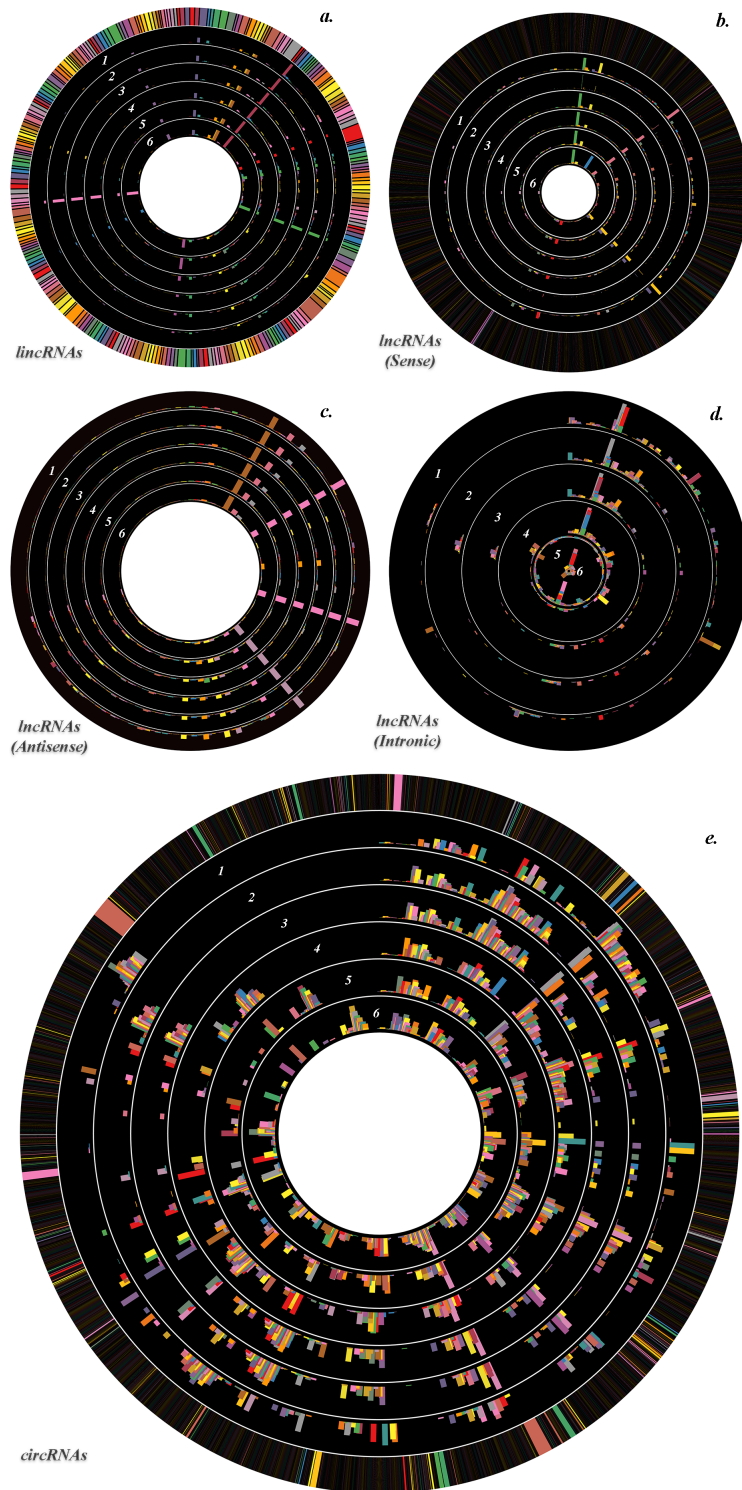


Fig. 25. Circular plot of most altered ncRNAs FCs. The expression profile of analyzed lincRNAs (a), sense lincRNAs (b), antisense lincRNAs (c), intronic lincRNAs (d) and circRNAs (e) with $0 < FC < 1$ (formerly $FC < -2$ in the manuscript) or $FC > +2$ between treated and untreated RPE samples was visualized in Circos. All FCs are \log_2 transformed. The expression profile of each considered time point is represented as a single circle, and FCs of the individual ncRNAs are proportional to histogram bar height. The time point – related order of the ncRNAs expression profile samples is from the outer circle to the inside, as depicted by inserted numbers. 1. 0h vs 1h – Treated. 2. 0h vs 1h – Untreated. 3. 1h (Treated vs Untreated). 4. 2h (Treated vs Untreated). 5. 4h (Treated vs Untreated). 6. 6h (Treated vs Untreated). It is evident a clustering of several groups of ncRNAs which follow the same trend through all considered time points.

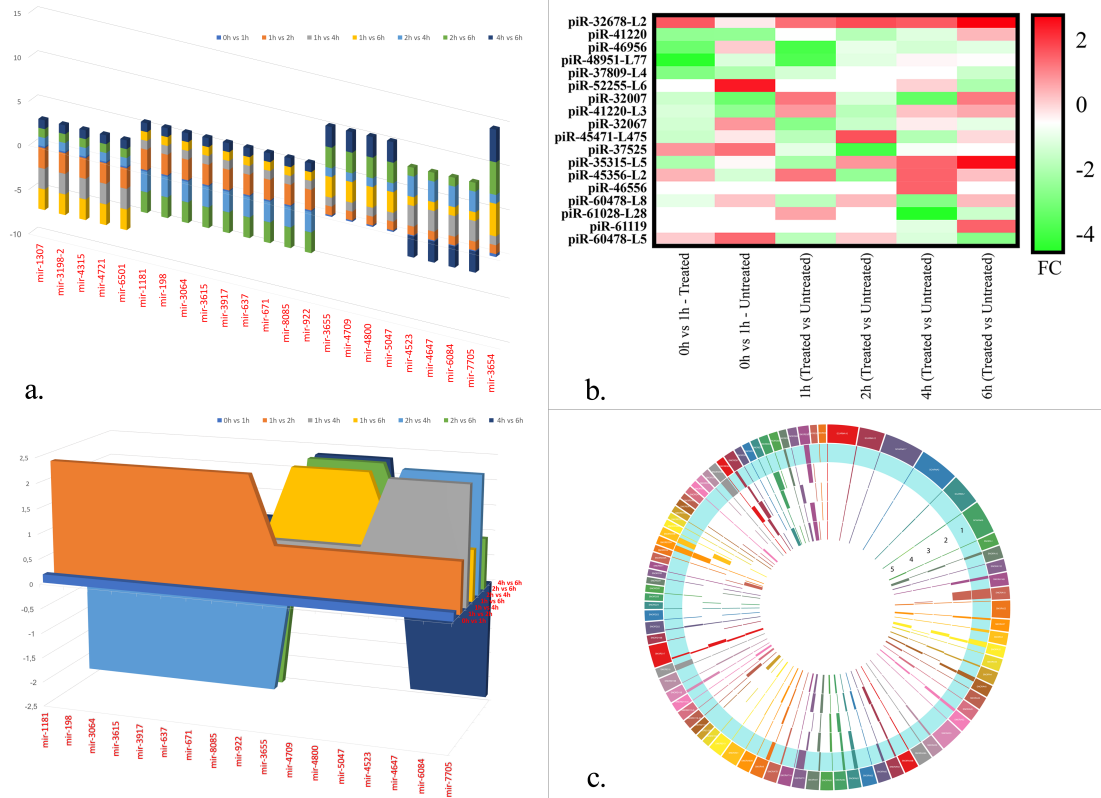


Fig. 26. Graphical representations of small non – coding RNAs FCs through selected time points. a. 3D histogram and 3D area graph of selected miRNA fold – change throughout all considered time points, highlighting five clusters emerged from analysis. For any value smaller than 1 we chose to replace the value by its negative reciprocal value, in order to make the variation more noticeable. b. Heat map with piRNA FCs through selected time points. The heat map correlates most altered piRNAs with their own FC (log2 transformed), in a range starting from down – regulated piRNAs (green) to up – regulated ones (red). It is highlighted that down – regulated represent the prevalent altered piRNAs in all selected time points. c. Circular plot made by CIRCOS (<http://circos.ca>) highlighting FCs of all analyzed snoRNA during selected time points in each concentric circle. 1. 0h vs 1h – Treated. 2. 1h (Treated vs Untreated). 3. 2h (Treated vs Untreated). 4. 4h (Treated vs Untreated). 5. 6h (Treated vs Untreated). Histogram and 3D area graph of miRNA fold – change trends during analyzed time points.

- miRNA differential expression analysis: the predominant length of 23 found altered miRNAs resulted mature miRNAs was 21 bp. A total of 55 mature miRNAs, with an average expression level of 3 reads across all considered treated and untreated RPE cells cultures, were identified. The variability was low across samples, with an expected higher trend for miRNAs expressed at lower levels. As highlighted in Table 3 and in Fig. 1, there are few values of fold – change that repeat during analyzed time points, with the highest value of 3.7 reached by mir-3654. Interestingly, five clusters of miRNAs showing particular trends through analyzed time points were found: *Cluster 1* (mir-1307, mir-3198, mir-4315, mir-4721, mir-6501) showed a little decrease (fold change = - 0.2) in treated samples after 1h, followed by a greater diminution

(fold change = - 2.3) from 2h up to 6h. *Cluster 2*, showing the highest number of deregulated miRNAs (mir-1181, mir-198, mir-3064, mir-3615, mir-3917, mir-637, mir-671, mir-8085, mir-922), evidenced a little increase (fold change = + 0.2) in treated samples after 1h, than boosted (fold change = + 2.3) up to 2h, and finally diminished of the same entity (fold change = - 2.3) at 4h, remaining unchanged up to 6h. *Cluster 3* (mir-4523, mir-4647, mir-6084, mir-7705) highlighted a little increase (fold change = + 0.2) in treated samples after 1h, maintained constant up to 2h, then increasing noticeably (fold change = + 2.3) at 4h, and decreasing again (fold change = - 2.3) at 6h. *Cluster 4* (mir-3655, mir-4709, mir-4800, mir-5047) showed a little increase (fold change = + 0.2) in treated samples after 1h, maintained constant up to 4h, then increasing noticeably (fold change = + 2.3) at 6h. *Cluster 5*, made of the single mir-3654, presented a little increase (fold change = + 0.3) in treated samples after 1h, maintained constant up to 4h, then increasing noticeably (fold change = + 3.7) at 6h (Fig. 1). The expressed miRNAs were, then, ranked based on their abundance (Table 1). The ten top-ranked miRNAs accounted for almost 80% of the total count and the top five for 60%.

- *snoRNA differential expression analysis*: the mean length of 84 found altered snoRNAs was 129.6 bp for snoRNAs, with an average value of 354 bp for scaRNAs. A total of 84 snoRNAs, with an average expression level of 23.615 reads across all considered treated and untreated RPE cells cultures, were identified. The variability was significant across samples, with an expected lower trend for expressed scaRNAs. There is a specific fold – change range during analyzed time points, with the highest value of 9.583 reached by SNORD55 and the lowest of -8.361 expressed by SNORD110. Interestingly, seven clusters of snoRNAs showing interesting trends through analyzed time points were found: *Cluster 1*, showing the highest number (26) of deregulated snoRNAs, evidenced a global increase of expression in treated samples (average fold – change = 2.169). *Cluster 2*, made of 17 snoRNAs, evidenced a huge decrease (average fold change = -0.915) in treated samples through all selected time points. *Cluster 3*, represented by 14 snoRNAs, and *Cluster 4*, made of 12 elements, highlighted only one variation during a single time point,

with a positive value of fold change (average fold change = 0.768) and a negative one (average fold – change = -0.603), respectively. *Cluster 5* and *Cluster 6*, made of 5 snoRNAs each other, showed a curious trend similar to the last two previously described ones, but with two down – regulations (fold change = -1.949) or two up – regulations (average fold – change = 1.539) through all selected time points. Finally, *Cluster 7*, made of 4 snoRNAs, resulted up – regulated in 50% of time points and down – regulated in the other 50% (average fold – change = 0.084). Only SNORD69 showed no expression changes during the experiment. Detailed expression data is available in Table 12.

	ref_gene_id	cuff_gene_id	length	0h vs 1h (T)	0h vs 1h (U)	1h (T vs U)	2h (T vs U)	4h (T vs U)	6h (T vs U)
lincRNAs	LINC01184	FLJ33630	2977	3,13	2,08	1,05	2,77	0,53	1,20
	LINC00663	LOC284440	1357	5,03	3,25	1,78	0,00	1,03	0,27
	LINC00852	GHRLOS2	1328	2,28	0,08	2,19	0,00	-2,56	0,62
	LINC00476	LINC00476	809	4,40	1,25	3,15	-0,47	-0,12	0,03
	LINC01094	LOC100505702	1985	2,58	0,08	2,50	0,53	0,00	0,00
	LINC01354	LOC100506795	2860	2,28	0,08	2,19	0,00	1,76	1,84
	LINC00472	LINC00472	2958	2,90	1,31	1,60	3,48	3,44	2,08
	LINC00115	LINC00115	1317	2,45	1,67	0,78	0,00	-2,14	-1,55
	LINC-PINT	FLJ43663	3505	-2,05	0,08	-2,14	0,30	0,44	2,44
	LINC00116	LINC00116	2051	-2,41	-0,28	-2,13	-1,30	-0,68	-0,35
	LINC00266-1	LINC00266-1	928	-2,31	0,00	0,00	2,31	0,00	-0,33
	LINC01123	LOC440894	2436	-2,02	-0,55	-1,48	0,28	1,32	2,37
	LINC01630	LOC100287225	3188	-2,27	-0,70	-1,57	0,00	0,00	0,00
	LINC00511	LINC00511	2265	-1,14	3,52	-4,65	5,04	-4,96	0,62
	LINC01023	HP07349	436	-0,72	2,89	-3,61	-2,27	-2,14	-1,55
	LINC00634	BK250D10.8	1510	-0,72	2,89	-3,61	-3,50	0,00	0,00
	LINC00665	LOC100506930	1749	0,00	2,77	-2,77	-1,78	-2,23	-3,44
	LINC00639	LOC283547	4364	-0,31	2,20	-2,51	-0,27	1,03	-0,70
	LINC01426	LOC100506385	2632	1,28	3,67	-2,39	-1,13	-0,38	0,00
	LINC00324	LINC00324	2082	1,28	2,25	-0,98	-1,17	1,76	-0,38
	LINC00893	LOC100131434	2344	1,39	2,50	-1,11	-1,39	-1,41	1,54
	LINC00685	PPP2R3B-AS1	428	-0,99	-2,50	1,52	-0,83	-1,88	-0,97
	LINC00922	LOC283867	1760	-0,46	-2,24	1,78	-0,69	0,44	0,00
	LINC00998	LOC401397	1070	0,79	-1,53	2,31	2,30	0,02	2,59
	LINC00242	LINC00242	2418	0,86	-1,50	2,36	-1,69	0,86	1,70
	LINC00707	LOC100507127	3070	1,67	-0,33	2,00	1,16	1,51	0,39
	LINC01012	LOC100507173	675	0,00	0,00	5,44	0,00	0,00	0,00
	LINC01252	LOC338817	3673	0,00	0,00	3,00	0,00	0,00	0,00
	LINC00520	LINC00520	778	0,00	0,00	-2,39	0,48	0,44	0,03
	LINC00630	LOC100287765	2101	1,69	0,08	1,61	3,12	-0,82	0,03
	LINC00641	LOC283624	1763	1,95	0,12	1,83	2,05	1,03	-0,38
	LINC02210	C17orf69	2458	-0,62	-1,18	0,56	2,77	-0,70	1,87
	LINC02062	LOC100289230	478	-1,05	0,57	-1,61	-3,69	-0,29	2,20
	LINC00910	LOC100130581	2438	1,92	0,00	0,00	-5,69	-1,97	-1,29
	LINC00514	LINC00514	2216	0,00	0,00	0,00	-6,60	0,00	0,00
	LINC00282	LINC00282	4008	0,00	0,00	0,00	0,00	2,03	0,00
	LINC00174	LINC00174	4702	-1,38	-0,57	-0,81	-0,91	-2,20	-0,06
	LINC01105	LOC400940	3329	-0,72	0,08	-0,81	-0,43	-2,46	0,62
	LINC01125	LOC728537	1356	-1,72	0,08	-1,81	1,31	-2,56	1,49
	LINC01140	LOC339524	751	0,00	0,00	0,40	1,63	-2,09	-1,97
	LINC01160	LOC100129269	894	0,00	0,00	1,19	0,00	-4,02	-0,97
	LINC00176	LINC00176	4303	-1,26	-0,45	-0,81	-0,80	0,44	2,05
lincRNAs (intronic)	LINC01239	FLJ35282	2347	0,95	1,08	-0,13	0,69	1,11	2,18
	RABGAP1L-IT1	RABGAP1L	737	2,38	0,26	2,12	3,29	0,35	-1,55
	WWTR1-IT1	WWTR1	451	2,09	-1,50	3,59	0,05	3,31	0,50
	ARHGEF9-IT1	ARHGEF9	394	-2,14	0,12	-2,26	1,61	-2,12	-0,98
	ZBTB40-IT1	ZBTB40	273	-3,24	0,08	-3,32	0,21	0,05	0,31
	LARGE-IT1	LARGE	558	1,26	2,48	-1,22	2,56	-0,88	-0,03
	IMMP2L-IT1	IMMP2L	557	1,68	-2,39	4,07	0,63	2,50	1,34
	TSPAN9-IT1	TSPAN9	562	-0,08	-2,34	2,26	-0,30	-1,48	-3,09
	RNF216-IT1	RNF216	337	0,46	-1,80	2,26	0,50	1,11	1,67
	FMR1-IT1	FMR1	343	-0,84	-0,01	-0,82	4,09	2,36	2,21
	ARHGAP22-IT1	ARHGAP22	470	-0,47	0,29	-0,76	-2,61	1,96	0,00
	SMYD3-IT1	SMYD3	361	0,38	0,45	-0,07	-2,02	-1,42	-0,53
	ARID4B-IT1	ARID4B	463	0,63	1,15	-0,52	0,33	3,08	-0,49
	ZNRF3-IT1	ZNRF3	674	0,05	-0,34	0,39	-1,06	2,40	-1,43
	AGAP1-IT1	AGAP1	664	-1,84	-0,96	-0,88	-0,91	-2,10	-1,63
circRNAs	NM_022763	FNDC3B	280	2,87	-0,58	3,46	0,00	0,00	0,00
	NM_001204387	DLG1	177	2,32	0,00	0,00	0,00	0,00	0,00
	NM_001305275	AGR1	98	1,00	4,95	-3,95	0,00	0,00	0,00
	NM_001110556	FLNA	153	0,00	2,17	0,00	-2,54	0,00	0,00
	NM_001194947	EIF4G1	98	0,00	3,09	0,00	0,00	0,00	0,00
	ENST00000369856	FLNA	153	0,00	3,17	0,00	0,00	0,00	0,00
	ENST00000512968	GNB2L1	126	0,00	-2,32	0,00	0,00	0,00	0,00
	ENST00000552461	RPLP0	218	0,00	-2,32	0,00	0,00	0,00	0,00
	ENST00000492719	GAPDH	105	0,00	0,00	2,81	0,00	0,00	0,00
	NM_022748	TNS3	38	0,00	0,00	-3,81	0,00	0,00	0,00
	ENST00000355730	TNS3	38	0,00	0,00	-3,46	0,00	0,00	0,00
	NM_001161560	TNFR	205	0,00	0,00	0,00	2,81	0,00	0,00
	ENST00000442909	NBPF12	217	-0,22	0,89	-1,12	-2,38	1,74	0,51
	NM_016441	CRIM1	174	0,00	0,00	0,00	0,00	2,58	0,00

	NM_002026	FN1	138	0,00	0,00	0,00	0,00	2,58	0,00
	NM_00117712	RBMS3	107	0,00	0,00	0,00	0,00	2,32	0,00
	NM_024947	PHC3	247	0,00	0,00	0,00	0,00	-2,32	0,00
	ENST00000524698	TXNRD1	2420	0,00	0,00	0,00	0,00	0,00	3,17
	ENST00000456556	ANKRD36C	915	0,00	0,00	0,00	0,00	0,58	2,70
	NM_001002800	SMC4	234	0,00	0,00	0,00	0,00	0,00	2,32
	NM_014607	UBXN4	177	0,00	0,00	0,00	0,00	0,00	2,32
	NM_003380	VIM	162	-2,00	0,00	-2,00	1,22	0,00	-2,81
piRNAs	piR-32678-L2	RN5-8S1	30	2,16	0,28	1,88	2,32	2,14	3,31
	piR-41220	LOC727849	32	-2,03	-2,01	-0,03	-1,34	-0,59	0,93
	piR-46956	LOC100630918	30	-2,72	0,67	-3,39	-0,43	-0,82	-0,55
	piR-48951-L77	ESRG	30	-3,92	-0,68	-3,24	-0,54	0,11	0,02
	piR-37809-L4	LOC100507053	32	-2,31	-1,50	-0,81	0,00	0,00	-0,97
	piR-52255-L6	POM121L1P	32	0,00	2,99	0,00	0,00	0,59	-1,51
	piR-32007	LOC653712	32	-0,95	-2,72	1,78	-0,69	-2,88	1,73
	piR-41220-L3	LOC727849	32	-0,71	-2,03	1,32	-1,29	0,78	1,12
	piR-32067	LOC100129534	31	-0,84	1,36	-2,20	-1,01	0,24	-0,49
	piR-45471-L475	LINC00340	30	-0,99	0,31	-1,29	2,25	-1,41	0,49
	piR-37525	MIR17HG	30	1,36	1,85	-0,48	-3,42	-0,14	0,00
	piR-35315-L5	LOC653061	32	-1,53	0,08	-1,61	1,37	2,00	3,17
	piR-45356-L2	LOC100288069	30	0,99	-0,79	1,78	-1,95	2,03	0,82
	piR-46556	RNF126P1	31	0,00	0,00	0,00	0,00	2,03	0,00
	piR-60478-L8	FAM27B	30	-0,46	0,76	-1,22	0,90	-2,26	0,88
	piR-61028-L28	LOC100129269	32	0,00	0,00	1,19	0,00	-4,02	-0,97
	piR-61119	LOC100288428	32	0,00	0,00	0,00	0,00	-0,56	2,03
	piR-60478-L5	FAM27A	30	0,67	1,94	-1,27	0,67	-0,68	-2,19
miRNAs	hsa-mir-1181		21	0,17	2,33	-2,33	1,00	1,00	-2,33
	hsa-mir-1307-3p		22	-0,17	-2,33	1,00	1,00	-2,33	1,00
	hsa-mir-198		22	0,17	2,33	-2,33	1,00	1,00	-2,33
	hsa-mir-3064-3p		23	0,17	2,33	-2,33	1,00	1,00	-2,33
	hsa-mir-3198		22	-0,17	-2,33	1,00	1,00	-2,33	1,00
	hsa-mir-3615		21	0,17	2,33	-2,33	1,00	1,00	-2,33
	hsa-mir-3654		19	0,33	1,00	1,00	3,69	3,69	3,69
	hsa-mir-3655		21	0,17	1,00	1,00	2,33	2,33	2,33
	hsa-mir-3917		20	0,17	2,33	-2,33	1,00	1,00	-2,33
	hsa-mir-4315		18	-0,17	-2,33	1,00	1,00	-2,33	1,00
	hsa-mir-4523		21	0,17	1,00	2,33	-2,33	1,00	1,00
	hsa-mir-4647		23	0,17	1,00	2,33	-2,33	1,00	1,00
	hsa-mir-4709-3p		23	0,17	1,00	1,00	2,34	2,34	2,34
	hsa-mir-4721		22	-0,17	-2,33	1,00	1,00	-2,33	1,00
	hsa-mir-4800-3p		19	0,17	1,00	1,00	2,34	2,34	2,34
	hsa-mir-5047		21	0,17	1,00	1,00	2,34	2,34	2,34
	hsa-mir-6084		20	0,17	1,00	2,33	-2,33	1,00	1,00
	hsa-mir-637		24	0,17	2,33	-2,33	1,00	1,00	-2,33
	hsa-mir-6501-3p		23	-0,17	-2,33	1,00	1,00	-2,33	1,00
	hsa-mir-671-3p		21	0,17	2,33	-2,33	1,00	1,00	-2,33
	hsa-mir-7705		23	0,17	1,00	2,33	-2,33	1,00	1,00
	hsa-mir-8085		21	0,17	2,33	-2,33	1,00	1,00	-2,33
	hsa-mir-922		23	0,17	2,33	-2,33	1,00	1,00	-2,33
snoRNA	SCARNA10		330	0,00	0,00	0,00	0,00	0,86	0,00
	SCARNA12		270	0,00	2,32	2,32	2,37	1,25	0,00
	SCARNA17		421	0,96	0,69	-0,27	0,42	1,00	-0,34
	SCARNA2		420	-0,82	-0,82	0,00	0,57	-0,78	-0,34
	SCARNA7		330	0,71	-0,36	-1,07	2,35	0,00	-1,19
	SCARNA9		353	0,80	-0,67	-1,47	-1,09	0,24	0,64
	SNORA1		130	0,00	0,00	0,00	0,00	0,00	3,75
	SNORA10		133	-4,56	-4,56	0,00	3,94	0,00	-5,52
	SNORA11D		128	0,00	0,00	0,00	0,00	0,00	2,95
	SNORA14B		135	0,00	4,75	4,75	0,00	0,00	0,00
	SNORA18		132	0,00	6,82	6,82	8,13	0,00	7,89
	SNORA23		189	0,00	0,00	0,00	0,00	0,00	-2,95
	SNORA27		126	0,00	4,13	4,13	0,00	0,00	-4,81
	SNORA3		130	-4,67	-4,67	0,00	0,00	0,00	0,00
	SNORA32		121	5,09	5,85	0,76	5,35	0,00	5,61
	SNORA33		133	0,00	0,00	0,00	0,00	0,00	3,64
	SNORA4		138	4,49	3,73	-0,76	3,80	0,00	3,50
	SNORA40		127	4,60	5,53	0,93	0,00	4,54	3,85
	SNORA42		134	0,00	0,00	0,00	0,00	0,00	-4,51
	SNORA45		131	0,00	0,00	0,00	0,00	-4,53	0,00
	SNORA52		134	0,00	4,79	4,79	0,00	-4,42	3,61
	SNORA53		250	0,00	0,00	0,00	0,00	0,00	1,26
	SNORA56		129	0,00	4,01	4,01	0,00	0,00	0,00
	SNORA59A		152	0,00	2,41	2,41	0,00	2,46	0,00
	SNORA59B		152	0,00	2,41	2,41	0,00	2,46	0,00
	SNORA5A		134	0,00	3,84	3,84	-4,56	-5,39	0,00
	SNORA60		136	-4,45	-4,45	0,00	0,00	0,00	0,00
	SNORA62		153	0,00	0,00	0,00	0,00	4,74	0,00
	SNORA63		123	0,00	5,32	5,32	0,00	-4,39	0,00
	SNORA64		134	0,08	-4,52	-4,60	-5,53	0,00	-4,51
	SNORA65		137	4,53	0,00	-4,53	-4,49	0,00	-4,44
	SNORA67		137	5,46	3,73	-1,73	0,30	5,31	5,00
	SNORA70		135	-2,45	-1,70	0,75	0,00	1,71	-0,95
	SNORA71A		139	0,00	0,00	0,00	0,00	0,00	-4,37
	SNORA7B		139	0,00	3,67	3,67	0,00	0,00	0,00
	SNORA8		139	-5,31	-5,31	0,00	-4,38	3,73	-0,90
	SNORA80B		136	0,00	0,00	0,00	0,00	-4,35	3,54
	SNORA81		178	0,00	0,00	0,00	-0,60	0,00	0,00
	SNORD10		148	0,00	0,00	0,00	0,00	0,00	-4,04
	SNORD104		80	7,12	0,00	-7,12	0,00	-6,94	0,00
	SNORD109B		67	0,00	8,21	8,21	7,87	0,00	5,98
	SNORD110		75	-8,36	-8,36	0,00	0,00	0,00	6,40
	SNORD116-24		94	0,00	0,00	0,00	0,00	5,59	0,00
	SNORD116-6		98	0,00	0,00	0,00	0,00	0,00	5,09
	SNORD116-8		97	0,00	0,00	0,00	0,00	0,00	5,14
	SNORD11B		90	0,00	4,68	4,68	0,00	0,00	0,00
	SNORD15B		146	0,00	0,00	0,00	3,51	3,50	0,00
	SNORD16		101	-5,94	-5,94	0,00	0,00	0,00	0,00
	SNORD17		237	-1,25	-0,50	0,74	1,59	1,66	1,66
	SNORD19B		84	7,37	0,00	-7,37	7,22	0,00	0,00
	SNORD22		126	0,57	-0,21	-0,79	-0,24	-0,12	-0,03
	SNORD23		110	0,00	0,00	0,00	6,80	0,00	0,00
	SNORD24		75	7,45	0,00	-7,45	0,00	0,00	0,00
	SNORD26		75	0,08	1,27	1,19	0,00	-8,26	0,00
	SNORD28		75	0,00	0,00	0,00	7,71	6,71	7,97
	SNORD29		65	0,00	7,38	7,38	7,45	0,00	0,00
	SNORD30		70	0,00	0,00	0,00	-0,68	0,00	0,00
	SNORD31		71	0,00	0,00	0,00	0,00	0,00	6,90
	SNORD32A		77	0,08	-7,91	-8,00	-2,26	0,00	5,96
	SNORD34		66	0,00	0,00	0,00	0,00	-0,55	0,00
	SNORD35A		86	0,00	5,97	5,97	0,00	0,00	0,00
	SNORD35B		88	6,71	5,91	-0,80	5,98	-0,55	-1,95
	SNORD36A		72	0,00	0,00	0,00	0,00	-0,55	0,00

SNORD36C	68	0,00	0,00	0,00	0,00	0,00	-7,93
SNORD38B	69	0,00	0,00	0,00	0,00	0,00	6,82
SNORD41	70	-7,71	-7,71	0,00	0,00	0,00	0,00
SNORD42A	58	0,00	7,54	7,54	7,61	0,00	0,00
SNORD47	65	0,00	6,52	6,52	0,31	6,58	0,00
SNORD52	64	0,00	0,00	0,00	0,00	0,00	4,92
SNORD55	74	-0,50	0,01	0,51	9,58	-0,55	-1,55
SNORD57	72	0,00	0,00	0,00	6,92	0,00	7,60
SNORD58C	65	-6,46	-6,46	0,00	0,00	0,00	0,00
SNORD62A	86	0,00	0,00	0,00	-5,73	0,00	0,00
SNORD67	111	5,51	4,73	-0,78	-1,65	-5,33	0,03
SNORD69	77	0,00	0,00	0,00	0,00	0,00	0,00
SNORD76	80	0,00	0,00	0,00	0,00	0,00	-6,97
SNORD79	85	0,00	0,00	0,00	0,00	0,00	6,02
SNORD83A	95	6,27	0,00	-6,27	5,55	0,00	0,00
SNORD83B	93	0,00	0,00	0,00	6,64	-1,54	0,00
SNORD84	78	0,08	-4,42	-4,50	0,00	0,00	0,00
SNORD88B	97	0,00	0,00	0,00	5,45	0,00	5,14
SNORD89	114	0,08	1,26	1,17	6,95	6,21	6,31
SNORD96A	72	-7,57	-7,57	0,00	0,00	6,92	0,00
SNORD99	80	7,12	0,00	-7,12	0,00	0,00	-7,04

Tab. 12. ncRNAs expression variations throughout all analyzed time points. All selected ncRNAs showed particular fold – change trends, between treated and untreated samples, during evaluated time points (0h, 1h, 2h, 4h, 6h). Altered Sense and Antisense ncRNAs are not shown, due to their high number. The whole results were statistically validated by Bonferroni – corrected EDGE test, and p – values are all about 0 (values not shown).

- qRT-PCR verification: in order to validate the authenticity and reproducibility of the RNA-Seq results, 63 among the most altered analyzed ncRNAs were selected for qRT-PCR analysis, and the obtained expression profiles were similar to the results of transcriptome analysis (data not shown). The linear regression analysis showed a significantly positive correlation of the relationship between gene expression ratios of qRT-PCR and RNA-Seq for all selected time points (Fig. 31), confirming our transcriptomic data validity.

Correlation analysis of fold change data between qRT-PCR and RNA-seq

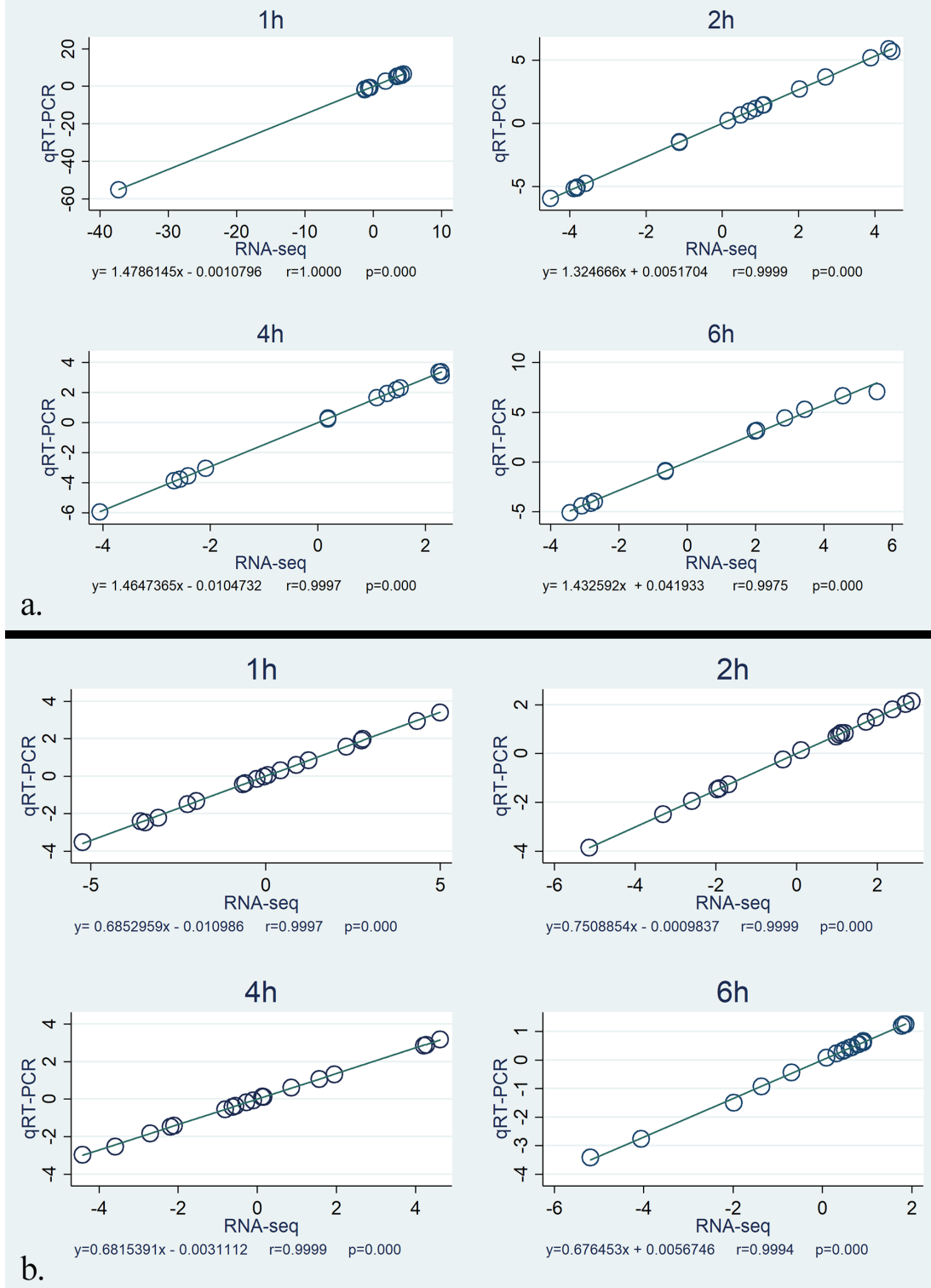


Fig. 27. Correlation analysis of fold – change data between qRT – PCR and RNA – Seq. Expression data of 20 selected genes (a) and 20 selected ncRNAs (b) from qRT – PCR and RNA – Seq are means of three replicates, considering all selected time points. Scatterplots were generated by the fold – change values from RNA – Seq (x – axis) and qRT – PCR (y – axis).

- Pathway analysis of genes generating altered ncRNAs*: a pathway enrichment analysis by Cytoscape and its plugins was performed on the host genes that produce the most altered ncRNAs in exam. Although such enrichment was primarily intended to reflect functions of proteins derived from a given gene, it is possible that loss of function studies contributing to these annotations might also have disrupted the ncRNAs loci. Moreover, changes in back – splicing to generate circRNAs could impact protein expression from a gene. Pathway analysis showed statistically significant associations between altered circRNA genes and several categories linked to intracellular transport and oxidative stress induced effects. Altered lincRNA genes, instead, showed statistically significant association with “C – terminal protein tyrosinilation” and “Negative regulation of complement activation, lectin pathway”, both with a P of about zero. Very interestingly, Antisense and Sense lincRNA host genes with the highest expression differences shared many significant pathways involved in acetylation and deacetylation. However, many other terms resulted significantly associated to Antisense lincRNA genes only (“Mitochondrial ABC transporters”, P=0.00; “Response to copper ion”, P=0.01, “Globo sphingolipid metabolism”, P=0.04) or to Sense ones (“TFIIH – class transcription factor binding”, P=0.00; “Alpha-methylbutyryl CoA + FAD → Tiglyl-CoA + FADH₂”, P=0.00). Intronic lincRNAs, instead, showed a unique clustering of terms for their altered host genes, consisting of “Protein export” (P=0.00) and “RUNX proteins bind the p14-ARF promoter at the CDKN2A locus” (P=0.01). Finally, piRNA altered genes highlighted significance in “Catalitic activity” (P=0.05), “Hydrolase activity, hydrolyzing O-glycosyl compounds” (P=0.04), “miRNA Regulation of DNA Damage Response” (P=0.04) and “Transporter activity” (P=0.05). Detailed results of most altered pathways and subpathways are available in Fig. 28.



Fig. 28. Sunburst chart of most altered ncRNAs. This type of visualization shows hierarchy through a series of rings, that are sliced for each category node. Each ring corresponds to a GO level in the hierarchy, with the central circle representing the root node made of analyzed ncRNAs categories, and the hierarchy moving outwards from it. The angle of each slice is either divided equally under its parent node or made proportional to the percentage of most altered ncRNAs involved in each GO categories. Different colors highlight hierarchical groupings, while font dimension is proportional to up – regulated pathway and sub – pathways (bigger font) and down – regulated ones (smaller font).

- miRNA target identification and pathway analysis: 1402 genes resulted experimentally validated targets of 23 found altered miRNAs in miRTarBase. Five miRNAs (hsa-miR-1307-3p, hsa-miR-3064-3p, hsa-miR-4709-3p, hsa-miR-3615 and hsa-miR-637) are able to regulate five already known RP causative genes [Kelch-like protein 7 (*KLHL7*), Retinol Dehydrogenase 11 (*RDH11*), CeramideKinase Like (*CERKL*), Aryl hydrocarbon receptor interacting protein like1 (*AIPL1*) and Usher syndrome type 1G (*USH1G*)], as

demonstrated by high-throughput sequencing of RNA isolated by cross-linking immunoprecipitation (HITS-CLIP), Photoactivatable-Ribonucleoside-Enhanced Cross-linking and Immunoprecipitation (PAR-CLIP) and crosslinking, ligation, and sequencing of hybrids (CLASH). 810 genes, instead, resulted common to ones emerged from microT prediction, which totally showed 7351 target genes. Subsequently, mirPath KEGG analysis showed a statistically significant association between six analyzed miRNAs (hsa-miR-3615, hsa-miR-922, hsa-miR-4523, hsa-miR-671-3p, hsa-miR-198, hsa-miR-1307-3p) and “NF-kappa B signaling pathway”, and two miRNAs (hsa-miR-922 and hsa-miR-1307-3p) and “Fatty acids biosynthesis and metabolism”. mirPath GO analysis, instead, showed a statistically significant association between six miRNAs (hsa-miR-3615, hsa-miR-922, hsa-miR-637, hsa-miR-671-3p, hsa-miR-198, hsa-miR-1307-3p) and four categories (“Cellular nitrogen compound”, “Metabolic process”, “Organelle”, “RNA binding and poly(A) RNA binding”), five miRNAs (hsa-miR-3615, hsa-miR-922, hsa-miR-637, hsa-miR-198, hsa-miR-1307-3p) and three categories (“Cytosol”, “Biosynthetic process”, “Mitotic cell cycle”), four miRNAs (hsa-miR-3615, hsa-miR-922, hsa-miR-198, hsa-miR-1307-3p) and six categories (“Gene expression”, “Nucleoplasm”, “Protein complex”, “Molecular function”, “Cellular component”). Once obtained experimental validated pathways, we enriched previously gathered data with pathway analysis based on miRTarBase and microTcommon gene targets, realized by Cytoscape and its plugin ClueGO. Pathways with the highest number of involved miRNA – regulated genes could be clustered in “Intracellular organelle”, “Regulation of cellular process”, “Organic cyclic, hetero cycle, cellular nitrogen and aromatic compounds metabolic process”, “Protein metabolic process”, “Nucleic acid binding”, “Macromolecule modification”, “Regulation of transcription”, “Regulation of response to stimulus”, “Proteosomal cleavage of substrate” “IRS – and SOS – mediated signaling”, “ER – Phagosome pathway”, “Inflammation”, “ABC – transporters disorders”, “Signaling by Hedgehog”.

- *miRNAs and RBPs targeting to most altered RPE expressed circRNAs*: only five known mature circRNAs were found in Circular RNA Interactome database: hsa_circ_0007345, originated from DLG1, interacting with 11RBPs (especially with EIF4A3) and 30 miRNAs (particularly with hsa-miR-515-5p); hsa_circ_0080164, coming from TNS3, and interacting with 4 RBPs (especially with EIF4A3) and 5 miRNAs; hsa_circ_0064644, originated from RBMS3, and interacting with 2 RBPs only by circRNA flanking regions, and with 15 miRNAs; hsa_circ_0067946, coming from TNIK gene, and interacting with 3 RBPs (especially with EIF4A3) and 29 miRNAs (particularly with hsa-miR-646, hsa-miR-766 and hsa-miR-767-3p); hsa_circ_0017874, originated from VIM, and interacting with 14 RBPs (especially with FMRP and AGO2) and with 19 miRNAs (particularly with hsa-miR-1290 and hsa-miR-885-3p). Details about the exact number of RNA-binding protein sites matching to circular RNAs or their flanking regions, along with TargetScan miRNA predictions are available in Table 13.

CircRNA ID	Gene Symbol	RBP	Binding Sites	miRNA	#Sites
<i>hsa_circ_0007345</i>	DLG1	O2	4	hsa-miR-1208	1
		DGCR8	1	hsa-miR-1229	1
		EIF4A3	9	hsa-miR-1231	1
		FMRP	1	hsa-miR-1248	1
		HuR	3	hsa-miR-1252	1
		IGF2BP2	1	hsa-miR-1253	1
		IGF2BP3	1	hsa-miR-1270	1
		LIN28A	3	hsa-miR-1278	1
		LIN28B	1	hsa-miR-1305	1
		PTB	1	hsa-miR-136	1
		ZC3H7B	1	hsa-miR-149	2
				hsa-miR-338-3p	1
				hsa-miR-409-3p	1
				hsa-miR-421	1
				hsa-miR-503	1
				hsa-miR-515-5p	3
				hsa-miR-577	1
				hsa-miR-589	1
				hsa-miR-620	1
				hsa-miR-623	1
				hsa-miR-630	1
				hsa-miR-638	1
				hsa-miR-646	1
				hsa-miR-649	1
				hsa-miR-653	1
				hsa-miR-661	1
				hsa-miR-671-5p	1
				hsa-miR-758	1
				hsa-miR-767-3p	2
				hsa-miR-942	1
<i>hsa_circ_0064644</i>	RBMS3	EIF4A3	3	hsa-miR-1183	1
		FUS	1	hsa-miR-153	1
				hsa-miR-1827	1
				hsa-miR-183	1
				hsa-miR-330-3p	1
				hsa-miR-492	1
				hsa-miR-507	1
				hsa-miR-545	1
				hsa-miR-557	1
				hsa-miR-576-3p	1
				hsa-miR-615-5p	1
				hsa-miR-637	1
				hsa-miR-652	1
				hsa-miR-654-3p	1
				hsa-miR-885-3p	1
<i>hsa_circ_0067946</i>	TNIK	AGO2	2	hsa-miR-1184	1
		EIF4A3	12	hsa-miR-1200	1
		HuR	2	hsa-miR-1208	1
				hsa-miR-1296	1
				hsa-miR-1305	1
				hsa-miR-151-3p	1
				hsa-miR-203	1
				hsa-miR-224	1
				hsa-miR-331-3p	1
				hsa-miR-375	1

				hsa-miR-383	1
				hsa-miR-492	1
				hsa-miR-512-5p	1
				hsa-miR-513a-5p	1
				hsa-miR-526b	1
				hsa-miR-545	1
				hsa-miR-5481	1
				hsa-miR-571	1
				hsa-miR-599	1
				hsa-miR-629	1
				hsa-miR-646	2
				hsa-miR-657	1
				hsa-miR-668	1
				hsa-miR-766	2
				hsa-miR-767-3p	2
				hsa-miR-874	1
				hsa-miR-889	1
				hsa-miR-938	1
				hsa-miR-95	1
<i>hsa_circ_0080164</i>	TNS3	AGO2	1	hsa-miR-1179	1
		EIF4A3	13	hsa-miR-1197	1
		FUS	1	hsa-miR-1205	1
		PTB	1	hsa-miR-1256	1
				hsa-miR-1257	1
				hsa-miR-1265	1
				hsa-miR-1286	1
				hsa-miR-1287	1
				hsa-miR-1294	1
				hsa-miR-1322	1
				hsa-miR-139-3p	1
				hsa-miR-145	1
				hsa-miR-153	1
				hsa-miR-197	2
				hsa-miR-198	1
				hsa-miR-203	1
				hsa-miR-370	1
				hsa-miR-488	1
				hsa-miR-510	1
				hsa-miR-518a-5p	1
				hsa-miR-527	1
				hsa-miR-578	2
				hsa-miR-579	1
				hsa-miR-581	2
				hsa-miR-636	1
				hsa-miR-649	1
				hsa-miR-657	1
				hsa-miR-873	1
<i>hsa_circ_0017874</i>	VIM	AGO1	1	hsa-miR-1184	1
		AGO2	6	hsa-miR-1200	1
		C22ORF28	1	hsa-miR-1205	1
		CAPRIN1	1	hsa-miR-1279	1
		DGCR8	2	hsa-miR-1288	1
		EIF4A3	2	hsa-miR-1290	2
		FMRP	13	hsa-miR-1294	1
		IGF2BP1	3	hsa-miR-370	1
		IGF2BP2	1	hsa-miR-494	1
		IGF2BP3	3	hsa-miR-510	1
		LIN28A	1	hsa-miR-512-5p	1
		PTB	2	hsa-miR-513a-5p	1
		SFRS1	1	hsa-miR-545	1
		ZC3H7B	1	hsa-miR-598	1
				hsa-miR-616	1
				hsa-miR-657	1
				hsa-miR-661	1
				hsa-miR-885-3p	2
				hsa-miR-890	1

Tab. 13. CircInteractome results of RNA-binding protein sites and miRNAs matching to circular RNAs. Table shows RBPs binding in different regions of analyzed circRNAs or in their flanking regions, along with TargetScan predictions of miRNA “sponged” by given circRNAs.

- snoRNAs target identification and host genes pathway analysis: 68 different residues of ribosomal RNAs resulted as targets of 84 found altered snoRNAs in snoRNABase, snOPY and Ingenuity Target Explorer. Specific targets of 5 H/ACA box snoRNAs (SNORA18, SNORA53, SNORA59A, SNORA59B, SNORA11D) and of 10 C/D box snoRNAs (SNORD23, SNORD89, SNORD109B, SNORD116-24, SNORD116-6, SNORD116-8, SNORD22, SNORD83A, SNORD83B, SNORD84) resulted, instead, still unknown. Afterwards, 6 “macro – pathways” (“L-13-mediated translational silencing of Ceruloplasmin expression”, “Cytoplasmic translation”, “RNA helicase activity”, “Dissociation of L13a from the 60S ribosomal subunit”, “eIF3 and eIF1A bind to the 40S subunit” and “Association of phosphor-L13a with GAIT

element of Ceruloplasmin mRNA”) and 125 “sub – pathways” resulted from host genes pathway analysis.

5. DISCUSSION

5.1. CLASSIFICATION OF NEW RP FORMS BY NEW GENOTYPE – PHENOTYPE ASSOCIATIONS

RP is a highly heterogeneous disease in clinical features and genetics, and association of mutations/variants in at least 80 genes to the various forms of the disease (recessive, dominant, and X – linked) (Sorrentino, Gallenga, Bonifazzi, & Perri, 2016) is not immediate. Furthermore, it is highly likely that mutations/variants in other still unidentified genes, as well as non – coding RNAs (Donato, Bramanti, et al., 2018), could contribute to RP pathogenesis. The complexity of the situation is compounded by the variety of genotype-phenotype combinations that occur. Heterogeneity depends on various factors. First, the allelic factor: each gene may present various disease-causing mutations leading to the same phenotype. Secondly, the genetic factor: different genes, when mutated, might induce the same pathological phenotype. Thirdly, the phenotypic factor: different mutations in the same gene can lead to different clinical pictures (Donato, Scimone, Rinaldi, et al., 2018). Fourthly, the clinical factor: the same gene mutation can cause different signs and symptoms, even in members of the same family (Reiff et al., 2016).

Affected family members reported in this work showed a wide range of phenotypes. Such clinical heterogeneity could result from a combination of previously described factors. WGS (Park & Kim, 2016) permitted to investigate the whole genome of the proband and find new potentially RP-associated gene variants, which were then studied in the other family members. By applying previously described filtering criteria and grounding our search on quality score analysis and homopolymeric filtering, we discarded most false positive results. Negative results were dealt with using the highly sensitive algorithm Fixed Ploidy Variant Caller from Qiagen. Then, to discriminate the actual involvement of all previously selected variants in the etiopathogenesis of the unknown form of RP reported here, data mining with eye-related pathway analysis per phenotypes of each patient were combined. In the end, nine variants, distributed within six genes (*PAX2*, *RXRG*, *CACNG8*, *CCDC175*,

PDE4DIP, and *LTF*), emerged as potentially associated with RP in analyzed cases. *PAX2*, *RXRG* and *CACNG8* variants will be deeply discussed in section 6.2.

- *PDE4DIP* (Phosphodiesterase 4D Interacting Protein, 1q21.1) gene product, also known as myomegalin, anchors the phosphodiesterase 4D (PDE4D) at centrosome-Golgi cell region (Shapshak, 2012), acting as a scaffolding protein (Roubin et al., 2013) necessary for the polymerization of centrosomal and Golgi-derived microtubules. It was seen that depletion of myomegalin decreased directional migration of RPE cells (Di Gioia et al., 2015). Due to its direct interaction with SANS (scaffold protein containing ankyrin repeats and SAM domain, *USH1G*), myomegalin can be implicated in the USH photoreceptor transport network, targeting vesicles from the Golgi apparatus to the outer segment, or from this compartment to the periciliary target membrane (Overlack et al., 2011).
- The lactotransferrin gene (*LTF*, 3p21.31) and protein expression have been detected at high levels in adipose tissue, directly associated with adipogenesis and insulin signaling-related pathways and inversely associated with inflammatory markers (Moreno-Navarrete et al., 2014). Large *LTF* expression was seen in all 3 types of secondary corneal amyloidosis (Araki-Sasaki et al., 2013), but had never been previously linked to RT.
- Little is known about *CCDC175* (coiled-coiledomain containing 175, 14q23.1), especially in homo sapiens. The only available data come from the STRING database and highlight an interaction between the *Mus musculus* *ccdc175* protein and IL23R (Interleukin 23 Receptor), which is associated with two eye-relevant and rare diseases, Behçet's Disease and Vogt-Koyanagi-Harada Syndrome (Cao et al., 2016; Hou et al., 2015; H. Yu et al., 2016). We conducted a whole transcriptome analysis on human RPE cells which showed a decreased expression of *CCDC175*, after an oxidant chemical compound treatment. Therefore, we can say that expression of *CCDC175* occurs in the human retina, as well as other considered genes, established by the same RNA – Seq experiment (submitted data, partially shown in Supplementary Table S1).

This scenario could promote cone and rod death, due to the lack of fundamental anti-inflammatory activity of lactotransferrin, which failed because of the presence of *LTF* rs1126477:G>A and rs1126478:A>G and, probably, *CCDC175* rs7141565:C>G and c.76 C>T. Additionally, photoreceptor death may be due to reduced expression of *PDE4DIP* variants, the 3' UTR variants rs141564171:G>A and c.*105 G>A. These variants might determine the block of microtubule polymerization, preventing the proper transport of phototransduction proteins between the inner and the outer photoreceptor segments.

- *GLO1* (Glyoxalase I, 6p21.2) encodes the main of two enzymes (Glo I and Glo II) that constitute the Glyoxalase system, which plays an important role in detoxification of MGO. GloI catalyzes the conversion of methylglyoxal into to (S)-D-lactoylglutathione. Glo-II hydrolyses the reaction of S-D-Lactoylglutathione to H₂O and D-lactate (Chang & Wu, 2006). In the retina, defense against oxidative stress (one of the first cause of RP) is principally carried out by glyoxalase system (Berner et al., 2012). However, the activity of glyoxalase depends on adequate levels of GSH that can be reduced by the same MGO, making the cells more sensitive to oxidative stress. Furthermore, an excess of MGO inactivates antioxidant enzymes such as glutathione peroxidase and SOD, which impairs degradation of MGO. Since MGO is an important precursor for AGEs, Glyoxalase 1 activity indirectly determines the rate of AGEs formation, and therefore, might be of particular interest in AGEs accumulation. AGEs act as mediators of neurodegeneration, induce irreversible changes in the extracellular matrix, vascular dysfunction and pro-inflammatory signalling. Cells and tissues of the eye are profoundly influenced by such processes, and consequently AGEs can have a pathogenic role in onset and progression of retinal diseases including Retinitis pigmentosa.

Analyzed polymorphisms could alter the enzymatic activity of GLO1, contributing to oxidative damage that causes the gradual death of cones after the complete loss of rods. Frequencies of rs2736654 (c. A332C, p.E111A), rs1130534 (c.372A>T, p.G124G), and rs1049346 (c.-7 C>T, 5'-UTR) *GLO1* gene polymorphisms were evaluated in a control sample and in a population of patients with RP (Donato, Scimone, Nicocia, et

al., 2018). Relatively to rs1130534 polymorphism, known to reduce the activity of enzyme in whole blood lysates (Peculis et al., 2013), an association between T allele and RP was found. About the rs1049346 (c.-7 C>T, 5'-UTR) polymorphism, located in the 5' –UTR of *GLO1* gene, a protective role of CT/TT genotypes was found, as also demonstrated by AAT (++-) (rs1130534-rs2736654- rs1049346), TCT (---) and TAT (-+-) haplotypes with a higher frequency in the control group than in RP patients. These data disagreed with some studies reporting the association between rs1049346 C>T polymorphism and *GLO1* expression levels. *GLO1* enzyme activity was detected in whole blood lysates from patients with diabetes and a significant association between C allele and decreased *GLO1* enzyme activity was found (Peculis et al., 2013). The reduction was observed also in a study on *GLO1* promoter activity by reporter gene assays (Junaid et al., 2004). As other ambiguous roles played by the same SNP (D'Angelo et al., 2017), the protective role allele c.-7T indicated by us, in contrast with the enzymatic reduction observed elsewhere, could be explained by considering that these analyses were performed in whole blood lysates and not in the retina where the presence of specific factors could modulate the enzymatic activity. In particular, there could be RNA-binding proteins for *GLO1* 5'-UTR able to modulate the levels of glyoxalase protein by acting on mRNA stability. Furthermore, the current state, it is not possible excluded that the reduction in the activity of *GLO1* and the consequent increase of the levels of MGO do not play a role in cell proliferation and viability. In this regard, experiments document both the increased vulnerability of si*GLO1*-transfected melanoma cells to the cytotoxic effects of exogenous methylglyoxal and upregulation of cellular levels of MGO modified heat-shock protein (Hsp27) that contributes to protection from caspase-dependent cell death (Bair, Cabello, Uchida, Bause, & Wondrak, 2010). Therefore, further functional studies are needed to test these hypotheses. If obtained data will be confirmed by further studies, also in non – Sicilian populations, the examination of these haplotypes may represent a potential biomarker and a useful tool to screen risk individuals of RP.

- *PPEF2* (Protein phosphatase with EF-hand domains 2, 4q21.1) encodes a potent negative regulator of apoptosis signal regulating kinase-1 (ASK1), a MAP kinase kinase kinase implicated, among the others, in neurodegenerative diseases. ASK1 is activated by oxidative stress and induces pro-apoptotic or

inflammatory signaling. So PPEF2 expression may correlate with stress protective responses, cell survival, growth, proliferation, or neoplastic transformation (Kutuzov, Bennett, & Andreeva, 2010).

- *RNF144B* (Ring Finger Protein 144B, 6p22.3), encoding an IBR-type RING-finger E3 ubiquitin ligase, regulates the levels of the pro-apoptotic Bax and protects cells from unprompted Bax activation and cell death. Downregulation of RNF144B induces increased cellular levels and accumulation of the active form of Bax (Benard et al., 2010). Moreover, in the regulation of p53-dependent apoptosis, the miR-100 antagonism inhibits ubiquitin-mediated p53 protein degradation by activating RNF144B (G. Yang, Gong, Wang, Wang, & Zhang, 2016).
- *RDH13* (Retinol dehydrogenase 13, 19q13.42) encodes a recently discovered short-chain dehydrogenase/reductase, related to microsomal retinoid oxidoreductase RDH11. Retinol dehydrogenases (RDHs) reduce all-trans retinal to all-trans retinol after bleaching of visual pigment in vertebrate photoreceptors. The localization of RDH13 on the outer side of the inner mitochondrial membrane suggests that it may act protecting mitochondria against oxidative stress associated with the highly reactive retinaldehyde produced from dietary β -carotene (Belyaeva, Korkina, Stetsenko, & Kedishvili, 2008). The possible inhibition of the mitochondrial apoptosis pathway could protect the retina against acute light-induced retinopathy (H. Wang et al., 2012).
- Activation of *FLT3* (Fms Related Tyrosine Kinase 3, 13q12.2) with its ligand could inhibit the proliferation of neural progenitor cells and promote neuron survival, along with NGF (Mitton et al., 2003). Fiz1 (Flt3-interacting zinc-finger protein) acts as transcriptional repressor of neural retina leucine zipper (NRL) function in photoreceptors, providing a possible role into retina impairment (Mitton et al., 2003).

The last intron variants were analyzed to discover their possible negative role into the splicing events. The sequences that allow the recognition of splice sites are called exonic or intronic splicing enhancers (ESE or ISE), recognized by proteins belonging to the SR family. In addition, the sequences that mask those sites are called exonic or intronic splicing silencers (ESS or ISS) and are recognized by heterogeneous nuclear ribonucleoproteins (hnRNPs). Therefore, the selection of a given splice site (and, consequently, the possibility of alternative splicing), depends on the presence of ESE sequences, ISE, ESS or ISS, and on the availability of the proteins that bind them. According to what described, it is clear that, alterations in the nucleotide sequence of the gene, can be translated in the abolition of enhancers sequences or, on the contrary, in the creation of silencers sequences, responsible for the lack of recognition of canonical splice sites. Moreover, mutations in the nucleotide sequence, could lead to a removal of the canonical sites and the creation of new cryptic splice sites. Variants in *PPEF2* rs1976518 and *RDH13* rs2569513 were predicted to brake exonic ESE sites, while exonic ESS sites could be destroyed by *FLT3* rs17086226 or created by the previous *RDH13* polymorphism and *RNF144B* rs1886248. The latter, furthermore, could be involved into the activation of an exonic cryptic donor site. Less deleterious intronic ESE sites could be created by *PPEF2* rs12498639 and the yet cited *FLT3* variant, while the *PPEF2* rs1566975 also involved into the brake of an intron ESS site. The other deep intronic variants, characterized by a more intricate splicing alteration pattern, should also determine a relevant modification to the process. The interrupted balance caused by the contemporary presence of all analyzed variants could create a scenario rich of altered proteins, which might increase oxidative stress (*RDH13*) that, along with the pro-apoptotic role determined by *PPEF2*, *RNF144B* and *FLT3* alterations, could lead to photoreceptors death and the onset of retinitis pigmentosa. Further steps, already started, consist of functional assays able to demonstrate, in vitro and in vivo, in silico obtained results.

- *RCVRN* (Recoverin, 17p13.1): this gene encodes a member of the recoverin family of neuronal calcium sensors, which contains three calcium-binding EF-hand domains. It may delay phototransduction cascade termination in the retina by blocking the phosphorylation of photo-activated rhodopsin (Maeda,

Imanishi, & Palczewski, 2003; Strissel et al., 2005). Recoverin may be the antigen responsible for cancer-associated retinopathy (Bazhin, Schadendorf, Philippov, & Eichmuller, 2007).

- *GNB1* (G Protein Subunit Beta 1, 1p36.33) and *GNGT1* (G Protein Subunit Gamma Transducin 1, 7q21.3): heterotrimeric guanine nucleotide-binding proteins (G proteins), which transduce extracellular signals received by transmembrane receptors to effector proteins (Mylvaganam, McGee, Berson, & Dryja, 2006). They are membrane bound GTPases that are linked to 7-TM receptors. Each G protein contains an α -, β - and γ -subunit and is bound to GDP in the “off” state. Ligand-receptor binding results in detachment of the G protein, switching it to an “on” state and permitting G_{α} activation of second messenger signalling cascades. Transducin is one of these proteins, found specifically in rod outer segments, where it mediates the activation of a cyclic GTP-specific guanosine monophosphate phosphodiesterase by rhodopsin (Clack, Juhl, Rice, Li, & Witzmann, 2003). *GNB1* encodes a β subunit, while *GNGT1* the gamma one (Hurley & Stryer, 1982) (Scherer, Feinstein, Oliveira, Tsui, & Pittler, 1996). The α subunit is encoded by *GNAT1* gene. The β and γ chains are required for the GTPase activity, for replacement of GDP by GTP, and for G protein-effector interaction (provided by RefSeq, Sep 2013).
- *GRK7* (G Protein-Coupled Receptor Kinase 7, 3q23): This gene encodes a member of the guanine nucleotide-binding protein (G protein)-coupled receptor kinase subfamily of the Ser/Thr protein kinase family (GRK) (C. K. Chen et al., 2001). It is a retina-specific kinase involved in the shutoff of the photoresponse and adaptation to changing light conditions via cone opsin phosphorylation, including rhodopsin (RHO) (Osawa & Weiss, 2012). It is believed that the movements of intracytoplasmic loop of activated RHO are responsible for the activation of the GRK7, in a way similar to GRK1 (Horner, Osawa, Schaller, & Weiss, 2005).
- *ARRB1* (Arrestin Beta 1, 11q13.4): members of arrestin/beta-arrestin protein

family are thought to participate in agonist-mediated desensitization of G-protein-coupled receptors and cause specific dampening of cellular responses to stimuli such as hormones, neurotransmitters, or sensory signals (P. Wang et al., 2014). Arrestin beta 1 is a cytosolic protein and acts as a cofactor in the beta-adrenergic receptor kinase (BARK) mediated desensitization of beta-adrenergic receptors. During homologous desensitization, beta-arrestins bind to the GPRK-phosphorylated receptor and sterically preclude its coupling to the cognate G – protein; the binding appears to require additional receptor determinants exposed only in the active receptor conformation (Y. X. Zhang et al., 2017). The beta-arrestins target many receptors for internalization by acting as endocytic adapters (CLASPs, clathrin-associated sorting proteins) and recruiting the GPRCs to the adapter protein 2 complex 2 (AP-2) in clathrin-coated pits (CCPs). However, the extent of beta-arrestin involvement appears to vary significantly depending on the receptor, agonist and cell type. Internalized arrestin-receptor complexes traffic to intracellular endosomes, where they remain uncoupled from G-proteins (Bhattacharyya, Hope, & Young, 2011). Beta-arrestins function as multivalent adapter proteins that can act as signaling scaffold for MAPK pathways, like several other proteins as CCM proteins (Scimone, Bramanti, et al., 2017; Scimone et al., 2015), in the so-called beta-arrestin signalosomes (McLaughlin et al., 2006). Moreover, they can be involved in IGF1-stimulated AKT1 signaling leading to increased protection from apoptosis, in activation of the p38 MAPK signaling pathway and in actin bundle formation, in F2RL1-mediated cytoskeletal rearrangement and chemotaxis, and in AGTR1-mediated stress fiber formation by acting together with GNAQ to activate RHOA (Barnes et al., 2005).

As highlighted by the pathway database Reactome, all five gene products cooperate during phototransductional activation, especially in the dark adaptation, as confirmed by KEGG. Thanks to BioGraph web service, STRING, GeneAnalytics and VarElect, it could be conjectured how these genes should be involved into etiopathogenesis of retinitis pigmentosa (Donato & Denaro, 2018). All five analyzed genes share annotation or pathways with already known causative ones: in detail, they are *TULP1* (required for normal photoreceptor function and for long-term survival of

photoreceptor cells, interacts with cytoskeleton proteins and may play a role in protein transport of these cells), *PROM1* (during early retinal development acts as a key regulator of disk morphogenesis; it is also involved in regulation of MAPK and Akt signaling pathways), *RPI* (encoding a MAP needed for the correct stacking of disc in the outer segment of photoreceptor), *RPGR* (guanine-nucleotide releasing factor, which plays a role in ciliogenesis and in intraflagellar transport processes by regulating actin stress filaments and cell contractility), *CNGA1* (the encoded protein can be activated by cyclic GMP which leads to an opening of the cation channel and thereby causing a depolarization of rod photoreceptors), *GUCAIB* (calcium-binding protein that activates photoreceptor guanylate cyclases; this Ca²⁺-sensitive regulation of GC is a key event in recovery of the dark state of rod photoreceptors following light exposure), *PDE6A-B* (these genes encode alfa and beta subunits of the phosphodiesterase 6 holoenzyme, which regulate the rod cGMP concentration, an important regulator of cell membrane current), and *CNGB1* (subunit of cyclic nucleotide-gated channels, nonselective cation channels, involved in the regulation of ion flow into the rod photoreceptor outer segment (ROS) in response to light-induced alteration of cGMP intracellular levels). *GNGT1* shares many targets of *GNB1*, but also shows a protein interaction with *RHO* and involvement in eye photoreceptor cell development and light signal transduction, annotating with *RGR* (putative retinal G-protein coupled receptor for all-trans- and 11-cis-retinal; it binds preferentially to the former and may catalyze the isomerization of the chromophore by a retinochrome-like mechanism). *RCVRN* stands for the calcium sensitive guanylate cyclase activator activity, requested for its fine molecular regulation. *GRK7* evidences a protein interaction with *PDE6D* (another subunity of the PDE complex, that also binds to prenyl groups of proteins to target them to subcellular organelles called cilia) and annotation with genes appointed to vision, *FAMI61A* (involved in ciliogenesis) and *SPATA7* (required for the stable assembly and localization of the ciliary RPGRIP1 protein complex in the connecting cilium). *ARRB1*, instead, shows a fundamental protein interaction with *SAG* (member of arrestin/beta-arrestin protein family, is a major soluble photoreceptor protein that is involved in desensitization of the photoactivated transduction cascade) and *DPY30*, component of a multiprotein histone methyltransferase complex, which regulates the causative *PRPF3* gene (participates in

pre-mRNA splicing).

- *RLBP1* (Retinaldehyde Binding Protein 1, 15q26.1) is expressed in retinal pigment epithelium (RPE) and encodes for the cellular retinaldehyde-binding protein 1, CRALBP, involved in visual cycle. Particularly, CRALBP binds 11-cis-retinol which needs to be oxidized in 11-cis-retinal; 11-cis-retinal is carried into photoreceptors where combines with opsin, resulting in visual pigments formations (Kennedy et al., 2003). This process is common in both cones and rods. Different *RLBP1* mutations were linked to a wider spectrum of phenotype as Bothnia retinal dystrophy (BD), Newfoundland rod-cone dystrophy (NFRCD), fundus albipunctatus (FA). Such forms differ for age of onset, progression and severity (Hipp et al., 2015). A founder effect was proven for mutation p.R234W, causing Bothnia phenotype (Burstedt et al., 2013), as well as for splice-junctions mutations detected in NFRCD cases (Eichers et al., 2002). Therefore, different clinical manifestations are tightly linked to the effects of mutations on protein structure.

Molecular screening of all known RPA causative genes in Sicilian family n°3 of section 3.1.1 showed a novel single base-pair frameshift deletion, c.398delC, in exon 6 of *RLBP1*. It leads to a truncated 258 aminoacids protein. Premature stop codon falls within exon 8. CRALBP protein contains one CRAL-TRIO lipid binding domain, of 162 aminoacids (136-297). As predicted by in-silico analysis, the c.398delC affects proline 133 and causes total disruption of CRAL-TRIO domain, resulting in a loss of ability to bind its ligands. CRAL-TRIO motifs usually bind small hydrophobic molecules. In CRALBP, aminoacids 136 – 297 form CRAL-TRIO domain and, 12 of these, form the retinoid binding pocket (Wu, Hasan, Liu, Teller, & Crabb, 2004). Therefore, c.398delC has deleterious effects on protein's functionality (Scimone, Donato, et al., 2017). Presence of variant c.398delC was assessed also in the other family's members, despite they show no pathological phenotypes. Of these, the healthy father and other relatives showed this variant, in a heterozygous condition. This confirms autosomal recessive model of inheritance of RPA. The proband carries the novel c.398delC mutation in a homozygous condition. We proceeded to investigate frequency of variant in Fiumedinisi's population. Fiumedinisi, a small town in

province of Messina, is located on the Ionian side, at the height of 190 above sea level. It has an area of 36 km² and extends along Nisi's valley, at Mt. Belvedere's slopes, behind Valle del Mela. The city was founded in VII century b. C., by a group of Calcedesi Greek colonists, attracted by mineral deposits, who inhabited the high area of Mt. Belvedere. Later, Roman, Arab, Norman, Angevin and Spanish dominions went on. During these centuries, the town was moved to the foot of mountain (where it remains today) and renamed as FlumenDionisyi. Still today, it results not easy for getting to. Two big disasters hit the city: an epidemic plague in 1743 and a big flood in 1855. A period of decline, then, started due to high immigration's phenomenon. To date, Fiumedinisi's population counts about 1400 inhabitants, most of which are over age of 50 years. After the screening of about 25% of population, c.398delC was found in 0,01% and it is in HWE. No other RPA cases were detected in the town. Although high rate of consanguinity in Fiumedinisi's population, its low frequency may be attributed to both several dominations, repeated drastic reductions in population, the probable selective disadvantage, a recent founder effect. This last hypothesis can be demonstrated by several statistic approaches. Among these, the method proposed by Slatkin and Rannala (Slatkin & Rannala, 2000) based on allele frequency and coalescent process (Goldstein et al., 1999) is what it should be applied to estimate the age of c.398delC mutation, as next development of realized work.

The role of each gene described in this section is represented in Fig. 29.

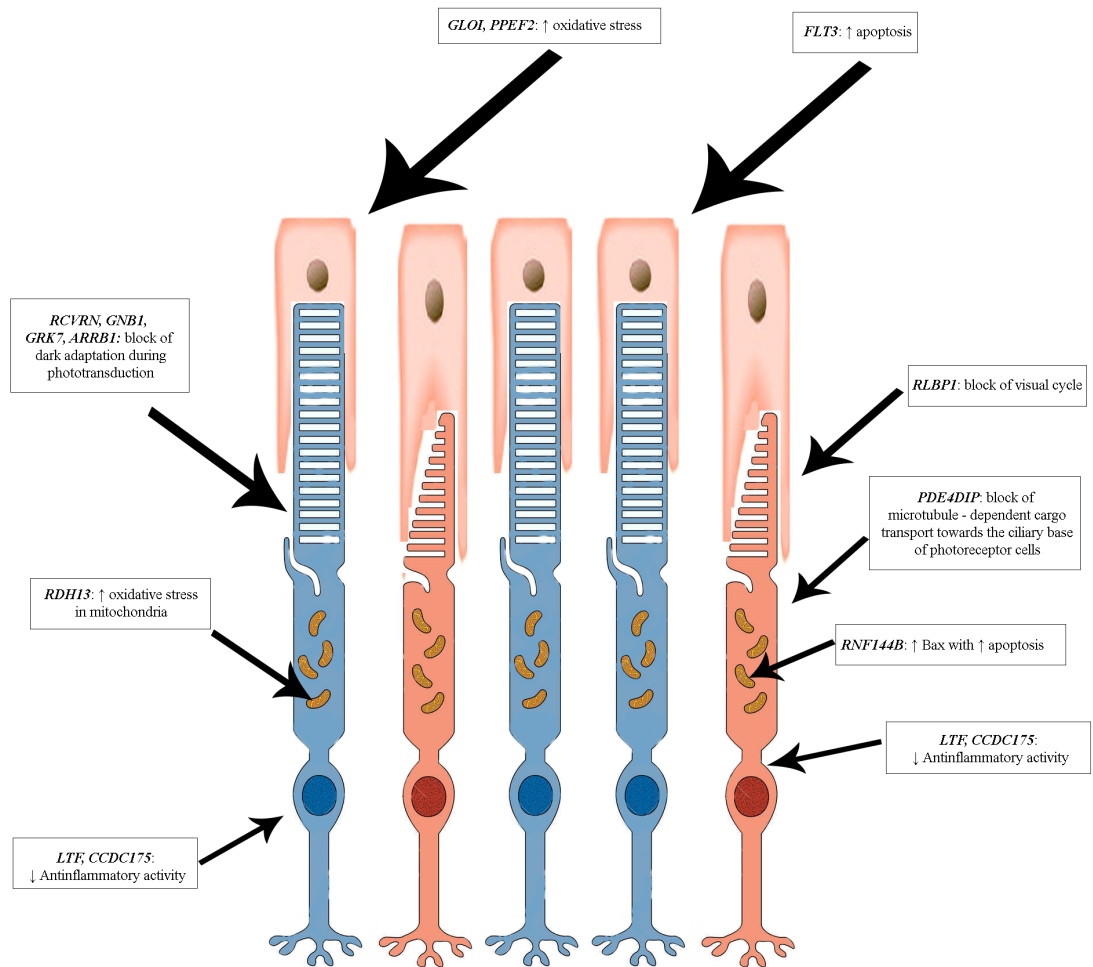


Fig. 29. Proposed RP pathogenic mechanism of involving variants in new candidate genes. Mutations in 13 analyzed genes could determine a serious oxidative stress to photoreceptors and RPE cells and, along with an impairment of their main functions (visual cycle and phototransduction), could increase their apoptotic rate. Details in the text.

5.2. IMPAIRED BIDIRECTIONAL NEUROTRANSMISSION IN THE INNER RETINA LAYERS AS RP FIRST PATHOGENETIC MECHANISM (AND NOT AS EFFECT)

Results from all realized experiments suggest us a possible non – syndromic RP etiopathogenesis lead by inner retinal cells, whose death could be determined by an impairment of their primary neurotransmission function. There were found 51 coding and 28 non-coding genes (6 as target of circRNAs and 22 as target of Sense lncRNAs) involved in neurotransmission and synapses pathways, all genes showing expression changes between selected time points earlier than other genes involved in pathways already associated to RP (e. g. photoreceptor death). Previously cited 79 genes could

be involved in a strong scenario, corroborated by particular phenotypes of affected members of the fourth family in 3.1.1 section (e. g. optic nerve impairment before other symptoms related to photoreceptor degeneration), in which cooperate with 3 mutated genes, came from genome sequencing of just mentioned family, probably representing the driver elements able to cause the onset of a new specific RP form:

- CACNG8 (Calcium voltage-gated channel auxiliary subunit gamma 8, 19q13.4) encodes the γ -8 member of transmembrane AMPA receptor-associated regulatory proteins (TARPs). They represent a family of auxiliary proteins that modulate the kinetics of α -amino-3-hydroxy-5-methyl-4-isoxazolepropionic acid (AMPA) receptors (AMPA receptors) (Khodosevich et al., 2014). These molecules, increasing receptor surface trafficking and unitary conductance (E. Suzuki, Kessler, & Arai, 2008), regulate receptor localization to post-synaptic sites (Itakura, Watanabe, Sugaya, & Takahashi, 2014). In particular, TARP γ -8 is an N-glycosylated protein, which contains two glycosylation sites, Asn⁵³ and Asn⁵⁶. TARP γ -8 glycosylation is critical for surface expression of both TARP γ -8 and GluA1 AMPAR subunit in neurons (Zheng, Chang, Suh, & Roche, 2015). Moreover, it was demonstrated that the deactivation and desensitization time constants of GluR3 receptors were greatly increased by TARP γ -8 (E. Suzuki et al., 2008). Additionally, the γ -8 proline/alanine (P/A) rich region was seen to be essential for binding calcineurin (Cn) (Itakura et al., 2014). Cn is a Ca²⁺/calmodulin-dependent Ser/Thr phosphatase involved in synaptic transmission and plasticity pathways, such as long-term plasticity (LTP) and long-term depression (LTD) (Itakura et al., 2014). Cn is transported to the plasma membrane through interaction with γ -8, suggesting that the γ -8/calcineurin complex may modulate AMPA receptor phosphorylation (especially GluA1) and trafficking (Itakura et al., 2014). Furthermore, since Cn anchored to γ -8 is also localized in close proximity to the postsynaptic membrane, it is assumed to dephosphorylate ionotropic glutamate receptors in a neural activity – dependent manner and to influence synaptic functions in γ -8 positive neurons. TARPs control synaptic strength both by targeting AMPARs to synapses through an intracellular PDZ-binding motif and by

regulating their gating through an extracellular domain (Sumioka et al., 2011). Although the extracellular domain of γ -8 can determine slower AMPAR decay kinetics, it is constrained by an inhibitory influence of AMPAR channel gating exerted by the intracellular domains of γ -8 (Milstein & Nicoll, 2009).

- RXRG (Retinoid X Receptor Gamma, 1q22-q23) is one of the members of the steroid/thyroid hormone superfamily of nuclear receptors, involved in the vitamin D pathway (Grave et al., 2016) and in lipid homeostasis (Sentinelli et al., 2013). RXRG, activated by 9-cis retinoic acid, plays also an important role in the differentiation of cones (Onishi, Peng, Chen, & Blackshaw, 2010; Swaroop, Kim, & Forrest, 2010), especially short-wavelength (S) and long/middle-wavelength (L/M) ones, heterodimerizing with the thyroid hormone receptor β 2 (TR β 2) (Forrest & Swaroop, 2012; Ng et al., 2001).
- PAX2 (Paired Box 2, 10q24.31) is a member of the paired box genes cluster, expressed by glial cells within the optic nerve, and is required for the correct closure of the cephalic neural tube in eye morphogenesis (Torres, Gomez-Pardo, & Gruss, 1996). Furthermore PAX2, together with its main molecular partner PAX6, regulates cell proliferation and differentiation in developing neural retina, as well as the activation of pigmentation genes in normal RPE and the regulation of cell proliferation in transdifferentiated RPE (Fujimura et al., 2015). It seems likely that different combinations of binding partners, phosphorylation states, DNA/promoter methylation, and possibly splice variants decrease the activity of the transactivation domain and establish whether reciprocal inhibition of PAX6 and PAX2 occurs. It is also possible that the tissue-specific PAX2 isoform in Muller glia, especially when it is up-regulated, lacks the capacity to inhibit *PAX6* expression (Fischer & Reh, 2001).

The developed working hypothesis, explained below, is based on the recent discovery regarding photosensitive retinal ganglion cells (ipRGCs), and their capacity of expressing melanopsin intrinsically (J. Zhang, Wang, Wu, Liu, & Wang, 2017). These cells represent the third class of retinal photoreceptors whose axon collaterals

constitute a centrifugal pathway to upstream dopaminergic amacrine cells (DACs) forwarding melanopsin-based signals from the innermost retina to the outer retina (Prigge et al., 2016). Melanopsin-based membrane depolarization could trigger glutamate release locally onto DACs, as RGC dendrites contain synaptic vesicle, and AMPA receptors of DACs are located in close proximity to melanopsin-immunopositive dendrites of ipRGCs (Prigge et al., 2016). Activation of the ipRGC axon collateral triggers Ca^{2+} influx via N-type voltage-dependent calcium channels (VGCCs) into the collateral terminals, resulting in glutamate release onto postsynaptic DACs (X. Zhao et al., 2017). Glutamate excites DACs through activation of AMPA glutamate receptors, which depolarizes DACs and increases action potential firing frequency, triggering dopamine release (Prigge et al., 2016). Increased dopamine release mediated by ipRGC activity (which integrates light-adapted cone and melanopsin signals) can also act through D4 dopamine receptors expressed on cones. Cones are known to affect cGMP metabolism, gene expression, and rod-cone coupling, regulating cone photoreceptor adaptation. In addition, the loss of M1 subtype of ipRGCs attenuates light adaptation. This is evidenced by an impaired electroretinogram b-wave from cones (Prigge et al., 2016). This scenario highlights the possibility that RGCs provide physiological signals to the brain but, above all, a retrograde melanopsin-based signaling influencing visual function within the retina. This concept represents the starting point of our hypothesis. All affected family members present a phenotype most likely related to cone impairment already at disease onset, as evidenced by clinical exams (reduced b-wave amplitudes in scotopic ERGs, with increased latency) and by altered color perception. As previously reported, the frequency of *CACNG8* rs66507429:A>T, is extremely low in the Messina population. This variant is candidate to decrease the expression of TARP γ -8 physiologically, interacting with DACs and RGCs AMPARs and reducing both retrograde and anterograde signal transmissions. The arrest of the anterograde pathway may send a stop signal to RGCs, impairing optic nerve activity, (evidenced in IV1 and IV4) by altered evoked potentials. Interruption of retrograde signaling may involve cones, which consequently may die, due to inability to perform neuronal transmission function. Additionally, the presence of the *RXRG* splicing variant rs283696:A>G, not frequent in the Messina population, may also alter the phenotypic proportion of L and

S cones and their differentiation from birth, leading to confused color perception. An altered expression of *PAX2* rs7094977:C>A could also decrease cone cell genesis and correct glial phenotype manifestation. That is a consequence of impairing astrocytes and other neural supporting cells, especially in RPE, preventing it from ensuring a trophic and protective role towards the underlying photoreceptor layer of the retina. The hypothetical compromised functional scenario is represented in Fig. 30. This pathophysiological model appears consistent with bioinformatic and literature data and is currently being experimentally tested.

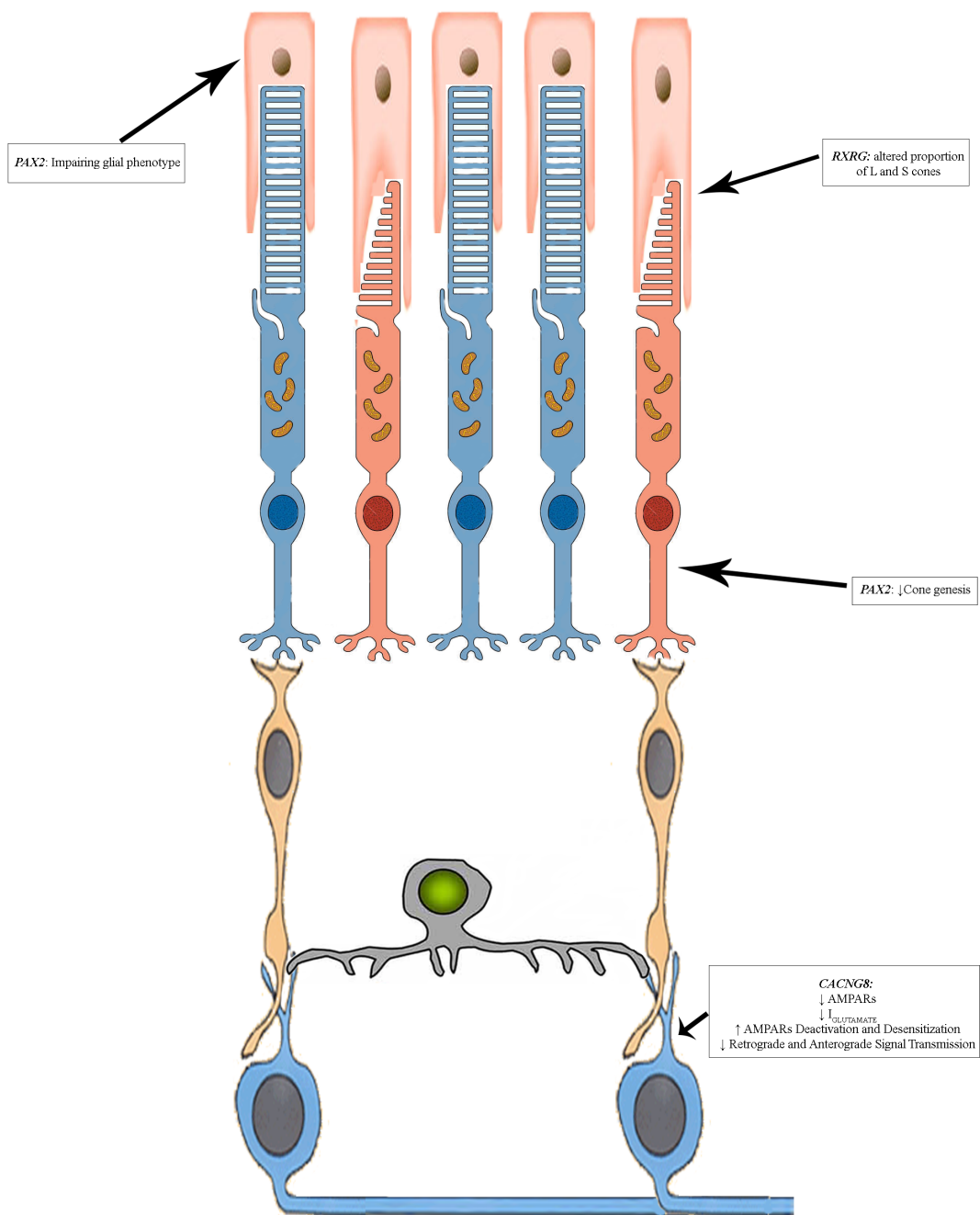


Fig. 30. Proposed pathogenic mechanism of impaired bidirectional neurotransmission in the inner retina layers. Our hypothesis is based on the recent discovery of melanopsin – expressing intrinsically photosensitive retinal ganglion cells (ipRGCs). *CACNG8* rs66507429:A>T could decrease the expression of TARP γ -8 physiologically interacting with DACs and RGCs AMPARs, reducing the retrograde and anterograde signal transmission determining, respectively, an impairment of optic nerve activity and co death. Additionally, the presence of the *RXRG* rs283696:A>G and *PAX2* rs7094977:C>A may have already compromised cones and their differentiation, probably involving astrocytes and other neural supporting cells, especially in RPE. More details in the text.

5.3. EVALUATION OF NEW CONSEQUENCES DETERMINED BY ALREADY KNOWN VARIANTS IN RP CAUSATIVE GENES

- *EYS* (Eyes Shut Homolog – Drosophila -, 6q12) encodes a protein found in the ciliary axoneme, which suggested that it could play an important role in the organization/function of microtubule structures such as the primary cilium (Alfano et al., 2016). Furthermore, EYS is also considered vital for the correct activity of cones (Alfano et al., 2016). Interestingly, the inner segment ellipsoid band length (ISe) of several RP patients with EYS mutations resulted shortened during a 5 year of observation (Miyata et al., 2016). Moreover, variants in EYS were associated to several retinal dystrophies in Tunisian (Habibi et al., 2016), Japanese (Arai et al., 2015) and Indian (Di et al., 2016) populations, but never in Italian one. Despite this, only coding sequence variations were linked to retinal diseases, although it is known the EYS has four isoforms expressed in the retina, regulated by alternative splicing (Alfano et al., 2016).
- *MYO7A* (Myosin VIIA, 11q13.5) encodes a protein localized in retinal pigmented epithelial (RPE) cells, where plays a fundamental role in organelle motility and in light-dependent translocation of the visual cycle enzyme RPE65 (Goldenberg-Cohen et al., 2013). A small quantity of myosin VIIA is also associated with the connecting cilium of photoreceptor cells, probably maintaining a diffusion barrier (Williams & Lopes, 2011). Mutations in Myosin VIIA gene are known to be causative of Usher's Syndrome (Ben-Rebeh et al., 2016). Interestingly, splicing variants of MYO7A were yet analyzed (Jaijo et al., 2011), and several could determine mild forms of retinopathy (Ben Rebeh et al., 2010).

As cited in previous sections, the possible negative role of intron variants into the splicing events was emphasized, evaluating the presence of ESE sequences, ISE, ESS or ISS, and the availability of the proteins that bind them (Donato, 2017). Variants in *EYS* (rs149849078 and rs71638759) were predicted to brake exonic ESE sites, while the *MYO7A* rs2276283 is involved into the brake of an intron ESS site. The other deep intronic variants, characterized by a more intricate splicing alteration pattern, should

also determine a relevant modification to the process. The interrupted balance caused by the contemporary presence of all analyzed variants belonging to both genes could create a scenario rich of altered proteins, which might impair the trafficking through the photoreceptors connecting cilium, leading to photoreceptors death and the onset of retinitis pigmentosa. Further steps, already started, consist of functional assays able to demonstrate, in vitro and in vivo, in silico obtained results.

- *RPI* (Retinitis Pigmentosa 1 Protein, 8q11.23) encodes a protein located in the region of the axoneme of rod and cone photo-receptors. The photo-receptor axoneme begins at the basal body in the distal inner segment and passes through the connecting cilium. It is considered the primary pass for continuous polarized transport of proteins and membrane needed in outer segments to substitute older discs with new ones. (Anderson, Fisher, & Steinberg, 1978; Young, 1967). The junction between the connecting cilium and the outer segment is also where disc morphogenesis occurs (Kinney & Fisher, 1978; Steinberg, Fisher, & Anderson, 1980). It has been pointed out (Q. Liu, Lyubarsky, Skalet, Pugh, & Pierce, 2003) that *RPI* could have a role in controlling the orientation and organization of outer segment discs. It may function as a connection between newly formed discs and the axoneme, and this interaction helps discs form in the correct orientation and stack up into outer segments. Several RP1 mutations are causative of many forms of RP (D. Y. Wang, W. M. Chan, et al., 2005).
- *ABCA4* (ATP Binding Cassette Subfamily A Member 4, 1p22.1) encodes for a cytospecific member of the ATP – binding cassette (ABC) transporter superfamily, retina photoreceptor specific. It is an allosteric protein, acting as an inward-directed retinoid flipase, which imports substrates from the lumen to the cytoplasmic side of retinal disc membranes. The substrates are the all-trans-retinaldehyde (ATR) and N-retinyl-phosphatidyl-ethanolamine (NR-PE), an intermediate derived from the reaction of ATR with phosphatidyl-ethanolamine (PE) located in disc membranes. ATR, once transported to the cytoplasmic side, is reduced to vitamin A by trans-retinol dehydrogenase

(tRDH). Then, transferred to the retinal pigment epithelium (RPE), it is converted to 11-cis-retinal. Abca4 protein is involved in photoresponse, removing ATR/NR-PE from the extracellular photoreceptor surfaces during bleach recovery. An altered Abca4 protein cannot remove NR-PE from photoreceptor cells, thus it combines with other ATR molecules, and this, in turn, leads to condensation, oxidation, hydrolysis and rearrangements. All these reactions produce the bisretinoid Di-retinoid-pyridinium-ethanolamine (A2E) (Jang, Matsuda, Itagaki, Nakanishi, & Sparrow, 2005), among which lipofuscin, one of the constituents of fatty yellow pigments that builds up in retinal cells (Cideciyan et al., 2004). This is toxic to the retina, leading to photoreceptor apoptosis and non – syndromic/syndromic (such as Stargardt macular degeneration) progressive vision loss in patients. Therefore, different phenotypes are associated to variable residual functions of the protein, due to several variants of the *ABCA4* gene.

It was supposed that *RPI* homozygous mutations found in the proband could be responsible for his phenotype. His wife, instead, although carrying a triple homozygous in the “hot-spot” region of *RPI*, normally associated with retinitis pigmentosa pathology (El Shamieh et al., 2015), is only mildly affected. Regarding *ABCA4* gene, she is carrying the c. 1268, A>G in heterozygosity. The non-affected daughter, inherited a condition of heterozygosity for all analyzed variants of both genes, manifesting no typical symptoms of retinal pathologies in exam. Online genetic databases (EMBASE, ENSEMBL and PUBMED) report found mutations as polymorphisms. The Human Gene Mutation Database (HGMD) classifies two of them (c. 5008G>A for *RP1* and c. 1268A>G for *ABCA4*) as disease-causing mutations with a question mark (DM?), denoting a probable/possible pathological mutation, reported to be pathogenic in the corresponding report, but where the author has indicated that there may be some degree of uncertainty. The c. 5008G>A, present in wild type condition in the proband, implies the change of an alanine in position 1670 with a threonine implemented by this variation and represents a regulatory region modification, due to its location in a promoter flanking region. As with other *RPI* analyzed SNPs, it would appear to be implicated in retinitis pigmentosa phenotype of Chinese (Sheng et al., 2008; D. Y. Wang, B. J. Fan, et al., 2005; X. Zhang et al., 2010;

X. Zhang et al., 2002) and Indian (Gandra et al., 2008) populations, as well as associated as a member of the “hot-spot” high causative region of *RPI* (Schwartz et al., 2003). The c. 1268A>G, also found in the wild type condition in the proband, represents a missense variation, which changes the histidine in position 423 with a proline, is located within a regulatory region, showing enhancer features, involving one of two transmembrane domains (TMD). It was regarded as a polymorphism found in heterozygosity in 101/440 controls in a comprehensive survey of sequence variation in the *ABCA4* of a German population (Rivera et al., 2000). The same variant results as a high-penetrance disease-causing mutation in a cohort of patients with Stargardt disease in a study from 2004 (Oh et al., 2004), and as a reducing risk factor more recently, also in a heterozygous model (Aguirre-Lamban et al., 2011; Brion et al., 2011; Webster et al., 2001). Bioinformatic software predictions (Sift, PolyPhen 2, PROVEAN), analyzing non-synonymous coding SNPs effects on protein function, give this mutation the status of tolerated or neutral. Furthermore, literature reports the c. 1268, A>G as associated to late-onset Stargardt disease (Yatsenko et al., 2001), to macular degeneration (Baum et al., 2003) and to retinitis pigmentosa (Valverde et al., 2007), depending on severity of symptoms manifested. Despite all these studies, the phenotype associated with this *ABCA* variant is not clear. According to our hypotheses, the c. 1268A>G missense variant may play a protective role against the damaging *RPI* “hot-spot” region variants in syndromic retinitis pigmentosa. These findings suggest that, in our family case, the variant examined leads to an asymptomatic visual phenotype, without any typical features of Stargardt disease or syndromic retinitis pigmentosa. Obtained data is corroborated by the genetic and phenotypic (only a slight reduction of sensitivity on peripheral areas) condition of the proband’s wife and daughter (the latter without any typical or atypical symptomatology), suggesting the likely delaying effect of analyzed polymorphisms regarding pathology onset. Probably, *Rp1* and *Abca4* could interact, directly or indirectly, in order to extend the half-life of photoreceptors. In particular, it could be speculated that the missense variant 1268A>G of *ABCA4* induces a misfolding into encoded protein, which decreases the transport of ATR/NR-PE and, consequently, a lower quantity of PE from disc membranes is consumed in spontaneous adduct formation with ATR. This renewed stability of disc membrane lipids could compensate for the lack due to *RPI*

homozygous mutation in the “hot–spot” region, which results in a misfolded protein unable to guarantee the correct stacking of discs and, above all, proper lipid transport from the inner to the outer segment, in order to build new functional discs.

- *ELOVL4* (ELOVL Fatty Acid Elongase 4, 6q14.1) encodes a member of the elongase family, expressed in retina, brain, skin and sperm, involved in the elongation of very long-chain fatty acids (Bennett & Anderson, 2016). Although little is known about the role of this protein, data reports that the contribution of the enzyme is to be found in the initial rate of VLC-PUFA production and condensation reactions between a fatty acyl-CoA and malonyl-CoA (Agbaga et al., 2014). The role of VLC- PUFA is fundamental. The most reliable hypothesis argues that the VLC-PUFA acyl chain may cover the entire bilayer, representing a flexible hinge at the rim site where the curvature of photoreceptor disk membranes is the greatest (Harkewicz et al., 2012). At rim level, alteration of *ELOVL4* could impair the turnover of photoreceptor disk membranes, due to a modified balance of fatty acid precursors. The direct consequence of this variation leads to an abnormal accumulation of lipofuscin granules, observed in the RPE of mutant retinas, that may could impair retinoic acid trafficking between RPE and photoreceptors (Bennett, Brush, et al., 2014). Recent experiments have shown a reduction in rods ERG oscillatory potentials and scotopic threshold responses in *ELOVL4* KO mice, and presented biomorphologic evidence that the ERG changes are correlated with reduced VLC-PUFA and synaptic architecture. It may affect vesicle tethering or recycling pathways, as well as glutamate release mechanisms, due to VLC-PUFA interaction with synaptic proteins that mediate endo/exocytic activity or that were localized to the synaptic ribbon in photoreceptor terminals (Bennett, Hopiavuori, et al., 2014). It is known that *ELOVL4* mutations, alone or with *PROM1* mutations, could cause enzyme activity loss and, subsequently, the onset of the dominant form of Stargardt disease (Palejwala et al., 2016).

Analysis of *ELOVL4* gene sequence in our patient affected by Stargardt disease permitted to identify two variants, trans-configured on the gene promoter. It was demonstrated that the coexistence of two variants determined the down regulation of

gene transcription, reducing the amount of enzyme. To be precise, the Dual-Luciferase Reporter assay highlighted the down regulation of *ELOVL4* transcription by 97% in the patient's sample (c. -90 G>C and c. -236 C>T). The protein elongating activity loss could lead to several consequences:

- a) Compromising the integrity of photoreceptor membrane compartments, such as Golgi, or even the retinal pigment epithelium (Vasireddy et al., 2009).
- b) Causing a corresponding reduction of rhodopsin levels within outer segment disk membranes, or the production of abnormal hetero-oligomers with its membrane proteins, which may lead to alterations in membrane ultrastructure or biochemistry (Okuda et al., 2010).
- c) Altering VLC-PUFA direct signaling and possible alteration of the rim site where the curvature of photoreceptor disk membranes is greater or the greatest. It was proposed that lipid molecules, such as docosahexaenoic (DHA), eicosapentaenoic and arachidonic acids could activate specific receptors or modulate transient receptor potential cation channel activity. The latter task is enforced by the presence of VLC-PUFAs also in ribbon synapses, as well as the smaller conventional synapses in the retina (Bennett, Hopiavuori, et al., 2014).

Results showed that many TF binding sites were altered in the *ELOVL4* promoter, both for activators (ETF (Kageyama, Merlino, & Pastan, 1989), FBI-I (Maeda et al., 2009), HDAC2 (Fan et al., 2013; X. Kong, Fang, Li, Fang, & Xu, 2009; Koriyama et al., 2013; Lebrun-Julien & Suter, 2015) and TAFII250 (Herzfeld, Nolte, & Muller, 2007; Piper, Dwivedy, Leung, Bradley, & Holt, 2008), Spi-B (Ray et al., 1992), Pax-4 (Rath et al., 2009; Reichman et al., 2010), POLR3A (Natalizio, Robson-Dixon, & Garcia-Blanco, 2009; Sepehri & Hernandez, 1997), TFII-I (Grueneberg et al., 1997; Palmer et al., 2007), PAX-5 (Bougel et al., 2010; Livide et al., 2012), TP53 (Polato et al., 2014; Y. Wang, Wong, Zhang, & Chiu, 2015; Yasuda, Tanaka, Nishiguchi, et al., 2014), SP1 (Alfonso-Jaume, Mahimkar, & Lovett, 2004; Bikbova, Oshitari, Baba, & Yamamoto, 2015; Donovan, Alekseev, Qi, Cho, & Azizkhan-Clifford, 2014) and GR-alpha (Cubilla, Bermudez, Marquioni Ramella, Bachor, & Suburo, 2013; Nader, Chrousos, & Kino, 2009)) and repressors (ZF5 (Orlov et al., 2007), EZF-6 (Trimarchi et al., 1998), CPBP (Koritschoner et al., 1997; Nakamura, Edward, Sugar, & Yue,

2007; Steketee et al., 2014), BCL6B (Lim, Lu, & He, 2012), GKLF (J. Fang, Shaw, Wang, & Goldberg, 2016; Rowland & Peeper, 2006; Villarreal et al., 2010) and RXR-alpha (H. Chen & Privalsky, 1995; Y. Chen et al., 2015; Cvekl & Wang, 2009; J. J. Janssen et al., 1999)). As emerged from Cytoscape pathway analysis, the *ELOVL4* expression reduction in the proband could derive from a complex balance of all TFs, most of which could present a mutual influence in determining the final effect. Focusing on TFs binding sites that have formed as a result of the presence of both examined variants, SP1 probably represents the key node around which other factors determine the overall *ELOVL4* protein under expression. As literature evidences, SP1 should be enhanced by RXR-alpha activity (Y. Suzuki et al., 1999), but this positive status should be repressed or seized by interaction with TFII-I (Bu, Gao, & Gelman, 2011), TP53 (X. Kong et al., 2013) and KLF6 (L. M. Kong et al., 2016), the latter stimulated by KLF4 (Okano et al., 2000). The direct consequences of SP1 inhibition could be related to a decrease of connected PAX-5 (Miranda et al., 2002; C. X. Wu et al., 2004), in turn influencing PAX-4 (Chalepakis & Gruss, 1995). Although there is no solid proof, in literature, of a possible direct interaction, we can hypothesize, basing on previous assumptions, that TFII-I, usually acting as a repressor, could contribute to the inhibition of SP1, as well as the possibility that SP1 impairment could reflect on POLR3A, reducing its activity. Analysing, instead, the TF binding sites lost in the patient, the situation is less clear, because of no data available on involved TF interactions. We can only speculate that, because HDAC2 usually acts as a repressor, with FBI-I as co-repressor (W. I. Choi et al., 2009), both could down regulate another two inhibitors, ZF5 and E2F-6. This situation leaves most of the transcriptional activity to TAFII250, which functions as an activator, and which presents many binding sites in wild-type genotype.

Mutations in previously cited genes could lead to serious impairments in connecting cilium physiology, as represented in Fig. 31.

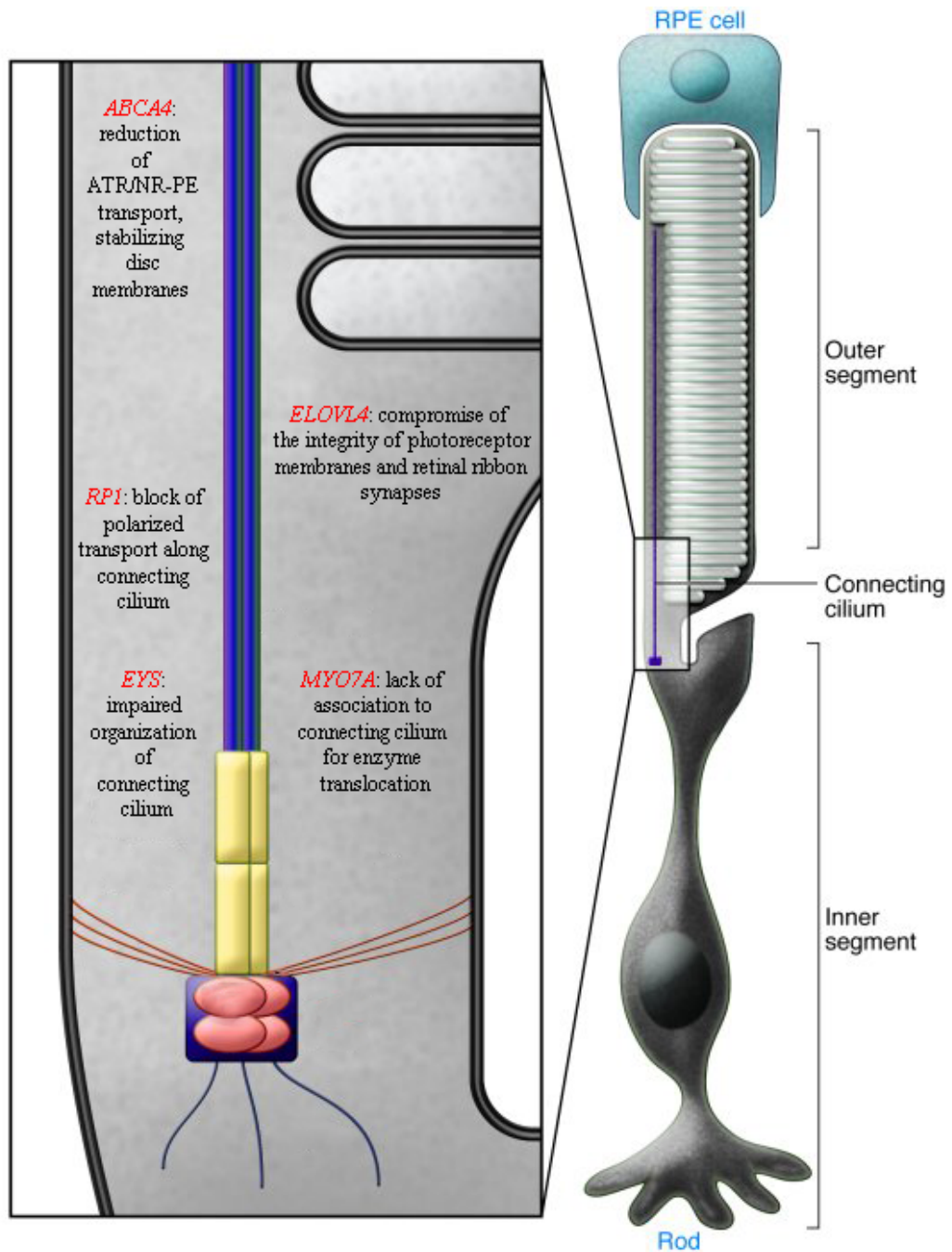


Fig. 31. Already known variants in RP causative could determine new consequences in photoreceptors. Previously described genes are yet associated to RP, but the exact pathogenic mechanisms are still undeciphered. Our hypothesis foresees a serious compromise of connecting cilium activities, leading to photoreceptor apoptosis. Details in the text.

5.4. CLASSIFICATION OF NEW NON – SYNDROMIC RP FORMS BY DISCOVERY OF NEW BIOCHEMICAL PATHWAYS (Fig. 32)

In this study, the whole transcriptome of RPE cells was deeply analyzed. It is known that RPE provides many vital functions for photoreceptor cells, such as involvement in visual cycle (Muniz A, 2009), metabolite transport and photoreceptor excitability (PA, 2015), phagocytosis of photoreceptor outer segments (POSSs) (Nguyen-Legros J, 2000), secretion of growth factors (King GL, 2000), and oxidative stress protection (Beatty S, 2001). In this study, we treated RPE with ox-LDL, during a follow-up of four time points (1h, 2h, 4h and 6h) after exposure, and compared to untreated ones. The oxidative stress is one of the most prevalent cause of RP (Campochiaro & Mir, 2017), and ox-LDL is an oxidative stress product already associated to other ocular diseases, as age macular disease (AnandBabu et al., 2016). The oxidized low-density lipoprotein is able to increase the RPE apoptosis (Yating et al., 2015), senescent changes (Marazita, Dugour, Marquioni-Ramella, Figueroa, & Suburo, 2016), synthesis of extracellular matrix (ECM) components (Shaw et al., 2016), expression of transforming growth factor-beta2 (TGF-b2) (A. L. Yu et al., 2009), inhibition of processing of photoreceptor outer segments by RPE (Mao et al., 2014) and outer blood–retinal barrier dysfunction (Arredondo Zamarripa et al., 2014). Thus, developed hypothesis foresaw that the expression analysis, in these altered conditions, could give new potentially RP involved pathways, with many new candidate genes that could be associated or causative of Retinitis pigmentosa. From initial 16,799 sequenced transcripts, about 4,000 showed changes in their expression level, with a raising up-regulation and a decreasing down-regulation from time zero and final considered time point (6h). Selected altered genes were, then, functional annotated by several databases and combined with statistical analysis of GSEA, clustering them into final 14 candidate “macro-pathways”. Afterwards, new aspects of pathways made of genes already associated to RP or consisting of new candidate genes were analyzed. Main described pathways are summarized in Table 14.

CANDIDATE PATHWAY	DESCRIPTION OF PATWAY ACTIVITY AND/OR IMPAIRMENT
INFLAMMATION	Increase inflammasome activity when macrophages accumulate in Bruch's membrane
MITOCHONDRION	Apoptotic induction, increase of ROS and mtDNA mutations
RNA PROCESSING	RNA maturation enzyme alterations
CIRCADIAN RHYTHMS	Dysregulation of shed POSs phagocytosis and accumulation of lipofuscin
EPIGENETIC	Up - regulation of methylation - realed genes
FATTY ACID METABOLISM	Peroxidation of LC - PUFAs and lipofuscin accumulation
OXIDATIVE STRESS	Altered balance of oxidant/antioxidant activity
APOPTOSIS AND CELL DEATH	Increased apoptosis and autophagy
CYTOSKELETON	Alteration in retinal vesicular trafficking mediated by connecting cilium
PROTEOSTASIS	Misfolding of proteins involved into retinal survival and vision process, with deactivation of several chaperones
SIGNAL TRANSDUCTION	Block of ciliary targeting of several proteins in photoreceptors and of ionotropic glutamate receptors in RGCs
PHOTOTRANSDUCTION	Altered phototransduction
NEURON	Reprogramming of RPE to differentiate towards retinal neurons and alteration of synpatic plasticity
SPLICING	Decrease of normal splicing (generally high in the retina)
ER STRESS AND UPR	Persistence of ER stress induces UPR to trigger intrinsic apoptotic pathway
VESICULAR TRAFFICKING CONTROL	Attempt to renew damage cellular components
SPECIFIC TF REGULATIVE NETWORK	Impairment of opsin expression and possible adaptive protection from lipid deposits
ECM REMODELING	ECM alterations could induce apoptosis
CELLULAR CYCLE REGULATION	Alterations in mitotic spindle development, as well as increased apoptosis and autophagy
PHAGOCYTOSIS AND MELANOSOMES TRANSPORT IN RPE	Accumulation of waste components of photoreceptor outer segment, leading to apoptosis
RETINOIC ACID CYCLE	Block of redox reactions needed for visual cycle

Tab. 14. New RP candidate pathway emerged from RNA – Seq analysis. This table shows the possible involvement of new candidate pathways in etiopathogenesis of RP, with the final induction of photoreceptor and/or RPE cell deaths. A detailed description of each pathways could be found in the text.

5.4.1. Candidate “macro-pathways” analysis.

The 14 candidate “macro-pathways” showed a time of exposure-related trend very variable for each one.

- *Inflammation*. It is one of the two involved pathways with the highest score, reached at first and final considered time points, with a flexion at intermediate ones. It could be reasonably explained by the initial aggressive response by preformed cellular mediators, like histamine and lysosomal enzymes, followed by a slow activation of inactive mediators of the fluid phase (e. g. complement and kinin system) (Brandstetter, Patt, Holz, & Krohne, 2016; Kauppinen, Paterno, Blasiak, Salminen, & Kaarniranta, 2016; L. Wang et al., 2016). Such protective response in early RP could became damaging when macrophages accumulate in Bruch's membrane, also favored by altered autophagy (Y. Liu et

al., 2016), potentially increasing inflammasome activity (Dick, 2017; Marneros, 2016), as showed by the climax at 6h.

- Mitochondrion. It represents the second most altered pathway, with a score growing from 1h to 2h, when it remains unchanged till 6h, time point that shows a little reduction. The observed trend is probably due to an increase of p53/Bcl-2 proteins complex, promoting mitochondrial outer membrane permeabilization (MOMP) and triggering the release of proapoptotic factors from the intermembrane space. Apoptotic induction, along with high level of reactive oxygen species (ROS) (Matsunaga et al., 2016) and mutations in mtDNA, could lead to retinal degeneration (Chichagova et al., 2017).
- RNA Processing. Alterations in pre – mRNA splicing can induce a cytotype – specific defect, especially in tissue like retina, in which there is a high number of mature mRNA derived from alternative splicing (Pinelli et al., 2016). Consequently, vulnerability of retinal cells to impairments in spliceosome building blocks, such as U4/U6.U5 triple small nuclear ribonucleoprotein (tri – snRNP) complex (Schmidt-Kastner et al., 2008), might result from an unsatisfied requirement for the production of sufficient amounts of needed retinal mRNAs. This pathway shows a constant score of 13 till 6h, time point in which it decreases slightly. It probably happens because enzymes involved in maturation process could be immediately altered by a serious stress like oxLDL presence; this scenario leads cells to death, that means that only survived ones are able to continue the genetic flow, with a reduced number of post – transcriptional enzyme which could still be the target of induced stress.
- Circadian Rhythms. The tight link between neural retina and the underlying RPE is essential for vision, while the diurnal and circadian rhythmicity of the RPE is needed for photoreceptor support and retinal function (Besharse & McMahon, 2016). A dysregulation of shed photoreceptors outer segments (POSS) phagocytosis by RPE (Sethna et al., 2016), triggered by the dark/light periods of the daily rhythm (Fanjul-Moles & Lopez-Riquelme, 2016) and

synchronized under circadian control like retinal melatonin and dopamine (Laurent, Sengupta, Sanchez-Bretano, Hicks, & Tosini, 2017), is sufficient to induce rapid photoreceptor degeneration by disk shedding (Yao et al., 2014) and accumulation of lipofuscin (Olchawa, Furso, Szewczyk, & Sarna, 2017). This pathway shows a rising score till 2h, then falls steeply at 4h, remaining the same at 6h. The explanation may involve pathway master genes that, once dysregulated, impair cell rhythms, leading to RPE disruption. Only a few cells, already compromised, could survive, showing alterations in a little group of late involved genes.

- *Epigenetic*. Exposure to oxidative agents induces epigenetics modifications, especially DNA methylation, triggered by the hypoxia condition (Hunter et al., 2012). Such data is also confirmed in retinal models, in which selective inhibition of DNA methyltransferases (DNMTs) and demethylation of Ten-eleven translocation (TET) enzymes promoters associated with the Hypoxia Inducible Factors 1 and 2 (HIF-1, -2) could reduce photoreceptor death (Alivand, Soheili, Pornour, Solali, & Sabouni, 2017), representing a promising therapeutic target (Amram, Cohen-Tayar, David, & Ashery-Padan, 2017). Score of this pathway shows a sinusoidal trend; probably it reflects an initial up-regulation of methylation-related genes, exasperating the silencing activity whose effects determining the reduced score at 2h. After 4 hours, the incremented oxidative stress could develop a second methylation “boost”, which implies the small score of 6h time point.
- *Fatty acids metabolism*. Fatty acids modulate cell loss observed in RP and other degenerative eye diseases (Y. Gong et al., 2017). As epigenetic pathway, also the fatty acids metabolism one shows a sinusoidal trend. It could be explained by a starting phase (1h – 2h) in which the induced oxidative stress determines the peroxidation of the long – chain polyunsaturated fatty acids (LC-PUFAs), such as the exquisitely sensitive docosahexaenoic acid (DHA) (Rice et al., 2015), physiologically needed for photoreceptor survive and rescue from damage (Gorusupudi, Liu, Hageman, & Bernstein, 2016). Afterwards,

retinal biosynthesis of lipofuscin and its accumulation in the RPE cells is consequence of both visual processes taking place in photoreceptor – RPE functional complex and metabolic insufficiency of RPE lysosomal compartment. The highest score of genes related to metabolism of all-*trans* retinal, lipofuscin's precursor, observed at 6h time point is well explained by cytotoxic and complement activation increasing upon oxidation.

- *Oxidative stress*. All described pathways represent many different faces of oxidative stress (Kruk, Kubasik-Kladna, & Aboul-Enein, 2015). The score of this pathway rapidly raises in the first hour, probably due to primary lipids peroxidation, and decreases at 2h, reasonably for antioxidant activity of specific gene products which slow down the oxidative alterations. From 4h and till 6h, a new increase of score is highlighted, most likely due to an altered balance of oxidant/antioxidant activity which, as long – term effects, damages DNA.
- *Apoptosis and cell death*. Autophagy regulates the structural integrity and physiological functions of retinal cells and contributes to the pathogenesis of RP (Bo et al., 2015). Autophagy represents the high score of the first time point, followed by a possible necroptosis induced by inflammation. In the meantime, survived cells organized themselves towards apoptosis (2h), which is probably realized starting from 4h. Finally, in 6h time point, dead cells could give signals to adjacent cells to die, with a little reduced number of directly involved and altered genes.
- *Cytoskeleton and Trafficking*. Various genes, like Retinitis Pigmentosa GTPase Regulator (RPGR) (Dutta & Seo, 2016), Family With Sequence Similarity 161 Member A (FAM161A) (Di Gioia et al., 2015), Retinitis Pigmentosa 1 (RP1) (Kabir et al., 2016) and 2 (RP2) (Schwarz et al., 2017b), are known to be involved into retinal vesicular trafficking, mediated by connecting cilium, and cytoskeleton rearrangement (Azadi, Brush, Anderson, & Rajala, 2016). According to our observation, the increasing score till 2h is

probably due to alterations of actin microfilaments, especially the basolateral cellular junctions and the apical surface with microvilli, which break the interdigitations with the adjacent photoreceptor outer segment. At 4h, alterations in the polarized distribution of microtubules block the vectorial targeting of membrane vesicles by motor microtubule-associated proteins (MAPs). Finally, at 6h, the residual score is probably due to intermediate filaments disruption, interrupting the attachment of RPE cells to other cells and the basement lamina.

- Proteostasis. Misfolding of several proteins involved into retinal survival and vision process, like rhodopsin, can result in disruptions of cellular protein homeostasis (Proteostasis) (J. H. Lin & Lavail, 2010). Probably the interaction between several chaperones could be altered by oxidant agents, due to activation/deactivation switches that induce certain chaperones – encoding genes and repress other ones. According to this scenario, several chaperones – encoding genes, like C1GALT1 Specific Chaperone 1 (*C1GALT1C1*) (L. S. Xie et al., 2010) and Ubiquitin Conjugating Enzyme E2 T (*UBE2T*) (Alpi, Chaugule, & Walden, 2016), or co – chaperones, like SGT1 Homolog, MIS12 Kinetochores Complex Assembly Co-chaperone (*SUGT1*) (Niikura, Kitagawa, Ogi, & Kitagawa, 2017), could increase their expression during initial stages of oxLDL exposure, due to increased levels or de novo biosynthesis of their substrates. Afterwards, the possible “switch – off” given by down – regulation of other chaperones – encoding genes, like Apolipoprotein E (*APOE*) (P. Yang et al., 2017), could explain the possible reduced score of 4h and 6h time points.
- Signal transduction. Most inherited forms of blindness are caused by mutations that lead to photoreceptors death, but little is known of second – and third – order retinal neurons involvement. At this level, the regulation of intracellular trafficking is highly depending on signal transduction, mainly mediated by Small guanosine triphosphate (GTPase) ADP – ribosylation factors (Arfs) (R. Luo et al., 2017) and phosphodiesterase 6 (PDE6D) (J. J. Lee & Seo, 2015), whose ablation could blocks ciliary targeting of various proteins like RPGR.

Moreover, the expression of the light – gated excitatory mammalian ion channel light – gated ionotropic glutamate receptor (LiGluR) in retinal ganglion cells (RGCs) could partially restore visual functions when stimulated by UV light (Gaub et al., 2014). From 1h to 4h this pathway shows a decreasing score, probably due to a compensatory cross – talk which permits the RPE cells to progressively reduce the number of altered involved genes. Nevertheless, the oxLDL long – term effects could alter also the “compensatory genes” (6h).

- *Phototransduction*. Several RPE proteins, such as membrane frizzled – related protein (MFRP/Mftp) (Fogerty & Besharse, 2011) or the beta – V spectrins (Papal et al., 2013) significantly modulate the expression of genes involved in visual cycle and phototransduction (Fogerty & Besharse, 2011), impairing rod and cone functions when mutated (Nash, Wright, Grigg, Bennetts, & Jamieson, 2015). This pathway shows the lowest average score, probably because of the most involved genes are expressed in photoreceptors and not in RPE. The highest score is reached at 4 hours, reasonably when the most genes involved into phototransduction cascades should be actively expressed.
- *Neuron*. The score of this pathway increase a little until 2h, when it becomes stable. These results could be indicative of a reprogramming of RPE cells to differentiate towards retinal neurons, in which a limited number of genes is involved. Simultaneously, RPE cells play a pivotal role in organizing the spatial structure of the retina, probably with a constant set of genes involved in neurite outgrowth and synaptic plasticity of altered retina (Sugitani, Koriyama, Ogai, Wakasugi, & Kato, 2016), along with abnormally elongated and branched axons of peripheral cones (Z. Y. Li, Kljavin, & Milam, 1995). Interestingly, it was seen that the block of gamma-aminobutyric acid c (GABA_c) receptors increases light responsiveness of retinal ganglion cells in a rat model of RP (Jensen, 2012).
- *Splicing*. Retina cells express unusually high amounts of spliceosome components, which indicates a high demand for splicing (Karunakaran et al.,

2016). Moreover, inefficient splicing and alterations in alternative splicing have been reported in cell culture experiments, animal models and blood cells derived from RP patients (Tanackovic et al., 2011). This pathway shows the lowest average score, with a drop at 2 hours, probably due to corrupted splicing process realized during the first hour. The activation of alternative splicing probably determines the score increase from 4h time point.

5.4.2. Pathway analysis of altered genes yet associated to retinal diseases

Several genes yet known to be causative/associated to retinal degenerations showed sensible time – dependent expression variations, probably related to specific pathways activated/inhibited during oxLDL exposure. Considering the average fold – change of each one and their reciprocal connections, we highlighted a more detailed pathways network. Such connections could help to depict several “causative/associative clusters”, underlining a more complex pattern of possible RP etiologies.

- *Endoplasmic Reticulum Stress and Unfolded Protein Response*. The most of analyzed genes involved in endoplasmic reticulum stress and unfolded protein response resulted up – regulated (*ATF6*, *BBS10*, *PRPF8*, *TOPORS*, *SNRNP200*), while only two (*WFS1* and *KLHL7*) showed a down – regulation. Mutations in these genes were reported in patients affected by RP. Endoplasmic reticulum (ER) stress and Unfolded Protein Response (UPR) signaling have been implicated in the etiopathogenesis of heritable forms of retinitis pigmentosa (Shinde, Kotla, Strang, & Gorbatyuk, 2016). UPR determines an initial inhibition of translation to prevent further accumulation of misfolded proteins, and an up – regulation of chaperones genes to improve protein folding, followed by activation of the ER – associated degradation system, which retro – translocates misfolded proteins from the ER for proteasome – dependent degradation. If ER stress persists, UPR signaling “switches” to trigger cell death by activating the intrinsic apoptosis pathway (Hiramatsu, Chiang, Kurt, Sigurdson, & Lin, 2015). Particularly, Activating Transcription Factor 6 (*ATF6*), Bardet-Biedl Syndrome 10 (*BBS10*) and Top 1

Binding Arginine/Serine Rich Protein (*TOPORS1*) encode for proteins involved in response to misfolded proteins (Esposito et al., 2017; Farkas et al., 2014; Jerry Chiang & Lin, 2014; Ruzickova & Stanek, 2017; Yoshikawa et al., 2011). Our data show that signaling triggered by oxidative damage leads to a protective response, as well as reported in presence of gene mutations. The UPR response in RPE cells is also activated by accumulation of mutant EGF Containing Fibulin Like Extracellular Matrix Protein 1 (EFEMP1), which should involve wolframin, an ER protein encoded by Wolframin ER Transmembrane Glycoprotein (*WFS1*) gene (Schmidt-Kastner et al., 2009). A new intriguing gene, involved in poly – ubiquitinating target proteins for proteasome – mediated degradation, is Kelch Like Family Member 7 (*KLHL7*). Mutations in *KLHL7* have recently been reported as causative of an autosomal – dominant form of retinitis pigmentosa (RP42), preferentially affecting the rod photoreceptors (Angius et al., 2016). Patients with mutations in *KLHL7* showed thinner – than – normal RPE (Y. Wen et al., 2011). Too little is known about the real involvement of *WFS1* and *KLHL7* in these processes, and further insights are required to elucidate their role and the meaning of their down – expression induced by oxidative stress.

- *Vesicular trafficking control.* A very intense vesicular flow characterizes communication between RPE and photoreceptors and Bruch's Membrane (BM). RP may be also caused by vesicular trafficking impairment, and mutations in several involved genes were reported. Among these, Nephrocystin 3 (*NPHP3*) (Wright et al., 2011), Inversin (*INVS*) (Lienkamp, Ganner, & Walz, 2012), Dehydrodolichyl Diphosphate Synthase Subunit (*DHDDS*) (R. Wen et al., 2014), Rab Escort Protein 1 (*CHM*) (Gordiyenko, Fariss, Zhi, & MacDonald, 2010) and Patatin Like Phospholipase Domain Containing 6 (*PNPLA6*) (Hufnagel et al., 2015) showed a significant fold-change, after oxLDL treatment. Particularly, genes promoting vesicles formation *NPHP3*, *INVS*, *DHDDS* and *CHM* resulted up – regulated, while a decreased expression level was observed for *PNPLA6*, involved in membrane's integrity maintenance. Globally, these data suggest that vesicular trafficking is

promoted under stress condition, probably in order to trigger the renewal of damaged cellular components disrupted by oxidative agent.

- *Specific transcription factors regulative network*. Two transcription factors encoding genes linked to RP development, Zinc Finger Protein 513 (*ZNF513*) and Nuclear Receptor Subfamily 2 Group F Member 1 (*NR2F1*), resulted down – regulated in our experiment. Znf513 regulates expression of genes involved in retinal development and photoreceptor maintenance (L. Li et al., 2010). NR2F1, together with NR2F2, promotes optic vesicle development (K. Tang et al., 2010) and regulates lipid homeostasis under stress condition (Cho, Yi, Tserentsoodol, Searle, & Ferreira, 2010). The observed decreased expression level may indicate both an impairment of opsin expression together with cones activity and, conversely, a possible adaptive protection from lipid deposits, as final attempt to escape from retinal cells death.
- *Extracellular matrix (ECM) remodeling*. Two genes, TIMP Metallopeptidase Inhibitor 3 (*TIMP3*) and Collagen Type XI Alpha 1 Chain (*COL11A1*), resulted up – regulated after oxLDL exposure; their proteins are synthesized in RPE and then secreted in BM. Advanced glycation end –products (AGEs) and confluent drusen accumulate in BM, resulting in an uncontrolled activation of the complement cascade with onset of RP symptoms (Booij, Baas, Beisekeeva, Gorgels, & Bergen, 2010). *TIMP3* encodes for an inhibitor of matrix metalloproteinases (MMPs). The balance between proteolytic MMPs and TIMPs underlies the ECM remodeling. An increase of *TIMP3* mRNA expression in retinas affected by simplex RP is documented (Jomary, Neal, & Jones, 1995). The ECM – involved *COL11A1* resulted, also, modified in its expression. *Col11a1a* is detectable in the RPE (M. Fang, Adams, McMahan, Brown, & Oxford, 2010). Although over – expression of ECM and pro – fibrotic proteins, like *col11a1*, is not yet related to specific form of RP, it was reported in primary open angle glaucoma (POAG) cells, compared with normal Gliar fibrillary acidic protein (GFAP)-negative lamina cribrosa (LC) cells (Kirwan, Wordinger, Clark, & O'Brien, 2009). The up – regulation of *TIMP3* and *COL11A1* could determine retinal cells apoptosis, induced by ECM

alterations due to oxidative stress.

- Cellular cycle regulation. In RPE, among several genes involved in cell cycle progression, Polo like kinase 4 (*PLK4*), Kinesin family member 11 (*KIF11*), Ceramide kinase like (*CERKL*) and RB1 inducible coiled-coil 1 (*RB1CC1*) resulted over - expressed after oxLDL treatment. Mutations in the *PLK4* kinase determine microcephalic primordial dwarfism with additional congenital anomalies including retinopathy. The retinal pathology may result from perturbed mitosis in the eye, or as a consequence of impaired cilia formation leading to photoreceptor death (Martin et al., 2014). Also mutations in the mitotic spindle binding motor kinesin *KIF11* cause microcephaly and retinopathy (S. H. Choi & McCollum, 2012). *CERKL* and *RB1CC1*, instead, regulate the phagocytosis of outer segments (OSs) by the RPE (Yao et al., 2015; S. Yu et al., 2017). Observed increase in gene expression indicates an alteration in mitotic spindle development, as well as increased apoptosis and autophagy, symptoms of retinal degeneration progression.
- Phagocytosis and melanosomes transport in RPE. Photoreceptors maintain specific structure and dimensions by continuously renewal of outer segments, while simultaneously old and waste outer segments are phagocytized by the RPE. Perturbations in OS digestion can lead to retinopathies (Kevany & Palczewski, 2010). Myosin VIIA (*MYO7A*) encodes for the unconventional Myosin – VIIa, whose mutations cause Usher syndrome type 1B, a disorder involving profound congenital deafness and progressive blindness (Xia et al., 2017). In the retina, most of *MYO7A* is localized in the apical region of the RPE cells, where participates in the localization of RPE melanosomes and in the delivery of phagosomes to lysosomes in the basal RPE. An additional role of *MYO7A* in the RPE is suggested by its requirement for light – dependent translocation of the ER – associated visual cycle enzyme, RPE65, and normal visual retinoid cycle physiology (Williams & Lopes, 2011). The down – regulation of *MYO7A* we observed could represent the impairment of RPE phagocytosis activity, which leads to accumulation of waste components, with

the following induced apoptosis.

- Retinoic acid cycle. Some RP cases are caused by an impaired retinoid cycle (Travis, Golczak, Moise, & Palczewski, 2007). Several enzymes belonging to Retinal Dehydrogenases (RDHs) family take part to visual cycle. RDH5 is very abundant in the RPE, where it is able to oxidize or to reduce all common cis – retinoid isomers (Parker & Crouch, 2010). However, its expression decreases after oxLDL treatment, as well as after exposure to proinflammatory cytokines Interferon- γ (IFN- γ), Tumor necrosis factor- α (TNF- α), and Interleukin-1 β (IL-1 β) (Kutty et al., 2016). Moreover, mevalonate kinase gene (*MVK*) results down – regulated in the same condition. *MVK* is involved in the isoprenoid pathway resulting in biosynthesis of glycoproteins, coenzyme Q, vitamin K and carotenoids (retinol biosynthesis). Furthermore, RP was described in several patients with *MVK* mutations (Siemiakowska et al., 2013). Down – regulation of both *RDH5* and *MVK* suggests that oxidant agents alter retinoic acid cycle, inducing defects in physiological visual functions exerted by retina.

5.4.3. New candidate genes and their possible impact on RP etiopathogenesis

Aim of this study is to understand how oxidative stress may induce RP progression and, above all, to discover new candidate genes that can lead to disease development, in all those patients with no detected mutations in already known genes. Very interesting, although apoptosis represents the common last solution, it is clear that cells try to rescue themselves before die. Curiously, this scenario is determined by highlighted contrasting effects of many gene expression alterations, frequently in the same pathway.

- Cell cycle regulators. In presence of oxLDL, RPE cells showed an altered expression of genes encoding cyclin-dependent kinases (CDKs) and their inhibitors, involved in cell cycle regulations (Rajapakse, Chen, Curtis, & Xu, 2017). Cell cycle proteins alterations could determine neuron death but, because they are usually expressed at a late stage of cell death, they could also attempt to save cells (Frade & Ovejero-Benito, 2015). In *Rdl* mutant retina explants, the inhibition of CDK activity rescued about half photoreceptors

(Cunningham et al., 2002). One of hub gene is *CDK1*, a serine/threonine kinase that drives cell from late G2 to mitosis. Cdk1, in complex with cyclin B1, is strongly involved into regulation of mitochondrial activities, stimulating cell death via direct phosphorylation of Bcl-2, Bcl-XL, and Mcl1-1 proteins (Telegina, Korbolina, Ershov, Kolosova, & Kozhevnikova, 2015) or suppressing eye impairments and mitochondrial alterations caused by mRpl10 deficiency (H. B. Li et al., 2016). As we demonstrated, *CDK1* is up-regulated under stress condition, together with *CDK4* and *CDK6*, involved in Rb phosphorylation and subsequent inactivation. Phospho – Rb was detected in degenerating photoreceptors for both inherited diseases and acute injury, as well as an over – expression of CDK4 (Pei, Bai, Tsutsui, Kiyokawa, & Xiong, 2004). Conversely, CDK5, involved in the cell cycle regulation by recruiting p27 in the nucleus to maintain neurons in a postmitotic state, is down – expressed. In degenerative neurons, CDK5 is combined with Mekk1 mediating a signaling pathway required for ER-stress-induced apoptosis. Interruption of this pathway could slow the progression of age-related retinal degeneration in a Drosophila model of retinitis pigmentosa (Kang, Chung, & Ryoo, 2012). Additionally, CDK5 could promote retinal degeneration through increased intracellular Ca²⁺ and calpain – mediated apoptosis (Shinde et al., 2016). Moreover, two families of Cdk inhibitors (CKI) further control the transitions between the different cell cycle phases: the Ink family, which regulates the quiescent state blocking the binding of Cdk4/6 with Cyclin D, and the Cip/Kip family, which inactivate Cyclin/Cdk complexes (Ovejero-Benito & Frade, 2015). In details, *CDKN2D* (Ink4d) is expressed in progenitors and selects neurons in the mature retina, and *CDKN1B* (p27kip1) mediates exit from the cell cycle. Retinas devoid of only Ink4d showed an extended period of replication, followed by apoptosis, while retinas missing both proteins continued the hyperproliferation, implicating that a huge number of horizontal cells and differentiated neurons reentered the cell cycle (Cunningham et al., 2002). We observed a down expression of *CDKN2D* and an up regulation of *CDKN1B* resulting in apoptosis induction. Moreover, *CDKN2A* and *CDKN2B*, encode for tumor suppressor proteins p16^{INK4A} and p15^{INK4B}, respectively,

which inhibit cell cycle progression, binding CDK4 or CDK6. *CDKN2B* is up-regulated by transforming growth factor (TGF)- β in several models of glaucoma and optic nerve damage (S. Gao & Jakobs, 2016). As evidenced by our results, the up – regulation of CDKs 1, 4 and 6, with the contemporary down – expression of the only CDK5, could increase the apoptotic cell rate, mediated by a possible accumulation of phospho – Rb and p53. This cell death stimulation could be additionally enforced by the down – expression of *CDKN2D* and the over – expression of *CDKN1B*. Curiously, an ambiguous data seems to arise from the contrasting values of average fold – change for *CDKN2A* and *CDKN2B*, but the power of the first (-4,31) is greater than the second (+1,38), favoring the loss of CDK4 and CDK6 inhibition.

- *Zinc fingers transcription factors*. As previously described, RP may be caused by mutations at zinc finger (ZNF) proteins. These include a huge number of small functional domains that require at least one zinc ion, and are involved in a wide variety of biological functions. Zinc finger containing domains generally act as interactors, binding RNA, DNA, proteins or small molecules (Laity, Lee, & Wright, 2001). Targets of many ZNFs are still unknown, as well as biological processes in which they are involved. RPE cells treated with oxLDL showed an increased expression level for many ZNF genes. Particularly, TIZ (TRAF-6 inhibitory zinc finger protein) can significantly inhibit cell proliferation, as observed in epithelial ovarian cancer cells (H. Y. Zheng et al., 2015). ZNF174 acts as transcriptional repressor (Yee & Yu, 1998), ZNF325 is involved in MAPK signaling pathway (Y. Zhao et al., 2006). Expression of ZNF845, instead, is misregulated in a human thyroid epithelial cell line after exposure to high – dose of γ – radiation (Bang, Choi, Kim, & Choi, 2016). ZNF585 has a closer resemblance to PR Domain Zinc Finger 9 (PRDM9)

[http://genomewiki.ucsc.edu/index.php/PRDM9:_meiosis_and_recombination], while ZNF708 (Kox8) and ZNF700 are involved in immune response. Particularly, the first one was isolated from human T – cell lines (Thiesen, Bellefroid, Revelant, & Martial, 1991), while ZNF700 acts as capture antigen

for detection of autoantibodies in colorectal cancer (O'Reilly et al., 2015). A down – expression was observed for *ZFPM-1* and *ZNF580*. *ZFPM-1* suppression accelerates the erythropoietic differentiation of human CD34⁺ cells (H. Y. Yang et al., 2007). Expression of *ZNF580*, instead, is increased in hydrogen peroxide (H₂O₂)-regulated inflammation-related signaling pathways (DangLi, HeKong, JiQin, MingHua, & WenCheng, 2012) and regulated by LDL and HDL, depending on the oxLDL/LDL-ratio, and representing a novel factor in the lipoprotein-dependent regulation of IL-8 and monocyte arrest (Hoffmann et al., 2011). These observations counteract with our results, according to which oxLDL determines a reduction of *ZNF580* expression; this evidence could be due to different considered tissues. Moreover, *ZNF580* could be involved in the maintenance of vascular endothelium homeostasis (Luo et al., 2011), mediating endothelial nitric oxide synthase (eNOS) expression and endothelial cell migration/proliferation via the TGF- β 1/ALK5/Smad2 pathway (Luo, Zhao, Li, Zhao, & Zhang, 2014). The main ZNFs transcription factor cluster suggested us that the cell proliferation is highly inhibited but, in the meantime, the down – expression of *ZNF580* and *ZFPM-1* could increase angiogenesis and phagocytosis. Probably the meaning of this scenario is that the arrest of cell cycle could reduce oxidative damages induced by oxLDL, with increase of contemporary altered cells phagocytosis followed by neoangiogenesis, in order to attempt a final rescue of retinal tissue.

- *Vesicular trafficking and cell migration*. Rho GTPases include proteins involved in the organization of the actin cytoskeleton, determining the regulation of many cellular processes like cell migration, cell division and vesicle trafficking (Cerutti & Ridley, 2017). Ras homolog family member D (*RHOD*) and RAS related 2 (*RRAS2*), two of most important hub genes involved in this latter, belong to the GTPase family. Expression of *RHOD* gene decreases after oxLDL treatment. Its deficiency increases actin filament-containing structures, such as cortical actin and stress fibers, and impairs cell migration and proliferation (Blom, Reis, Heldin, Kreuger, & Aspenstrom, 2017). *RRAS2* permits to establish and maintain cell polarity, and to modulate

the formation and release of ECM attachments. Furthermore, it enhances cell spreading (lamellipodial extension around the cell perimeter) and motility via RalBP1/RLIP76, an R-Ras effector that links GTP-R-Ras to activation of Arf6 and Rac1 GTPases (Wurtzel et al., 2015). According to our results, oxidative stress induces expression of *RRAS2*. In order to relate these data with RP pathogenesis, we can hypothesize that the down – expression of *RHOD* could impair migration and proliferation of RPE cells. At the same time, the over – expression of *RRAS2* indicates an increase in cell spreading, probably related to a possible increased chemotaxis of inflammatory cells.

- *Chaperones, UPR and ER stress.* As previously evidenced, UPR activation following ER stress represents one of the most altered pathways related to oxidative stress, probably leading to retinal degeneration. Several new candidate genes, involved in these pathways, emerged from final enrichment. Polyubiquitination by E2 and E3 enzymes represents the main mechanism regulating protein activity (Brandstetter et al., 2016). One of the biggest RING (Really Interesting New Gene domain) E3s is the Anaphase Promoting Complex/Cyclosome (APC). APC, with the help of its RING partner APC11, controls cell proliferation by ubiquitinating cell cycle regulators and managing their programmed degradation (Brown et al., 2015). Another way occurring in response to ER stress involves the *xbp1* protein which, by ire-1-mediated unconventional splicing and the induction of the ER chaperone heat shock cognate protein 3 (*hsc3*), induces apoptosis (Ryoo, Domingos, Kang, & Steller, 2007). Interestingly, in retinas of Rho mutants was observed an up-regulation of *Xbp1* (Kunte et al., 2012), suggesting that a chronic and excessive UPR activation might be pro-apoptotic. However, a moderate increase in UPR activation (via the Ire1/*Xbp1* pathway) could be protective for photoreceptors neurons (PNs) (Griciuc et al., 2010). To support this hypothesis, a reduction of the UPR through a mutation in *xbp1* could aggravates the course of retinal degeneration, as seen in the *Drosophila* model (Kang & Ryoo, 2009). Furthermore, ER stress induces the transcription of the BiP co-chaperone and reductase protein ERdj5 (DNAJC10), probably involved in protein folding and

translocation across the ER membrane (Cunnea et al., 2003). ERdj5 is a member of the proteostasis network that regulates rhodopsin biogenesis, promoting its disulphide bond formation/reduction. Moreover, it was highlighted that ERdj5 overexpression favors the degradation, improves the ER mobility and prevents the aggregation of mutant rhodopsin (Athanasίου et al., 2014). Besides these recently discovered ER – related chaperones, heat shock protein family A Member 1A (HSPA1A) was yet partially associated to retinal degeneration. It encodes for the inducible heat shock protein 70 (HSP70), already known to protect cells against environmental and physiological stresses. HSP70 inducers, such as valproic acid and geranylgeranylacetone, attenuated photoreceptor cell death (Koriyama & Furukawa, 2015). HSP70 antiapoptotic activity could be explicated in two stages: the early one foresees the HSP70 cleavage through protein carbonylation by production of reactive oxygen species, lipid peroxidation and Ca²⁺influx/calpain activation, followed by the late stage of cathepsin and/or caspase activation. Thus, the upregulation of functional HSP70 by its inducer probably protects photoreceptor cells (Furukawa & Koriyama, 2016) and promotes the survival of injured RGCs (Kwong et al., 2015). Curiously, a chaperone activity is also relevant at histones level. Anti-silencing function 1 histone chaperone (ASF1A) is a highly-conserved histone H3/H4 chaperone that plays a role in the efficiency of DNA synthesis-coupled and DNA synthesis-independent nucleosome assembly (Galvani et al., 2008). In details, ASF1 binds a heterodimeric histone H3-H4 complex and impedes the formation of the (H3-H4)₂tetramer both inside the nucleus and in the cytoplasm (H. Wang, Wang, Yang, & Xu, 2015). Under stress conditions, the Asf1 histone chaperone buffers excess histones then rapidly used, during recovery, as replication resumes. This shows that replication stress interferes with predeposition marking and histone recycling, influencing the epigenetic stability. The chaperones involvement into retinal degeneration could be also elicited by metal ion. Poly(rC)-binding protein PCBP1 can bind iron and deliver it to ferritin for storage or to prolyl and asparagyl hydroxylases to metallate their iron center, such as deoxyhypusine hydroxylase (DOHH)

required for the activity of the translation factor eukaryotic initiation factor 5A (Frey et al., 2014). If over – expressed, the PCBP1 iron chaperone inhibits autophagy in favor of apoptosis (W. Zhang et al., 2016). According to these evidences, the over – expression of XBP1 and ASF1A we observed, together with down – expression of APC11 and PCBP1, indicate a possible increased apoptosis, induced by cell cycle regulator impaired ubiquitination, translation arrest and epigenetic instability. Additionally, the UPR activation and an attempt to correct protein folding could be favorite by the over – expression of DNAJC10 (average fold – change = +2.73). The down – expression of HSPA1A could be explained considering the reduction of the synthesis of proteins substrate of Hsp70.

- *Small GTPase superfamily altered signaling.* Small GTPases are a family of GDP-/GTP-binding proteins. They control many essential cellular processes, like subcellular localization regulation, cellular transport and selective membrane localization, actin organization, cell shape and polarity, movement, cell–cell and cell–matrix interactions (Cromm, Spiegel, Grossmann, & Waldmann, 2015). K-Ras (Kirsten-Ras), encoded by *KRAS* (KRAS Proto-Oncogene, GTPase), is a proto – oncogene belonging to the subfamily of Ras GTPases and regulates cell proliferation and differentiation. KRAS is involved in many signaling pathways (Ostrem & Shokat, 2016), such as MAPK/ERK (RAF–MAPK/ERK kinase–extracellular signal-regulated kinase), PI3K-AKT (phosphoinositide 3-kinase–AKT–mechanistic target of rapamycin) and RALGDS-RAL (RAL guanine nucleotide-dissociation stimulator–RAL). KRAS mutations cause the Noonan syndrome, a condition that affects many areas of the body, with multiple genetic bases associated with an extensive variety of congenital ocular abnormalities, like amblyopia, myopia, astigmatism, strabismus (van Trier et al., 2016). Under stress conditions, we observed that KRAS up – regulation could determine an uncontrolled RPE cell proliferation or functional alterations. Our data are also supported by a recent study in which an increased expression of KRAS in astrocytes, after acute stress stimulation, was reported (Messina, Di Zazzo, & Moncharmont, 2017).

- *Inflammation*. Two new candidate genes related to oxidative stress, B-cell CLL/lymphoma-3 (*BCL-3*) and Inhibin Beta A Subunit (*INHBA*), are involved in inflammatory response. *BCL-3* is a member of the inhibitor of NF- κ B proteins (I κ B). Nuclear factor kappa B (NF- κ B) is a key regulator of the immune response, but could also induce inflammation and proliferation, and could regulate apoptosis (Bourteele et al., 2007). *BCL3* expression seems to reduce the inflammatory response in several tissues by blocking ubiquitination and proteasome – mediated degradation of p50 homodimers (L. Song et al., 2016). Absence of *BCL-3* severely inhibits cell viability, proliferation and cell cycle progression, while its overexpression promotes these cellular processes (Tu et al., 2016). We found a down – expression of *BCL-3* in RPE cells exposed to the oxidant agent, leading to a cell proliferation arrest. Furthermore, it is well known that most vision loss arise from the transition between inflammation and cell death. In RPE cells, this switch is driven by lasting activation of the TGF- β pathway (Radeke et al., 2015). *INHBA* encodes for the inhibin, a subunit of the dimeric activin and inhibin protein complexes, related to TGF- β . Inhibin regulates follicle stimulating hormone (FSH) secretion from the pituitary gland, but it is also involved in eye, tooth and testis development. *INHBA* results over-expressed by our RPE cells. Possible involvement of *INHBA* gene in RP development is not easy to hypothesize; however, pathological conditions in which RP coexist with FSH disorders were reported (Edwards, Sethi, Scoma, Bannerman, & Frohman, 1976; Faraci et al., 1984).
- *Retinoic acid effects on epigenetics*. Retinoic acid is fundamental for RPE structure and activity (S. Wang, Liu, Mao, & Wen, 2014). All–trans retinoic acid (ATRA) regulates cytokines release towards SUV39H2. This is a histone methyltransferase that inhibits cytokines expression; particularly, ATRA induces Suppressor of variegation 3-9 homolog 2 (*SUV39H2*) expression (Arts et al., 2015). We detected an over – expression of *SUV39H2* that could impair inflammatory responses and improve cellular homeostasis, probably as a defensive attempt to survive, after serious induced stress.

- DNA breaks repair.* Sirtuins constitute a family of nicotinamide adenine dinucleotide (NAD)-dependent protein deacetylases/ADP-ribosyltransferases able to modulate various metabolic processes like development, cell survival, stress resistance, energy metabolism, and aging. Compared with other tissues, all sirtuins are highly expressed in the retina, showing mRNA levels affected by light–dark condition (Ban et al., 2013). In particular, lower expression and mislocalization of Sirtuin 1 (SIRT1), involved in the repair of DNA double – strand breaks, were found in Age macular degeneration(AMD) RPE-induced pluripotent stem cell (iPSC)-RPE (Golestaneh et al., 2016), showing an accelerated retinal cell apoptosis (Ozawa et al., 2010). At the same time, a significant under – expression of SIRT1 was observed in oxidative stress-induced damaged retinal cells, negatively correlated with the level of intracellular reactive oxygen species production (Peng et al., 2010). Probably, one of the mechanism involving the anti-inflammatory response involves the regulation of AGE (Advanced glycation end products)-induced pro-inflammatory cytokines and chemokines, like demonstrated in retinal ARPE-19 cells (Y. F. Zhang et al., 2015). Therefore, increasing SIRT1 expression could protect retinal neurons (Zuo et al., 2013) and visual function, probably via regulating neurotrophin and its receptor (Zeng & Yang, 2015) or via SIRT1-regulated lipid metabolism (Y. Zhang, Li, Cao, Zhang, & Wei, 2015). SIRT1 over – expression could be induced by resveratrol (Kubota et al., 2010; Mimura, Kaji, Noma, Funatsu, & Okamoto, 2013), fullerenol (Zhuge et al., 2014) and Vitamin C (Wei et al., 2014). *SIRT1* resulted over – expressed in our experiment, highlighting how injured cells try to fight their damaging cause, by increasing antinflammatory activities and, above all, by improve the ability to repair DNA. Such molecular adaptations, combined with an increased neurotrophic response and a better regulation of lipid metabolism, could give RPE cells a fundamental neuroprotection, required to avoid retinal degeneration.
- Early response to oxidative stress could impair synapses.* Although degeneration mechanisms require activation of several steps, the impact of

early response to oxidative stress could play a fundamental role in progressive retinal impairment. Most likely, the early control is mediated by phosphorylation and activation of several protein pools. Among these, early growth response-1 (EGR-1) induces the transcription of genes controlling both cell proliferation and apoptosis (Chaum, Yin, & Lang, 2011). EGR-1 is a transcription factor encoding a nuclear protein with a zinc finger-binding domain, involved in the regulation of eye growth (Ashby, Zeng, Leotta, Tse, & McFadden, 2014), which also carries a cytoplasmic polyadenylation element able to respond to NMDA receptor activation (Simon, Schott, Williams, & Schaeffel, 2004). Our data showed a marked reduction of *EGRI* expression in RPE cells, following oxLDL treatment. Interestingly, it was seen that *Egr1* knockdown mice selectively suppressed the differentiation of amacrine cells (ACs) and horizontal cells (HCs), adding a general delay of development of the other retinal cell types. Such scenario led to compromise the integrity of the inner and outer plexiform layers (L. Zhang, Cho, Ptak, & Leung, 2013). However, it is upregulated in glaucoma (Yasuda, Tanaka, Ryu, Tsuda, & Nakazawa, 2014) and in retina degeneration slow (*rds*) mouse models, where it was associated with microglial activation and migration into the outer retina, after the major peak of photoreceptors death (Sharma et al., 2012). According to our data, EGR-1 involvement in RP pathogenesis may be explained considering its role in impairments of retinal cells growth and differentiation and, very interestingly, in potential disruption of synaptic communications.

- *Fatty acids metabolism and circadian rhythms*. Nuclear transcription factor Y (NF-Y) is a trimeric protein, made of three subunits, NF-YA, NF-YB and NF-YC, regulating expression of genes that control cell proliferation. NF-Y controls the biosynthesis of polyamines and purines, and *de novo* biosynthetic pathways of lipids, activating glycolytic genes, but, surprisingly, repressing mitochondrial respiratory genes (Benatti et al., 2016). NF-Y is also involved into circadian rhythms regulation, activating and generating the daily cycle of *Bmal1* expression (J. Xiao et al., 2013). In our experiment, we only found an over expression of YA subunit; no variations were reported for both YB and

YC mRNA levels. NF-YA is the regulatory subunit of the trimer, and its increasing is able to activate the fatty acid synthase (FASN) signaling pathway (Guo et al., 2016). FASN is also over – expressed in several tumor tissues (Fraser, Frank, & Dalakas, 1991). However, we observed a decreased expression of FASN. A reduction of FASN level was only reported in sons of patients underwent a calorie – restricted diet, during pregnancy. Particularly, this was related to high level of plasma LDL (Ramirez-Lopez et al., 2016). Following this data, we hypothesize that the down – expression observed is consequence of oxLDL treatment. Moreover, high FASN expression was shown by renal epithelial cells during maturation; however, this value decreases once the cells reach the confluence (Aschauer et al., 2013). In order to understand RP pathogenesis, altered FASN expression induced by oxidative stress may interfere with the normal RPE morphogenesis, leading to pathological phenotype.

- Microvascular impairments. Integrin alpha2beta1 (ITGA2) is an important platelet receptor for collagen fibers (J. Y. Gong, Deng, & Sun, 2015). ITGA2 and nitric oxide (NO) play an important role in the pathogenesis of microvascular complications in diabetic retinopathy (Azmy et al., 2012). The over – expression of the integrin alpha2beta1 coding gene could represent one of the most interesting damage caused by oxLDL, which could imply the thrombosis of retinal microcirculation, leading to cell death (Cehofski et al., 2016).
- Chromosome instability induction. Chromosome instability (CIN) is a condition which leads normal cells to death. One event that could induce CIN is the disruption of the spindle assembly checkpoint (SAC), required to detect misoriented or detached kinetochores. CIN determines mitosis stop until pairs of sister chromatids achieve the bipolar geometry, the uniquely compatible with normal chromosome disjunction. Mitotic arrest deficient 2 like 1 (Mad211) is an essential component of the SAC and its deletion lead to impairments of this control sensor (Foijer et al., 2017). Our experiment showed

an over – expression of *MAD2L1*, which could determine an early exit from mitosis.

- *JUN complex and retinal cell rescue.* Jun proto-oncogene (JUN) is a transcription factor, expressed in the inner nuclear layer (INL) of retina, which inhibit the AP – 1 complex (Rouit & Schorderet, 2008). In light-exposed mutant retinas, a change in the composition of the AP-1 protein complex, from c-Jun/Fra-1/c-Fos to JunB/ c-Fos, was detected (Gu, Beltran, Li, Acland, & Aguirre, 2007). Moreover, in RP models, it was seen that JUN may mediate photoreceptor rescue indirectly, at early stage, especially if corroborated by brain derived neurotrophic factor (BDNF) delivery (R. Chen, Yin, Peng, & Li, 2012). The down – expression of *JUN* could improve the activation of AP – 1 complex, leading to an increased cellular proliferation, but without the possibility to rescue impaired retinal cells.
- *Mitochondrion – induced apoptosis.* Histone deacetylase 10 (HDAC10) represents a novel class IIb histone deacetylase, present in both the nucleus and cytoplasm. HDAC10 is involved in transcriptional down – regulation of the endogenous inhibitor of cellular antioxidant TXNIP (thioredoxin-interacting protein), leading to altered ROS signaling. In details, it was observed that inhibition of HDAC10 induced release of cytochrome c and activated apoptotic signaling molecules, through accumulation of reactive oxygen species (ROS) (J. H. Lee et al., 2010). Furthermore, HDAC10 could promote autophagy-mediated survival in neuroblastoma cells (Oehme et al., 2013). As highlighted in results, *HDAC10* was down – expressed in our experiment, suggesting a relevant induction of mitochondrion – induced apoptosis of RPE cells.

5.5. CLASSIFICATION OF NEW NON – SYNDROMIC RP FORMS CAUSED BY ALTERATIONS IN REGULATION OF NEW SPECIFIC PATHWAYS (Fig. 33)

Until last 10 years, the scientific community claimed that RNAs transcribed from human genome coded only for proteins. Nowadays, thanks to deep sequencing technologies and advances in bioinformatics, it was discovered that the transcription of Eukaryotic genomes produces a huge variety of RNA species, many of them without coding potential, referred to as non-coding RNAs (ncRNAs) (Patil, Zhou, & Rana, 2014). During past years, ncRNAs were considered as “evolutionary junk”, but increasing evidence suggests a huge impact on several molecular mechanisms, from protein translation to the copying of DNA during cell replication (Santosh, Varshney, & Yadava, 2015). Moreover, the amount of ncRNAs in an organism correlates with its complexity, suggesting a relevant role on development and organization of higher structured animals (Johnsson, Lipovich, Grander, & Morris, 2014). Specific biological functions of ncRNAs depend on their structure and length, which permit us to classify them in small non-coding RNAs (sncRNAs) and long non-coding RNAs (lncRNAs) (Johnsson et al., 2014). A summary of main candidate pathways regulated by analyzed ncRNAs could be found in Table 15.

CANDIDATE PATHWAY	DESCRIPTION OF PATWAY ACTIVITY AND/OR IMPAIRMENT
lncRNAs	Ion channel regulation in ribbon synapses Synaptic vesicle transport Alteration of neurotransmitter levels Cell junction organization Cell - matrix adhesion and actin cytoskeleton organization Alteration of glucose and fatty acid metabolism Increased oxidoreductase activity Induction of apoptosis BRB dysfunctions
piRNAs	Decrease of miRNA silencing activity towards DNA damage response and transporter activity of RPE cells
miRNAs	ABC - transporter disorders Inflammation ER - phagosome pathway Ubiquitin - proteasome pathway
circRNAs	Retinal neurotransmission impairment ECM adhesion structures impairment
snoRNAs	Retinal development and activity Chromatin remodeling, post - post transcriptional silencing and RNA splicing modulation Copper metabolism

Tab. 15. New RP candidate pathway emerged from ncRNA – Seq analysis. This table shows the possible involvement of new candidate pathways in etiopathogenesis of RP, due to increased or decreased regulator activities of analyzed ncRNAs. A detailed description of each pathways could be found in the text.

The relevance of the non-coding RNAs to human disease was initially studied in the context of human cancer (Slaby, Laga, & Sedlacek, 2017), and then was extended to several other diseases (Donato, Scimone, Alibrandi, D'Angelo, & A, 2017). Today, it is widely known that many ncRNAs, such as PIWI-interacting RNAs (piRNAs), large intergenic non-coding RNAs (lincRNAs) and long non-coding RNAs (lncRNAs) are emerging as key elements of cellular homeostasis (Amaral, Dinger, & Mattick, 2013). Along with microRNAs (miRNAs) and other small non-coding RNAs (snoRNAs), dysregulation of these ncRNAs is being found to have relevance not only to tumorigenesis, but also to neurological, cardiovascular, developmental and other diseases (Xue, Zhuo, & Shan, 2017). Among them, Retinitis pigmentosa, an ocular disease with very heterogeneous phenotypes, shows unusually complex molecular genetic causes, most of which still unknown (Bolz, 2017). Using high-throughput sequencing technologies, the whole transcriptome of RPE cells was analyzed, exposed to ox-LDL, during a follow-up of four time points (1h, 2h, 4h and 6h) after exposure, and compared to untreated ones. Thanks to the high coverage of performed sequencing experiment, along with parallel analysis of three replicates for each selected group for each time point, and with the use of multiple algorithms, reliable data was obtained, overcoming possible bias – related variability in ncRNA expression levels and nucleotide sequences. Oxidative stress plays a critical role in RP etiopathogenesis. In particular, it targets RPE cells, very sensible because of high metabolic demand, needed for processes like physiological phagocytosis and life-long light illumination (Inana et al., 2018). Impairment of such functions could lead to pathobiological modifications like outer blood-retinal barrier (BRB) dysfunctions (de Hoz et al., 2016), alterations of extracellular matrix (ECM) components (Shin et al., 2016), inhibition of photoreceptors outer segments processing (Platon-Corchado et al., 2017), increasing of RPE cells senescence and/or apoptosis (Parmar et al., 2018). Our results evidenced that up – regulated circular RNAs could enhance the transcription of their host genes involved in ion channel regulator activity, integrity of basal membrane and receptor clustering. Such functions are well known to be related to RP etiopathogenesis (Giblin, Comes, Strauss, & Gasull, 2016). Very interesting, the ion channel regulation is crucial for ribbon synapses between retina cells (Haumann, Junghans, Anstotz, & Frotscher, 2017), and synaptic vesicle transport could be altered by lncRNAs. It could be

speculated that the global downregulation of Intronic lncRNAs might weaken RPE protein export pathway, along with a reduction of neuroplastin mediated GABA A receptors localization to synapse. This possible effect, along with increased GABA – mediated Cl⁻ import, might inhibit the downstream signal transmission in the retina. Such function could also be influenced by an altered regulation of neurotransmitter levels by down – regulated Sense lncRNAs. About integrity of RPE cell connection to other retina layers, up – regulated Antisense and Sense lncRNAs could alter cell junction organization, cell – matrix adhesion and actin cytoskeleton organization, probably modifying cell morphogenesis, and possibly leading to RPE loss of trophic function towards photoreceptors. Impairment of this vital activity could also be evidenced by alteration in glucose and unsaturated fatty acid metabolic process due to Antisense and Sense lncRNAs over – expressed, respectively. All previously described pathways, along with a possible increased oxidoreductase activity by up – regulated Sense lncRNAs, indicates an intense oxidative stress condition, which finally determine cell death. Induction of apoptotic signaling involves the up – regulation of both Antisense and Sense lncRNAs, especially in the intrinsic pathways for the latter. In such scenario, the small piRNAs assumes the key role of junction ring between long non – coding RNAs and small non-coding RNAs, both influencing regulation of epigenetic changes (Assumpcao et al., 2015; Fok, Scholefield, Fanucchi, & Mhlanga, 2017). It was seen that both PIWI target silencing and piRNA precursor specification can be determined by similar types of chromatin that are characterized by H3K9me3 marks and HP1-like proteins (Toth, Pezic, Stuwe, & Webster, 2016). Very curiously, it was established that the silencing activity of a Piwi pathway can turn a target locus (such as a protein-coding gene) into a piRNA-generating locus (Yamamoto et al., 2013). During and after this process, the locus continues to be transcribed, but rather than leading to protein expression, the transcripts are now processed into piRNAs. Subsequently, the resulting piRNAs can silence, in trans, other loci of similar sequence, showing effects that can be kept over generations without alterations of the involved Piwi pathway, in a way very similar to paramutation (Hovel, Pearson, & Stam, 2015). So, a global down – regulation of detected piRNAs could be interpreted as a decrease of silencing activity of miRNA regulation of DNA damage response and transporter activity of RPE cells, representations of reaction attempt to induced

oxidative stress. Moreover, the ox-LDL probably regulates miRNAs both directly (especially as shown by down – regulated miRNAs) and indirectly by Dicer (particularly when it is up-regulated and over-expresses miRNAs), probably altering several new interesting pathways emerging from target gene predictions. Cellular nitrogen compound metabolic process seems to be impaired and, as already highlighted in aqueous humor and peripheral blood of RP patients (Martinez-Fernandez de la Camara et al., 2013), leading to nitrosative stress. Additionally, alterations of metabolic process involving organic cyclic, cellular aromatic and heterocycle compounds, such as reaction intermediates of retinoid cycle, could lead to retinal degeneration (Bassolino et al., 2014). Furthermore, three signaling pathways were predicted to be altered by selected miRNA dysregulation: Insulin Receptor Signaling (IRS), possibly related to glucose sequestration by RPE in RP dominant subjects (W. Wang et al., 2016), Son of Sevenless (SOS) mediated signaling, already associated to ocular manifestations in Noonan Syndrome (Roberts et al., 2007; van Trier et al., 2016), and Hedgehog signaling, whose impairments could lead to ciliary trafficking defects (Schwarz et al., 2017a). All described pathways, along with ABC – transporters disorders (D'Angelo et al., 2017), inflammation (Appelbaum, Santana, & Aguirre, 2017), Endoplasmic Reticulum (ER) – phagosome pathways (Williams & Lopes, 2011), and Ubiquitin Proteasome pathway (Juuti-Uusitalo et al., 2017), represent all possible targets of miRNA regulation in RPE cells. Finally, miRTarBase showed experimentally verified gene targets of several considered miRNAs, already known to be causative of different forms of RP: Kelch Like Family Member 7 (*KLHL7*, target of hsa-miR-1307), whose mutations could determine alterations in ubiquitination of target proteins for proteasome-mediated degradation (Angius et al., 2018), Retinol Dehydrogenase 11 (*RDH11*, target of hsa-miR-3064), a fundamental enzyme needed for vision-related and systemic retinoic acid metabolism (Y. A. Xie et al., 2014), Ceramide Kinase Like (*CERKL*, target of hsa-miR-4709), encoding an antioxidant protein which is crucial to photoreceptor survival (J. Chen et al., 2015; Fathinajafabadi, Perez-Jimenez, Riera, Knecht, & Gonzalez-Duarte, 2014), Aryl Hydrocarbon Receptor Interacting Protein Like 1 (*AIPLI*, target of hsa-miR-3615), whose mutations cause various form of recessive RP and Leber Congenital Amaurosis (Sundaramurthy et al., 2016), and USH1 Protein Network Component Sans (*USH1G*,

target of hsa-miR-637), one of best known causative gene of Usher Syndrome Type I (Lenarduzzi et al., 2015). Additionally, as yet evidenced, miRNA silencing is also a relevant target of altered circular RNAs (Hsiao, Sun, & Tsai, 2017), especially those coming from *DLG1*, *RBMS3* and *TNIK* (globally up – regulated), and from *TNS3* and *VIM* (globally down – regulated). *DLG1* and *RBMS3* are tumor suppressor genes. *DLG1* encoded product act as protein scaffold at the outer plexiform layer of the retina, maintaining photoreceptor – Muller glia cell adhesion, and as regulator of K⁺ - voltage dependent channels distributed in amacrine cholinergic and bipolar cells (Vieira et al., 2008). Moreover, *Dlg1* is a member of CRB1 – membrane – associated palmitoylated protein (MPP) 5 protein complex, and it is already known that mutation in *CRB1* are frequent causes of various forms of Retinitis pigmentosa (Alves & Wijnholds, 2018). *Rbms3* post– transcriptionally regulates members of the TGF – Beta pathway, influencing cellular proliferation and differentiation (Jayasena & Bronner, 2012). Cellular adhesion and migration are also regulated by tensin 3 (*TNS3*), an adaptor of Rho GTPase signaling at extracellular matrix adhesion structures (Blangy, 2017). The small GTPase signaling pathway, involving *RAP2*, presents *Tnik* as a specific effector, able to regulate dendritogenesis and glutamatergic signaling. Over – expression of *TNIK* results in disruption of F – actine structures and activation of c-Jun N-terminal kinase (*JNK*) signaling, determining cell spreading and neuronal degeneration (Larhammar, Huntwork-Rodriguez, Rudhard, Sengupta-Ghosh, & Lewcock, 2017). Curiously, the last most interesting altered circRNA host gene, *VIM*, is yet known to be susceptible to different forms of metabolic and oxidative stress (Velez et al., 2018). Additionally, it was yet seen that retinas without *Vim* show attenuated Muller cell reactivity, with altered Kir channel distribution, determining reduced retinal cell survival (Wunderlich et al., 2015). So, alteration in previously described circRNAs might impair retina neurotransmission and extracellular matrix adhesion structures, leading to possible block of visual signaling pathways. Involvement of ion channels regulation and synaptic impairments is a new branch of retinitis pigmentosa research field, already analyzed by our team in several patients by whole genome sequencing analyses (data under publication). An interesting data emerged from two altered lncRNA host genes, *ABCC6* and *VCAN*, already present in RetNet official database and known as causative of retinal pathologies. In details, *ABCC6* is expressed in brain

microvascular endothelial cells (BMEC), suggesting that it may contribute to the inner blood – retina barrier (BRB) as well as the blood – brain barrier BBB (Tachikawa, Toki, Tomi, & Hosoya, 2008). Alterations of *ABCC6*, as ones in the other ABC family member *ABCA4* (D'Angelo et al., 2017), are involved in syndromic/systemic diseases with retinopathy, as pseudoxanthoma elasticum (S. Yoshida et al., 2005). *VCAN*, instead, coding for versican, is a chondroitin sulfate proteoglycan particularly abundant in extracellular matrix of nervous system cells, retina included (Popp, Maurel, Andersen, & Margolis, 2004). Mutations in *VCAN* cause several ocular – retinal developmental disease, like Wagner syndrome (Araujo et al., 2018). Obtained data showed an up – regulation of antisense lncRNA from *ABCC6* and a down – regulation sense lncRNA from *VCAN*, which might play a pathogenic role impairing retina structures.

Finally, a special mention goes to found snoRNAs with altered expression. Several snoRNAs were already detected in murine retina, suggesting a possible involvement in retinal development and activity (C. H. Liu, Wang, Sun, SanGiovanni, & Chen, 2016). Although how such functions could be explicated need to be yet totally understood, several evidences highlight snoRNAs role in influencing translational fidelity, stop codon recognition and ribosome – ligand interactions (Wilusz & Wilusz, 2014). Additionally, snoRNAs could play a fundamental role in chromatin remodeling, in miRNA – like post – transcriptional gene silencing and in lncRNA – like RNA splicing modulation (McMahon, Contreras, & Ruggero, 2015). Intriguingly, the most interesting snoRNAs research area regards the ability for pseudouridine in nonsense codon suppression, potentially altering the coding potential of non-canonical RNA substrates, such as mRNAs (Weischenfeldt, Lykke-Andersen, & Porse, 2005). For this purpose, a pathway analysis of snoRNAs host genes was realized, in order to highlight possible involvement in Retinitis pigmentosa pathology. Host gene pathway analysis evidenced that alteration of found snoRNAs expression could impair the interferon- γ -activated inhibitor of translation (GAIT) translational control system, made of glutamyl-prolyl tRNA synthetase (EPRS), NS1-associated protein 1 (NSAP1), ribosomal protein L13a (L13a), and glyceraldehyde-3-phosphate dehydrogenase (GAPDH) (Mukhopadhyay, Jia, Arif, Ray, & Fox, 2009). It controls the transcript – selective translation of functionally related genes, binding structural GAIT elements

in the 3'-untranslated regions (UTRs) of multiple inflammation – related mRNAs, including ceruloplasmin (Cp), and represses their translation (Fox, 2015). Ceruloplasmin is a multifunctional, copper-binding α -globulin, with antioxidant capabilities, due to the discharge of electrons, e.g. during conversion of Fe(II) to Fe(III) (Eid, Hemadi, Ha-Duong, & El Hage Chahine, 2014). Interestingly, several changes in pathways involving L13a, an integral constituent of the ribosome 60S subunit (Eid et al., 2014), emerged from analysis. In details, it was highlighted a possible alteration in dissociation of L13a from the 60S ribosomal subunit, following DAPK-ZIPK kinase axis phosphorylation, and an association of phospho-L13a with GAIT element of ceruloplasmin, with the possible block of eIF3-containing 43S pre-initiation complex, thereby promoting the L-13a-mediated translational silencing of ceruloplasmin expression. *RPL13A* mRNA is co – transcribed with four box C/D snoRNA genes, U32a, U33, U34 and U35a, located within four *RPL13A* introns (Michel et al., 2011), and globally down – expressed in our data. Such results could be compatible with alterations in ceruloplasmin levels, influencing both the transport of copper and the functioning of RPE (Hadziahmetovic et al., 2008), as seen in Indian patients of RP (Gahlot, Khosla, Makashir, Vasuki, & Basu, 1976) and macular degeneration (Newsome et al., 1986). Additionally, alterations of copper metabolism could impair allosteric effects on reducing misfolded aggregates, as in other neurodegenerative disorders including Alzheimer disease (Pal, Kumar, & Prasad, 2014). Moreover, DAPK and ZIPK are validated regulators of programmed cell death pathways, suggesting the possibility that GAIT – mediated translational repression of the kinases could contribute to regulation of apoptosis. Additionally, it was seen that GAIT complex assembly is inhibited by ox – LDL, resulting in sustained production and accumulation of GAIT system target proteins like Cp (Arif et al., 2017). Additionally, deletion of the Rpl13a snoRNA in a mouse model, while leaving the coding and regulatory regions intact, profoundly influenced mitochondrial metabolism, resulting in enhanced systemic glucose tolerance and protection against oxidative stress (J. Lee et al., 2016). Therefore, the delayed inhibition of expression of multiple inflammation – related proteins by the GAIT complex suggests that this system represent a post-transcriptional off – switch that also contributes to inflammation – resolution. The other group that showed altered expression consists of

small Cajal body – Specific RNAs (scaRNAs), a sub – group of snoRNAs associated to Cajal body. Cajal bodies, distinct sub – domains of interphase nucleus, represent specific and dynamic assemblies of proteins and RNA factors involved in various aspect of gene expression, such the biogenesis and/or transport of small nuclear ribonucleoproteins (snRNP) and small nucleolar ribonucleoproteins (snoRNPs) (Darzacq et al., 2002). It was seen that U85 (over – expressed through our experiment) is able to realize the 2'-O-methylation and psudouridylation of snRNA U5, while U89 and U91 (also over – expressed in our results) could direct post – transcriptional modification of pol II – specific spliceosomal snRNAs, as well as U91 (the only scaRNA over – expressed in our analysis). Following this data, we could speculate that the overall down – regulation of found scaRNAs could impair specific modifications controlled by them, leading the spliceosome to function properly.

6. CONCLUSIONS

In this work, an intricate set of experiments based on omics approaches were realized, in order to improve the classification of RP orphan forms and to clarify the etiopathogenesis of already known ones. It was identified a complex cluster of candidate gene-variants closely associated with a form of RP whose genetic causes were previously unknown. These genes (*PDE4DIP*, *LTF*, *CCDC175*, *GLO1*, *PPEF2*, *RNF144B*, *RDH13*, *FLT3*, *RCVRN*, *GNB1*, *GNGT1*, *GRK7*, *ARRB1*, *RLBP1*, *CACNG8*, *RXRG*, *PAX2*, *EYS*, *MYO7A*, *RP1*, *ABCA4*, *ELOVL4*) encode several fundamental proteins involved in retina and eye physiology. Moreover, there were found new candidate “macro – pathways” with many related sub – pathways that could be involved in RP etiopathogenesis. Among them, resulted very interesting the expression changes in genes involved in cell cycle regulation, vesicular trafficking, cell migration, endoplasmic reticulum stress, chaperones activity, small GTPase signaling, retinoic acid cycle in relation with epigenetics, microvascular impairments, chromosome instability, circadian rhythms related with fatty acids metabolism, synapses integrity, JUN complex and retinal cells rescue. In addition to coding genes, 3155 lncRNAs and 162 sncRNAs exhibited expression alterations in transcriptomic experiments, targeting host genes involved in several biochemical pathways related to visual functions. One of them, corroborated by WGS analyses, regards the synaptic impairment of neurotransmission in the retina, which might be seriously associated for the first time to RP etiopathogenesis. Obtained results could represent an important step towards detection and classification of unknown forms of RP. The following steps could foresee the genetic analysis of patients affected by such orphan RP forms, looking for variations in previously selected candidate genes, in order to establish a specific genotype – phenotype correlation. Finally, “molecular characterization” of patients will allow future inclusion in clinical trials based on gene therapy. Such model represents a predictive and personalized approach to RP (Donato, Scimone, D’Angelo, & Sidoti, 2017), which nowadays still present several challenges to win: 1) The analysis of epigenetic modifications (Mensaert et al., 2014); 2) Extension of predictive models to the widest different clinical populations (Brunotto & Zarate, 2012); 3) A more intensive application of NGS (Ballester, Luthra, Kanagal-Shamanna, & Singh,

2016); 4) Use of machine learning approaches to genetic data develop more powerful and accurate prognostic tests (Dale, Popescu, & Karp, 2010);(Calamuneri et al., 2017); 5) Reduce disease complexity and improve genetic susceptibility by classifying diseases by molecular subtypes (Berger, Wang, & Shen, 2014). Finally, even if prediction will continue to be challenging, it could give researchers and clinicians a relevant help to discover new possible models to detect the real ethiopathology of many complex genetic and not diseases.

7. BIBLIOGRAPHY

- Abdelhakim, A., & Rasool, N. (2018). Neuroretinitis: a review. *Curr Opin Ophthalmol*. doi:10.1097/ICU.0000000000000527
- Abraham, F. A., Ivry, M., & Tsvieli, R. (1976). Sector retinitis pigmentosa: a fluorescein angiographic study. *Ophthalmologica*, 172(4), 287-297. doi:10.1159/000307727
- Acharya, S., Foletta, V. C., Lee, J. W., Rayborn, M. E., Rodriguez, I. R., Young, W. S., 3rd, & Hollyfield, J. G. (2000). SPACRCAN, a novel human interphotoreceptor matrix hyaluronan-binding proteoglycan synthesized by photoreceptors and pinealocytes. *J Biol Chem*, 275(10), 6945-6955.
- Acton, J. H., Greenberg, J. P., Greenstein, V. C., Marsiglia, M., Tabacaru, M., Theodore Smith, R., & Tsang, S. H. (2013). Evaluation of multimodal imaging in carriers of X-linked retinitis pigmentosa. *Exp Eye Res*, 113, 41-48. doi:10.1016/j.exer.2013.05.003
- Adams, J. C., & Zhang, L. (1999). cDNA cloning of human muskelin and localisation of the muskelin (MKLN1) gene to human chromosome 7q32 and mouse chromosome 6 B1/B2 by physical mapping and FISH. *Cytogenet Cell Genet*, 87(1-2), 19-21. doi:10.1159/000015385
- Agbaga, M. P., Tam, B. M., Wong, J. S., Yang, L. L., Anderson, R. E., & Moritz, O. L. (2014). Mutant ELOVL4 that causes autosomal dominant stargardt-3 macular dystrophy is misrouted to rod outer segment disks. *Invest Ophthalmol Vis Sci*, 55(6), 3669-3680. doi:10.1167/iovs.13-13099
- Aguirre-Lamban, J., Gonzalez-Aguilera, J. J., Riveiro-Alvarez, R., Cantalapiedra, D., Avila-Fernandez, A., Villaverde-Montero, C., . . . Ayuso, C. (2011). Further associations between mutations and polymorphisms in the ABCA4 gene: clinical implication of allelic variants and their role as protector/risk factors. *Invest Ophthalmol Vis Sci*, 52(9), 6206-6212. doi:10.1167/iovs.10-5743
- Ajmal, M., Khan, M. I., Neveling, K., Khan, Y. M., Azam, M., Waheed, N. K., . . . Cremers, F. P. (2014). A missense mutation in the splicing factor gene DHX38 is associated with early-onset retinitis pigmentosa with macular coloboma. *J Med Genet*, 51(7), 444-448. doi:10.1136/jmedgenet-2014-102316
- Aken, B. L., Ayling, S., Barrell, D., Clarke, L., Curwen, V., Fairley, S., . . . Searle, S. M. (2016). The Ensembl gene annotation system. *Database (Oxford)*, 2016. doi:10.1093/database/baw093

- Al Rashaed, S., Khan, A. O., Nowilaty, S. R., Edward, D. P., & Kozak, I. (2016). Spectral-domain optical coherence tomography reveals prelaminar membranes in optic nerve head pallor in eyes with retinitis pigmentosa. *Graefes Arch Clin Exp Ophthalmol*, 254(1), 77-81. doi:10.1007/s00417-015-3015-1
- Al-Ubaidi, M. R., Naash, M. I., & Conley, S. M. (2013). A perspective on the role of the extracellular matrix in progressive retinal degenerative disorders. *Invest Ophthalmol Vis Sci*, 54(13), 8119-8124. doi:10.1167/iovs.13-13536
- Aleman, T. S., Cideciyan, A. V., Aguirre, G. K., Huang, W. C., Mullins, C. L., Roman, A. J., . . . Jacobson, S. G. (2011). Human CRB1-associated retinal degeneration: comparison with the rd8 Crb1-mutant mouse model. *Invest Ophthalmol Vis Sci*, 52(9), 6898-6910. doi:10.1167/iovs.11-7701
- Aleman, T. S., Cideciyan, A. V., Sumaroka, A., Schwartz, S. B., Roman, A. J., Windsor, E. A., . . . Jacobson, S. G. (2007). Inner retinal abnormalities in X-linked retinitis pigmentosa with RPGR mutations. *Invest Ophthalmol Vis Sci*, 48(10), 4759-4765. doi:10.1167/iovs.07-0453
- Alfano, G., Kruczek, P. M., Shah, A. Z., Kramarz, B., Jeffery, G., Zelhof, A. C., & Bhattacharya, S. S. (2016). EYS Is a Protein Associated with the Ciliary Axoneme in Rods and Cones. *PLoS One*, 11(11), e0166397. doi:10.1371/journal.pone.0166397
- Alfonso-Jaume, M. A., Mahimkar, R., & Lovett, D. H. (2004). Co-operative interactions between NFAT (nuclear factor of activated T cells) c1 and the zinc finger transcription factors Sp1/Sp3 and Egr-1 regulate MT1-MMP (membrane type 1 matrix metalloproteinase) transcription by glomerular mesangial cells. *Biochem J*, 380(Pt 3), 735-747. doi:10.1042/BJ20031281
- Ali, M. U., Rahman, M. S. U., Cao, J., & Yuan, P. X. (2017). Genetic characterization and disease mechanism of retinitis pigmentosa; current scenario. *3 Biotech*, 7(4), 251. doi:10.1007/s13205-017-0878-3
- Alivand, M. R., Soheili, Z. S., Pornour, M., Solali, S., & Sabouni, F. (2017). Novel Epigenetic Controlling of Hypoxia Pathway Related to Overexpression and Promoter Hypomethylation of TET1 and TET2 in RPE Cells. *J Cell Biochem*, 118(10), 3193-3204. doi:10.1002/jcb.25965
- Allison, D. B., Cui, X., Page, G. P., & Sabripour, M. (2006). Microarray data analysis: from disarray to consolidation and consensus. *Nat Rev Genet*, 7(1), 55-65. doi:10.1038/nrg1749

- Alpi, A. F., Chaugule, V., & Walden, H. (2016). Mechanism and disease association of E2-conjugating enzymes: lessons from UBE2T and UBE2L3. *Biochem J*, 473(20), 3401-3419. doi:10.1042/BCJ20160028
- Alves, C. H., & Wijnholds, J. (2018). AAV Gene Augmentation Therapy for CRB1-Associated Retinitis Pigmentosa. *Methods Mol Biol*, 1715, 135-151. doi:10.1007/978-1-4939-7522-8_10
- Amaral, P. P., Dinger, M. E., & Mattick, J. S. (2013). Non-coding RNAs in homeostasis, disease and stress responses: an evolutionary perspective. *Brief Funct Genomics*, 12(3), 254-278. doi:10.1093/bfgp/elt016
- Amram, B., Cohen-Tayar, Y., David, A., & Ashery-Padan, R. (2017). The retinal pigmented epithelium - from basic developmental biology research to translational approaches. *Int J Dev Biol*, 61(3-4-5), 225-234. doi:10.1387/ijdb.160393ra
- AnandBabu, K., Bharathidevi, S. R., Sripriya, S., Sen, P., Prakash, V. J., Bindu, A., . . . Angayarkanni, N. (2016). Serum Paraoxonase activity in relation to lipid profile in Age-related Macular Degeneration patients. *Exp Eye Res*, 152, 100-112. doi:10.1016/j.exer.2016.09.009
- Andersen, K. M., Sauer, L., Gensure, R. H., Hammer, M., & Bernstein, P. S. (2018). Characterization of Retinitis Pigmentosa Using Fluorescence Lifetime Imaging Ophthalmoscopy (FLIO). *Transl Vis Sci Technol*, 7(3), 20. doi:10.1167/tvst.7.3.20
- Anderson, D. H., Fisher, S. K., & Steinberg, R. H. (1978). Mammalian cones: disc shedding, phagocytosis, and renewal. *Invest Ophthalmol Vis Sci*, 17(2), 117-133.
- Andrews, S. (2014). FastQC A Quality Control tool for High Throughput Sequence Data. Retrieved from <http://www.bioinformatics.babraham.ac.uk/projects/fastqc/>
- Angius, A., Uva, P., Buers, I., Oppo, M., Puddu, A., Onano, S., . . . Rutsch, F. (2016). Bi-allelic Mutations in KLHL7 Cause a Crisponi/CISS1-like Phenotype Associated with Early-Onset Retinitis Pigmentosa. *Am J Hum Genet*, 99(1), 236-245. doi:10.1016/j.ajhg.2016.05.026
- Angius, A., Uva, P., Buers, I., Oppo, M., Puddu, A., Onano, S., . . . Rutsch, F. (2018). Bi-allelic Mutations in KLHL7 Cause a Crisponi/CISS1-like Phenotype Associated with Early-Onset Retinitis Pigmentosa. *Am J Hum Genet*, 102(4), 713. doi:10.1016/j.ajhg.2018.03.020
- Appelbaum, T., Santana, E., & Aguirre, G. D. (2017). Strong upregulation of inflammatory genes accompanies photoreceptor demise in canine models of retinal degeneration. *PLoS One*, 12(5), e0177224. doi:10.1371/journal.pone.0177224

- Arai, Y., Maeda, A., Hiram, Y., Ishigami, C., Kosugi, S., Mandai, M., . . . Takahashi, M. (2015). Retinitis Pigmentosa with EYS Mutations Is the Most Prevalent Inherited Retinal Dystrophy in Japanese Populations. *J Ophthalmol*, 2015, 819760. doi:10.1155/2015/819760
- Araki-Sasaki, K., Hirano, K., Osakabe, Y., Kuroda, M., Kitagawa, K., Mishima, H., . . . Kinoshita, S. (2013). Classification of secondary corneal amyloidosis and involvement of lactoferrin. *Ophthalmology*, 120(6), 1166-1172. doi:10.1016/j.ophtha.2012.11.047
- Araujo, J. R., Tavares-Ferreira, J., Estrela-Silva, S., Rocha, P., Brandao, E., Faria, P. A., . . . Rocha-Sousa, A. (2018). WAGNER syndrome: anatomic, functional and genetic characterization of a Portuguese family. *Graefes Arch Clin Exp Ophthalmol*, 256(1), 163-171. doi:10.1007/s00417-017-3800-0
- Arif, A., Yao, P., Terenzi, F., Jia, J., Ray, P. S., & Fox, P. L. (2017). The GAIT translational control system. *Wiley Interdiscip Rev RNA*. doi:10.1002/wrna.1441
- Arno, G., Carss, K. J., Hull, S., Zihni, C., Robson, A. G., Fiorentino, A., . . . Webster, A. R. (2017). Biallelic Mutation of ARHGEF18, Involved in the Determination of Epithelial Apicobasal Polarity, Causes Adult-Onset Retinal Degeneration. *Am J Hum Genet*, 100(2), 334-342. doi:10.1016/j.ajhg.2016.12.014
- Arno, G., Hull, S., Carss, K., Dev-Borman, A., Chakarova, C., Bujakowska, K., . . . Webster, A. R. (2016). Reevaluation of the Retinal Dystrophy Due to Recessive Alleles of RGR With the Discovery of a Cis-Acting Mutation in CDHR1. *Invest Ophthalmol Vis Sci*, 57(11), 4806-4813. doi:10.1167/iovs.16-19687
- Arredondo Zamarripa, D., Diaz-Lezama, N., Melendez Garcia, R., Chavez Balderas, J., Adan, N., Ledesma-Colunga, M. G., . . . Thebault, S. (2014). Vasoinhibins regulate the inner and outer blood-retinal barrier and limit retinal oxidative stress. *Front Cell Neurosci*, 8, 333. doi:10.3389/fncel.2014.00333
- Arts, R. J., Blok, B. A., van Crevel, R., Joosten, L. A., Aaby, P., Benn, C. S., & Netea, M. G. (2015). Vitamin A induces inhibitory histone methylation modifications and down-regulates trained immunity in human monocytes. *J Leukoc Biol*, 98(1), 129-136. doi:10.1189/jlb.6AB0914-416R
- Aschauer, L., Gruber, L. N., Pfaller, W., Limonciel, A., Athersuch, T. J., Cavill, R., . . . Jennings, P. (2013). Delineation of the key aspects in the regulation of epithelial monolayer formation. *Mol Cell Biol*, 33(13), 2535-2550. doi:10.1128/MCB.01435-12

- Ashby, R. S., Zeng, G., Leotta, A. J., Tse, D. Y., & McFadden, S. A. (2014). Egr-1 mRNA expression is a marker for the direction of mammalian ocular growth. *Invest Ophthalmol Vis Sci*, *55*(9), 5911-5921. doi:10.1167/iovs.13-11708
- Assumpcao, C. B., Calcagno, D. Q., Araujo, T. M., Santos, S. E., Santos, A. K., Riggins, G. J., . . . Assumpcao, P. P. (2015). The role of piRNA and its potential clinical implications in cancer. *Epigenomics*, *7*(6), 975-984. doi:10.2217/epi.15.37
- Athanasidou, D., Bevilacqua, D., Aguila, M., McCulley, C., Kanuga, N., Iwawaki, T., . . . Cheetham, M. E. (2014). The co-chaperone and reductase ERdj5 facilitates rod opsin biogenesis and quality control. *Hum Mol Genet*, *23*(24), 6594-6606. doi:10.1093/hmg/ddu385
- Azadi, S., Brush, R. S., Anderson, R. E., & Rajala, R. V. (2016). Class I Phosphoinositide 3-Kinase Exerts a Differential Role on Cell Survival and Cell Trafficking in Retina. *Adv Exp Med Biol*, *854*, 363-369. doi:10.1007/978-3-319-17121-0_48
- Azmy, R., Dawood, A., Kilany, A., El-Ghobashy, Y., Ellakwa, A. F., & El-Daly, M. (2012). Association analysis of genetic variations of eNOS and alpha2beta1 integrin genes with type 2 diabetic retinopathy. *Appl Clin Genet*, *5*, 55-65. doi:10.2147/TACG.S31979
- Bagheri, S., Pantrangi, M., Sodhi, S. K., Bagheri, S., Oellers, P., & Scholl, H. P. N. (2017). A Novel Large Homozygous Deletion in the Cellular Retinaldehyde-Binding Protein Gene (Rlbp1) in a Patient with Retinitis Punctata Albescens. *Retin Cases Brief Rep*. doi:10.1097/ICB.0000000000000628
- Bainbridge, J. W. (2009). Prospects for gene therapy of inherited retinal disease. *Eye (Lond)*, *23*(10), 1898-1903. doi:10.1038/eye.2008.412
- Bair, W. B., 3rd, Cabello, C. M., Uchida, K., Bause, A. S., & Wondrak, G. T. (2010). GLO1 overexpression in human malignant melanoma. *Melanoma Res*, *20*(2), 85-96. doi:10.1097/CMR.0b013e3283364903
- Ballester, L. Y., Luthra, R., Kanagal-Shamanna, R., & Singh, R. R. (2016). Advances in clinical next-generation sequencing: target enrichment and sequencing technologies. *Expert Rev Mol Diagn*, *16*(3), 357-372. doi:10.1586/14737159.2016.1133298
- Ban, N., Ozawa, Y., Inaba, T., Miyake, S., Watanabe, M., Shinmura, K., & Tsubota, K. (2013). Light-dark condition regulates sirtuin mRNA levels in the retina. *Exp Gerontol*, *48*(11), 1212-1217. doi:10.1016/j.exger.2013.04.010
- Bandah-Rozenfeld, D., Mizrahi-Meissonnier, L., Farhy, C., Obolensky, A., Chowers, I., Pe'er, J., . . . Sharon, D. (2010). Homozygosity mapping reveals null mutations in FAM161A

- as a cause of autosomal-recessive retinitis pigmentosa. *Am J Hum Genet*, 87(3), 382-391. doi:10.1016/j.ajhg.2010.07.022
- Bang, H. S., Choi, M. H., Kim, C. S., & Choi, S. J. (2016). Gene expression profiling in undifferentiated thyroid carcinoma induced by high-dose radiation. *J Radiat Res*, 57(3), 238-249. doi:10.1093/jrr/rrw002
- Barnes, W. G., Reiter, E., Violin, J. D., Ren, X. R., Milligan, G., & Lefkowitz, R. J. (2005). beta-Arrestin 1 and Galphaq/11 coordinately activate RhoA and stress fiber formation following receptor stimulation. *J Biol Chem*, 280(9), 8041-8050. doi:10.1074/jbc.M412924200
- Barsky, A., Gardy, J. L., Hancock, R. E., & Munzner, T. (2007). Cerebral: a Cytoscape plugin for layout of and interaction with biological networks using subcellular localization annotation. *Bioinformatics*, 23(8), 1040-1042. doi:10.1093/bioinformatics/btm057
- Bassolino, G., Sovdat, T., Liebel, M., Schnedermann, C., Odell, B., Claridge, T. D., . . . Fletcher, S. P. (2014). Synthetic control of retinal photochemistry and photophysics in solution. *J Am Chem Soc*, 136(6), 2650-2658. doi:10.1021/ja4121814
- Battaglia Parodi, M., La Spina, C., Triolo, G., Riccieri, F., Pierro, L., Gagliardi, M., & Bandello, F. (2016). Correlation of SD-OCT findings and visual function in patients with retinitis pigmentosa. *Graefes Arch Clin Exp Ophthalmol*, 254(7), 1275-1279. doi:10.1007/s00417-015-3185-x
- Baum, L., Chan, W. M., Li, W. Y., Lam, D. S., Wang, P. B., & Pang, C. P. (2003). ABCA4 sequence variants in Chinese patients with age-related macular degeneration or Stargardt's disease. *Ophthalmologica*, 217(2), 111-114. doi:68553
- Bazhin, A. V., Schadendorf, D., Philippov, P. P., & Eichmuller, S. B. (2007). Recoverin as a cancer-retina antigen. *Cancer Immunol Immunother*, 56(1), 110-116. doi:10.1007/s00262-006-0132-z
- Beatty S, M. I., Henson DB, Carden D, Koh H, Boulton ME. (2001). Macular pigment and risk for age-related macular degeneration in subjects from a Northern European population. *Invest Ophthalmol Vis Sci*, 42(2), 439-446.
- Bellingrath, J. S., Ochakovski, G. A., Seitz, I. P., Kohl, S., Zrenner, E., Hanig, N., . . . Fischer, M. D. (2017). High Symmetry of Visual Acuity and Visual Fields in RPGR-Linked Retinitis Pigmentosa. *Invest Ophthalmol Vis Sci*, 58(11), 4457-4466. doi:10.1167/iovs.17-22077
- Belyaeva, O. V., Korkina, O. V., Stetsenko, A. V., & Kedishvili, N. Y. (2008). Human retinol dehydrogenase 13 (RDH13) is a mitochondrial short-chain dehydrogenase/reductase

- with a retinaldehyde reductase activity. *FEBS J*, 275(1), 138-147. doi:10.1111/j.1742-4658.2007.06184.x
- Ben Rebeh, I., Moriniere, M., Ayadi, L., Benzina, Z., Charfedine, I., Feki, J., . . . Masmoudi, S. (2010). Reinforcement of a minor alternative splicing event in MYO7A due to a missense mutation results in a mild form of retinopathy and deafness. *Mol Vis*, 16, 1898-1906.
- Ben-Rebeh, I., Grati, M., Bonnet, C., Bouassida, W., Hadjamor, I., Ayadi, H., . . . Masmoudi, S. (2016). Genetic analysis of Tunisian families with Usher syndrome type 1: toward improving early molecular diagnosis. *Mol Vis*, 22, 827-835.
- Benard, G., Neutzner, A., Peng, G., Wang, C., Livak, F., Youle, R. J., & Karbowski, M. (2010). IBRDC2, an IBR-type E3 ubiquitin ligase, is a regulatory factor for Bax and apoptosis activation. *EMBO J*, 29(8), 1458-1471. doi:10.1038/emboj.2010.39
- Benatti, P., Chiaramonte, M. L., Lorenzo, M., Hartley, J. A., Hochhauser, D., Gnesutta, N., . . . Dolfini, D. (2016). NF-Y activates genes of metabolic pathways altered in cancer cells. *Oncotarget*, 7(2), 1633-1650. doi:10.18632/oncotarget.6453
- Bennett, L. D., & Anderson, R. E. (2016). Current Progress in Deciphering Importance of VLC-PUFA in the Retina. *Adv Exp Med Biol*, 854, 145-151. doi:10.1007/978-3-319-17121-0_20
- Bennett, L. D., Brush, R. S., Chan, M., Lydic, T. A., Reese, K., Reid, G. E., . . . Anderson, R. E. (2014). Effect of reduced retinal VLC-PUFA on rod and cone photoreceptors. *Invest Ophthalmol Vis Sci*, 55(5), 3150-3157. doi:10.1167/iovs.14-13995
- Bennett, L. D., Hopiavuori, B. R., Brush, R. S., Chan, M., Van Hook, M. J., Thoreson, W. B., & Anderson, R. E. (2014). Examination of VLC-PUFA-deficient photoreceptor terminals. *Invest Ophthalmol Vis Sci*, 55(7), 4063-4072. doi:10.1167/iovs.14-13997
- Bennett, L. D., Klein, M., Locke, K. G., Kiser, K., & Birch, D. G. (2017). Dark-Adapted Chromatic Perimetry for Measuring Rod Visual Fields in Patients with Retinitis Pigmentosa. *Transl Vis Sci Technol*, 6(4), 15. doi:10.1167/tvst.6.4.15
- Bennis, A., Gorgels, T. G., Ten Brink, J. B., van der Spek, P. J., Bossers, K., Heine, V. M., & Bergen, A. A. (2015). Comparison of Mouse and Human Retinal Pigment Epithelium Gene Expression Profiles: Potential Implications for Age-Related Macular Degeneration. *PLoS One*, 10(10), e0141597. doi:10.1371/journal.pone.0141597
- Berger, J. O., Wang, X., & Shen, L. (2014). A Bayesian approach to subgroup identification. *J Biopharm Stat*, 24(1), 110-129. doi:10.1080/10543406.2013.856026
- Berner, A. K., Brouwers, O., Pringle, R., Klaassen, I., Colhoun, L., McVicar, C., . . . Stitt, A. W. (2012). Protection against methylglyoxal-derived AGEs by regulation of

- glyoxalase 1 prevents retinal neuroglial and vasodegenerative pathology. *Diabetologia*, 55(3), 845-854. doi:10.1007/s00125-011-2393-0
- Berson, E. L. (1993). Retinitis pigmentosa. The Friedenwald Lecture. *Invest Ophthalmol Vis Sci*, 34(5), 1659-1676.
- Besharse, J. C., & McMahon, D. G. (2016). The Retina and Other Light-sensitive Ocular Clocks. *J Biol Rhythms*, 31(3), 223-243. doi:10.1177/0748730416642657
- Bhattacharya, A., Ziebarth, J. D., & Cui, Y. (2014). PolymiRTS Database 3.0: linking polymorphisms in microRNAs and their target sites with human diseases and biological pathways. *Nucleic Acids Res*, 42(Database issue), D86-91. doi:10.1093/nar/gkt1028
- Bhattacharyya, S., Hope, T. J., & Young, J. A. (2011). Differential requirements for clathrin endocytic pathway components in cellular entry by Ebola and Marburg glycoprotein pseudovirions. *Virology*, 419(1), 1-9. doi:10.1016/j.virol.2011.07.018
- Bikbova, G., Oshitari, T., Baba, T., & Yamamoto, S. (2015). Altered Expression of NF- kappa B and SP1 after Exposure to Advanced Glycation End-Products and Effects of Neurotrophic Factors in AGEs Exposed Rat Retinas. *J Diabetes Res*, 2015, 543818. doi:10.1155/2015/543818
- Bindea, G., Galon, J., & Mlecnik, B. (2013). CluePedia Cytoscape plugin: pathway insights using integrated experimental and in silico data. *Bioinformatics*, 29(5), 661-663. doi:10.1093/bioinformatics/btt019
- Bindea, G., Mlecnik, B., Hackl, H., Charoentong, P., Tosolini, M., Kirilovsky, A., . . . Galon, J. (2009). ClueGO: a Cytoscape plug-in to decipher functionally grouped gene ontology and pathway annotation networks. *Bioinformatics*, 25(8), 1091-1093. doi:10.1093/bioinformatics/btp101
- Birch, D. G., Wen, Y., Locke, K., & Hood, D. C. (2011). Rod sensitivity, cone sensitivity, and photoreceptor layer thickness in retinal degenerative diseases. *Invest Ophthalmol Vis Sci*, 52(10), 7141-7147. doi:10.1167/iovs.11-7509
- Bittner, A. K., Haythornthwaite, J. A., Diener-West, M., & Dagnelie, G. (2012). Photopsias are related in part to perceived stress and positive mood in retinitis pigmentosa. *Eye (Lond)*, 26(1), 101-108. doi:10.1038/eye.2011.247
- Blangy, A. (2017). Tensins are versatile regulators of Rho GTPase signalling and cell adhesion. *Biol Cell*, 109(3), 115-126. doi:10.1111/boc.201600053
- Blom, M., Reis, K., Heldin, J., Kreuger, J., & Aspenstrom, P. (2017). The atypical Rho GTPase RhoD is a regulator of actin cytoskeleton dynamics and directed cell migration. *Exp Cell Res*, 352(2), 255-264. doi:10.1016/j.yexcr.2017.02.013

- Bo, Q., Ma, S., Han, Q., Wang, F. E., Li, X., & Zhang, Y. (2015). Role of autophagy in photoreceptor cell survival and death. *Crit Rev Eukaryot Gene Expr*, 25(1), 23-32.
- Bolz, H. J. (2017). [Next-Generation Sequencing: A Quantum Leap in Ophthalmology Research and Diagnostics]. *Klin Monbl Augenheilkd*, 234(3), 280-288. doi:10.1055/s-0043-103962
- Bonnici, V., Russo, F., Bombieri, N., Pulvirenti, A., & Giugno, R. (2014). Comprehensive reconstruction and visualization of non-coding regulatory networks in human. *Front Bioeng Biotechnol*, 2, 69. doi:10.3389/fbioe.2014.00069
- Booij, J. C., Baas, D. C., Beisekeeva, J., Gorgels, T. G., & Bergen, A. A. (2010). The dynamic nature of Bruch's membrane. *Prog Retin Eye Res*, 29(1), 1-18. doi:10.1016/j.preteyeres.2009.08.003
- Bougel, S., Renaud, S., Braunschweig, R., Loukinov, D., Morse, H. C., 3rd, Bosman, F. T., . . . Benhattar, J. (2010). PAX5 activates the transcription of the human telomerase reverse transcriptase gene in B cells. *J Pathol*, 220(1), 87-96. doi:10.1002/path.2620
- Bourteele, S., Oesterle, K., Weinzierl, A. O., Paxian, S., Riemann, M., Schmid, R. M., & Planz, O. (2007). Alteration of NF-kappaB activity leads to mitochondrial apoptosis after infection with pathological prion protein. *Cell Microbiol*, 9(9), 2202-2217. doi:10.1111/j.1462-5822.2007.00950.x
- Brandstetter, C., Patt, J., Holz, F. G., & Krohne, T. U. (2016). Inflammasome priming increases retinal pigment epithelial cell susceptibility to lipofuscin phototoxicity by changing the cell death mechanism from apoptosis to pyroptosis. *J Photochem Photobiol B*, 161, 177-183. doi:10.1016/j.jphotobiol.2016.05.018
- Branham, K., & Yashar, B. M. (2013). Providing comprehensive genetic-based ophthalmic care. *Clin Genet*, 84(2), 183-189. doi:10.1111/cge.12192
- Brion, M., Sanchez-Salorio, M., Corton, M., de la Fuente, M., Pazos, B., Othman, M., . . . Spanish multi-centre group of, A. M. D. (2011). Genetic association study of age-related macular degeneration in the Spanish population. *Acta Ophthalmol*, 89(1), e12-22. doi:10.1111/j.1755-3768.2010.02040.x
- Brito-Garcia, N., Del Pino-Sedeno, T., Trujillo-Martin, M. M., Coco, R. M., Rodriguez de la Rúa, E., Del Cura-Gonzalez, I., & Serrano-Aguilar, P. (2017). Effectiveness and safety of nutritional supplements in the treatment of hereditary retinal dystrophies: a systematic review. *Eye (Lond)*, 31(2), 273-285. doi:10.1038/eye.2016.286
- Broadgate, S., Yu, J., Downes, S. M., & Halford, S. (2017). Unravelling the genetics of inherited retinal dystrophies: Past, present and future. *Prog Retin Eye Res*, 59, 53-96. doi:10.1016/j.preteyeres.2017.03.003

- Brown, N. G., VanderLinden, R., Watson, E. R., Qiao, R., Grace, C. R., Yamaguchi, M., . . . Schulman, B. A. (2015). RING E3 mechanism for ubiquitin ligation to a disordered substrate visualized for human anaphase-promoting complex. *Proc Natl Acad Sci U S A*, *112*(17), 5272-5279. doi:10.1073/pnas.1504161112
- Bruno, M., Nebbioso, M., Rigoni, E., Gagliardi, A., & Vingolo, E. M. (2015). Posterior capsule opacity in Retinitis Pigmentosa according to different biomaterials of intraocular lenses: Our clinical experience. *Clin Ter*, *166*(5), 191-193. doi:10.7417/CT.2015.1876
- Brunotto, M., & Zarate, A. M. (2012). [Predictive models for complex diseases]. *Rev Fac Cien Med Univ Nac Cordoba*, *69*(1), 33-41.
- Bu, Y., Gao, L., & Gelman, I. H. (2011). Role for transcription factor TFII-I in the suppression of SSeCKS/Gravin/Akap12 transcription by Src. *Int J Cancer*, *128*(8), 1836-1842. doi:10.1002/ijc.25524
- Burstedt, M., Jonsson, F., Kohn, L., Burstedt, M., Kivitalo, M., & Golovleva, I. (2013). Genotype-phenotype correlations in Bothnia dystrophy caused by RLBP1 gene sequence variations. *Acta Ophthalmol*, *91*(5), 437-444. doi:10.1111/j.1755-3768.2012.02431.x
- Byrne, L. C., Dalkara, D., Luna, G., Fisher, S. K., Clerin, E., Sahel, J. A., . . . Flannery, J. G. (2015). Viral-mediated RdCVF and RdCVFL expression protects cone and rod photoreceptors in retinal degeneration. *J Clin Invest*, *125*(1), 105-116. doi:10.1172/JCI65654
- Calamuneri, A., Donato, L., Scimone, C., Costa, A., D'Angelo, R., & Sidoti, A. (2017). On Machine Learning in Biomedicine. *Life Safety And Security*. doi:10.12882/2283-7604.2017.5.12
- Campochiaro, P. A., & Mir, T. A. (2017). The mechanism of cone cell death in Retinitis Pigmentosa. *Prog Retin Eye Res*. doi:10.1016/j.preteyeres.2017.08.004
- Cao, S., Chee, S. P., Yu, H. G., Sukavatcharin, S., Wu, L., Kijlstra, A., . . . Yang, P. (2016). Investigation of the association of Vogt-Koyanagi-Harada syndrome with IL23R-C1orf141 in Han Chinese Singaporean and ADO-ZNF365-EGR2 in Thai. *Br J Ophthalmol*, *100*(3), 436-442. doi:10.1136/bjophthalmol-2015-307366
- Carrigan, M., Duignan, E., Humphries, P., Palfi, A., Kenna, P. F., & Farrar, G. J. (2016). A novel homozygous truncating GNAT1 mutation implicated in retinal degeneration. *Br J Ophthalmol*, *100*(4), 495-500. doi:10.1136/bjophthalmol-2015-306939
- Carss, K. J., Arno, G., Erwood, M., Stephens, J., Sanchis-Juan, A., Hull, S., . . . Raymond, F. L. (2017). Comprehensive Rare Variant Analysis via Whole-Genome Sequencing to

- Determine the Molecular Pathology of Inherited Retinal Disease. *Am J Hum Genet*, 100(1), 75-90. doi:10.1016/j.ajhg.2016.12.003
- Casper, J., Zweig, A. S., Villarreal, C., Tyner, C., Speir, M. L., Rosenbloom, K. R., . . . Kent, W. J. (2018). The UCSC Genome Browser database: 2018 update. *Nucleic Acids Res*, 46(D1), D762-D769. doi:10.1093/nar/gkx1020
- Cehofski, L. J., Kruse, A., Bogsted, M., Magnusdottir, S. O., Stensballe, A., Honore, B., & Vorum, H. (2016). Retinal proteome changes following experimental branch retinal vein occlusion and intervention with ranibizumab. *Exp Eye Res*, 152, 49-56. doi:10.1016/j.exer.2016.09.002
- Cerutti, C., & Ridley, A. J. (2017). Endothelial cell-cell adhesion and signaling. *Exp Cell Res*, 358(1), 31-38. doi:10.1016/j.yexcr.2017.06.003
- Chakradhar, S. (2016). An eye to the future: Researchers debate best path for stem cell-derived therapies. *Nat Med*, 22(2), 116-119. doi:10.1038/nm0216-116
- Chalepakis, G., & Gruss, P. (1995). Identification of DNA recognition sequences for the Pax3 paired domain. *Gene*, 162(2), 267-270.
- Chang, T., & Wu, L. (2006). Methylglyoxal, oxidative stress, and hypertension. *Can J Physiol Pharmacol*, 84(12), 1229-1238. doi:10.1139/y06-077
- Chang, J., Cideciyan, A. V., Jacobson, S. G., Sumaroka, A., Schwartz, S. B., Swider, M., . . . Swaroop, A. (2016). Variegated yet non-random rod and cone photoreceptor disease patterns in RPGR-ORF15-associated retinal degeneration. *Hum Mol Genet*, 25(24), 5444-5459. doi:10.1093/hmg/ddw361
- Chaum, E., Yin, J., & Lang, J. C. (2011). Molecular responses transduced by serial oxidative stress in the retinal pigment epithelium: feedback control modeling of gene expression. *Neurochem Res*, 36(4), 574-582. doi:10.1007/s11064-010-0370-5
- Chebil, A., & El Matri, L. (2016). [Retinitis pigmentosa associated with coats-like fundus]. *J Fr Ophtalmol*, 39(2), 235-236. doi:10.1016/j.jfo.2015.09.007
- Chen, C. K., Zhang, K., Church-Kopish, J., Huang, W., Zhang, H., Chen, Y. J., . . . Baehr, W. (2001). Characterization of human GRK7 as a potential cone opsin kinase. *Mol Vis*, 7, 305-313.
- Chen, H., & Privalsky, M. L. (1995). Cooperative formation of high-order oligomers by retinoid X receptors: an unexpected mode of DNA recognition. *Proc Natl Acad Sci U S A*, 92(2), 422-426.
- Chen, J., Liu, F., Li, H., Archacki, S., Gao, M., Liu, Y., . . . Liu, M. (2015). pVHL interacts with Ceramide kinase like (CERKL) protein and ubiquitinates it for oxygen dependent

- proteasomal degradation. *Cell Signal*, 27(11), 2314-2323. doi:10.1016/j.cellsig.2015.08.011
- Chen, R., Yin, X. B., Peng, C. X., & Li, G. L. (2012). Effect of brain-derived neurotrophic factor on c-jun expression in the rd mouse retina. *Int J Ophthalmol*, 5(3), 266-271. doi:10.3980/j.issn.2222-3959.2012.03.03
- Chen, Y., Huang, L., Jiao, X., Riazuddin, S., Riazuddin, S. A., & Fielding Hetmancik, J. (2018). A novel LRAT mutation affecting splicing in a family with early onset retinitis pigmentosa. *Hum Genomics*, 12(1), 35. doi:10.1186/s40246-018-0165-3
- Chen, Y., Wang, W., Liu, F., Tang, L., Tang, R., & Li, W. (2015). 9-cis-retinoic acid improves sensitivity to platelet-derived growth factor-BB via RXRalpha and SHP-1 in diabetic retinopathy. *Biochem Biophys Res Commun*, 465(4), 810-816. doi:10.1016/j.bbrc.2015.08.093
- Cheng, D. L., Greenberg, P. B., & Borton, D. A. (2017). Advances in Retinal Prosthetic Research: A Systematic Review of Engineering and Clinical Characteristics of Current Prosthetic Initiatives. *Curr Eye Res*, 42(3), 334-347. doi:10.1080/02713683.2016.1270326
- Chichagova, V., Hallam, D., Collin, J., Buskin, A., Saretzki, G., Armstrong, L., . . . Steel, D. H. (2017). Human iPSC disease modelling reveals functional and structural defects in retinal pigment epithelial cells harbouring the m.3243A > G mitochondrial DNA mutation. *Sci Rep*, 7(1), 12320. doi:10.1038/s41598-017-12396-2
- Cho, K. I., Yi, H., Tserentsoodol, N., Searle, K., & Ferreira, P. A. (2010). Neuroprotection resulting from insufficiency of RANBP2 is associated with the modulation of protein and lipid homeostasis of functionally diverse but linked pathways in response to oxidative stress. *Dis Model Mech*, 3(9-10), 595-604. doi:10.1242/dmm.004648
- Choi, S. H., & McCollum, D. (2012). A role for metaphase spindle elongation forces in correction of merotelic kinetochore attachments. *Curr Biol*, 22(3), 225-230. doi:10.1016/j.cub.2011.12.022
- Choi, W. I., Jeon, B. N., Yun, C. O., Kim, P. H., Kim, S. E., Choi, K. Y., . . . Hur, M. W. (2009). Proto-oncogene FBI-1 represses transcription of p21CIP1 by inhibition of transcription activation by p53 and Sp1. *J Biol Chem*, 284(19), 12633-12644. doi:10.1074/jbc.M809794200
- Cideciyan, A. V., Aleman, T. S., Swider, M., Schwartz, S. B., Steinberg, J. D., Brucker, A. J., . . . Jacobson, S. G. (2004). Mutations in ABCA4 result in accumulation of lipofuscin before slowing of the retinoid cycle: a reappraisal of the human disease sequence. *Hum Mol Genet*, 13(5), 525-534. doi:10.1093/hmg/ddh048

- Clack, J. W., Juhl, M., Rice, C. A., Li, J., & Witzmann, F. A. (2003). Proteomic analysis of transducin beta-subunit structural heterogeneity. *Electrophoresis*, 24(19-20), 3493-3499. doi:10.1002/elps.200305520
- CLC Genomics Workbench 9.5.3. (2016). Retrieved from <https://www.qiagenbioinformatics.com>
- Cromm, P. M., Spiegel, J., Grossmann, T. N., & Waldmann, H. (2015). Direct Modulation of Small GTPase Activity and Function. *Angew Chem Int Ed Engl*, 54(46), 13516-13537. doi:10.1002/anie.201504357
- Cubilla, M. A., Bermudez, V., Marquioni Ramella, M. D., Bachor, T. P., & Suburo, A. M. (2013). Mifepristone, a blocker of glucocorticoid receptors, promotes photoreceptor death. *Invest Ophthalmol Vis Sci*, 54(1), 313-322. doi:10.1167/iovs.12-10014
- Cunnea, P. M., Miranda-Vizueté, A., Bertoli, G., Simmen, T., Damdimopoulos, A. E., Hermann, S., . . . Spyrou, G. (2003). ERdj5, an endoplasmic reticulum (ER)-resident protein containing DnaJ and thioredoxin domains, is expressed in secretory cells or following ER stress. *J Biol Chem*, 278(2), 1059-1066. doi:10.1074/jbc.M206995200
- Cunningham, J. J., Levine, E. M., Zindy, F., Goloubeva, O., Roussel, M. F., & Smeyne, R. J. (2002). The cyclin-dependent kinase inhibitors p19(Ink4d) and p27(Kip1) are coexpressed in select retinal cells and act cooperatively to control cell cycle exit. *Mol Cell Neurosci*, 19(3), 359-374. doi:10.1006/mcne.2001.1090
- Cvekl, A., & Wang, W. L. (2009). Retinoic acid signaling in mammalian eye development. *Exp Eye Res*, 89(3), 280-291. doi:10.1016/j.exer.2009.04.012
- D'Angelo, R., Donato, L., Venza, I., Scimone, C., Aragona, P., & Sidoti, A. (2017). Possible protective role of the ABCA4 gene c.1268A>G missense variant in Stargardt disease and syndromic retinitis pigmentosa in a Sicilian family: Preliminary data. *Int J Mol Med*, 39(4), 1011-1020. doi:10.3892/ijmm.2017.2917
- D'Orazi, F. D., Suzuki, S. C., & Wong, R. O. (2014). Neuronal remodeling in retinal circuit assembly, disassembly, and reassembly. *Trends Neurosci*, 37(10), 594-603. doi:10.1016/j.tins.2014.07.009
- Dale, J. M., Popescu, L., & Karp, P. D. (2010). Machine learning methods for metabolic pathway prediction. *BMC Bioinformatics*, 11, 15. doi:10.1186/1471-2105-11-15
- Dalkara, D., Kolstad, K. D., Guerin, K. I., Hoffmann, N. V., Visel, M., Klimczak, R. R., . . . Flannery, J. G. (2011). AAV mediated GDNF secretion from retinal glia slows down retinal degeneration in a rat model of retinitis pigmentosa. *Mol Ther*, 19(9), 1602-1608. doi:10.1038/mt.2011.62

- Dalvin, L. A., Abou Chehade, J. E., Chiang, J., Fuchs, J., Iezzi, R., & Marmorstein, A. D. (2016). Retinitis pigmentosa associated with a mutation in BEST1. *Am J Ophthalmol Case Rep*, 2, 11-17. doi:10.1016/j.ajoc.2016.03.005
- DangLi, R., HeKong, W., JiQin, L., MingHua, Z., & WenCheng, Z. (2012). ROS-induced ZNF580 expression: a key role for H2O2/NF-kappaB signaling pathway in vascular endothelial inflammation. *Mol Cell Biochem*, 359(1-2), 183-191. doi:10.1007/s11010-011-1013-0
- Darzacq, X., Jady, B. E., Verheggen, C., Kiss, A. M., Bertrand, E., & Kiss, T. (2002). Cajal body-specific small nuclear RNAs: a novel class of 2'-O-methylation and pseudouridylation guide RNAs. *EMBO J*, 21(11), 2746-2756. doi:10.1093/emboj/21.11.2746
- de Hoz, R., Rojas, B., Ramirez, A. I., Salazar, J. J., Gallego, B. I., Trivino, A., & Ramirez, J. M. (2016). Retinal Macroglial Responses in Health and Disease. *Biomed Res Int*, 2016, 2954721. doi:10.1155/2016/2954721
- Delori, F. C., Dorey, C. K., Staurenghi, G., Arend, O., Goger, D. G., & Weiter, J. J. (1995). In vivo fluorescence of the ocular fundus exhibits retinal pigment epithelium lipofuscin characteristics. *Invest Ophthalmol Vis Sci*, 36(3), 718-729.
- Demirci, F. Y., Rigatti, B. W., Mah, T. S., & Gorin, M. B. (2006). A novel RPGR exon ORF15 mutation in a family with X-linked retinitis pigmentosa and Coats'-like exudative vasculopathy. *Am J Ophthalmol*, 141(1), 208-210. doi:10.1016/j.ajo.2005.07.077
- den Hollander, A. I., Heckenlively, J. R., van den Born, L. I., de Kok, Y. J., van der Velde-Visser, S. D., Kellner, U., . . . Cremers, F. P. (2001). Leber congenital amaurosis and retinitis pigmentosa with Coats-like exudative vasculopathy are associated with mutations in the crumbs homologue 1 (CRB1) gene. *Am J Hum Genet*, 69(1), 198-203.
- Denecker, G., Vandamme, N., Akay, O., Koludrovic, D., Taminau, J., Lemeire, K., . . . Berx, G. (2014). Identification of a ZEB2-MITF-ZEB1 transcriptional network that controls melanogenesis and melanoma progression. *Cell Death Differ*, 21(8), 1250-1261. doi:10.1038/cdd.2014.44
- Desmet, F. O., Hamroun, D., Lalande, M., Collod-Beroud, G., Claustres, M., & Beroud, C. (2009). Human Splicing Finder: an online bioinformatics tool to predict splicing signals. *Nucleic Acids Res*, 37(9), e67. doi:10.1093/nar/gkp215
- Dessalces, E., Bocquet, B., Bourien, J., Zanlonghi, X., Verdet, R., Meunier, I., & Hamel, C. P. (2013). Early-onset foveal involvement in retinitis punctata albescens with

- mutations in RLBPI. *JAMA Ophthalmol*, 131(10), 1314-1323. doi:10.1001/jamaophthalmol.2013.4476
- Dharmat, R., Eblimit, A., Robichaux, M. A., Zhang, Z., Nguyen, T. T., Jung, S. Y., . . . Chen, R. (2018). SPATA7 maintains a novel photoreceptor-specific zone in the distal connecting cilium. *J Cell Biol*, 217(8), 2851-2865. doi:10.1083/jcb.201712117
- Di Gioia, S. A., Farinelli, P., Letteboer, S. J., Arsenijevic, Y., Sharon, D., Roepman, R., & Rivolta, C. (2015). Interactome analysis reveals that FAM161A, deficient in recessive retinitis pigmentosa, is a component of the Golgi-centrosomal network. *Hum Mol Genet*, 24(12), 3359-3371. doi:10.1093/hmg/ddv085
- Di, Y., Huang, L., Sundaresan, P., Li, S., Kim, R., Ballav Saikia, B., . . . Yang, Z. (2016). Whole-exome Sequencing Analysis Identifies Mutations in the EYS Gene in Retinitis Pigmentosa in the Indian Population. *Sci Rep*, 6, 19432. doi:10.1038/srep19432
- Dick, A. D. (2017). Doyne lecture 2016: intraocular health and the many faces of inflammation. *Eye (Lond)*, 31(1), 87-96. doi:10.1038/eye.2016.177
- Ding, J. D., Salinas, R. Y., & Arshavsky, V. Y. (2015). Discs of mammalian rod photoreceptors form through the membrane evagination mechanism. *J Cell Biol*, 211(3), 495-502. doi:10.1083/jcb.201508093
- Dobin, A., Davis, C. A., Schlesinger, F., Drenkow, J., Zaleski, C., Jha, S., . . . Gingeras, T. R. (2013). STAR: ultrafast universal RNA-seq aligner. *Bioinformatics*, 29(1), 15-21. doi:10.1093/bioinformatics/bts635
- Donato, L. (2017). Novel intronic variants in unconventional gene cluster could lead to Retinitis pigmentosa phenotype. *EMBJ*. doi:10.3269/1970-5492.2017.12.7
- Donato, L., Bramanti, P., Scimone, C., Rinaldi, C., D'Angelo, R., & Sidoti, A. (2018). miRNA expression profile of retinal pigment epithelial cells under oxidative stress conditions. *FEBS Open Bio*, 8(2), 219-233. doi:10.1002/2211-5463.12360
- Donato, L., & Denaro, L. (2018). Bioinformatic analysis of a “functional cluster” probably related to retinitis pigmentosa. *The Open Bioinformatic Journal*. doi:10.2174/1875036201811010089
- Donato, L., Scimone, C., Alibrandi, S., D'Angelo, R., & A, A. S. (2017). The new era of non-coding RNAs: the state of art and future perspectives in advanced molecular therapies. *Life Safety And Security*. doi:10.12882/2283-7604.2017.5.10.
- Donato, L., Scimone, C., D'Angelo, R., & Sidoti, A. (2017). Predictive and personalized approaches towards retinitis pigmentosa and cerebral cavernous malformations. *Life Safety And Security*. doi:10.12882/2283-7604.2017.5.2

- Donato, L., Scimone, C., Nicocia, G., Denaro, L., Robledo, R., Sidoti, A., & D'Angelo, R. (2018). GLO1 gene polymorphisms and their association with retinitis pigmentosa: a case-control study in a Sicilian population. *Mol Biol Rep*. doi:10.1007/s11033-018-4295-4
- Donato, L., Scimone, C., Rinaldi, C., Aragona, P., Briuglia, S., D'Ascola, A., . . . Sidoti, A. (2018). Stargardt Phenotype Associated With Two ELOVL4 Promoter Variants and ELOVL4 Downregulation: New Possible Perspective to Etiopathogenesis? *Invest Ophthalmol Vis Sci*, *59*(2), 843-857. doi:10.1167/iovs.17-22962
- Donovan, K., Alekseev, O., Qi, X., Cho, W., & Azizkhan-Clifford, J. (2014). O-GlcNAc modification of transcription factor Sp1 mediates hyperglycemia-induced VEGF-A upregulation in retinal cells. *Invest Ophthalmol Vis Sci*, *55*(12), 7862-7873. doi:10.1167/iovs.14-14048
- Dudekula, D. B., Panda, A. C., Grammatikakis, I., De, S., Abdelmohsen, K., & Gorospe, M. (2016). CircInteractome: A web tool for exploring circular RNAs and their interacting proteins and microRNAs. *RNA Biol*, *13*(1), 34-42. doi:10.1080/15476286.2015.1128065
- Duncker, T., Tabacaru, M. R., Lee, W., Tsang, S. H., Sparrow, J. R., & Greenstein, V. C. (2013). Comparison of near-infrared and short-wavelength autofluorescence in retinitis pigmentosa. *Invest Ophthalmol Vis Sci*, *54*(1), 585-591. doi:10.1167/iovs.12-11176
- Durlu, Y. K., Koroglu, C., & Tolun, A. (2014). Novel recessive cone-rod dystrophy caused by POC1B mutation. *JAMA Ophthalmol*, *132*(10), 1185-1191. doi:10.1001/jamaophthalmol.2014.1658
- Dutta, N., & Seo, S. (2016). RPGR, a prenylated retinal ciliopathy protein, is targeted to cilia in a prenylation- and PDE6D-dependent manner. *Biol Open*, *5*(9), 1283-1289. doi:10.1242/bio.020461
- Dysli, C., Schurch, K., Pascal, E., Wolf, S., & Zinkernagel, M. S. (2018). Fundus Autofluorescence Lifetime Patterns in Retinitis Pigmentosa. *Invest Ophthalmol Vis Sci*, *59*(5), 1769-1778. doi:10.1167/iovs.17-23336
- Edwards, J. A., Sethi, P. K., Scoma, A. J., Bannerman, R. M., & Frohman, L. A. (1976). A new familial syndrome characterized by pigmentary retinopathy, hypogonadism, mental retardation, nerve deafness and glucose intolerance. *Am J Med*, *60*(1), 23-32.
- Eichers, E. R., Green, J. S., Stockton, D. W., Jackman, C. S., Whelan, J., McNamara, J. A., . . . Katsanis, N. (2002). Newfoundland rod-cone dystrophy, an early-onset retinal

- dystrophy, is caused by splice-junction mutations in RLBP1. *Am J Hum Genet*, 70(4), 955-964. doi:10.1086/339688
- Eid, C., Hemadi, M., Ha-Duong, N. T., & El Hage Chahine, J. M. (2014). Iron uptake and transfer from ceruloplasmin to transferrin. *Biochim Biophys Acta*, 1840(6), 1771-1781. doi:10.1016/j.bbagen.2014.01.011
- El Shamieh, S., Boulanger-Scemama, E., Lancelot, M. E., Antonio, A., Demontant, V., Condroyer, C., . . . Zeitz, C. (2015). Targeted next generation sequencing identifies novel mutations in RP1 as a relatively common cause of autosomal recessive rod-cone dystrophy. *Biomed Res Int*, 2015, 485624. doi:10.1155/2015/485624
- Escher, P., Tran, H. V., Vaclavik, V., Borruat, F. X., Schorderet, D. F., & Munier, F. L. (2012). Double concentric autofluorescence ring in NR2E3-p.G56R-linked autosomal dominant retinitis pigmentosa. *Invest Ophthalmol Vis Sci*, 53(8), 4754-4764. doi:10.1167/iovs.11-8693
- Esposito, G., Testa, F., Zacchia, M., Crispo, A. A., Di Iorio, V., Capolongo, G., . . . Salvatore, F. (2017). Genetic characterization of Italian patients with Bardet-Biedl syndrome and correlation to ocular, renal and audio-vestibular phenotype: identification of eleven novel pathogenic sequence variants. *BMC Med Genet*, 18(1), 10. doi:10.1186/s12881-017-0372-0
- Estrada-Cuzcano, A., Roepman, R., Cremers, F. P., den Hollander, A. I., & Mans, D. A. (2012). Non-syndromic retinal ciliopathies: translating gene discovery into therapy. *Hum Mol Genet*, 21(R1), R111-124. doi:10.1093/hmg/dds298
- Fabregat, A., Sidiropoulos, K., Garapati, P., Gillespie, M., Hausmann, K., Haw, R., . . . D'Eustachio, P. (2016). The Reactome pathway Knowledgebase. *Nucleic Acids Res*, 44(D1), D481-487. doi:10.1093/nar/gkv1351
- Faktorovich, E. G., Steinberg, R. H., Yasumura, D., Matthes, M. T., & LaVail, M. M. (1990). Photoreceptor degeneration in inherited retinal dystrophy delayed by basic fibroblast growth factor. *Nature*, 347(6288), 83-86. doi:10.1038/347083a0
- Falsini, B., Galli-Resta, L., Fadda, A., Ziccardi, L., Piccardi, M., Iarossi, G., & Resta, G. (2012). Long-term decline of central cone function in retinitis pigmentosa evaluated by focal electroretinogram. *Invest Ophthalmol Vis Sci*, 53(12), 7701-7709. doi:10.1167/iovs.12-11017
- Fan, J., Alsarraf, O., Dahrouj, M., Platt, K. A., Chou, C. J., Rice, D. S., & Crosson, C. E. (2013). Inhibition of HDAC2 protects the retina from ischemic injury. *Invest Ophthalmol Vis Sci*, 54(6), 4072-4080. doi:10.1167/iovs.12-11529

- Fang, J., Shaw, P. X., Wang, Y., & Goldberg, J. L. (2016). Kruppel-Like Factor 4 (KLF4) Is Not Required for Retinal Cell Differentiation. *eNeuro*, 3(1). doi:10.1523/ENEURO.0117-15.2016
- Fang, M., Adams, J. S., McMahan, B. L., Brown, R. J., & Oxford, J. T. (2010). The expression patterns of minor fibrillar collagens during development in zebrafish. *Gene Expr Patterns*, 10(7-8), 315-322. doi:10.1016/j.gep.2010.07.002
- Fanjul-Moles, M. L., & Lopez-Riquelme, G. O. (2016). Relationship between Oxidative Stress, Circadian Rhythms, and AMD. *Oxid Med Cell Longev*, 2016, 7420637. doi:10.1155/2016/7420637
- Faraci, C., Galmozzi, A., Sesini, E., Ianniello, A., Milesi, S., & Saija, A. (1984). [Lawrence Moon Biedl Bardet, a polymorphic syndrome]. *Pediatr Med Chir*, 6(4), 529-534.
- Farkas, M. H., Lew, D. S., Sousa, M. E., Bujakowska, K., Chatagnon, J., Bhattacharya, S. S., . . . Nandrot, E. F. (2014). Mutations in pre-mRNA processing factors 3, 8, and 31 cause dysfunction of the retinal pigment epithelium. *Am J Pathol*, 184(10), 2641-2652. doi:10.1016/j.ajpath.2014.06.026
- Farrar, G. J., Carrigan, M., Dockery, A., Millington-Ward, S., Palfi, A., Chadderton, N., . . . Humphries, P. (2017). Toward an elucidation of the molecular genetics of inherited retinal degenerations. *Hum Mol Genet*, 26(R1), R2-R11. doi:10.1093/hmg/ddx185
- Farre, D., Roset, R., Huerta, M., Adsuara, J. E., Rosello, L., Alba, M. M., & Messeguer, X. (2003). Identification of patterns in biological sequences at the ALGGEN server: PROMO and MALGEN. *Nucleic Acids Res*, 31(13), 3651-3653.
- Fathinajafabadi, A., Perez-Jimenez, E., Riera, M., Knecht, E., & Gonzalez-Duarte, R. (2014). CERKL, a retinal disease gene, encodes an mRNA-binding protein that localizes in compact and untranslated mRNPs associated with microtubules. *PLoS One*, 9(2), e87898. doi:10.1371/journal.pone.0087898
- Finn, R. D., Attwood, T. K., Babbitt, P. C., Bateman, A., Bork, P., Bridge, A. J., . . . Mitchell, A. L. (2017). InterPro in 2017-beyond protein family and domain annotations. *Nucleic Acids Res*, 45(D1), D190-D199. doi:10.1093/nar/gkw1107
- Fischer, A. J., & Reh, T. A. (2001). Muller glia are a potential source of neural regeneration in the postnatal chicken retina. *Nat Neurosci*, 4(3), 247-252. doi:10.1038/85090
- Flynn, O. J., Cukras, C. A., & Jeffrey, B. G. (2018). Characterization of Rod Function Phenotypes Across a Range of Age-Related Macular Degeneration Severities and Subretinal Drusenoid Deposits. *Invest Ophthalmol Vis Sci*, 59(6), 2411-2421. doi:10.1167/iovs.17-22874

- Fogerty, J., & Besharse, J. C. (2011). 174delG mutation in mouse MFRP causes photoreceptor degeneration and RPE atrophy. *Invest Ophthalmol Vis Sci*, *52*(10), 7256-7266. doi:10.1167/iovs.11-8112
- Foijer, F., Albacker, L. A., Bakker, B., Spierings, D. C., Yue, Y., Xie, S. Z., . . . Sorger, P. K. (2017). Deletion of the MAD2L1 spindle assembly checkpoint gene is tolerated in mouse models of acute T-cell lymphoma and hepatocellular carcinoma. *Elife*, *6*. doi:10.7554/eLife.20873
- Fok, E. T., Scholefield, J., Fanucchi, S., & Mhlanga, M. M. (2017). The emerging molecular biology toolbox for the study of long noncoding RNA biology. *Epigenomics*, *9*(10), 1317-1327. doi:10.2217/epi-2017-0062
- Forrest, D., & Swaroop, A. (2012). Minireview: the role of nuclear receptors in photoreceptor differentiation and disease. *Mol Endocrinol*, *26*(6), 905-915. doi:10.1210/me.2012-1010
- Forsythe, E., Kenny, J., Bacchelli, C., & Beales, P. L. (2018). Managing Bardet-Biedl Syndrome-Now and in the Future. *Front Pediatr*, *6*, 23. doi:10.3389/fped.2018.00023
- Fox, P. L. (2015). Discovery and investigation of the GAIT translational control system. *RNA*, *21*(4), 615-618. doi:10.1261/rna.050187.115
- Frade, J. M., & Ovejero-Benito, M. C. (2015). Neuronal cell cycle: the neuron itself and its circumstances. *Cell Cycle*, *14*(5), 712-720. doi:10.1080/15384101.2015.1004937
- Franke, M., Rauschenberger, L., & Fluri, F. (2018). Challenges of diagnosing and treating Charles Bonnet syndrome. *Neurol Clin Pract*, *8*(4), 359-361. doi:10.1212/CPJ.0000000000000484
- Fraser, D. D., Frank, J. A., & Dalakas, M. C. (1991). Inflammatory myopathies: MR imaging and spectroscopy. *Radiology*, *179*(2), 341-342; discussion 343-344. doi:10.1148/radiology.179.2.2064655
- Frey, A. G., Nandal, A., Park, J. H., Smith, P. M., Yabe, T., Ryu, M. S., . . . Philpott, C. C. (2014). Iron chaperones PCBP1 and PCBP2 mediate the metallation of the dinuclear iron enzyme deoxyhypusine hydroxylase. *Proc Natl Acad Sci U S A*, *111*(22), 8031-8036. doi:10.1073/pnas.1402732111
- Fu, J., Ma, L., Cheng, J., Yang, L., Wei, C., Fu, S., . . . Fu, J. (2018). A novel, homozygous nonsense variant of the CDHR1 gene in a Chinese family causes autosomal recessive retinal dystrophy by NGS-based genetic diagnosis. *J Cell Mol Med*. doi:10.1111/jcmm.13841

- Fujimura, N., Klimova, L., Antosova, B., Smolikova, J., Machon, O., & Kozmik, Z. (2015). Genetic interaction between Pax6 and beta-catenin in the developing retinal pigment epithelium. *Dev Genes Evol*, 225(2), 121-128. doi:10.1007/s00427-015-0493-4
- Fujiwara, K., Ikeda, Y., Murakami, Y., Nakatake, S., Tachibana, T., Yoshida, N., . . . Ishibashi, T. (2016). Association Between Aqueous Flare and Epiretinal Membrane in Retinitis Pigmentosa. *Invest Ophthalmol Vis Sci*, 57(10), 4282-4286. doi:10.1167/iovs.16-19686
- Furukawa, A., & Koriyama, Y. (2016). A role of Heat Shock Protein 70 in Photoreceptor Cell Death: Potential as a Novel Therapeutic Target in Retinal Degeneration. *CNS Neurosci Ther*, 22(1), 7-14. doi:10.1111/cns.12471
- Gahlot, D. K., Khosla, P. K., Makashir, P. D., Vasuki, K., & Basu, N. (1976). Copper metabolism in retinitis pigmentosa. *Br J Ophthalmol*, 60(11), 770-774.
- Galli-Resta, L., Piccardi, M., Ziccardi, L., Fadda, A., Minnella, A., Marangoni, D., . . . Falsini, B. (2013). Early detection of central visual function decline in cone-rod dystrophy by the use of macular focal cone electroretinogram. *Invest Ophthalmol Vis Sci*, 54(10), 6560-6569. doi:10.1167/iovs.13-12676
- Galvani, A., Courbeyrette, R., Agez, M., Ochsenbein, F., Mann, C., & Thuret, J. Y. (2008). In vivo study of the nucleosome assembly functions of ASF1 histone chaperones in human cells. *Mol Cell Biol*, 28(11), 3672-3685. doi:10.1128/MCB.00510-07
- Gandra, M., Anandula, V., Authiappan, V., Sundaramurthy, S., Raman, R., Bhattacharya, S., & Govindasamy, K. (2008). Retinitis pigmentosa: mutation analysis of RHO, PRPF31, RP1, and IMPDH1 genes in patients from India. *Mol Vis*, 14, 1105-1113.
- Gao, M., Zhang, S., Liu, C., Qin, Y., Archacki, S., Jin, L., . . . Liu, M. (2016). Whole exome sequencing identifies a novel NRL mutation in a Chinese family with autosomal dominant retinitis pigmentosa. *Mol Vis*, 22, 234-242.
- Gao, S., & Jakobs, T. C. (2016). Mice Homozygous for a Deletion in the Glaucoma Susceptibility Locus INK4 Show Increased Vulnerability of Retinal Ganglion Cells to Elevated Intraocular Pressure. *Am J Pathol*, 186(4), 985-1005. doi:10.1016/j.ajpath.2015.11.026
- Gao, Y., Wang, J., & Zhao, F. (2015). CIRI: an efficient and unbiased algorithm for de novo circular RNA identification. *Genome Biol*, 16, 4. doi:10.1186/s13059-014-0571-3
- Garanto, A., & Collin, R. W. J. (2018). Design and In Vitro Use of Antisense Oligonucleotides to Correct Pre-mRNA Splicing Defects in Inherited Retinal Dystrophies. *Methods Mol Biol*, 1715, 61-78. doi:10.1007/978-1-4939-7522-8_5

- Garcia-Cazorla, A., Mochel, F., Lamari, F., & Saudubray, J. M. (2015). The clinical spectrum of inherited diseases involved in the synthesis and remodeling of complex lipids. A tentative overview. *J Inherit Metab Dis*, *38*(1), 19-40. doi:10.1007/s10545-014-9776-6
- Garcia-Gonzalo, F. R., Corbit, K. C., Sirerol-Piquer, M. S., Ramaswami, G., Otto, E. A., Noriega, T. R., . . . Reiter, J. F. (2011). A transition zone complex regulates mammalian ciliogenesis and ciliary membrane composition. *Nat Genet*, *43*(8), 776-784. doi:10.1038/ng.891
- Gaub, B. M., Berry, M. H., Holt, A. E., Reiner, A., Kienzler, M. A., Dolgova, N., . . . Isacoff, E. Y. (2014). Restoration of visual function by expression of a light-gated mammalian ion channel in retinal ganglion cells or ON-bipolar cells. *Proc Natl Acad Sci U S A*, *111*(51), E5574-5583. doi:10.1073/pnas.1414162111
- Gene Ontology, C. (2015). Gene Ontology Consortium: going forward. *Nucleic Acids Res*, *43*(Database issue), D1049-1056. doi:10.1093/nar/gku1179
- Ghazi, N. G., Abboud, E. B., Nowilaty, S. R., Alkuraya, H., Alhommadi, A., Cai, H., . . . Alkuraya, F. S. (2016). Treatment of retinitis pigmentosa due to MERTK mutations by ocular subretinal injection of adeno-associated virus gene vector: results of a phase I trial. *Hum Genet*, *135*(3), 327-343. doi:10.1007/s00439-016-1637-y
- Giblin, J. P., Comes, N., Strauss, O., & Gasull, X. (2016). Ion Channels in the Eye: Involvement in Ocular Pathologies. *Adv Protein Chem Struct Biol*, *104*, 157-231. doi:10.1016/bs.apcsb.2015.11.006
- Godino, L., Turchetti, D., Jackson, L., Hennessy, C., & Skirton, H. (2016). Impact of presymptomatic genetic testing on young adults: a systematic review. *Eur J Hum Genet*, *24*(4), 496-503. doi:10.1038/ejhg.2015.153
- Goldberg, A. F., Moritz, O. L., & Williams, D. S. (2016). Molecular basis for photoreceptor outer segment architecture. *Prog Retin Eye Res*, *55*, 52-81. doi:10.1016/j.preteyeres.2016.05.003
- Goldberg, N. R., Greenberg, J. P., Laud, K., Tsang, S., & Freund, K. B. (2013). Outer retinal tubulation in degenerative retinal disorders. *Retina*, *33*(9), 1871-1876. doi:10.1097/IAE.0b013e318296b12f
- Goldenberg-Cohen, N., Banin, E., Zalzstein, Y., Cohen, B., Rotenstreich, Y., Rizel, L., . . . Ben-Yosef, T. (2013). Genetic heterogeneity and consanguinity lead to a "double hit": homozygous mutations of MYO7A and PDE6B in a patient with retinitis pigmentosa. *Mol Vis*, *19*, 1565-1571.

- Goldstein, D. B., Reich, D. E., Bradman, N., Usher, S., Seligsohn, U., & Peretz, H. (1999). Age estimates of two common mutations causing factor XI deficiency: recent genetic drift is not necessary for elevated disease incidence among Ashkenazi Jews. *Am J Hum Genet*, *64*(4), 1071-1075.
- Golestaneh, N., Chu, Y., Cheng, S. K., Cao, H., Poliakov, E., & Berinstein, D. M. (2016). Repressed SIRT1/PGC-1alpha pathway and mitochondrial disintegration in iPSC-derived RPE disease model of age-related macular degeneration. *J Transl Med*, *14*(1), 344. doi:10.1186/s12967-016-1101-8
- Goncalves, J., & Pelletier, L. (2017). The Ciliary Transition Zone: Finding the Pieces and Assembling the Gate. *Mol Cells*, *40*(4), 243-253. doi:10.14348/molcells.2017.0054
- Gong, J. Y., Deng, D. T., & Sun, Y. H. (2015). Association of platelet glycoprotein receptor alpha2beta1 integrin and glycoprotein IIIa gene polymorphisms with diabetic retinopathy: evidence from 3007 subjects. *Curr Eye Res*, *40*(5), 476-483. doi:10.3109/02713683.2014.932386
- Gong, Y., Fu, Z., Liegl, R., Chen, J., Hellstrom, A., & Smith, L. E. (2017). omega-3 and omega-6 long-chain PUFAs and their enzymatic metabolites in neovascular eye diseases. *Am J Clin Nutr*, *106*(1), 16-26. doi:10.3945/ajcn.117.153825
- Goo, Y. S., Ahn, K. N., Song, Y. J., Ryu, S. B., & Kim, K. H. (2011). Comparison of basal oscillatory rhythm of retinal activities in rd1 and rd10 mice. *Conf Proc IEEE Eng Med Biol Soc*, *2011*, 1093-1096. doi:10.1109/IEMBS.2011.6090255
- Gordiyenko, N. V., Fariss, R. N., Zhi, C., & MacDonald, I. M. (2010). Silencing of the CHM gene alters phagocytic and secretory pathways in the retinal pigment epithelium. *Invest Ophthalmol Vis Sci*, *51*(2), 1143-1150. doi:10.1167/iovs.09-4117
- Gorovoy, I. R., Gallagher, D. S., Eller, A. W., Mayercik, V. A., Friberg, T. R., & Schuman, J. S. (2013). Cystoid macular edema in retinitis pigmentosa patients without associated macular thickening. *Semin Ophthalmol*, *28*(2), 79-83. doi:10.3109/08820538.2012.760614
- Gorusupudi, A., Liu, A., Hageman, G. S., & Bernstein, P. S. (2016). Associations of human retinal very long-chain polyunsaturated fatty acids with dietary lipid biomarkers. *J Lipid Res*, *57*(3), 499-508. doi:10.1194/jlr.P065540
- Grave, N., Tovo-Rodrigues, L., da Silveira, J., Rovaris, D. L., Dal Bosco, S. M., Contini, V., & Genro, J. P. (2016). A vitamin D pathway gene-gene interaction affects low-density lipoprotein cholesterol levels. *J Nutr Biochem*, *38*, 12-17. doi:10.1016/j.jnutbio.2016.08.002

- Griciuc, A., Aron, L., Roux, M. J., Klein, R., Giangrande, A., & Ueffing, M. (2010). Inactivation of VCP/ter94 suppresses retinal pathology caused by misfolded rhodopsin in *Drosophila*. *PLoS Genet*, *6*(8). doi:10.1371/journal.pgen.1001075
- Grueneberg, D. A., Henry, R. W., Brauer, A., Novina, C. D., Cheriya, V., Roy, A. L., & Gilman, M. (1997). A multifunctional DNA-binding protein that promotes the formation of serum response factor/homeodomain complexes: identity to TFII-I. *Genes Dev*, *11*(19), 2482-2493.
- Grunwald, J. E., Maguire, A. M., & Dupont, J. (1996). Retinal hemodynamics in retinitis pigmentosa. *Am J Ophthalmol*, *122*(4), 502-508.
- Gu, D., Beltran, W. A., Li, Z., Acland, G. M., & Aguirre, G. D. (2007). Clinical light exposure, photoreceptor degeneration, and AP-1 activation: a cell death or cell survival signal in the rhodopsin mutant retina? *Invest Ophthalmol Vis Sci*, *48*(11), 4907-4918. doi:10.1167/iovs.07-0428
- Guo, J., Kong, L. M., Peng, A. F., Long, X. H., Zhou, Y., & Shu, Y. (2016). Transcription factor NFYA promotes a malignant phenotype by upregulating fatty acid synthase expression. *Mol Med Rep*, *14*(6), 5007-5014. doi:10.3892/mmr.2016.5897
- Habibi, I., Chebil, A., Falfoul, Y., Allaman-Pillet, N., Kort, F., Schorderet, D. F., & El Matri, L. (2016). Identifying mutations in Tunisian families with retinal dystrophy. *Sci Rep*, *6*, 37455. doi:10.1038/srep37455
- Habibi, I., Chebil, A., Kort, F., Schorderet, D. F., & El Matri, L. (2017). Exome sequencing confirms ZNF408 mutations as a cause of familial retinitis pigmentosa. *Ophthalmic Genet*, *38*(5), 494-497. doi:10.1080/13816810.2016.1275020
- Hadziiahmetovic, M., Dentchev, T., Song, Y., Haddad, N., He, X., Hahn, P., . . . Dunaief, J. L. (2008). Ceruloplasmin/hephaestin knockout mice model morphologic and molecular features of AMD. *Invest Ophthalmol Vis Sci*, *49*(6), 2728-2736. doi:10.1167/iovs.07-1472
- Haer-Wigman, L., van Zelst-Stams, W. A., Pfundt, R., van den Born, L. I., Klaver, C. C., Verheij, J. B., . . . Yntema, H. G. (2017). Diagnostic exome sequencing in 266 Dutch patients with visual impairment. *Eur J Hum Genet*, *25*(5), 591-599. doi:10.1038/ejhg.2017.9
- Haeseleer, F., Sokal, I., Li, N., Pettenati, M., Rao, N., Bronson, D., . . . Palczewski, K. (1999). Molecular characterization of a third member of the guanylyl cyclase-activating protein subfamily. *J Biol Chem*, *274*(10), 6526-6535.
- Hageman, G. S., Marmor, M. F., Yao, X. Y., & Johnson, L. V. (1995). The interphotoreceptor matrix mediates primate retinal adhesion. *Arch Ophthalmol*, *113*(5), 655-660.

- Hanein, S., Perrault, I., Gerber, S., Tanguy, G., Rozet, J. M., & Kaplan, J. (2006). Leber congenital amaurosis: survey of the genetic heterogeneity, refinement of the clinical definition and phenotype-genotype correlations as a strategy for molecular diagnosis. Clinical and molecular survey in LCA. *Adv Exp Med Biol*, 572, 15-20. doi:10.1007/0-387-32442-9_3
- Hariri, A. H., Zhang, H. Y., Ho, A., Francis, P., Weleber, R. G., Birch, D. G., . . . Trial of Oral Valproic Acid for Retinitis Pigmentosa, G. (2016). Quantification of Ellipsoid Zone Changes in Retinitis Pigmentosa Using en Face Spectral Domain-Optical Coherence Tomography. *JAMA Ophthalmol*, 134(6), 628-635. doi:10.1001/jamaophthalmol.2016.0502
- Harkewicz, R., Du, H., Tong, Z., Alkuraya, H., Bedell, M., Sun, W., . . . Zhang, K. (2012). Essential role of ELOVL4 protein in very long chain fatty acid synthesis and retinal function. *J Biol Chem*, 287(14), 11469-11480. doi:10.1074/jbc.M111.256073
- Harrow, J., Frankish, A., Gonzalez, J. M., Tapanari, E., Diekhans, M., Kokocinski, F., . . . Hubbard, T. J. (2012). GENCODE: the reference human genome annotation for The ENCODE Project. *Genome Res*, 22(9), 1760-1774. doi:10.1101/gr.135350.111
- Haumann, I., Junghans, D., Anstötz, M., & Frotscher, M. (2017). Presynaptic localization of GluK5 in rod photoreceptors suggests a novel function of high affinity glutamate receptors in the mammalian retina. *PLoS One*, 12(2), e0172967. doi:10.1371/journal.pone.0172967
- Heckenlively, J. R. (1987). RP cone-rod degeneration. *Trans Am Ophthalmol Soc*, 85, 438-470.
- Hendriks, M., Verhoeven, V. J. M., Buitendijk, G. H. S., Polling, J. R., Meester-Smoor, M. A., Hofman, A., . . . Klaver, C. C. W. (2017). Development of Refractive Errors-What Can We Learn From Inherited Retinal Dystrophies? *Am J Ophthalmol*, 182, 81-89. doi:10.1016/j.ajo.2017.07.008
- Herse, P. (2005). Retinitis pigmentosa: visual function and multidisciplinary management. *Clin Exp Optom*, 88(5), 335-350.
- Herzfeld, T., Nolte, D., & Muller, U. (2007). Structural and functional analysis of the human TAF1/DYT3 multiple transcript system. *Mamm Genome*, 18(11), 787-795. doi:10.1007/s00335-007-9063-z
- Hipp, S., Zobor, G., Glockle, N., Mohr, J., Kohl, S., Zrenner, E., . . . Zobor, D. (2015). Phenotype variations of retinal dystrophies caused by mutations in the RLBP1 gene. *Acta Ophthalmol*, 93(4), e281-286. doi:10.1111/aos.12573

- Hiramatsu, N., Chiang, W. C., Kurt, T. D., Sigurdson, C. J., & Lin, J. H. (2015). Multiple Mechanisms of Unfolded Protein Response-Induced Cell Death. *Am J Pathol*, *185*(7), 1800-1808. doi:10.1016/j.ajpath.2015.03.009
- Hoffmann, C. J., Hohberg, M., Chlench, S., Maroski, J., Drab, M., Siegel, G., . . . Zakrzewicz, A. (2011). Suppression of zinc finger protein 580 by high oxLDL/LDL-ratios is followed by enhanced expression of endothelial IL-8. *Atherosclerosis*, *216*(1), 103-108. doi:10.1016/j.atherosclerosis.2011.01.017
- Hollyfield, J. G. (1999). Hyaluronan and the functional organization of the interphotoreceptor matrix. *Invest Ophthalmol Vis Sci*, *40*(12), 2767-2769.
- Honavar, S. G. (2018). Retinal vasoproliferative tumor - A proposal for classification. *Indian J Ophthalmol*, *66*(2), 185-186. doi:10.4103/ijo.IJO_128_18
- Hood, D. C., Lazow, M. A., Locke, K. G., Greenstein, V. C., & Birch, D. G. (2011). The transition zone between healthy and diseased retina in patients with retinitis pigmentosa. *Invest Ophthalmol Vis Sci*, *52*(1), 101-108. doi:10.1167/iovs.10-5799
- Horner, T. J., Osawa, S., Schaller, M. D., & Weiss, E. R. (2005). Phosphorylation of GRK1 and GRK7 by cAMP-dependent protein kinase attenuates their enzymatic activities. *J Biol Chem*, *280*(31), 28241-28250. doi:10.1074/jbc.M505117200
- Hou, S., Liao, D., Zhang, J., Fang, J., Chen, L., Qi, J., . . . Yang, P. (2015). Genetic variations of IL17F and IL23A show associations with Behcet's disease and Vogt-Koyanagi-Harada syndrome. *Ophthalmology*, *122*(3), 518-523. doi:10.1016/j.ophtha.2014.09.025
- Hovel, I., Pearson, N. A., & Stam, M. (2015). Cis-acting determinants of paramutation. *Semin Cell Dev Biol*, *44*, 22-32. doi:10.1016/j.semcdb.2015.08.012
- Hsiao, K. Y., Sun, H. S., & Tsai, S. J. (2017). Circular RNA - New member of noncoding RNA with novel functions. *Exp Biol Med (Maywood)*, *242*(11), 1136-1141. doi:10.1177/1535370217708978
- Huang, X. F., Wu, J., Lv, J. N., Zhang, X., & Jin, Z. B. (2015). Identification of false-negative mutations missed by next-generation sequencing in retinitis pigmentosa patients: a complementary approach to clinical genetic diagnostic testing. *Genet Med*, *17*(4), 307-311. doi:10.1038/gim.2014.193
- Hufnagel, R. B., Arno, G., Hein, N. D., Hersheson, J., Prasad, M., Anderson, Y., . . . Ahmed, Z. M. (2015). Neuropathy target esterase impairments cause Oliver-McFarlane and Laurence-Moon syndromes. *J Med Genet*, *52*(2), 85-94. doi:10.1136/jmedgenet-2014-102856

- Hunter, A., Spechler, P. A., Cwanger, A., Song, Y., Zhang, Z., Ying, G. S., . . . Dunaief, J. L. (2012). DNA methylation is associated with altered gene expression in AMD. *Invest Ophthalmol Vis Sci*, *53*(4), 2089-2105. doi:10.1167/iovs.11-8449
- Hurley, J. B., & Stryer, L. (1982). Purification and characterization of the gamma regulatory subunit of the cyclic GMP phosphodiesterase from retinal rod outer segments. *J Biol Chem*, *257*(18), 11094-11099.
- Illumina. iGenomes Ready-To-Use Reference Sequences and Annotations. Retrieved from https://support.illumina.com/sequencing/sequencing_software/igenome.html
- Inana, G., Murat, C., An, W., Yao, X., Harris, I. R., & Cao, J. (2018). RPE phagocytic function declines in age-related macular degeneration and is rescued by human umbilical tissue derived cells. *J Transl Med*, *16*(1), 63. doi:10.1186/s12967-018-1434-6
- Inooka, D., Ueno, S., Kominami, T., Sayo, A., Okado, S., Ito, Y., & Terasaki, H. (2018). Quantification of Macular Microvascular Changes in Patients With Retinitis Pigmentosa Using Optical Coherence Tomography Angiography. *Invest Ophthalmol Vis Sci*, *59*(1), 433-438. doi:10.1167/iovs.17-23202
- Inui, E., Oishi, A., Oishi, M., Ogino, K., Makiyama, Y., Gotoh, N., . . . Yoshimura, N. (2014). Tomographic comparison of cone-rod and rod-cone retinal dystrophies. *Graefes Arch Clin Exp Ophthalmol*, *252*(7), 1065-1069. doi:10.1007/s00417-014-2570-1
- Ishikawa, M., Sawada, Y., & Yoshitomi, T. (2015). Structure and function of the interphotoreceptor matrix surrounding retinal photoreceptor cells. *Exp Eye Res*, *133*, 3-18. doi:10.1016/j.exer.2015.02.017
- Itakura, M., Watanabe, I., Sugaya, T., & Takahashi, M. (2014). Direct association of the unique C-terminal tail of transmembrane AMPA receptor regulatory protein gamma-8 with calcineurin. *FEBS J*, *281*(5), 1366-1378. doi:10.1111/febs.12708
- Jaijo, T., Aller, E., Aparisi, M. J., Garcia-Garcia, G., Hernan, I., Gamundi, M. J., . . . Millan, J. M. (2011). Functional analysis of splicing mutations in MYO7A and USH2A genes. *Clin Genet*, *79*(3), 282-288. doi:10.1111/j.1399-0004.2010.01454.x
- Jaissle, G. B., May, C. A., van de Pavert, S. A., Wenzel, A., Claes-May, E., Giessel, A., . . . Seeliger, M. W. (2010). Bone spicule pigment formation in retinitis pigmentosa: insights from a mouse model. *Graefes Arch Clin Exp Ophthalmol*, *248*(8), 1063-1070. doi:10.1007/s00417-009-1253-9
- Jang, Y. P., Matsuda, H., Itagaki, Y., Nakanishi, K., & Sparrow, J. R. (2005). Characterization of peroxy-A2E and furan-A2E photooxidation products and detection in human and mouse retinal pigment epithelial cell lipofuscin. *J Biol Chem*, *280*(48), 39732-39739. doi:10.1074/jbc.M504933200

- Janssen, J. J., Kuhlmann, E. D., van Vugt, A. H., Winkens, H. J., Janssen, B. P., Deutman, A. F., & Driessen, C. A. (1999). Retinoic acid receptors and retinoid X receptors in the mature retina: subtype determination and cellular distribution. *Curr Eye Res*, *19*(4), 338-347.
- Janssen, S. F., van der Spek, S. J., Ten Brink, J. B., Essing, A. H., Gorgels, T. G., van der Spek, P. J., . . . Bergen, A. A. (2013). Gene expression and functional annotation of the human and mouse choroid plexus epithelium. *PLoS One*, *8*(12), e83345. doi:10.1371/journal.pone.0083345
- Jayasena, C. S., & Bronner, M. E. (2012). Rbms3 functions in craniofacial development by posttranscriptionally modulating TGF-beta signaling. *J Cell Biol*, *199*(3), 453-466. doi:10.1083/jcb.201204138
- Jensen, R. J. (2012). Blocking GABA(C) receptors increases light responsiveness of retinal ganglion cells in a rat model of retinitis pigmentosa. *Exp Eye Res*, *105*, 21-26. doi:10.1016/j.exer.2012.10.005
- Jerry Chiang, W. C., & Lin, J. H. (2014). The effects of IRE1, ATF6, and PERK signaling on adRP-linked rhodopsins. *Adv Exp Med Biol*, *801*, 661-667. doi:10.1007/978-1-4614-3209-8_83
- Johnsson, P., Lipovich, L., Grander, D., & Morris, K. V. (2014). Evolutionary conservation of long non-coding RNAs; sequence, structure, function. *Biochim Biophys Acta*, *1840*(3), 1063-1071. doi:10.1016/j.bbagen.2013.10.035
- Jomary, C., Neal, M. J., & Jones, S. E. (1995). Increased expression of retinal TIMP3 mRNA in simplex retinitis pigmentosa is localized to photoreceptor-retaining regions. *J Neurochem*, *64*(5), 2370-2373.
- Jones, B. W., Marc, R. E., & Pfeiffer, R. L. (1995). Retinal Degeneration, Remodeling and Plasticity. In H. Kolb, E. Fernandez, & R. Nelson (Eds.), *Webvision: The Organization of the Retina and Visual System*. Salt Lake City (UT).
- Junaid, M. A., Kowal, D., Barua, M., Pullarkat, P. S., Sklower Brooks, S., & Pullarkat, R. K. (2004). Proteomic studies identified a single nucleotide polymorphism in glyoxalase I as autism susceptibility factor. *Am J Med Genet A*, *131*(1), 11-17. doi:10.1002/ajmg.a.30349
- Juuti-Uusitalo, K., Koskela, A., Kivinen, N., Viiri, J., Hyttinen, J. M. T., Reinisalo, M., . . . Kaamiranta, K. (2017). Autophagy Regulates Proteasome Inhibitor-Induced Pigmentation in Human Embryonic Stem Cell-Derived Retinal Pigment Epithelial Cells. *Int J Mol Sci*, *18*(5). doi:10.3390/ijms18051089

- Kabir, F., Ullah, I., Ali, S., Gottsch, A. D., Naeem, M. A., Assir, M. Z., . . . Riazuddin, S. A. (2016). Loss of function mutations in RP1 are responsible for retinitis pigmentosa in consanguineous familial cases. *Mol Vis*, *22*, 610-625.
- Kageyama, R., Merlino, G. T., & Pastan, I. (1989). Nuclear factor ETF specifically stimulates transcription from promoters without a TATA box. *J Biol Chem*, *264*(26), 15508-15514.
- Kanehisa, M. (2002). The KEGG database. *Novartis Found Symp*, *247*, 91-101; discussion 101-103, 119-128, 244-152.
- Kanehisa, M., Furumichi, M., Tanabe, M., Sato, Y., & Morishima, K. (2017). KEGG: new perspectives on genomes, pathways, diseases and drugs. *Nucleic Acids Res*, *45*(D1), D353-D361. doi:10.1093/nar/gkw1092
- Kang, M. J., Chung, J., & Ryoo, H. D. (2012). CDK5 and MEKK1 mediate pro-apoptotic signalling following endoplasmic reticulum stress in an autosomal dominant retinitis pigmentosa model. *Nat Cell Biol*, *14*(4), 409-415. doi:10.1038/ncb2447
- Kang, M. J., & Ryoo, H. D. (2009). Suppression of retinal degeneration in *Drosophila* by stimulation of ER-associated degradation. *Proc Natl Acad Sci U S A*, *106*(40), 17043-17048. doi:10.1073/pnas.0905566106
- Karunakaran, D. K., Al Seesi, S., Bandy, A. R., Baumgartner, M., Olthof, A., Lemoine, C., . . . Kanadia, R. N. (2016). Network-based bioinformatics analysis of spatio-temporal RNA-Seq data reveals transcriptional programs underpinning normal and aberrant retinal development. *BMC Genomics*, *17 Suppl 5*, 495. doi:10.1186/s12864-016-2822-z
- Kauppinen, A., Paterno, J. J., Blasiak, J., Salminen, A., & Kaarniranta, K. (2016). Inflammation and its role in age-related macular degeneration. *Cell Mol Life Sci*, *73*(9), 1765-1786. doi:10.1007/s00018-016-2147-8
- Keilhauer, C. N., & Delori, F. C. (2006). Near-infrared autofluorescence imaging of the fundus: visualization of ocular melanin. *Invest Ophthalmol Vis Sci*, *47*(8), 3556-3564. doi:10.1167/iovs.06-0122
- Kennedy, B. N., Li, C., Ortego, J., Coca-Prados, M., Sarthy, V. P., & Crabb, J. W. (2003). CRALBP transcriptional regulation in ciliary epithelial, retinal Muller and retinal pigment epithelial cells. *Exp Eye Res*, *76*(2), 257-260.
- Kevany, B. M., & Palczewski, K. (2010). Phagocytosis of retinal rod and cone photoreceptors. *Physiology (Bethesda)*, *25*(1), 8-15. doi:10.1152/physiol.00038.2009

- Khan, A. O., Abu-Safieh, L., Eisenberger, T., Bolz, H. J., & Alkuraya, F. S. (2013). The RPGRIP1-related retinal phenotype in children. *Br J Ophthalmol*, *97*(6), 760-764. doi:10.1136/bjophthalmol-2012-303050
- Khan, K. N., Robson, A., Mahroo, O. A. R., Arno, G., Inglehearn, C. F., Armengol, M., . . . Consortium, U. K. I. R. D. (2018). A clinical and molecular characterisation of CRB1-associated maculopathy. *Eur J Hum Genet*, *26*(5), 687-694. doi:10.1038/s41431-017-0082-2
- Khodosevich, K., Jacobi, E., Farrow, P., Schulmann, A., Rusu, A., Zhang, L., . . . von Engelhardt, J. (2014). Coexpressed auxiliary subunits exhibit distinct modulatory profiles on AMPA receptor function. *Neuron*, *83*(3), 601-615. doi:10.1016/j.neuron.2014.07.004
- Kim, D., Pertea, G., Trapnell, C., Pimentel, H., Kelley, R., & Salzberg, S. L. (2013). TopHat2: accurate alignment of transcriptomes in the presence of insertions, deletions and gene fusions. *Genome Biol*, *14*(4), R36. doi:10.1186/gb-2013-14-4-r36
- King GL, S. K. (2000). Pigment-epithelium-derived factor--a key coordinator of retinal neuronal and vascular functions. *N Engl J Med*, *342*(5), 349-351.
- Kinney, M. S., & Fisher, S. K. (1978). The photoreceptors and pigment epithelium of the adult *Xenopus* retina: morphology and outer segment renewal. *Proc R Soc Lond B Biol Sci*, *201*(1143), 131-147.
- Kirwan, R. P., Wordinger, R. J., Clark, A. F., & O'Brien, C. J. (2009). Differential global and extra-cellular matrix focused gene expression patterns between normal and glaucomatous human lamina cribrosa cells. *Mol Vis*, *15*, 76-88.
- Koenekoop, R. K. (2018). Revisiting Congenital Stationary Night Blindness in the Molecular Era. *JAMA Ophthalmol*, *136*(4), 398-399. doi:10.1001/jamaophthalmol.2018.0193
- Kominami, T., Ueno, S., Kominami, A., Nakanishi, A., Yasuda, S., Piao, C. H., . . . Terasaki, H. (2017). Associations Between Outer Retinal Structures and Focal Macular Electroretinograms in Patients With Retinitis Pigmentosa. *Invest Ophthalmol Vis Sci*, *58*(12), 5122-5128. doi:10.1167/iovs.17-22040
- Kong, L. M., Yao, L., Lu, N., Dong, Y. L., Zhang, J., Wang, Y. Q., . . . Liao, C. G. (2016). Interaction of KLF6 and Sp1 regulates basigin-2 expression mediated proliferation, invasion and metastasis in hepatocellular carcinoma. *Oncotarget*, *7*(19), 27975-27987. doi:10.18632/oncotarget.8564
- Kong, X., Fang, M., Li, P., Fang, F., & Xu, Y. (2009). HDAC2 deacetylates class II transactivator and suppresses its activity in macrophages and smooth muscle cells. *J Mol Cell Cardiol*, *46*(3), 292-299. doi:10.1016/j.yjmcc.2008.10.023

- Kong, X., Peng, B., Yang, Y., Zhang, P., Qin, B., Han, D., . . . Yu, L. (2013). p53 Represses transcription of RING finger LIM domain-binding protein RLIM through Sp1. *PLoS One*, 8(5), e62832. doi:10.1371/journal.pone.0062832
- Koritschoner, N. P., Bocco, J. L., Panzetta-Dutari, G. M., Dumur, C. I., Flury, A., & Patrito, L. C. (1997). A novel human zinc finger protein that interacts with the core promoter element of a TATA box-less gene. *J Biol Chem*, 272(14), 9573-9580.
- Koriyama, Y., & Furukawa, A. (2015). [Role of Heat Shock Protein 70 in Retinitis Pigmentosa and a Novel Strategy for Treatment]. *Brain Nerve*, 67(12), 1523-1531. doi:10.11477/mf.1416200332
- Koriyama, Y., Takagi, Y., Chiba, K., Yamazaki, M., Sugitani, K., Arai, K., . . . Kato, S. (2013). Requirement of retinoic acid receptor beta for genipin derivative-induced optic nerve regeneration in adult rat retina. *PLoS One*, 8(8), e71252. doi:10.1371/journal.pone.0071252
- Kozomara, A., & Griffiths-Jones, S. (2014). miRBase: annotating high confidence microRNAs using deep sequencing data. *Nucleic Acids Res*, 42(Database issue), D68-73. doi:10.1093/nar/gkt1181
- Kruk, J., Kubasik-Kladna, K., & Aboul-Enein, H. Y. (2015). The Role Oxidative Stress in the Pathogenesis of Eye Diseases: Current Status and a Dual Role of Physical Activity. *Mini Rev Med Chem*, 16(3), 241-257.
- Kubota, S., Kurihara, T., Ebinuma, M., Kubota, M., Yuki, K., Sasaki, M., . . . Tsubota, K. (2010). Resveratrol prevents light-induced retinal degeneration via suppressing activator protein-1 activation. *Am J Pathol*, 177(4), 1725-1731. doi:10.2353/ajpath.2010.100098
- Kunte, M. M., Choudhury, S., Manheim, J. F., Shinde, V. M., Miura, M., Chiodo, V. A., . . . Gorbatyuk, M. S. (2012). ER stress is involved in T17M rhodopsin-induced retinal degeneration. *Invest Ophthalmol Vis Sci*, 53(7), 3792-3800. doi:10.1167/iovs.11-9235
- Kutty, R. K., Samuel, W., Boyce, K., Cherukuri, A., Duncan, T., Jaworski, C., . . . Redmond, T. M. (2016). Proinflammatory cytokines decrease the expression of genes critical for RPE function. *Mol Vis*, 22, 1156-1168.
- Kutuzov, M. A., Bennett, N., & Andreeva, A. V. (2010). Protein phosphatase with EF-hand domains 2 (PPEF2) is a potent negative regulator of apoptosis signal regulating kinase-1 (ASK1). *Int J Biochem Cell Biol*, 42(11), 1816-1822. doi:10.1016/j.biocel.2010.07.014
- Kwong, J. M., Gu, L., Nassiri, N., Bekerman, V., Kumar-Singh, R., Rhee, K. D., . . . Piri, N. (2015). AAV-mediated and pharmacological induction of Hsp70 expression

- stimulates survival of retinal ganglion cells following axonal injury. *Gene Ther*, 22(2), 138-145. doi:10.1038/gt.2014.105
- Laity, J. H., Lee, B. M., & Wright, P. E. (2001). Zinc finger proteins: new insights into structural and functional diversity. *Curr Opin Struct Biol*, 11(1), 39-46.
- Larhammar, M., Huntwork-Rodriguez, S., Rudhard, Y., Sengupta-Ghosh, A., & Lewcock, J. W. (2017). The Ste20 Family Kinases MAP4K4, MINK1, and TNIK Converge to Regulate Stress-Induced JNK Signaling in Neurons. *J Neurosci*, 37(46), 11074-11084. doi:10.1523/JNEUROSCI.0905-17.2017
- Laurent, V., Sengupta, A., Sanchez-Bretano, A., Hicks, D., & Tosini, G. (2017). Melatonin signaling affects the timing in the daily rhythm of phagocytic activity by the retinal pigment epithelium. *Exp Eye Res*, 165, 90-95. doi:10.1016/j.exer.2017.09.007
- Lebrun-Julien, F., & Suter, U. (2015). Combined HDAC1 and HDAC2 Depletion Promotes Retinal Ganglion Cell Survival After Injury Through Reduction of p53 Target Gene Expression. *ASN Neuro*, 7(3). doi:10.1177/1759091415593066
- Lee, J., Harris, A. N., Holley, C. L., Mahadevan, J., Pyles, K. D., Lavagnino, Z., . . . Schaffer, J. E. (2016). Rpl13a small nucleolar RNAs regulate systemic glucose metabolism. *J Clin Invest*, 126(12), 4616-4625. doi:10.1172/JCI88069
- Lee, J. H., Jeong, E. G., Choi, M. C., Kim, S. H., Park, J. H., Song, S. H., . . . Kim, T. Y. (2010). Inhibition of histone deacetylase 10 induces thioredoxin-interacting protein and causes accumulation of reactive oxygen species in SNU-620 human gastric cancer cells. *Mol Cells*, 30(2), 107-112. doi:10.1007/s10059-010-0094-z
- Lee, J. J., & Seo, S. (2015). PDE6D binds to the C-terminus of RPGR in a prenylation-dependent manner. *EMBO Rep*, 16(12), 1581-1582. doi:10.15252/embr.201541220
- Lee, K. A., Nawrot, M., Garwin, G. G., Saari, J. C., & Hurley, J. B. (2010). Relationships among visual cycle retinoids, rhodopsin phosphorylation, and phototransduction in mouse eyes during light and dark adaptation. *Biochemistry*, 49(11), 2454-2463. doi:10.1021/bi1001085
- Lenarduzzi, S., Vozzi, D., Morgan, A., Rubinato, E., D'Eustacchio, A., Osland, T. M., . . . Giroto, G. (2015). Usher syndrome: an effective sequencing approach to establish a genetic and clinical diagnosis. *Hear Res*, 320, 18-23. doi:10.1016/j.heares.2014.12.006
- Lenzi, L., Coassin, M., Lambiase, A., Bonini, S., Amendola, T., & Aloe, L. (2005). Effect of exogenous administration of nerve growth factor in the retina of rats with inherited retinitis pigmentosa. *Vision Res*, 45(12), 1491-1500. doi:10.1016/j.visres.2004.12.020

- Lestrade, L., & Weber, M. J. (2006). snoRNA-LBME-db, a comprehensive database of human H/ACA and C/D box snoRNAs. *Nucleic Acids Res*, *34*(Database issue), D158-162. doi:10.1093/nar/gkj002
- Leung, Y. Y., Kuksa, P. P., Amlie-Wolf, A., Valladares, O., Ungar, L. H., Kannan, S., . . . Wang, L. S. (2016). DASHR: database of small human noncoding RNAs. *Nucleic Acids Res*, *44*(D1), D216-222. doi:10.1093/nar/gkv1188
- Li, B., Ruotti, V., Stewart, R. M., Thomson, J. A., & Dewey, C. N. (2010). RNA-Seq gene expression estimation with read mapping uncertainty. *Bioinformatics*, *26*(4), 493-500. doi:10.1093/bioinformatics/btp692
- Li, H. B., Wang, R. X., Jiang, H. B., Zhang, E. D., Tan, J. Q., Xu, H. Z., . . . Xia, X. B. (2016). Mitochondrial Ribosomal Protein L10 Associates with Cyclin B1/Cdk1 Activity and Mitochondrial Function. *DNA Cell Biol*, *35*(11), 680-690. doi:10.1089/dna.2016.3271
- Li, L., Nakaya, N., Chavali, V. R., Ma, Z., Jiao, X., Sieving, P. A., . . . Hejtmancik, J. F. (2010). A mutation in ZNF513, a putative regulator of photoreceptor development, causes autosomal-recessive retinitis pigmentosa. *Am J Hum Genet*, *87*(3), 400-409. doi:10.1016/j.ajhg.2010.08.003
- Li, Z. Y., Kljavin, I. J., & Milam, A. H. (1995). Rod photoreceptor neurite sprouting in retinitis pigmentosa. *J Neurosci*, *15*(8), 5429-5438.
- Li, Z. Y., Possin, D. E., & Milam, A. H. (1995). Histopathology of bone spicule pigmentation in retinitis pigmentosa. *Ophthalmology*, *102*(5), 805-816.
- Liang, F. Q., Aleman, T. S., Dejneka, N. S., Dudas, L., Fisher, K. J., Maguire, A. M., . . . Bennett, J. (2001). Long-term protection of retinal structure but not function using RAAV.CNTF in animal models of retinitis pigmentosa. *Mol Ther*, *4*(5), 461-472. doi:10.1006/mthe.2001.0473
- Lienkamp, S., Ganner, A., & Walz, G. (2012). Inversin, Wnt signaling and primary cilia. *Differentiation*, *83*(2), S49-55. doi:10.1016/j.diff.2011.11.012
- Liew, G., Moore, A. T., Webster, A. R., & Michaelides, M. (2015). Efficacy and prognostic factors of response to carbonic anhydrase inhibitors in management of cystoid macular edema in retinitis pigmentosa. *Invest Ophthalmol Vis Sci*, *56*(3), 1531-1536. doi:10.1167/iovs.14-15995
- Lim, J. Q., Lu, J., & He, B. P. (2012). Diva/BclB regulates differentiation by inhibiting NDPKB/Nm23H2-mediated neuronal differentiation in PC-12 cells. *BMC Neurosci*, *13*, 123. doi:10.1186/1471-2202-13-123

- Lima, L. H., Cella, W., Greenstein, V. C., Wang, N. K., Busuioc, M., Smith, R. T., . . . Tsang, S. H. (2009). Structural assessment of hyperautofluorescent ring in patients with retinitis pigmentosa. *Retina*, *29*(7), 1025-1031. doi:10.1097/IAE.0b013e3181ac2418
- Lin, J. H., & Lavail, M. M. (2010). Misfolded proteins and retinal dystrophies. *Adv Exp Med Biol*, *664*, 115-121. doi:10.1007/978-1-4419-1399-9_14
- Lin, Y., Golovkina, K., Chen, Z. X., Lee, H. N., Negron, Y. L., Sultana, H., . . . Harbison, S. T. (2016). Comparison of normalization and differential expression analyses using RNA-Seq data from 726 individual *Drosophila melanogaster*. *BMC Genomics*, *17*, 28. doi:10.1186/s12864-015-2353-z
- Littink, K. W., van Genderen, M. M., van Schooneveld, M. J., Visser, L., Riemsdag, F. C., Keunen, J. E., . . . van den Born, L. I. (2012). A homozygous frameshift mutation in LRAT causes retinitis punctata albescens. *Ophthalmology*, *119*(9), 1899-1906. doi:10.1016/j.ophtha.2012.02.037
- Liu, C. H., Wang, Z., Sun, Y., SanGiovanni, J. P., & Chen, J. (2016). Retinal expression of small non-coding RNAs in a murine model of proliferative retinopathy. *Sci Rep*, *6*, 33947. doi:10.1038/srep33947
- Liu, G., Du, Q., Keyal, K., & Wang, F. (2017). Morphologic characteristics and clinical significance of the macular-sparing area in patients with retinitis pigmentosa as revealed by multicolor imaging. *Exp Ther Med*, *14*(6), 5387-5394. doi:10.3892/etm.2017.5227
- Liu, G., Liu, X., Li, H., Du, Q., & Wang, F. (2016). Optical Coherence Tomographic Analysis of Retina in Retinitis Pigmentosa Patients. *Ophthalmic Res*, *56*(3), 111-122. doi:10.1159/000445063
- Liu, Q., Lyubarsky, A., Skalet, J. H., Pugh, E. N., Jr., & Pierce, E. A. (2003). RPI is required for the correct stacking of outer segment discs. *Invest Ophthalmol Vis Sci*, *44*(10), 4171-4183.
- Liu, X., Yu, X., Zack, D. J., Zhu, H., & Qian, J. (2008). TiGER: a database for tissue-specific gene expression and regulation. *BMC Bioinformatics*, *9*, 271. doi:10.1186/1471-2105-9-271
- Liu, Y., Zhou, J., Wang, L., Hu, X., Liu, X., Liu, M., . . . Tan, W. (2016). A Cyanine Dye to Probe Mitophagy: Simultaneous Detection of Mitochondria and Autolysosomes in Live Cells. *J Am Chem Soc*, *138*(38), 12368-12374. doi:10.1021/jacs.6b04048
- Livide, G., Epistolato, M. C., Amenduni, M., Disciglio, V., Marozza, A., Mencarelli, M. A., . . . Ariani, F. (2012). Epigenetic and copy number variation analysis in retinoblastoma by MS-MLPA. *Pathol Oncol Res*, *18*(3), 703-712. doi:10.1007/s12253-012-9498-8

- Lopez Torres, L. T., Turksever, C., Schotzau, A., Orgul, S., & Todorova, M. G. (2015). Peripapillary retinal vessel diameter correlates with mfERG alterations in retinitis pigmentosa. *Acta Ophthalmol*, 93(7), e527-533. doi:10.1111/aos.12707
- Lu, Z., Hu, X., Liu, F., Soares, D. C., Liu, X., Yu, S., . . . Liu, M. (2017). Ablation of EYS in zebrafish causes mislocalisation of outer segment proteins, F-actin disruption and cone-rod dystrophy. *Sci Rep*, 7, 46098. doi:10.1038/srep46098
- Luo, R., Reed, C. E., Sload, J. A., Wordeman, L., Randazzo, P. A., & Chen, P. W. (2017). Arf GAPs and molecular motors. *Small GTPases*, 1-14. doi:10.1080/21541248.2017.1308850
- Luo, W., Ruba, A., Takao, D., Zweifel, L. P., Lim, R. Y. H., Verhey, K. J., & Yang, W. (2017). Axonemal Lumen Dominates Cytosolic Protein Diffusion inside the Primary Cilium. *Sci Rep*, 7(1), 15793. doi:10.1038/s41598-017-16103-z
- Luo, Y., Hu, W., Xu, R., Hou, B., Zhang, L., & Zhang, W. (2011). ZNF580, a novel C2H2 zinc-finger transcription factor, interacts with the TGF-beta signal molecule Smad2. *Cell Biol Int*, 35(11), 1153-1157. doi:10.1042/CBI20110050
- Luo, Y., Zhao, Y., Li, X., Zhao, J., & Zhang, W. (2014). ZNF580 mediates eNOS expression and endothelial cell migration/proliferation via the TGF-beta1/ALK5/Smad2 pathway. *Mol Cell Biochem*, 393(1-2), 199-207. doi:10.1007/s11010-014-2061-z
- Ma, L., Sheng, X. L., Li, H. P., Zhang, F. X., Liu, Y. N., Rong, W. N., & Zhang, J. L. (2013). Identification of a novel p.R1443W mutation in RP1 gene associated with retinitis pigmentosa sine pigmento. *Int J Ophthalmol*, 6(4), 430-435. doi:10.3980/j.issn.2222-3959.2013.04.04
- Maeda, T., Imanishi, Y., & Palczewski, K. (2003). Rhodopsin phosphorylation: 30 years later. *Prog Retin Eye Res*, 22(4), 417-434.
- Maeda, T., Ito, K., Merghoub, T., Polisenno, L., Hobbs, R. M., Wang, G., . . . Pandolfi, P. P. (2009). LRF is an essential downstream target of GATA1 in erythroid development and regulates BIM-dependent apoptosis. *Dev Cell*, 17(4), 527-540. doi:10.1016/j.devcel.2009.09.005
- Mahajan, D., & Votruba, M. (2017). A novel NR2E3 gene mutation in autosomal recessive retinitis pigmentosa with cystic maculopathy. *Acta Ophthalmol*. doi:10.1111/aos.13629
- Makiyama, Y., Oishi, A., Otani, A., Ogino, K., Nakagawa, S., Kurimoto, M., & Yoshimura, N. (2014). Prevalence and spatial distribution of cystoid spaces in retinitis pigmentosa: investigation with spectral domain optical coherence tomography. *Retina*, 34(5), 981-988. doi:10.1097/IAE.000000000000010

- Mao, H., Seo, S. J., Biswal, M. R., Li, H., Conners, M., Nandyala, A., . . . Lewin, A. S. (2014). Mitochondrial oxidative stress in the retinal pigment epithelium leads to localized retinal degeneration. *Invest Ophthalmol Vis Sci*, *55*(7), 4613-4627. doi:10.1167/iovs.14-14633
- Marazita, M. C., Dugour, A., Marquioni-Ramella, M. D., Figueroa, J. M., & Suburo, A. M. (2016). Oxidative stress-induced premature senescence dysregulates VEGF and CFH expression in retinal pigment epithelial cells: Implications for Age-related Macular Degeneration. *Redox Biol*, *7*, 78-87. doi:10.1016/j.redox.2015.11.011
- Marnaros, A. G. (2016). VEGF-A and the NLRP3 Inflammasome in Age-Related Macular Degeneration. *Adv Exp Med Biol*, *854*, 79-85. doi:10.1007/978-3-319-17121-0_12
- Marre, E., & Walther, A. (1990). [Friedrich August von Ammon (1799-1861) and Dresden ophthalmology in the 1st half of the 19th century]. *Gesnerus*, *47 Pt 1*, 53-58.
- Martin, C. A., Ahmad, I., Klingseisen, A., Hussain, M. S., Bicknell, L. S., Leitch, A., . . . Jackson, A. P. (2014). Mutations in PLK4, encoding a master regulator of centriole biogenesis, cause microcephaly, growth failure and retinopathy. *Nat Genet*, *46*(12), 1283-1292. doi:10.1038/ng.3122
- Martinez-Fernandez de la Camara, C., Salom, D., Sequedo, M. D., Hervas, D., Marin-Lambies, C., Aller, E., . . . Rodrigo, R. (2013). Altered antioxidant-oxidant status in the aqueous humor and peripheral blood of patients with retinitis pigmentosa. *PLoS One*, *8*(9), e74223. doi:10.1371/journal.pone.0074223
- Massengill, M. T., Ahmed, C. M., Lewin, A. S., & Ildefonso, C. J. (2018). Neuroinflammation in Retinitis Pigmentosa, Diabetic Retinopathy, and Age-Related Macular Degeneration: A Minireview. *Adv Exp Med Biol*, *1074*, 185-191. doi:10.1007/978-3-319-75402-4_23
- Massof, R. W., Finkelstein, D., Starr, S. J., Kenyon, K. R., Fleischman, J. A., & Maumenee, I. H. (1979). Bilateral symmetry of vision disorders in typical retinitis pigmentosa. *Br J Ophthalmol*, *63*(2), 90-96.
- Mathijssen, I. B., Florijn, R. J., van den Born, L. I., Zekveld-Vroon, R. C., Ten Brink, J. B., Plomp, A. S., . . . van Schooneveld, M. J. (2017). LONG-TERM FOLLOW-UP OF PATIENTS WITH RETINITIS PIGMENTOSA TYPE 12 CAUSED BY CRB1 MUTATIONS: A Severe Phenotype With Considerable Interindividual Variability. *Retina*, *37*(1), 161-172. doi:10.1097/IAE.0000000000001127
- Mathur, P., & Yang, J. (2015). Usher syndrome: Hearing loss, retinal degeneration and associated abnormalities. *Biochim Biophys Acta*, *1852*(3), 406-420. doi:10.1016/j.bbadis.2014.11.020

- Matsui, R., Cideciyan, A. V., Schwartz, S. B., Sumaroka, A., Roman, A. J., Swider, M., . . . Jacobson, S. G. (2015). Molecular Heterogeneity Within the Clinical Diagnosis of Pericentral Retinal Degeneration. *Invest Ophthalmol Vis Sci*, *56*(10), 6007-6018. doi:10.1167/iovs.15-17174
- Matsunaga, D., Sreekumar, P. G., Ishikawa, K., Terasaki, H., Barron, E., Cohen, P., . . . Hinton, D. R. (2016). Humanin Protects RPE Cells from Endoplasmic Reticulum Stress-Induced Apoptosis by Upregulation of Mitochondrial Glutathione. *PLoS One*, *11*(10), e0165150. doi:10.1371/journal.pone.0165150
- Matys, V., Kel-Margoulis, O. V., Fricke, E., Liebich, I., Land, S., Barre-Dirrie, A., . . . Wingender, E. (2006). TRANSFAC and its module TRANSCompel: transcriptional gene regulation in eukaryotes. *Nucleic Acids Res*, *34*(Database issue), D108-110. doi:10.1093/nar/gkj143
- McCarthy, N. E., & Akhtar, M. (2002). Activation of rhodopsin kinase. *Biochem J*, *363*(Pt 2), 359-364.
- McIntyre, J. C., Hege, M. M., & Berbari, N. F. (2016). Trafficking of ciliary G protein-coupled receptors. *Methods Cell Biol*, *132*, 35-54. doi:10.1016/bs.mcb.2015.11.009
- McLaughlin, N. J., Banerjee, A., Kelher, M. R., Gamboni-Robertson, F., Hamiel, C., Sheppard, F. R., . . . Silliman, C. C. (2006). Platelet-activating factor-induced clathrin-mediated endocytosis requires beta-arrestin-1 recruitment and activation of the p38 MAPK signalosome at the plasma membrane for actin bundle formation. *J Immunol*, *176*(11), 7039-7050.
- McMahon, M., Contreras, A., & Ruggero, D. (2015). Small RNAs with big implications: new insights into H/ACA snoRNA function and their role in human disease. *Wiley Interdiscip Rev RNA*, *6*(2), 173-189. doi:10.1002/wrna.1266
- Mendis, R., & Lois, N. (2014). Fundus autofluorescence in patients with retinal pigment epithelial (RPE) tears: an in-vivo evaluation of RPE resurfacing. *Graefes Arch Clin Exp Ophthalmol*, *252*(7), 1059-1063. doi:10.1007/s00417-013-2549-3
- Mensaert, K., Denil, S., Trooskens, G., Van Criekinge, W., Thas, O., & De Meyer, T. (2014). Next-generation technologies and data analytical approaches for epigenomics. *Environ Mol Mutagen*, *55*(3), 155-170. doi:10.1002/em.21841
- Messina, S., Di Zazzo, E., & Moncharmont, B. (2017). Early and Late Induction of KRAS and HRAS Proto-Oncogenes by Reactive Oxygen Species in Primary Astrocytes. *Antioxidants (Basel)*, *6*(3). doi:10.3390/antiox6030048
- Michel, C. I., Holley, C. L., Scruggs, B. S., Sidhu, R., Brookheart, R. T., Listenberger, L. L., . . . Schaffer, J. E. (2011). Small nucleolar RNAs U32a, U33, and U35a are critical

- mediators of metabolic stress. *Cell Metab*, 14(1), 33-44. doi:10.1016/j.cmet.2011.04.009
- Milstein, A. D., & Nicoll, R. A. (2009). TARP modulation of synaptic AMPA receptor trafficking and gating depends on multiple intracellular domains. *Proc Natl Acad Sci U S A*, 106(27), 11348-11351. doi:10.1073/pnas.0905570106
- Mimura, T., Kaji, Y., Noma, H., Funatsu, H., & Okamoto, S. (2013). The role of SIRT1 in ocular aging. *Exp Eye Res*, 116, 17-26. doi:10.1016/j.exer.2013.07.017
- Miranda, G. A., Villalvazo, M., Galic, Z., Alva, J., Abrines, R., Yates, Y., . . . Aguilera, R. J. (2002). Combinatorial regulation of the murine RAG-2 promoter by Sp1 and distinct lymphocyte-specific transcription factors. *Mol Immunol*, 38(15), 1151-1159.
- Mitton, K. P., Swain, P. K., Khanna, H., Dowd, M., Apel, I. J., & Swaroop, A. (2003). Interaction of retinal bZIP transcription factor NRL with Flt3-interacting zinc-finger protein Fiz1: possible role of Fiz1 as a transcriptional repressor. *Hum Mol Genet*, 12(4), 365-373.
- Miyata, M., Ogino, K., Gotoh, N., Morooka, S., Hasegawa, T., Hata, M., & Yoshimura, N. (2016). Inner segment ellipsoid band length is a prognostic factor in retinitis pigmentosa associated with EYS mutations: 5-year observation of retinal structure. *Eye (Lond)*, 30(12), 1588-1592. doi:10.1038/eye.2016.196
- Moiseyev, G., Takahashi, Y., Chen, Y., Gentleman, S., Redmond, T. M., Crouch, R. K., & Ma, J. X. (2006). RPE65 is an iron(II)-dependent isomerohydrolase in the retinoid visual cycle. *J Biol Chem*, 281(5), 2835-2840. doi:10.1074/jbc.M508903200
- Molday, R. S., Molday, L. L., & Loewen, C. J. (2004). Role of subunit assembly in autosomal dominant retinitis pigmentosa linked to mutations in peripherin 2. *Novartis Found Symp*, 255, 95-112; discussion 113-116, 177-118.
- Moreno-Navarrete, J. M., Ortega, F., Moreno, M., Serrano, M., Ricart, W., & Fernandez-Real, J. M. (2014). Lactoferrin gene knockdown leads to similar effects to iron chelation in human adipocytes. *J Cell Mol Med*, 18(3), 391-395. doi:10.1111/jcmm.12234
- Mukhopadhyay, R., Holder, G. E., Moore, A. T., & Webster, A. R. (2011). Unilateral retinitis pigmentosa occurring in an individual with a germline mutation in the RP1 gene. *Arch Ophthalmol*, 129(7), 954-956. doi:10.1001/archophthalmol.2011.171
- Mukhopadhyay, R., Jia, J., Arif, A., Ray, P. S., & Fox, P. L. (2009). The GAIT system: a gatekeeper of inflammatory gene expression. *Trends Biochem Sci*, 34(7), 324-331. doi:10.1016/j.tibs.2009.03.004

- Muniz A, B. B., Trevino AR, Buddavarapu K, Roman R, Ma JX, Tsin AT. (2009). Evidence for two retinoid cycles in the cone-dominated chicken eye. *Biochemistry*, 48(29), 6854-6863.
- Murro, V., Mucciolo, D. P., Sodi, A., Vannozzi, L., De Libero, C., Simonini, G., & Rizzo, S. (2017). Retinal capillaritis in a CRB1-associated retinal dystrophy. *Ophthalmic Genet*, 38(6), 555-558. doi:10.1080/13816810.2017.1281966
- Mylvaganam, G. H., McGee, T. L., Berson, E. L., & Dryja, T. P. (2006). A screen for mutations in the transducin gene GNB1 in patients with autosomal dominant retinitis pigmentosa. *Mol Vis*, 12, 1496-1498.
- Na, K. H., Kim, H. J., Kim, K. H., Han, S., Kim, P., Hann, H. J., & Ahn, H. S. (2017). Prevalence, Age at Diagnosis, Mortality, and Cause of Death in Retinitis Pigmentosa in Korea-A Nationwide Population-based Study. *Am J Ophthalmol*, 176, 157-165. doi:10.1016/j.ajo.2017.01.014
- Nader, N., Chrousos, G. P., & Kino, T. (2009). Circadian rhythm transcription factor CLOCK regulates the transcriptional activity of the glucocorticoid receptor by acetylating its hinge region lysine cluster: potential physiological implications. *FASEB J*, 23(5), 1572-1583. doi:10.1096/fj.08-117697
- Nager, A. R., Goldstein, J. S., Herranz-Perez, V., Portran, D., Ye, F., Garcia-Verdugo, J. M., & Nachury, M. V. (2017). An Actin Network Dispatches Ciliary GPCRs into Extracellular Vesicles to Modulate Signaling. *Cell*, 168(1-2), 252-263 e214. doi:10.1016/j.cell.2016.11.036
- Nakamura, H., Edward, D. P., Sugar, J., & Yue, B. Y. (2007). Expression of Sp1 and KLF6 in the developing human cornea. *Mol Vis*, 13, 1451-1457.
- Napier, M. L., Durga, D., Wolsley, C. J., Chamney, S., Alexander, S., Brennan, R., . . . Willoughby, C. E. (2015). Mutational Analysis of the Rhodopsin Gene in Sector Retinitis Pigmentosa. *Ophthalmic Genet*, 36(3), 239-243. doi:10.3109/13816810.2014.958862
- Nash, B. M., Wright, D. C., Grigg, J. R., Bennetts, B., & Jamieson, R. V. (2015). Retinal dystrophies, genomic applications in diagnosis and prospects for therapy. *Transl Pediatr*, 4(2), 139-163. doi:10.3978/j.issn.2224-4336.2015.04.03
- Natalizio, B. J., Robson-Dixon, N. D., & Garcia-Blanco, M. A. (2009). The Carboxyl-terminal Domain of RNA Polymerase II Is Not Sufficient to Enhance the Efficiency of Pre-mRNA Capping or Splicing in the Context of a Different Polymerase. *J Biol Chem*, 284(13), 8692-8702. doi:10.1074/jbc.M806919200

- Naz, S., Riazuddin, S. A., Li, L., Shahid, M., Kousar, S., Sieving, P. A., . . . Riazuddin, S. (2010). A novel locus for autosomal recessive retinitis pigmentosa in a consanguineous Pakistani family maps to chromosome 2p. *Am J Ophthalmol*, *149*(5), 861-866. doi:10.1016/j.ajo.2009.12.034
- Newsome, D. A., Swartz, M., Leone, N. C., Hewitt, A. T., Wolford, F., & Miller, E. D. (1986). Macular degeneration and elevated serum ceruloplasmin. *Invest Ophthalmol Vis Sci*, *27*(12), 1675-1680.
- Ng, L., Hurley, J. B., Dierks, B., Srinivas, M., Salto, C., Vennstrom, B., . . . Forrest, D. (2001). A thyroid hormone receptor that is required for the development of green cone photoreceptors. *Nat Genet*, *27*(1), 94-98. doi:10.1038/83829
- Nguyen-Legros J, H. D. (2000). Renewal of photoreceptor outer segments and their phagocytosis by the retinal pigment epithelium. *Int Rev Cytol*, *196*, 245-313.
- Niikura, Y., Kitagawa, R., Ogi, H., & Kitagawa, K. (2017). SGT1-HSP90 complex is required for CENP-A deposition at centromeres. *Cell Cycle*, *16*(18), 1683-1694. doi:10.1080/15384101.2017.1325039
- North, V., Gelman, R., & Tsang, S. H. (2014). Juvenile-onset macular degeneration and allied disorders. *Dev Ophthalmol*, *53*, 44-52. doi:10.1159/000357293
- O'Neal, T. B., & Luther, E. E. (2018). Retinitis Pigmentosa. In *StatPearls*. Treasure Island (FL).
- O'Reilly, J. A., Fitzgerald, J., Fitzgerald, S., Kenny, D., Kay, E. W., O'Kennedy, R., & Kijanka, G. S. (2015). Diagnostic potential of zinc finger protein-specific autoantibodies and associated linear B-cell epitopes in colorectal cancer. *PLoS One*, *10*(4), e0123469. doi:10.1371/journal.pone.0123469
- Oehme, I., Linke, J. P., Bock, B. C., Milde, T., Lodrini, M., Hartenstein, B., . . . Witt, O. (2013). Histone deacetylase 10 promotes autophagy-mediated cell survival. *Proc Natl Acad Sci U S A*, *110*(28), E2592-2601. doi:10.1073/pnas.1300113110
- Oh, K. T., Weleber, R. G., Stone, E. M., Oh, D. M., Rosenow, J., & Billingslea, A. M. (2004). Electoretinographic findings in patients with Stargardt disease and fundus flavimaculatus. *Retina*, *24*(6), 920-928.
- Ohguro, H., Maeda, T., Yanagihashi, S., Miyakawa, Y., Maruyama, I., & Nakazawa, M. (2002). [Molecular pathology of retinitis pigmentosa]. *Nippon Ganka Gakkai Zasshi*, *106*(8), 461-473.
- Oishi, A., Ogino, K., Makiyama, Y., Nakagawa, S., Kurimoto, M., & Yoshimura, N. (2013). Wide-field fundus autofluorescence imaging of retinitis pigmentosa. *Ophthalmology*, *120*(9), 1827-1834. doi:10.1016/j.ophtha.2013.01.050

- Oishi, M., Oishi, A., Ogino, K., Makiyama, Y., Gotoh, N., Kurimoto, M., & Yoshimura, N. (2014). Wide-field fundus autofluorescence abnormalities and visual function in patients with cone and cone-rod dystrophies. *Invest Ophthalmol Vis Sci*, *55*(6), 3572-3577. doi:10.1167/iovs.14-13912
- Okano, J., Opitz, O. G., Nakagawa, H., Jenkins, T. D., Friedman, S. L., & Rustgi, A. K. (2000). The Kruppel-like transcriptional factors Zf9 and GKLf coactivate the human keratin 4 promoter and physically interact. *FEBS Lett*, *473*(1), 95-100.
- Okonechnikov, K., Conesa, A., & Garcia-Alcalde, F. (2016). Qualimap 2: advanced multi-sample quality control for high-throughput sequencing data. *Bioinformatics*, *32*(2), 292-294. doi:10.1093/bioinformatics/btv566
- Okoye, G., Zimmer, J., Sung, J., Gehlbach, P., Deering, T., Nambu, H., . . . Campochiaro, P. A. (2003). Increased expression of brain-derived neurotrophic factor preserves retinal function and slows cell death from rhodopsin mutation or oxidative damage. *J Neurosci*, *23*(10), 4164-4172.
- Okuda, A., Naganuma, T., Ohno, Y., Abe, K., Yamagata, M., Igarashi, Y., & Kihara, A. (2010). Hetero-oligomeric interactions of an ELOVL4 mutant protein: implications in the molecular mechanism of Stargardt-3 macular dystrophy. *Mol Vis*, *16*, 2438-2445.
- Olchawa, M. M., Furso, J. A., Szewczyk, G. M., & Sarna, T. J. (2017). Lipofuscin-mediated photic stress inhibits phagocytic activity of ARPE-19 cells; effect of donors' age and antioxidants. *Free Radic Res*, 1-13. doi:10.1080/10715762.2017.1380307
- Olivares-Gonzalez, L., Martinez-Fernandez de la Camara, C., Hervas, D., Millan, J. M., & Rodrigo, R. (2018). HIF-1alpha stabilization reduces retinal degeneration in a mouse model of retinitis pigmentosa. *FASEB J*, *32*(5), 2438-2451. doi:10.1096/fj.201700985R
- Onishi, A., Peng, G. H., Chen, S., & Blackshaw, S. (2010). Pias3-dependent SUMOylation controls mammalian cone photoreceptor differentiation. *Nat Neurosci*, *13*(9), 1059-1065. doi:10.1038/nn.2618
- Orchard, S., Ammari, M., Aranda, B., Breuza, L., Briganti, L., Broackes-Carter, F., . . . Hermjakob, H. (2014). The MIntAct project--IntAct as a common curation platform for 11 molecular interaction databases. *Nucleic Acids Res*, *42*(Database issue), D358-363. doi:10.1093/nar/gkt1115
- Orlov, S. V., Kuteykin-Teplyakov, K. B., Ignatovich, I. A., Dizhe, E. B., Mirgorodskaya, O. A., Grishin, A. V., . . . Perevozchikov, A. P. (2007). Novel repressor of the human FMR1 gene - identification of p56 human (GCC)(n)-binding protein as a Kruppel-like

- transcription factor ZF5. *FEBS J*, 274(18), 4848-4862. doi:10.1111/j.1742-4658.2007.06006.x
- Osawa, S., & Weiss, E. R. (2012). A tale of two kinases in rods and cones. *Adv Exp Med Biol*, 723, 821-827. doi:10.1007/978-1-4614-0631-0_105
- Ostrem, J. M., & Shokat, K. M. (2016). Direct small-molecule inhibitors of KRAS: from structural insights to mechanism-based design. *Nat Rev Drug Discov*, 15(11), 771-785. doi:10.1038/nrd.2016.139
- Ovejero-Benito, M. C., & Frade, J. M. (2015). p27(Kip1) participates in the regulation of endoreplication in differentiating chick retinal ganglion cells. *Cell Cycle*, 14(14), 2311-2322. doi:10.1080/15384101.2015.1044175
- Overlack, N., Kilic, D., Baus, K., Marker, T., Kremer, H., van Wijk, E., & Wolfrum, U. (2011). Direct interaction of the Usher syndrome 1G protein SANS and myomegalin in the retina. *Biochim Biophys Acta*, 1813(10), 1883-1892. doi:10.1016/j.bbamcr.2011.05.015
- Ozawa, Y., Kubota, S., Narimatsu, T., Yuki, K., Koto, T., Sasaki, M., & Tsubota, K. (2010). Retinal aging and sirtuins. *Ophthalmic Res*, 44(3), 199-203. doi:10.1159/000316484
- PA, C. (2015). Molecular pathogenesis of retinal and choroidal vascular diseases. *Prog Retin Eye Res*, 49, 67-81.
- Pal, A., Kumar, A., & Prasad, R. (2014). Predictive association of copper metabolism proteins with Alzheimer's disease and Parkinson's disease: a preliminary perspective. *Biometals*, 27(1), 25-31. doi:10.1007/s10534-013-9702-7
- Palejwala, N. V., Gale, M. J., Clark, R. F., Schlechter, C., Weleber, R. G., & Pennesi, M. E. (2016). Insights into Autosomal Dominant Stargardt-Like Macular Dystrophy through Multimodality Diagnostic Imaging. *Retina*, 36(1), 119-130. doi:10.1097/IAE.0000000000000659
- Palmer, S. J., Tay, E. S., Santucci, N., Cuc Bach, T. T., Hook, J., Lemckert, F. A., . . . Hardeman, E. C. (2007). Expression of Gtf2ird1, the Williams syndrome-associated gene, during mouse development. *Gene Expr Patterns*, 7(4), 396-404. doi:10.1016/j.modgep.2006.11.008
- Papal, S., Cortese, M., Legendre, K., Sorusch, N., Dragavon, J., Sahly, I., . . . El-Amraoui, A. (2013). The giant spectrin betaV couples the molecular motors to phototransduction and Usher syndrome type I proteins along their trafficking route. *Hum Mol Genet*, 22(18), 3773-3788. doi:10.1093/hmg/ddt228

- Park, S. T., & Kim, J. (2016). Trends in Next-Generation Sequencing and a New Era for Whole Genome Sequencing. *Int Neurol J*, 20(Suppl 2), S76-83. doi:10.5213/inj.1632742.371
- Parker, R. O., & Crouch, R. K. (2010). Retinol dehydrogenases (RDHs) in the visual cycle. *Exp Eye Res*, 91(6), 788-792. doi:10.1016/j.exer.2010.08.013
- Parmar, T., Parmar, V. M., Perusek, L., Georges, A., Takahashi, M., Crabb, J. W., & Maeda, A. (2018). Lipocalin 2 Plays an Important Role in Regulating Inflammation in Retinal Degeneration. *J Immunol*. doi:10.4049/jimmunol.1701573
- Patil, V. S., Zhou, R., & Rana, T. M. (2014). Gene regulation by non-coding RNAs. *Crit Rev Biochem Mol Biol*, 49(1), 16-32. doi:10.3109/10409238.2013.844092
- Patricio, M. I., Barnard, A. R., Xue, K., & MacLaren, R. E. (2018). Choroideremia: molecular mechanisms and development of AAV gene therapy. *Expert Opin Biol Ther*, 18(7), 807-820. doi:10.1080/14712598.2018.1484448
- Peculis, R., Konrade, I., Skapare, E., Fridmanis, D., Nikitina-Zake, L., Lejnicks, A., . . . Klovins, J. (2013). Identification of glyoxalase 1 polymorphisms associated with enzyme activity. *Gene*, 515(1), 140-143. doi:10.1016/j.gene.2012.11.009
- Pedersen, L. B., Schroder, J. M., Satir, P., & Christensen, S. T. (2012). The ciliary cytoskeleton. *Compr Physiol*, 2(1), 779-803. doi:10.1002/cphy.c110043
- Pei, X. H., Bai, F., Tsutsui, T., Kiyokawa, H., & Xiong, Y. (2004). Genetic evidence for functional dependency of p18Ink4c on Cdk4. *Mol Cell Biol*, 24(15), 6653-6664. doi:10.1128/MCB.24.15.6653-6664.2004
- Peng, C. H., Chang, Y. L., Kao, C. L., Tseng, L. M., Wu, C. C., Chen, Y. C., . . . Chen, S. J. (2010). SirT1--a sensor for monitoring self-renewal and aging process in retinal stem cells. *Sensors (Basel)*, 10(6), 6172-6194. doi:10.3390/s100606172
- Pierrache, L. H. M., Kimchi, A., Ratnapriya, R., Roberts, L., Astuti, G. D. N., Obolensky, A., . . . Cremers, F. P. M. (2017). Whole-Exome Sequencing Identifies Biallelic IDH3A Variants as a Cause of Retinitis Pigmentosa Accompanied by Pseudocoloboma. *Ophthalmology*, 124(7), 992-1003. doi:10.1016/j.optha.2017.03.010
- Pinckers, A., van Aarem, A., & Keunen, J. E. (1993). Colour vision in retinitis pigmentosa. Influence of cystoid macular edema. *Int Ophthalmol*, 17(3), 143-146.
- Pinelli, M., Carissimo, A., Cutillo, L., Lai, C. H., Mutarelli, M., Moretti, M. N., . . . di Bernardo, D. (2016). An atlas of gene expression and gene co-regulation in the human retina. *Nucleic Acids Res*, 44(12), 5773-5784. doi:10.1093/nar/gkw486

- Piper, M., Dwivedy, A., Leung, L., Bradley, R. S., & Holt, C. E. (2008). NF-protocadherin and TAF1 regulate retinal axon initiation and elongation in vivo. *J Neurosci*, *28*(1), 100-105. doi:10.1523/JNEUROSCI.4490-07.2008
- Platon-Corchado, M., Barcelona, P. F., Jmaeff, S., Marchena, M., Hernandez-Pinto, A. M., Hernandez-Sanchez, C., . . . de la Rosa, E. J. (2017). p75(NTR) antagonists attenuate photoreceptor cell loss in murine models of retinitis pigmentosa. *Cell Death Dis*, *8*(7), e2922. doi:10.1038/cddis.2017.306
- Pokorny, J., Lutze, M., Cao, D., & Zele, A. J. (2008). The color of night: surface color categorization by color defective observers under dim illuminations. *Vis Neurosci*, *25*(3), 475-480. doi:10.1017/S0952523808080486
- Polato, F., Rusconi, P., Zangrossi, S., Morelli, F., Boeri, M., Musi, A., . . . Broggin, M. (2014). DRAGO (KIAA0247), a new DNA damage-responsive, p53-inducible gene that cooperates with p53 as oncosuppressor. [Corrected]. *J Natl Cancer Inst*, *106*(4), dju053. doi:10.1093/jnci/dju053
- Popp, S., Maurel, P., Andersen, J. S., & Margolis, R. U. (2004). Developmental changes of aggrecan, versican and neurocan in the retina and optic nerve. *Exp Eye Res*, *79*(3), 351-356. doi:10.1016/j.exer.2004.05.016
- Prigge, C. L., Yeh, P. T., Liou, N. F., Lee, C. C., You, S. F., Liu, L. L., . . . Zhang, D. Q. (2016). M1 ipRGCs Influence Visual Function through Retrograde Signaling in the Retina. *J Neurosci*, *36*(27), 7184-7197. doi:10.1523/JNEUROSCI.3500-15.2016
- Priya, S., Nampoothiri, S., Sen, P., & Sripriya, S. (2016). Bardet-Biedl syndrome: Genetics, molecular pathophysiology, and disease management. *Indian J Ophthalmol*, *64*(9), 620-627. doi:10.4103/0301-4738.194328
- Radeke, M. J., Radeke, C. M., Shih, Y. H., Hu, J., Bok, D., Johnson, L. V., & Coffey, P. J. (2015). Restoration of mesenchymal retinal pigmented epithelial cells by TGFbeta pathway inhibitors: implications for age-related macular degeneration. *Genome Med*, *7*(1), 58. doi:10.1186/s13073-015-0183-x
- Rajapakse, D., Chen, M., Curtis, T. M., & Xu, H. (2017). PKCzeta-dependent upregulation of p27kip1 contributes to oxidative stress induced retinal pigment epithelial cell multinucleation. *Aging (Albany NY)*. doi:10.18632/aging.101299
- Ramirez-Lopez, M. T., Arco, R., Decara, J., Vazquez, M., Rivera, P., Blanco, R. N., . . . Rodriguez de Fonseca, F. (2016). Long-Term Effects of Prenatal Exposure to Undernutrition on Cannabinoid Receptor-Related Behaviors: Sex and Tissue-Specific Alterations in the mRNA Expression of Cannabinoid Receptors and Lipid Metabolic Regulators. *Front Behav Neurosci*, *10*, 241. doi:10.3389/fnbeh.2016.00241

- Ramon, E., Cordomi, A., Aguila, M., Srinivasan, S., Dong, X., Moore, A. T., . . . Garriga, P. (2014). Differential light-induced responses in sectorial inherited retinal degeneration. *J Biol Chem*, *289*(52), 35918-35928. doi:10.1074/jbc.M114.609958
- Rath, M. F., Bailey, M. J., Kim, J. S., Coon, S. L., Klein, D. C., & Moller, M. (2009). Developmental and daily expression of the Pax4 and Pax6 homeobox genes in the rat retina: localization of Pax4 in photoreceptor cells. *J Neurochem*, *108*(1), 285-294. doi:10.1111/j.1471-4159.2008.05765.x
- Rattner, A., Smallwood, P. M., & Nathans, J. (2000). Identification and characterization of all-trans-retinol dehydrogenase from photoreceptor outer segments, the visual cycle enzyme that reduces all-trans-retinal to all-trans-retinol. *J Biol Chem*, *275*(15), 11034-11043.
- Ray, D., Bosselut, R., Ghysdael, J., Mattei, M. G., Tavitian, A., & Moreau-Gachelin, F. (1992). Characterization of Spi-B, a transcription factor related to the putative oncoprotein Spi-1/PU.1. *Mol Cell Biol*, *12*(10), 4297-4304.
- Raya, A., Revert, F., Navarro, S., & Saus, J. (1999). Characterization of a novel type of serine/threonine kinase that specifically phosphorylates the human goodpasture antigen. *J Biol Chem*, *274*(18), 12642-12649.
- Rayapudi, S., Schwartz, S. G., Wang, X., & Chavis, P. (2013). Vitamin A and fish oils for retinitis pigmentosa. *Cochrane Database Syst Rev*(12), CD008428. doi:10.1002/14651858.CD008428.pub2
- Reichman, S., Kalathur, R. K., Lambard, S., Ait-Ali, N., Yang, Y., Lardenois, A., . . . Leveillard, T. (2010). The homeobox gene CHX10/VSX2 regulates RdCVF promoter activity in the inner retina. *Hum Mol Genet*, *19*(2), 250-261. doi:10.1093/hmg/ddp484
- Reiff, C., Owczarek-Lipska, M., Spital, G., Roger, C., Hinz, H., Juschke, C., . . . Neidhardt, J. (2016). The mutation p.E113K in the Schiff base counterion of rhodopsin is associated with two distinct retinal phenotypes within the same family. *Sci Rep*, *6*, 36208. doi:10.1038/srep36208
- Reiter, J. F., & Leroux, M. R. (2017). Genes and molecular pathways underpinning ciliopathies. *Nat Rev Mol Cell Biol*, *18*(9), 533-547. doi:10.1038/nrm.2017.60
- Rheinbay, E., Suva, M. L., Gillespie, S. M., Wakimoto, H., Patel, A. P., Shahid, M., . . . Bernstein, B. E. (2013). An aberrant transcription factor network essential for Wnt signaling and stem cell maintenance in glioblastoma. *Cell Rep*, *3*(5), 1567-1579. doi:10.1016/j.celrep.2013.04.021

- Rice, D. S., Calandria, J. M., Gordon, W. C., Jun, B., Zhou, Y., Gelfman, C. M., . . . Bazan, N. G. (2015). Adiponectin receptor 1 conserves docosahexaenoic acid and promotes photoreceptor cell survival. *Nat Commun*, *6*, 6228. doi:10.1038/ncomms7228
- Riveiro-Alvarez, R., Xie, Y. A., Lopez-Martinez, M. A., Gambin, T., Perez-Carro, R., Avila-Fernandez, A., . . . Allikmets, R. (2015). New mutations in the RAB28 gene in 2 Spanish families with cone-rod dystrophy. *JAMA Ophthalmol*, *133*(2), 133-139. doi:10.1001/jamaophthalmol.2014.4266
- Rivera, A., White, K., Stohr, H., Steiner, K., Hemmrich, N., Grimm, T., . . . Weber, B. H. (2000). A comprehensive survey of sequence variation in the ABCA4 (ABCR) gene in Stargardt disease and age-related macular degeneration. *Am J Hum Genet*, *67*(4), 800-813. doi:10.1086/303090
- Roberts, A. E., Araki, T., Swanson, K. D., Montgomery, K. T., Schiripo, T. A., Joshi, V. A., . . . Kucherlapati, R. S. (2007). Germline gain-of-function mutations in SOS1 cause Noonan syndrome. *Nat Genet*, *39*(1), 70-74. doi:10.1038/ng1926
- Robinson, M. D., McCarthy, D. J., & Smyth, G. K. (2010). edgeR: a Bioconductor package for differential expression analysis of digital gene expression data. *Bioinformatics*, *26*(1), 139-140. doi:10.1093/bioinformatics/btp616
- Robinson, M. D., & Oshlack, A. (2010). A scaling normalization method for differential expression analysis of RNA-seq data. *Genome Biol*, *11*(3), R25. doi:10.1186/gb-2010-11-3-r25
- Robson, A. G., Lenassi, E., Saihan, Z., Luong, V. A., Fitzke, F. W., Holder, G. E., & Webster, A. R. (2012). Comparison of fundus autofluorescence with photopic and scotopic fine matrix mapping in patients with retinitis pigmentosa: 4- to 8-year follow-up. *Invest Ophthalmol Vis Sci*, *53*(10), 6187-6195. doi:10.1167/iovs.12-10195
- Robson, A. G., Nilsson, J., Li, S., Jalali, S., Fulton, A. B., Tormene, A. P., . . . Brodie, S. E. (2018). ISCEV guide to visual electrodiagnostic procedures. *Doc Ophthalmol*, *136*(1), 1-26. doi:10.1007/s10633-017-9621-y
- Roduit, R., & Schorderet, D. F. (2008). MAP kinase pathways in UV-induced apoptosis of retinal pigment epithelium ARPE19 cells. *Apoptosis*, *13*(3), 343-353. doi:10.1007/s10495-008-0179-8
- Roepman, R., & Wolfrum, U. (2007). Protein networks and complexes in photoreceptor cilia. *Subcell Biochem*, *43*, 209-235.
- Roubin, R., Acquaviva, C., Chevrier, V., Sedjai, F., Zyss, D., Birnbaum, D., & Rosnet, O. (2013). Myomegalin is necessary for the formation of centrosomal and Golgi-derived microtubules. *Biol Open*, *2*(2), 238-250. doi:10.1242/bio.20123392

- Rowland, B. D., & Peeper, D. S. (2006). KLF4, p21 and context-dependent opposing forces in cancer. *Nat Rev Cancer*, 6(1), 11-23. doi:10.1038/nrc1780
- Russell, S., Bennett, J., Wellman, J. A., Chung, D. C., Yu, Z. F., Tillman, A., . . . Maguire, A. M. (2017). Efficacy and safety of voretigene neparvovec (AAV2-hRPE65v2) in patients with RPE65-mediated inherited retinal dystrophy: a randomised, controlled, open-label, phase 3 trial. *Lancet*, 390(10097), 849-860. doi:10.1016/S0140-6736(17)31868-8
- Ruzickova, S., & Stanek, D. (2017). Mutations in spliceosomal proteins and retina degeneration. *RNA Biol*, 14(5), 544-552. doi:10.1080/15476286.2016.1191735
- Ryoo, H. D., Domingos, P. M., Kang, M. J., & Steller, H. (2007). Unfolded protein response in a Drosophila model for retinal degeneration. *EMBO J*, 26(1), 242-252. doi:10.1038/sj.emboj.7601477
- Saari, J. C., Nawrot, M., Stenkamp, R. E., Teller, D. C., & Garwin, G. G. (2009). Release of 11-cis-retinal from cellular retinaldehyde-binding protein by acidic lipids. *Mol Vis*, 15, 844-854.
- Sahu, B., & Maeda, A. (2016). Retinol Dehydrogenases Regulate Vitamin A Metabolism for Visual Function. *Nutrients*, 8(11). doi:10.3390/nu8110746
- Salinas, R. Y., Pearing, J. N., Ding, J. D., Spencer, W. J., Hao, Y., & Arshavsky, V. Y. (2017). Photoreceptor discs form through peripherin-dependent suppression of ciliary ectosome release. *J Cell Biol*, 216(5), 1489-1499. doi:10.1083/jcb.201608081
- Salmon, A. E., Cooper, R. F., Langlo, C. S., Baghaie, A., Dubra, A., & Carroll, J. (2017). An Automated Reference Frame Selection (ARFS) Algorithm for Cone Imaging with Adaptive Optics Scanning Light Ophthalmoscopy. *Transl Vis Sci Technol*, 6(2), 9. doi:10.1167/tvst.6.2.9
- Santosh, B., Varshney, A., & Yadava, P. K. (2015). Non-coding RNAs: biological functions and applications. *Cell Biochem Funct*, 33(1), 14-22. doi:10.1002/cbf.3079
- Scherer, S. W., Feinstein, D. S., Oliveira, L., Tsui, L. C., & Pittler, S. J. (1996). Gene structure and chromosome localization to 7q21.3 of the human rod photoreceptor transducin gamma-subunit gene (GNGT1). *Genomics*, 35(1), 241-243. doi:10.1006/geno.1996.0346
- Schmidt-Kastner, R., Kreczmanski, P., Preising, M., Diederer, R., Schmitz, C., Reis, D., . . . Dorey, C. K. (2009). Expression of the diabetes risk gene wolframin (WFS1) in the human retina. *Exp Eye Res*, 89(4), 568-574. doi:10.1016/j.exer.2009.05.007
- Schmidt-Kastner, R., Yamamoto, H., Hamasaki, D., Yamamoto, H., Parel, J. M., Schmitz, C., . . . Preising, M. N. (2008). Hypoxia-regulated components of the U4/U6.U5 tri-small

- nuclear riboprotein complex: possible role in autosomal dominant retinitis pigmentosa. *Mol Vis*, *14*, 125-135.
- Scholl, H. P., Moore, A. T., Koenekoop, R. K., Wen, Y., Fishman, G. A., van den Born, L. I., . . . Group, R. I. S. (2015). Safety and Proof-of-Concept Study of Oral QLT091001 in Retinitis Pigmentosa Due to Inherited Deficiencies of Retinal Pigment Epithelial 65 Protein (RPE65) or Lecithin:Retinol Acyltransferase (LRAT). *PLoS One*, *10*(12), e0143846. doi:10.1371/journal.pone.0143846
- Schuerch, K., Woods, R. L., Lee, W., Duncker, T., Delori, F. C., Allikmets, R., . . . Sparrow, J. R. (2017). Quantifying Fundus Autofluorescence in Patients With Retinitis Pigmentosa. *Invest Ophthalmol Vis Sci*, *58*(3), 1843-1855. doi:10.1167/iovs.16-21302
- Schuster, A., Janecke, A. R., Wilke, R., Schmid, E., Thompson, D. A., Utermann, G., . . . Gal, A. (2007). The phenotype of early-onset retinal degeneration in persons with RDH12 mutations. *Invest Ophthalmol Vis Sci*, *48*(4), 1824-1831. doi:10.1167/iovs.06-0628
- Schwartz, S. B., Aleman, T. S., Cideciyan, A. V., Swaroop, A., Jacobson, S. G., & Stone, E. M. (2003). De novo mutation in the RP1 gene (Arg677ter) associated with retinitis pigmentosa. *Invest Ophthalmol Vis Sci*, *44*(8), 3593-3597.
- Schwarz, N., Lane, A., Jovanovic, K., Parfitt, D. A., Aguila, M., Thompson, C. L., . . . Cheetham, M. E. (2017a). Arl3 and RP2 regulate the trafficking of ciliary tip kinesins. *Hum Mol Genet*, *26*(17), 3451. doi:10.1093/hmg/ddx245
- Schwarz, N., Lane, A., Jovanovic, K., Parfitt, D. A., Aguila, M., Thompson, C. L., . . . Cheetham, M. E. (2017b). Arl3 and RP2 regulate the trafficking of ciliary tip kinesins. *Hum Mol Genet*, *26*(13), 2480-2492. doi:10.1093/hmg/ddx143
- Scimone, C., Bramanti, P., Alafaci, C., Granata, F., Piva, F., Rinaldi, C., . . . D'Angelo, R. (2017). Update on Novel CCM Gene Mutations in Patients with Cerebral Cavernous Malformations. *J Mol Neurosci*, *61*(2), 189-198. doi:10.1007/s12031-016-0863-z
- Scimone, C., Bramanti, P., Ruggeri, A., Donato, L., Alafaci, C., Crisafulli, C., . . . D'Angelo, R. (2016). CCM3/SERPINI1 bidirectional promoter variants in patients with cerebral cavernous malformations: a molecular and functional study. *BMC Med Genet*, *17*(1), 74. doi:10.1186/s12881-016-0332-0
- Scimone, C., Bramanti, P., Ruggeri, A., Katsarou, Z., Donato, L., Sidoti, A., & D'Angelo, R. (2015). Detection of Novel Mutation in Ccm3 Causes Familial Cerebral Cavernous Malformations. *J Mol Neurosci*, *57*(3), 400-403. doi:10.1007/s12031-015-0606-6
- Scimone, C., Donato, L., Esposito, T., Rinaldi, C., D'Angelo, R., & Sidoti, A. (2017). A novel RLBP1 gene geographical area-related mutation present in a young patient with

- retinitis punctata albescens. *Hum Genomics*, 11(1), 18. doi:10.1186/s40246-017-0114-6
- Sentinelli, F., Minicocci, I., Montali, A., Nanni, L., Romeo, S., Incani, M., . . . Baroni, M. G. (2013). Association of RXR-Gamma Gene Variants with Familial Combined Hyperlipidemia: Genotype and Haplotype Analysis. *J Lipids*, 2013, 517943. doi:10.1155/2013/517943
- Sepehri, S., & Hernandez, N. (1997). The largest subunit of human RNA polymerase III is closely related to the largest subunit of yeast and trypanosome RNA polymerase III. *Genome Res*, 7(10), 1006-1019.
- Sethna, S., Chamakkala, T., Gu, X., Thompson, T. C., Cao, G., Elliott, M. H., & Finnemann, S. C. (2016). Regulation of Phagolysosomal Digestion by Caveolin-1 of the Retinal Pigment Epithelium Is Essential for Vision. *J Biol Chem*, 291(12), 6494-6506. doi:10.1074/jbc.M115.687004
- Shamoto, N., Narita, K., Kubo, T., Oda, T., & Takeda, S. (2018). CFAP70 Is a Novel Axoneme-Binding Protein That Localizes at the Base of the Outer Dynein Arm and Regulates Ciliary Motility. *Cells*, 7(9). doi:10.3390/cells7090124
- Shannon, P., Markiel, A., Ozier, O., Baliga, N. S., Wang, J. T., Ramage, D., . . . Ideker, T. (2003). Cytoscape: a software environment for integrated models of biomolecular interaction networks. *Genome Res*, 13(11), 2498-2504. doi:10.1101/gr.1239303
- Shapshak, P. (2012). Molecule of the month, PDE4DIP. *Bioinformatics*, 8(16), 740-741. doi:10.6026/97320630008740
- Sharif, W., & Sharif, Z. (2017). Leber's congenital amaurosis and the role of gene therapy in congenital retinal disorders. *Int J Ophthalmol*, 10(3), 480-484. doi:10.18240/ijo.2017.03.24
- Sharma, Y. V., Cojocaru, R. I., Ritter, L. M., Khattree, N., Brooks, M., Scott, A., . . . Goldberg, A. F. (2012). Protective gene expression changes elicited by an inherited defect in photoreceptor structure. *PLoS One*, 7(2), e31371. doi:10.1371/journal.pone.0031371
- Shastry, B. S., & Trese, M. T. (1997). Identification of a polymorphic missense (G338D) and silent (106V and 121L) mutations within the coding region of the peripherin/RDS gene in a patient with retinitis punctata albescens. *Biochem Biophys Res Commun*, 231(1), 103-105. doi:10.1006/bbrc.1997.6052
- Shaw, P. X., Stiles, T., Douglas, C., Ho, D., Fan, W., Du, H., & Xiao, X. (2016). Oxidative stress, innate immunity, and age-related macular degeneration. *AIMS Mol Sci*, 3(2), 196-221. doi:10.3934/molsci.2016.2.196

- Shemesh, A., & Margolin, E. (2018). Kearns Sayre Syndrome. In *StatPearls*. Treasure Island (FL).
- Sheng, X., Zhang, X., Wu, W., Zhuang, W., Meng, R., & Rong, W. (2008). Variants of RP1 gene in Chinese patients with autosomal dominant retinitis pigmentosa. *Can J Ophthalmol*, *43*(2), 208-212. doi:10.3129/i08-004
- Shin, J. A., Kim, H. S., Vargas, A., Yu, W. Q., Eom, Y. S., Craft, C. M., & Lee, E. J. (2016). Inhibition of Matrix Metalloproteinase 9 Enhances Rod Survival in the S334ter-line3 Retinitis Pigmentosa Model. *PLoS One*, *11*(11), e0167102. doi:10.1371/journal.pone.0167102
- Shinde, V., Kotla, P., Strang, C., & Gorbatyuk, M. (2016). Unfolded protein response-induced dysregulation of calcium homeostasis promotes retinal degeneration in rat models of autosomal dominant retinitis pigmentosa. *Cell Death Dis*, *7*, e2085. doi:10.1038/cddis.2015.325
- Shokravi, M. T., & Dryja, T. P. (1993). Retinitis pigmentosa and the rhodopsin gene. *Int Ophthalmol Clin*, *33*(2), 219-228.
- Siemiakowska, A. M., van den Born, L. I., van Hagen, P. M., Stoffels, M., Neveling, K., Henkes, A., . . . Collin, R. W. (2013). Mutations in the mevalonate kinase (MVK) gene cause nonsyndromic retinitis pigmentosa. *Ophthalmology*, *120*(12), 2697-2705. doi:10.1016/j.ophtha.2013.07.052
- Simon, P., Schott, K., Williams, R. W., & Schaeffel, F. (2004). Posttranscriptional regulation of the immediate-early gene EGR1 by light in the mouse retina. *Eur J Neurosci*, *20*(12), 3371-3377. doi:10.1111/j.1460-9568.2004.03811.x
- Slaby, O., Laga, R., & Sedlacek, O. (2017). Therapeutic targeting of non-coding RNAs in cancer. *Biochem J*, *474*(24), 4219-4251. doi:10.1042/BCJ20170079
- Slatkin, M., & Rannala, B. (2000). Estimating allele age. *Annu Rev Genomics Hum Genet*, *1*, 225-249. doi:10.1146/annurev.genom.1.1.225
- Song, L., Wormann, S., Ai, J., Neuhofer, P., Lesina, M., Diakopoulos, K. N., . . . Algul, H. (2016). BCL3 Reduces the Sterile Inflammatory Response in Pancreatic and Biliary Tissues. *Gastroenterology*, *150*(2), 499-512 e420. doi:10.1053/j.gastro.2015.10.017
- Song, X., Zhang, N., Han, P., Moon, B. S., Lai, R. K., Wang, K., & Lu, W. (2016). Circular RNA profile in gliomas revealed by identification tool UROBORUS. *Nucleic Acids Res*, *44*(9), e87. doi:10.1093/nar/gkw075
- Sorrentino, F. S., Bonifazzi, C., & Perri, P. (2015). The Role of the Endothelin System in the Vascular Dysregulation Involved in Retinitis Pigmentosa. *J Ophthalmol*, *2015*, 405234. doi:10.1155/2015/405234

- Sorrentino, F. S., Gallenga, C. E., Bonifazzi, C., & Perri, P. (2016). A challenge to the striking genotypic heterogeneity of retinitis pigmentosa: a better understanding of the pathophysiology using the newest genetic strategies. *Eye (Lond)*, *30*(12), 1542-1548. doi:10.1038/eye.2016.197
- Souied, E., Soubrane, G., Benlian, P., Coscas, G. J., Gerber, S., Munnich, A., & Kaplan, J. (1996). Retinitis punctata albescens associated with the Arg135Trp mutation in the rhodopsin gene. *Am J Ophthalmol*, *121*(1), 19-25.
- Stanton, C. M., Borooah, S., Drake, C., Marsh, J. A., Campbell, S., Lennon, A., . . . Hayward, C. (2017). Novel pathogenic mutations in C1QTNF5 support a dominant negative disease mechanism in late-onset retinal degeneration. *Sci Rep*, *7*(1), 12147. doi:10.1038/s41598-017-11898-3
- Stecher, H., Gelb, M. H., Saari, J. C., & Palczewski, K. (1999). Preferential release of 11-cis-retinol from retinal pigment epithelial cells in the presence of cellular retinaldehyde-binding protein. *J Biol Chem*, *274*(13), 8577-8585.
- Steinberg, R. H., Fisher, S. K., & Anderson, D. H. (1980). Disc morphogenesis in vertebrate photoreceptors. *J Comp Neurol*, *190*(3), 501-508. doi:10.1002/cne.901900307
- Steketee, M. B., Oboudiyat, C., Daneman, R., Trakhtenberg, E., Lamoureux, P., Weinstein, J. E., . . . Goldberg, J. L. (2014). Regulation of intrinsic axon growth ability at retinal ganglion cell growth cones. *Invest Ophthalmol Vis Sci*, *55*(7), 4369-4377. doi:10.1167/iovs.14-13882
- Stingl, K., Schippert, R., Bartz-Schmidt, K. U., Besch, D., Cottrill, C. L., Edwards, T. L., . . . Zrenner, E. (2017). Interim Results of a Multicenter Trial with the New Electronic Subretinal Implant Alpha AMS in 15 Patients Blind from Inherited Retinal Degenerations. *Front Neurosci*, *11*, 445. doi:10.3389/fnins.2017.00445
- Strissel, K. J., Lishko, P. V., Trieu, L. H., Kennedy, M. J., Hurley, J. B., & Arshavsky, V. Y. (2005). Recoverin undergoes light-dependent intracellular translocation in rod photoreceptors. *J Biol Chem*, *280*(32), 29250-29255. doi:10.1074/jbc.M501789200
- Strong, S., Liew, G., & Michaelides, M. (2017). Retinitis pigmentosa-associated cystoid macular oedema: pathogenesis and avenues of intervention. *Br J Ophthalmol*, *101*(1), 31-37. doi:10.1136/bjophthalmol-2016-309376
- Sugitani, K., Koriyama, Y., Ogai, K., Wakasugi, K., & Kato, S. (2016). A Possible Role of Neuroglobin in the Retina After Optic Nerve Injury: A Comparative Study of Zebrafish and Mouse Retina. *Adv Exp Med Biol*, *854*, 671-675. doi:10.1007/978-3-319-17121-0_89

- Sujirakul, T., Lin, M. K., Duong, J., Wei, Y., Lopez-Pintado, S., & Tsang, S. H. (2015). Multimodal Imaging of Central Retinal Disease Progression in a 2-Year Mean Follow-up of Retinitis Pigmentosa. *Am J Ophthalmol*, *160*(4), 786-798 e784. doi:10.1016/j.ajo.2015.06.032
- Sumioka, A., Brown, T. E., Kato, A. S., Brecht, D. S., Kauer, J. A., & Tomita, S. (2011). PDZ binding of TARPgamma-8 controls synaptic transmission but not synaptic plasticity. *Nat Neurosci*, *14*(11), 1410-1412. doi:10.1038/nn.2952
- Sundaramurthy, S., Swaminathan, M., Sen, P., Arokiasamy, T., Deshpande, S., John, N., . . . Soumittra, N. (2016). Homozygosity mapping guided next generation sequencing to identify the causative genetic variation in inherited retinal degenerative diseases. *J Hum Genet*, *61*(11), 951-958. doi:10.1038/jhg.2016.83
- Suzuki, E., Kessler, M., & Arai, A. C. (2008). The fast kinetics of AMPA GluR3 receptors is selectively modulated by the TARPs gamma 4 and gamma 8. *Mol Cell Neurosci*, *38*(1), 117-123. doi:10.1016/j.mcn.2008.01.018
- Suzuki, Y., Shimada, J., Shudo, K., Matsumura, M., Crippa, M. P., & Kojima, S. (1999). Physical interaction between retinoic acid receptor and Sp1: mechanism for induction of urokinase by retinoic acid. *Blood*, *93*(12), 4264-4276.
- Swaroop, A., Kim, D., & Forrester, D. (2010). Transcriptional regulation of photoreceptor development and homeostasis in the mammalian retina. *Nat Rev Neurosci*, *11*(8), 563-576. doi:10.1038/nrn2880
- Swiersy, A., Klapper, S. D., & Busskamp, V. (2017). [Optogenetics: A Therapeutic Option for Advanced Retinal Dystrophies]. *Klin Monbl Augenheilkd*, *234*(3), 335-342. doi:10.1055/s-0043-101820
- Szabo, L., Morey, R., Palpant, N. J., Wang, P. L., Afari, N., Jiang, C., . . . Salzman, J. (2015). Statistically based splicing detection reveals neural enrichment and tissue-specific induction of circular RNA during human fetal development. *Genome Biol*, *16*, 126. doi:10.1186/s13059-015-0690-5
- Szklarczyk, D., Franceschini, A., Wyder, S., Forslund, K., Heller, D., Huerta-Cepas, J., . . . von Mering, C. (2015). STRING v10: protein-protein interaction networks, integrated over the tree of life. *Nucleic Acids Res*, *43*(Database issue), D447-452. doi:10.1093/nar/gku1003
- Tachibanaki, S., & Kawamura, S. (2005). [Molecular mechanisms of how we see]. *Tanpakushitsu Kakusan Koso*, *50*(15), 1979-1987.

- Tachikawa, M., Toki, H., Tomi, M., & Hosoya, K. (2008). Gene expression profiles of ATP-binding cassette transporter A and C subfamilies in mouse retinal vascular endothelial cells. *Microvasc Res*, *75*(1), 68-72. doi:10.1016/j.mvr.2007.05.002
- Talib, M., van Schooneveld, M. J., van Genderen, M. M., Wijnholds, J., Florijn, R. J., Ten Brink, J. B., . . . Boon, C. J. F. (2017). Genotypic and Phenotypic Characteristics of CRB1-Associated Retinal Dystrophies: A Long-Term Follow-up Study. *Ophthalmology*, *124*(6), 884-895. doi:10.1016/j.ophtha.2017.01.047
- Tanackovic, G., Ransijn, A., Thibault, P., Abou Elela, S., Klinck, R., Berson, E. L., . . . Rivolta, C. (2011). PRPF mutations are associated with generalized defects in spliceosome formation and pre-mRNA splicing in patients with retinitis pigmentosa. *Hum Mol Genet*, *20*(11), 2116-2130. doi:10.1093/hmg/ddr094
- Tang, K., Xie, X., Park, J. I., Jamrich, M., Tsai, S., & Tsai, M. J. (2010). COUP-TFs regulate eye development by controlling factors essential for optic vesicle morphogenesis. *Development*, *137*(5), 725-734. doi:10.1242/dev.040568
- Tang, P. H., Kono, M., Koutalos, Y., Ablonczy, Z., & Crouch, R. K. (2013). New insights into retinoid metabolism and cycling within the retina. *Prog Retin Eye Res*, *32*, 48-63. doi:10.1016/j.preteyeres.2012.09.002
- Tang, Z., Zhang, Y., Wang, Y., Zhang, D., Shen, B., Luo, M., & Gu, P. (2017). Progress of stem/progenitor cell-based therapy for retinal degeneration. *J Transl Med*, *15*(1), 99. doi:10.1186/s12967-017-1183-y
- Tarcea, V. G., Weymouth, T., Ade, A., Bookvich, A., Gao, J., Mahavisno, V., . . . Jagadish, H. V. (2009). Michigan molecular interactions r2: from interacting proteins to pathways. *Nucleic Acids Res*, *37*(Database issue), D642-646. doi:10.1093/nar/gkn722
- Taschner, M., Weber, K., Mourao, A., Vetter, M., Awasthi, M., Stiegler, M., . . . Lorentzen, E. (2016). Intraflagellar transport proteins 172, 80, 57, 54, 38, and 20 form a stable tubulin-binding IFT-B2 complex. *EMBO J*, *35*(7), 773-790. doi:10.15252/embj.201593164
- Telegina, D. V., Korbolina, E. E., Ershov, N. I., Kolosova, N. G., & Kozhevnikova, O. S. (2015). Identification of functional networks associated with cell death in the retina of OXYS rats during the development of retinopathy. *Cell Cycle*, *14*(22), 3544-3556. doi:10.1080/15384101.2015.1080399
- Teussink, M. M., Lambertus, S., de Mul, F. F., Rozanowska, M. B., Hoyng, C. B., Klevering, B. J., & Theelen, T. (2017). Lipofuscin-associated photo-oxidative stress during fundus autofluorescence imaging. *PLoS One*, *12*(2), e0172635. doi:10.1371/journal.pone.0172635

- The Gene Ontology, C. (2017). Expansion of the Gene Ontology knowledgebase and resources. *Nucleic Acids Res*, 45(D1), D331-D338. doi:10.1093/nar/gkw1108
- The UniProt, C. (2017). UniProt: the universal protein knowledgebase. *Nucleic Acids Res*, 45(D1), D158-D169. doi:10.1093/nar/gkw1099
- Thiesen, H. J., Bellefroid, E., Revelant, O., & Martial, J. A. (1991). Conserved KRAB protein domain identified upstream from the zinc finger region of Kox 8. *Nucleic Acids Res*, 19(14), 3996.
- Tian, L., Greenberg, S. A., Kong, S. W., Altschuler, J., Kohane, I. S., & Park, P. J. (2005). Discovering statistically significant pathways in expression profiling studies. *Proc Natl Acad Sci U S A*, 102(38), 13544-13549. doi:10.1073/pnas.0506577102
- Torres, M., Gomez-Pardo, E., & Gruss, P. (1996). Pax2 contributes to inner ear patterning and optic nerve trajectory. *Development*, 122(11), 3381-3391.
- Toth, K. F., Pezic, D., Stuwe, E., & Webster, A. (2016). The piRNA Pathway Guards the Germline Genome Against Transposable Elements. *Adv Exp Med Biol*, 886, 51-77. doi:10.1007/978-94-017-7417-8_4
- Trapnell, C., Hendrickson, D. G., Sauvageau, M., Goff, L., Rinn, J. L., & Pachter, L. (2013). Differential analysis of gene regulation at transcript resolution with RNA-seq. *Nat Biotechnol*, 31(1), 46-53. doi:10.1038/nbt.2450
- Travis, G. H., Golczak, M., Moise, A. R., & Palczewski, K. (2007). Diseases caused by defects in the visual cycle: retinoids as potential therapeutic agents. *Annu Rev Pharmacol Toxicol*, 47, 469-512. doi:10.1146/annurev.pharmtox.47.120505.105225
- Trimarchi, J. M., Fairchild, B., Verona, R., Moberg, K., Andon, N., & Lees, J. A. (1998). E2F-6, a member of the E2F family that can behave as a transcriptional repressor. *Proc Natl Acad Sci U S A*, 95(6), 2850-2855.
- Tu, K., Liu, Z., Yao, B., Xue, Y., Xu, M., Dou, C., . . . Wang, J. (2016). BCL-3 promotes the tumor growth of hepatocellular carcinoma by regulating cell proliferation and the cell cycle through cyclin D1. *Oncol Rep*, 35(4), 2382-2390. doi:10.3892/or.2016.4616
- Tzeng, D. T., Tseng, Y. T., Ung, M., Liao, I. E., Liu, C. C., & Cheng, C. (2014). DPRP: a database of phenotype-specific regulatory programs derived from transcription factor binding data. *Nucleic Acids Res*, 42(Database issue), D178-183. doi:10.1093/nar/gkt1254
- Uhlen, M., Zhang, C., Lee, S., Sjostedt, E., Fagerberg, L., Bidkhori, G., . . . Ponten, F. (2017). A pathology atlas of the human cancer transcriptome. *Science*, 357(6352). doi:10.1126/science.aan2507

- Valverde, D., Riveiro-Alvarez, R., Aguirre-Lamban, J., Baiget, M., Carballo, M., Antinolo, G., . . . Ayuso, C. (2007). Spectrum of the ABCA4 gene mutations implicated in severe retinopathies in Spanish patients. *Invest Ophthalmol Vis Sci*, *48*(3), 985-990. doi:10.1167/iovs.06-0307
- van den Born, L. I., van Soest, S., van Schooneveld, M. J., Riemsdag, F. C., de Jong, P. T., & Bleeker-Wagemakers, E. M. (1994). Autosomal recessive retinitis pigmentosa with preserved para-arteriolar retinal pigment epithelium. *Am J Ophthalmol*, *118*(4), 430-439.
- van Huet, R. A., Collin, R. W., Siemiakowska, A. M., Klaver, C. C., Hoyng, C. B., Simonelli, F., . . . Klevering, B. J. (2014). IMPG2-associated retinitis pigmentosa displays relatively early macular involvement. *Invest Ophthalmol Vis Sci*, *55*(6), 3939-3953. doi:10.1167/iovs.14-14129
- van Trier, D. C., Vos, A. M., Draaijer, R. W., van der Burgt, I., Draaisma, J. M., & Cruysberg, J. R. (2016). Ocular Manifestations of Noonan Syndrome: A Prospective Clinical and Genetic Study of 25 Patients. *Ophthalmology*, *123*(10), 2137-2146. doi:10.1016/j.ophtha.2016.06.061
- Van Woerkom, C., & Ferrucci, S. (2005). Sector retinitis pigmentosa. *Optometry*, *76*(5), 309-317.
- Vasireddy, V., Jablonski, M. M., Khan, N. W., Wang, X. F., Sahu, P., Sparrow, J. R., & Ayyagari, R. (2009). Elov14 5-bp deletion knock-in mouse model for Stargardt-like macular degeneration demonstrates accumulation of ELOVL4 and lipofuscin. *Exp Eye Res*, *89*(6), 905-912. doi:10.1016/j.exer.2009.07.021
- Velez, G., Machlab, D. A., Tang, P. H., Sun, Y., Tsang, S. H., Bassuk, A. G., & Mahajan, V. B. (2018). Proteomic analysis of the human retina reveals region-specific susceptibilities to metabolic- and oxidative stress-related diseases. *PLoS One*, *13*(2), e0193250. doi:10.1371/journal.pone.0193250
- Verbakel, S. K., van Huet, R. A. C., Boon, C. J. F., den Hollander, A. I., Collin, R. W. J., Klaver, C. C. W., . . . Klevering, B. J. (2018). Non-syndromic retinitis pigmentosa. *Prog Retin Eye Res*. doi:10.1016/j.preteyeres.2018.03.005
- Verhagen, F., Kuiper, J., Nierkens, S., Imhof, S. M., Radstake, T., & de Boer, J. (2016). Systemic inflammatory immune signatures in a patient with CRB1 linked retinal dystrophy. *Expert Rev Clin Immunol*, *12*(12), 1359-1362. doi:10.1080/1744666X.2016.1241709

- Vieira, V., de la Houssaye, G., Lacassagne, E., Dufier, J. L., Jais, J. P., Beermann, F., . . . Abitbol, M. (2008). Differential regulation of Dlg1, Scrib, and Lgl1 expression in a transgenic mouse model of ocular cancer. *Mol Vis*, *14*, 2390-2403.
- Villarreal, G., Jr., Zhang, Y., Larman, H. B., Gracia-Sancho, J., Koo, A., & Garcia-Cardena, G. (2010). Defining the regulation of KLF4 expression and its downstream transcriptional targets in vascular endothelial cells. *Biochem Biophys Res Commun*, *391*(1), 984-989. doi:10.1016/j.bbrc.2009.12.002
- Volders, P. J., Verheggen, K., Menschaert, G., Vandepoele, K., Martens, L., Vandesompele, J., & Mestdagh, P. (2015). An update on LNCipedia: a database for annotated human lncRNA sequences. *Nucleic Acids Res*, *43*(Database issue), D174-180. doi:10.1093/nar/gku1060
- Wagner, S. K., Jolly, J. K., Pefkianaki, M., Gekeler, F., Webster, A. R., Downes, S. M., & Maclaren, R. E. (2017). Transcorneal electrical stimulation for the treatment of retinitis pigmentosa: results from the TESOLAUk trial. *BMJ Open Ophthalmol*, *2*(1), e000096. doi:10.1136/bmjophth-2017-000096
- Wain, H. M., Bruford, E. A., Lovering, R. C., Lush, M. J., Wright, M. W., & Povey, S. (2002). Guidelines for human gene nomenclature. *Genomics*, *79*(4), 464-470. doi:10.1006/geno.2002.6748
- Wakabayashi, T., Sawa, M., Gomi, F., & Tsujikawa, M. (2010). Correlation of fundus autofluorescence with photoreceptor morphology and functional changes in eyes with retinitis pigmentosa. *Acta Ophthalmol*, *88*(5), e177-183. doi:10.1111/j.1755-3768.2010.01926.x
- Wang, D. Y., Chan, W. M., Tam, P. O., Chiang, S. W., Lam, D. S., Chong, K. K., & Pang, C. P. (2005). Genetic markers for retinitis pigmentosa. *Hong Kong Med J*, *11*(4), 281-288.
- Wang, D. Y., Fan, B. J., Chan, W. M., Tam, O. S., Chiang, W. Y., Lam, S. C., & Pang, C. P. (2005). [Digenic association of RHO and RP1 genes with retinitis pigmentosa among Chinese population in Hong Kong]. *Zhonghua Yi Xue Za Zhi*, *85*(23), 1613-1617.
- Wang, G. L., Lu, N., Zhang, F., Peng, X. Y., Li, Y., & Wang, M. Y. (2005). [The characteristics of retinitis pigmentosa with retinal vascular occlusion]. *Zhonghua Yan Ke Za Zhi*, *41*(5), 414-418.
- Wang, H., Cui, X., Gu, Q., Chen, Y., Zhou, J., Kuang, Y., . . . Xu, X. (2012). Retinol dehydrogenase 13 protects the mouse retina from acute light damage. *Mol Vis*, *18*, 1021-1030.

- Wang, H., Wang, M., Yang, N., & Xu, R. M. (2015). Structure of the quaternary complex of histone H3-H4 heterodimer with chaperone ASF1 and the replicative helicase subunit MCM2. *Protein Cell*, 6(9), 693-697. doi:10.1007/s13238-015-0190-0
- Wang, L., Cano, M., Datta, S., Wei, H., Ebrahimi, K. B., Gorashi, Y., . . . Handa, J. T. (2016). Pentraxin 3 recruits complement factor H to protect against oxidative stress-induced complement and inflammasome overactivation. *J Pathol*, 240(4), 495-506. doi:10.1002/path.4811
- Wang, P., Xu, T. Y., Wei, K., Guan, Y. F., Wang, X., Xu, H., . . . Miao, C. Y. (2014). ARRB1/beta-arrestin-1 mediates neuroprotection through coordination of BECN1-dependent autophagy in cerebral ischemia. *Autophagy*, 10(9), 1535-1548. doi:10.4161/auto.29203
- Wang, S., Liu, S., Mao, J., & Wen, D. (2014). Effect of retinoic acid on the tight junctions of the retinal pigment epithelium-choroid complex of guinea pigs with lens-induced myopia in vivo. *Int J Mol Med*, 33(4), 825-832. doi:10.3892/ijmm.2014.1651
- Wang, W., Lee, S. J., Scott, P. A., Lu, X., Emery, D., Liu, Y., . . . Dean, D. C. (2016). Two-Step Reactivation of Dormant Cones in Retinitis Pigmentosa. *Cell Rep*, 15(2), 372-385. doi:10.1016/j.celrep.2016.03.022
- Wang, Y., Wong, M. M., Zhang, X., & Chiu, S. K. (2015). Ectopic AP4 expression induces cellular senescence via activation of p53 in long-term confluent retinal pigment epithelial cells. *Exp Cell Res*, 339(1), 135-146. doi:10.1016/j.yexcr.2015.09.013
- Warde-Farley, D., Donaldson, S. L., Comes, O., Zuberi, K., Badrawi, R., Chao, P., . . . Morris, Q. (2010). The GeneMANIA prediction server: biological network integration for gene prioritization and predicting gene function. *Nucleic Acids Res*, 38(Web Server issue), W214-220. doi:10.1093/nar/gkq537
- Webster, A. R., Heon, E., Lotery, A. J., Vandenberg, K., Casavant, T. L., Oh, K. T., . . . Stone, E. M. (2001). An analysis of allelic variation in the ABCA4 gene. *Invest Ophthalmol Vis Sci*, 42(6), 1179-1189.
- Wei, W., Li, L., Zhang, Y., Geriletu, Yang, J., Zhang, Y., & Xing, Y. (2014). Vitamin C protected human retinal pigmented epithelium from oxidant injury depending on regulating SIRT1. *ScientificWorldJournal*, 2014, 750634. doi:10.1155/2014/750634
- Weischenfeldt, J., Lykke-Andersen, J., & Porse, B. (2005). Messenger RNA surveillance: neutralizing natural nonsense. *Curr Biol*, 15(14), R559-562. doi:10.1016/j.cub.2005.07.002

- Wen, R., Dallman, J. E., Li, Y., Zuchner, S. L., Vance, J. M., Pericak-Vance, M. A., & Lam, B. L. (2014). Knock-down DHDDS expression induces photoreceptor degeneration in zebrafish. *Adv Exp Med Biol*, *801*, 543-550. doi:10.1007/978-1-4614-3209-8_69
- Wen, Y., Locke, K. G., Klein, M., Bowne, S. J., Sullivan, L. S., Ray, J. W., . . . Hughbanks-Wheaton, D. K. (2011). Phenotypic characterization of 3 families with autosomal dominant retinitis pigmentosa due to mutations in KLHL7. *Arch Ophthalmol*, *129*(11), 1475-1482. doi:10.1001/archophthalmol.2011.307
- Williams, D. S., & Lopes, V. S. (2011). The many different cellular functions of MYO7A in the retina. *Biochem Soc Trans*, *39*(5), 1207-1210. doi:10.1042/BST0391207
- Wilusz, J. E., & Wilusz, J. (2014). Nonsense-mediated RNA decay: at the 'cutting edge' of regulated snoRNA production. *Genes Dev*, *28*(22), 2447-2449. doi:10.1101/gad.254193.114
- Wren, K. N., Craft, J. M., Tritchler, D., Schauer, A., Patel, D. K., Smith, E. F., . . . Lechtreck, K. F. (2013). A differential cargo-loading model of ciliary length regulation by IFT. *Curr Biol*, *23*(24), 2463-2471. doi:10.1016/j.cub.2013.10.044
- Wright, K. J., Baye, L. M., Olivier-Mason, A., Mukhopadhyay, S., Sang, L., Kwong, M., . . . Jackson, P. K. (2011). An ARL3-UNC119-RP2 GTPase cycle targets myristoylated NPHP3 to the primary cilium. *Genes Dev*, *25*(22), 2347-2360. doi:10.1101/gad.173443.111
- Wu, C. X., Zhao, W. P., Kishi, H., Dokan, J., Jin, Z. X., Wei, X. C., . . . Muraguchi, A. (2004). Activation of mouse RAG-2 promoter by Myc-associated zinc finger protein. *Biochem Biophys Res Commun*, *317*(4), 1096-1102. doi:10.1016/j.bbrc.2004.03.159
- Wu, Z., Hasan, A., Liu, T., Teller, D. C., & Crabb, J. W. (2004). Identification of CRALBP ligand interactions by photoaffinity labeling, hydrogen/deuterium exchange, and structural modeling. *J Biol Chem*, *279*(26), 27357-27364. doi:10.1074/jbc.M401960200
- Wucher, V., Legeai, F., Hedan, B., Rizk, G., Lagoutte, L., Leeb, T., . . . Derrien, T. (2017). FEELnc: a tool for long non-coding RNA annotation and its application to the dog transcriptome. *Nucleic Acids Res*, *45*(8), e57. doi:10.1093/nar/gkw1306
- Wunderlich, K. A., Tanimoto, N., Grosche, A., Zrenner, E., Pekny, M., Reichenbach, A., . . . Perez, M. T. (2015). Retinal functional alterations in mice lacking intermediate filament proteins glial fibrillary acidic protein and vimentin. *FASEB J*, *29*(12), 4815-4828. doi:10.1096/fj.15-272963
- Wurtzel, J. G., Lee, S., Singhal, S. S., Awasthi, S., Ginsberg, M. H., & Goldfinger, L. E. (2015). RLIP76 regulates Arf6-dependent cell spreading and migration by linking

- ARNO with activated R-Ras at recycling endosomes. *Biochem Biophys Res Commun*, 467(4), 785-791. doi:10.1016/j.bbrc.2015.10.064
- Xia, H., Hu, P., Yuan, L., Xiong, W., Xu, H., Yi, J., . . . Deng, H. (2017). A homozygous MYO7A mutation associated to Usher syndrome and unilateral auditory neuropathy spectrum disorder. *Mol Med Rep*, 16(4), 4241-4246. doi:10.3892/mmr.2017.7053
- Xiao, F., Zuo, Z., Cai, G., Kang, S., Gao, X., & Li, T. (2009). miRecords: an integrated resource for microRNA-target interactions. *Nucleic Acids Res*, 37(Database issue), D105-110. doi:10.1093/nar/gkn851
- Xiao, J., Zhou, Y., Lai, H., Lei, S., Chi, L. H., & Mo, X. (2013). Transcription factor NF-Y is a functional regulator of the transcription of core clock gene Bmal1. *J Biol Chem*, 288(44), 31930-31936. doi:10.1074/jbc.M113.507038
- Xie, L. S., Qin, W., Fan, J. M., Huang, J., Xie, X. S., & Li, Z. (2010). The role of C1GALT1C1 in lipopolysaccharide-induced IgA1 aberrant O-glycosylation in IgA nephropathy. *Clin Invest Med*, 33(1), E5-13.
- Xie, Y. A., Lee, W., Cai, C., Gambin, T., Noupou, K., Sujirakul, T., . . . Allikmets, R. (2014). New syndrome with retinitis pigmentosa is caused by nonsense mutations in retinol dehydrogenase RDH11. *Hum Mol Genet*, 23(21), 5774-5780. doi:10.1093/hmg/ddu291
- Xu, W., Dai, H., Lu, T., Zhang, X., Dong, B., & Li, Y. (2011). Seven novel mutations in the long isoform of the USH2A gene in Chinese families with nonsyndromic retinitis pigmentosa and Usher syndrome Type II. *Mol Vis*, 17, 1537-1552.
- Xue, M., Zhuo, Y., & Shan, B. (2017). MicroRNAs, Long Noncoding RNAs, and Their Functions in Human Disease. *Methods Mol Biol*, 1617, 1-25. doi:10.1007/978-1-4939-7046-9_1
- Yamamoto, Y., Watanabe, T., Hoki, Y., Shirane, K., Li, Y., Ichiiyanagi, K., . . . Sasaki, H. (2013). Targeted gene silencing in mouse germ cells by insertion of a homologous DNA into a piRNA generating locus. *Genome Res*, 23(2), 292-299. doi:10.1101/gr.137224.112
- Yamashita, T., Liu, J., Gao, J., LeNoue, S., Wang, C., Kaminoh, J., . . . Zuo, J. (2009). Essential and synergistic roles of RPI1 and RPI1L1 in rod photoreceptor axoneme and retinitis pigmentosa. *J Neurosci*, 29(31), 9748-9760. doi:10.1523/JNEUROSCI.5854-08.2009
- Yang, G., Gong, Y., Wang, Q., Wang, L., & Zhang, X. (2016). miR-100 antagonism triggers apoptosis by inhibiting ubiquitination-mediated p53 degradation. *Oncogene*. doi:10.1038/onc.2016.270

- Yang, H. Y., Kim, S. H., Kim, S. H., Kim, D. J., Kim, S. U., Yu, D. Y., . . . Lee, T. H. (2007). The suppression of zfp-1 accelerates the erythropoietic differentiation of human CD34+ cells. *Biochem Biophys Res Commun*, 353(4), 978-984. doi:10.1016/j.bbrc.2006.12.155
- Yang, P., Skiba, N. P., Tewkesbury, G. M., Treboschi, V. M., Baciuc, P., & Jaffe, G. J. (2017). Complement-Mediated Regulation of Apolipoprotein E in Cultured Human RPE Cells. *Invest Ophthalmol Vis Sci*, 58(7), 3073-3085. doi:10.1167/iovs.16-20083
- Yanik, M., Wende, W., & Stieger, K. (2017). [Genome Editing Tools and their Application in Experimental Ophthalmology]. *Klin Monbl Augenheilkd*, 234(3), 329-334. doi:10.1055/s-0042-119205
- Yao, J., Jia, L., Khan, N., Lin, C., Mitter, S. K., Boulton, M. E., . . . Zacks, D. N. (2015). Deletion of autophagy inducer RB1CC1 results in degeneration of the retinal pigment epithelium. *Autophagy*, 11(6), 939-953. doi:10.1080/15548627.2015.1041699
- Yao, J., Jia, L., Shelby, S. J., Ganiou, A. M., Feathers, K., Thompson, D. A., & Zacks, D. N. (2014). Circadian and noncircadian modulation of autophagy in photoreceptors and retinal pigment epithelium. *Invest Ophthalmol Vis Sci*, 55(5), 3237-3246. doi:10.1167/iovs.13-13336
- Yasuda, M., Tanaka, Y., Nishiguchi, K. M., Ryu, M., Tsuda, S., Maruyama, K., & Nakazawa, T. (2014). Retinal transcriptome profiling at transcription start sites: a cap analysis of gene expression early after axonal injury. *BMC Genomics*, 15, 982. doi:10.1186/1471-2164-15-982
- Yasuda, M., Tanaka, Y., Ryu, M., Tsuda, S., & Nakazawa, T. (2014). RNA sequence reveals mouse retinal transcriptome changes early after axonal injury. *PLoS One*, 9(3), e93258. doi:10.1371/journal.pone.0093258
- Yating, Q., Yuan, Y., Wei, Z., Qing, G., Xingwei, W., Qiu, Q., & Lili, Y. (2015). Oxidized LDL induces apoptosis of human retinal pigment epithelium through activation of ERK-Bax/Bcl-2 signaling pathways. *Curr Eye Res*, 40(4), 415-422. doi:10.3109/02713683.2014.927507
- Yatsenko, A., Shroyer, N., Lewis, R., & Lupski, J. (2001). Late-onset Stargardt disease is associated with missense mutations that map outside known functional regions of ABCR (ABCA4). *Hum Genet*, 108(4), 346-355. doi:10.1007/s004390100493
- Yee, K. S., & Yu, V. C. (1998). Isolation and characterization of a novel member of the neural zinc finger factor/myelin transcription factor family with transcriptional repression activity. *J Biol Chem*, 273(9), 5366-5374.

- Yoshida, N., Ikeda, Y., Murakami, Y., Nakatake, S., Tachibana, T., Notomi, S., . . . Ishibashi, T. (2015). Vitreous cysts in patients with retinitis pigmentosa. *Jpn J Ophthalmol*, 59(6), 373-377. doi:10.1007/s10384-015-0405-1
- Yoshida, S., Honda, M., Yoshida, A., Nakao, S., Goto, Y., Nakamura, T., . . . Ishibashi, T. (2005). Novel mutation in ABCC6 gene in a Japanese pedigree with pseudoxanthoma elasticum and retinitis pigmentosa. *Eye (Lond)*, 19(2), 215-217. doi:10.1038/sj.eye.6701449
- Yoshihama, M., Nakao, A., & Kenmochi, N. (2013). snOPY: a small nucleolar RNA orthological gene database. *BMC Res Notes*, 6, 426. doi:10.1186/1756-0500-6-426
- Yoshikawa, T., Ogata, N., Izuta, H., Shimazawa, M., Hara, H., & Takahashi, K. (2011). Increased expression of tight junctions in ARPE-19 cells under endoplasmic reticulum stress. *Curr Eye Res*, 36(12), 1153-1163. doi:10.3109/02713683.2011.606592
- Young, R. W. (1967). The renewal of photoreceptor cell outer segments. *J Cell Biol*, 33(1), 61-72.
- Yu, A. L., Fuchshofer, R., Kook, D., Kampik, A., Bloemendal, H., & Welge-Lussen, U. (2009). Subtoxic oxidative stress induces senescence in retinal pigment epithelial cells via TGF-beta release. *Invest Ophthalmol Vis Sci*, 50(2), 926-935. doi:10.1167/iovs.07-1003
- Yu, H., Zheng, M., Zhang, L., Li, H., Zhu, Y., Cheng, L., . . . Yang, P. (2016). Identification of susceptibility SNPs in IL10 and IL23R-IL12RB2 for Behcet's disease in Han Chinese. *J Allergy Clin Immunol*. doi:10.1016/j.jaci.2016.05.024
- Yu, S., Li, C., Biswas, L., Hu, X., Liu, F., Reilly, J., . . . Liu, M. (2017). CERKL gene knockout disturbs photoreceptor outer segment phagocytosis and causes rod-cone dystrophy in zebrafish. *Hum Mol Genet*, 26(12), 2335-2345. doi:10.1093/hmg/ddx137
- Yue, L., Weiland, J. D., Roska, B., & Humayun, M. S. (2016). Retinal stimulation strategies to restore vision: Fundamentals and systems. *Prog Retin Eye Res*, 53, 21-47. doi:10.1016/j.preteyeres.2016.05.002
- Zeng, Y., & Yang, K. (2015). Sirtuin 1 participates in the process of age-related retinal degeneration. *Biochem Biophys Res Commun*, 468(1-2), 167-172. doi:10.1016/j.bbrc.2015.10.139
- Zerbino, D. R., Achuthan, P., Akanni, W., Amode, M. R., Barrell, D., Bhai, J., . . . Flicek, P. (2018). Ensembl 2018. *Nucleic Acids Res*, 46(D1), D754-D761. doi:10.1093/nar/gkx1098

- Zhang, J., Wang, H., Wu, S., Liu, Q., & Wang, N. (2017). Regulation of Reentrainment Function Is Dependent on a Certain Minimal Number of Intact Functional ipRGCs in rd Mice. *J Ophthalmol*, 2017, 6804853. doi:10.1155/2017/6804853
- Zhang, L., Cho, J., Ptak, D., & Leung, Y. F. (2013). The role of *egr1* in early zebrafish retinogenesis. *PLoS One*, 8(2), e56108. doi:10.1371/journal.pone.0056108
- Zhang, W., Shi, H., Zhang, M., Liu, B., Mao, S., Li, L., . . . Wang, H. (2016). Poly C binding protein 1 represses autophagy through downregulation of LC3B to promote tumor cell apoptosis in starvation. *Int J Biochem Cell Biol*, 73, 127-136. doi:10.1016/j.biocel.2016.02.009
- Zhang, X., Chen, L. J., Law, J. P., Lai, T. Y., Chiang, S. W., Tam, P. O., . . . Pang, C. P. (2010). Differential pattern of RPI mutations in retinitis pigmentosa. *Mol Vis*, 16, 1353-1360.
- Zhang, X., Yeung, K. Y., Pang, C. P., & Fu, W. (2002). [Mutation analysis of retinitis pigmentosa 1 gene in Chinese with retinitis pigmentosa]. *Zhonghua Yi Xue Yi Chuan Xue Za Zhi*, 19(3), 194-197.
- Zhang, X. J., Gao, X. Z., Yao, W., & Cote, R. H. (2012). Functional mapping of interacting regions of the photoreceptor phosphodiesterase (PDE6) gamma-subunit with PDE6 catalytic dimer, transducin, and regulator of G-protein signaling9-1 (RGS9-1). *J Biol Chem*, 287(31), 26312-26320. doi:10.1074/jbc.M112.377333
- Zhang, X. O., Dong, R., Zhang, Y., Zhang, J. L., Luo, Z., Zhang, J., . . . Yang, L. (2016). Diverse alternative back-splicing and alternative splicing landscape of circular RNAs. *Genome Res*, 26(9), 1277-1287. doi:10.1101/gr.202895.115
- Zhang, Y., Li, H., Cao, Y., Zhang, M., & Wei, S. (2015). Sirtuin 1 regulates lipid metabolism associated with optic nerve regeneration. *Mol Med Rep*, 12(5), 6962-6968. doi:10.3892/mmr.2015.4286
- Zhang, Y. F., Wei, W., Li, L., Tu, G., Zhang, Y., Yang, J., & Xing, Y. (2015). Sirt1 and HMGB1 Regulate the AGE-Induced Pro-Inflammatory Cytokines in Human Retinal Cells. *Clin Lab*, 61(8), 999-1008.
- Zhang, Y. X., Li, X. F., Yuan, G. Q., Hu, H., Song, X. Y., Li, J. Y., . . . Wang, R. (2017). beta-Arrestin 1 has an essential role in neurokinin-1 receptor-mediated glioblastoma cell proliferation and G2/M phase transition. *J Biol Chem*, 292(21), 8933-8947. doi:10.1074/jbc.M116.770420
- Zhao, X., Reifler, A. N., Schroeder, M. M., Jaekel, E. R., Chervenak, A. P., & Wong, K. Y. (2017). Mechanisms creating transient and sustained photoresponses in mammalian retinal ganglion cells. *J Gen Physiol*, 149(3), 335-353. doi:10.1085/jgp.201611720

- Zhao, Y., Zhou, L., Liu, B., Deng, Y., Wang, Y., Wang, Y., . . . Li, Y. (2006). ZNF325, a novel human zinc finger protein with a RBAK-like RB-binding domain, inhibits AP-1- and SRE-mediated transcriptional activity. *Biochem Biophys Res Commun*, 346(4), 1191-1199. doi:10.1016/j.bbrc.2006.06.031
- Zheng, C. Y., Chang, K., Suh, Y. H., & Roche, K. W. (2015). TARP gamma-8 glycosylation regulates the surface expression of AMPA receptors. *Biochem J*, 465(3), 471-477. doi:10.1042/BJ20140806
- Zheng, H. Y., Zheng, H. Y., Zhou, Y. T., Liu, E. L., Li, J., & Zhang, Y. M. (2015). Changes of TIZ expression in epithelial ovarian cancer cells. *Asian Pac J Trop Med*, 8(2), 157-161. doi:10.1016/S1995-7645(14)60308-4
- Zhuge, C. C., Xu, J. Y., Zhang, J., Li, W., Li, P., Li, Z., . . . Xu, G. T. (2014). Fullerenol protects retinal pigment epithelial cells from oxidative stress-induced premature senescence via activating SIRT1. *Invest Ophthalmol Vis Sci*, 55(7), 4628-4638. doi:10.1167/iovs.13-13732
- Zou, X., Fu, Q., Fang, S., Li, H., Ge, Z., Yang, L., . . . Sui, R. (2018). Phenotypic Variability of Recessive Rdh12-Associated Retinal Dystrophy. *Retina*. doi:10.1097/IAE.0000000000002242
- Zuo, L., Khan, R. S., Lee, V., Dine, K., Wu, W., & Shindler, K. S. (2013). SIRT1 promotes RGC survival and delays loss of function following optic nerve crush. *Invest Ophthalmol Vis Sci*, 54(7), 5097-5102. doi:10.1167/iovs.13-12157